BED-LOAD TRANSPORT OF MIXED-SIZE SEDIMENT

by

Peter Richard Wilcock

B.S. (summa cum laude), University of Illinois (1978)

M.Sc., McGill University (1981)

Submitted to the Department of Earth,
Atmospheric, and Planetary Sciences
in partial fulfillment of the
requirements for the
Degree of

DOCTOR OF PHILOSOPHY

at the

MASSACHUSETTS INSTITUTE OF TECHNOLOGY

June 1987

Signature of Author:_____
Department of Earth, Atmospheric, and Planetary Sciences

Certified by:_____
John B. Southard, Thesis Supervisor

Accepted by:_____
Chairman, Department Committee on Graduate Students

BED-LOAD TRANSPORT OF MIXED-SIZE SEDIMENT

by

Peter Richard Wilcock

Submitted to the Department of Earth, Atmospheric, and Planetary Sciences on May 8, 1987 in partial fulfillment of the requirements for the Degree of Doctor of Philosophy

ABSTRACT

The physics of mixed-size sediment transport is sufficiently complex that empirical coefficients are an unavoidable component of a transport model. These coefficients may be quite general if the model is mechanically correct and functionally complete and if the empirical relations between the relevant variables are isolated and accurately measured. The leading variables that make mixed-size sediment transport different from the better understood uni-size case are the size of each grain relative to the others in the mixture and the sorting, or spread, of sizes in the mixture. An experimental program was conducted to isolate the effect of these variables on the transport rates of individual fractions in a mixed-size sediment, thereby permitting the definition of empirical relations that may be used in a general mixed-size sediment transport model. A wide range of transport rates were measured for five sediments. Three of the sediments had the same mean size, with standard deviations that varied from well sorted to poorly sorted. Because the same sources were used for each mixture (controlling grain shape, density, etc.) and because size-distribution shape, flow depth, and water temperature were held constant, we were able to isolate the effect of mixture sorting and/or a fraction's percentile position in the mixture on the transport rate of the same fraction in different mixtures. Two other sediments were close to uni-size, with mean sizes lying near the fine and coarse ends of the mixed-size sediments. These sediments permit a direct examination of the effect of relative grain size on the transport rates of particular fractions in the fine and coarse parts of a poorly sorted sediment.

We find that to a first approximation different size fractions in mixed-size sediment are transported as bed load at approximately the same rate. In particular, we find the variation of transport rate with bed shear stress to be very similar from fraction to fraction in a mixture and we find that all sizes in a mixture begin moving at close to the same value of bed shear stress. This second result is consistent with a reanalysis of previously published mixed-size sediment transport data. These data were collected for sediments that cover a tenfold range of mixture sorting, a thirtyfold range in mean grain size, and a wide variety of size-distribution shapes (lognormal, bimodal, highly skewed, and rectangular), yet all sizes in each sediment begin moving within a narrow range of bed shear stress that correlates well with the median size of the mixture. This result contrasts with most previous models of mixed-size sediment transport, wherein the shear stress for incipient motion of a particular fraction is assumed to increase directly with that fraction's grain size and, hence, its weight. We find that the effect of a fraction's relative size

within the mixture (a relatively rough bed and decreased exposure to the flow for finer fractions, a relatively smoother bed and increased exposure for coarser fractions) almost exactly counterbalances the differential flow resistance due to a fraction's weight.

Once the relative size of a fraction is accounted for by a size ratio such as D_i/D_{50}, the mixture sorting and the percentile position of individual fractions contribute little explanation to the variation of fractional transport rates. The primary deviations from perfect similarity of the relations between transport rate and shear stress for each fraction occur at intermediate transport rates of our most poorly sorted sediment. The finest and coarsest fractions are observed to be underrepresented in the transported sediment compared to their percentage in the bed. This result is related to the development of a coarse layer at the bed surface, which preferentially traps finer sediments and removes them from the actively transported sediment. The coarse surface layer apparently also decreases the transport rates of the coarser fractions, possibly by providing a rougher surface that decreases the flow exposure the coarse grains experience and increases the relative roughness of the bed over which they move. The coarse surface layer develops via a size-dependent sorting process wherein finer grains can work their way beneath coarse grains, but not vice versa. The coarse surface layer is able to develop at moderate transport rates and in the presence of bed forms of a regular two-dimensional shape. At higher flows, the increased bed shear stress and the irregular depths to which the bed forms scour apparently prevent a coarse surface layer from developing and the transport rates of each fraction in the mixture become nearly equal.

Thesis Supervisor: John B. Southard, Professor of Geology

ACKNOWLEGMENTS

It is a pleasure to thank my advisor, John Southard, for his contributions to this thesis. John has taught me a great deal, both directly and by example, about things both practical and profound. I am also grateful that he had an open mind in allowing someone with a different background and with different applications in mind to join his laboratory to pursue work in which we have a common interest.

Two others made fundamental contributions to my education at MIT. Ole Madsen gave me a solid grounding in sediment transport and open-channel flow. He also provided important comments and direction at the formative stages of my thesis work. Chris Paola taught me an enormous amount about science and its conduct. I can always count on him to clear my fuzzy thinking and jolt me forward in my research.

I thank Chris James for interrupting his sabbatical reverie to give my thesis a careful reading as a member of my thesis committee. I thank Wiki Royden for chairing the defense.

This project required an exceptional amount of labor. It is particularly true that the work could not have been completed without those who helped out in the lab. Just the mixing of the test mixtures (literally by hand) involved a quantity of sediment sufficient to build a dam eight feet high across a river fifty feet wide. Far greater quantities of sediment were involved in the painstaking and frustrating task of blending the mixtures to specifications. Joe Cerutti was an integral part of the project from start to finish. I am grateful to Joe for his able and tireless work; I could count on him to run the whole show and to work more carefully than I ever had the patience for. Scott Stull gave long hours of careful work; I could count on Scott to come up with simple, practical solutions to problems I could not solve. Jim Danna taught me the basics of machine tools, construction and plumbing with good humor and common sense, even when his own thesis was nearly due. Jennifer Putscher mixed sediment good naturedly and took the graveyard shift without complaint. Doug Walker provided endless enthusiasm for experimental work and used his practical understanding of fluid mechanics to improve my experiments in numerous ways. Cathy Summa provided soldering, common sense and muscle when they were sorely needed. Last, but never least, I'm grateful to Roger Kuhnle for his help in the lab and for the endless debates on hydraulics and sediment transport (and everything else) that sharpened my thinking and helped pass the hours in the lab.

I thank Mary Hubbard for having the presence of mind to go to Nepal and leave an empty desk during the months I was writing this thesis. I also thank Sang Mook Lee for not complaining when I growled at him. Cynthia Ebinger did things to my figures that my Mac could never do.

I thank my mother for convincing me that I could do well and for mailing college applications to general delivery addresses across the continent until I finally decided to get a college education. She taught me the ropes.

My family took my long absences and occasional grumpiness in stride and unfailingly made me keep the whole thing in perspective. My wife Barbara Ashley supported us financially, practically, and emotionally. She was my coach and friend through it all, for which I will always be grateful. Together, we were able to make the whole process far more pleasant than we ever expected. My sons Zachary and Jacob provided a new, much more important dimension to my life and emphatically forced me to live up to my bromides about priorities in one's life. It is to them — who understood least what I was doing, but always gave me what I most needed — that I dedicate this thesis.

Financial support for this work was provided by the Office of Naval Research under contract numbers N00014-80-C-0273 and N00014-86-K-0325.

TABLE OF CONTENTS

LIST OF FIGURES

LIST OF TABLES

CHAPTER ONE

INTRODUCTION

All natural sediments contain grains of different sizes. In some cases, the range of sizes is small enough that the sediment behaves as if all grains were identical in size. In other cases, the range of sizes is sufficiently broad that the hydrodynamic behavior of the sediment, and the transport rates of the individual grains within it, are fundamentally different. It is intuitively clear, and empirically well established, that grains in a mixed-size sediment are transported at rates very different from those of grains of the same size in a uni-size sediment. However, the transport rates of individual size fractions in mixed-size sediment (termed here the fractional transport rates) are not understood well enough to determine which fractions in a mixture move faster than others. Ample evidence exists that grains of different size in a single sediment are transported at different rates. The grain-size distribution of transported sediment is observed to vary with time and flow strength at a single place, as during the passage of a flood. Sediments become sorted by grain size over distances of meters to hundreds of kilometers in clastic sedimentary environments. To adequately describe such changes in grain-size distribution, or even to predict the transport rate of the entire mixture (which is only the sum of the fractional transport rates), a general model of mixed-size sediment transport must operate on a fraction-by-fraction basis, so that the transport rates of individual fractions — and the grain-size distribution of the transported sediment — may be determined.

The key to understanding fractional transport rates is to determine how the size of each fraction relative to the size of the others in the mixture affects the transport of that fraction. The intuitive argument for the variation in transport rates with grain size in a mixture is based on the relative grain size of the individual fractions. One might expect that relatively fine fractions in a mixture, being partially hidden from the flow by the larger grains, would experience a smaller driving force than as if they were present in a bed of

grains all of the same size. In addition, once these smaller grains are in motion, the bed over which they move is rough compared with a bed of uni-size sediment. Both of these factors should diminish the transport rate of the finer fractions relative to the uni-size case. On the other hand, the relatively coarse fractions might be expected to have transport rates that are greater in a mixture than in a uni-size bed. In the mixture case these grains are more exposed to the flow, and they traverse a relatively smooth bed that offers less resistance to their motion.

There are two fundamentally different ways to express the relative size of individual fractions in a size mixture. The first is a ratio of the fraction size D_i to some central measure of the grain-size distribution, such as the mean size D_m or the median size D_{50}. The second is the percentile position of a fraction within the mixture, such as the percentage of the mixture finer than P. These two relative-size parameters are related by the standard deviation of the grain-size distribution. The goal of the experimental work reported in this thesis is to isolate the effect of these three dominant grain-size parameters on the transport rates of individual fractions in different size mixtures. The primary experimental control that allows these variables to be isolated arises from the use of size mixtures whose grain-size distributions have been carefully tailored so that comparisons among fractions in different mixtures involve the variation of only a single relative-size parameter.

The results of our experiments will be examined in two parts. The first concerns the flow conditions necessary to initiate motion of the individual size fractions, commonly termed the threshold or critical shear stress. The second concerns how the fractional transport rates vary with the bed shear stress, once motion is established. These two parts may be thought of in terms of a graph of the relation between transport rate and bed shear stress, which we will term the transport function. Initial motion concerns the intercept, or *position*, of the transport function for each fraction in a mixture. Established motion concerns the *form* of the transport function. Much of the variation in transport rate among fractions in a mixture may be attributed to differences in

the value of bed shear stress at which transport of each fraction begins. If these threshold values of bed shear stress are determined first, the fractional transport rates may be expressed as a function of the excess of the bed shear stress above the threshold value. The transport function based on excess shear stress permits a direct evaluation of the variation in the *form* of the transport function with relative grain size. A two-part organization is also used here not only because the critical shear stress is an integral part of the transport-rate problem, but also because it is an important subject in its own right. The critical shear stress is of central importance for modeling a number of geomorphic and sedimentologic problems, including the stable form, shape, and slope of natural and artificial channels, and the sediment dispersal within and paleohydraulic interpretation of clastic sedimentary environments.

RELATIVE SIZE OF INDIVIDUAL FRACTIONS

The grain size of an individual size fraction in a mixture has two effects, one absolute and the other relative, on the transport rate of that fraction. First, for a given grain density and shape, the absolute size of the fraction determines the mass of the grain and the area of grain surface exposed to the flow. Grain area is proportional to D^2 and grain mass is proportional to D^3, so the ratio of driving forces to resisting forces for each fraction is represented by the classic Shields parameter

$$\tau_i^* = \frac{\tau_o}{(s-1)\rho g D_i}$$

where τ_o is bed shear stress, ρ is fluid density, s is the ratio of grain density to fluid density, g is acceleration due to gravity, and D_i is size of the ith fraction. For grains in a uni-size bed and a given τ_o, the ratio of driving to resisting forces, and hence the transport rate, increases with decreasing grain size. The size of each grain relative to others in the mixture controls the variation from fraction to fraction of both the value of bed shear stress acting on individual

grains and the resistance of those grains to movement. Because smaller grains in a mixture are more hidden from the flow and also more impeded in their motion than coarser grains, the relative-size effect counteracts the absolute-size effect by decreasing the mobility of the finer fractions and increasing the mobility of the coarser fractions. The essence of the mixed-size sediment transport problem lies in the balance between these two grain-size effects.

Because of its central role in mixed-size sediment transport, the relative size of each fraction must be described accurately. For the general case of a reasonably smooth grain-size distribution, relative grain size is completely described by three variables: the size ratio of the fraction (e.g., D_i/D_m), the percentile position of the fraction (e.g., percent finer than, P) and the mixture standard deviation σ. For a smooth size distribution reasonably symmetrical about its mean, two of these three variables are sufficient to describe the relative size of a fraction. For example, for a lognormal distribution (which we used in our experiments), the three are exactly related as

$$P = \frac{100}{\sqrt{2\pi}} \int_{-\infty}^{z} e^{\frac{-t^2}{2}} dt$$

where

$$z = \frac{\log_2 (D_i/D_m)}{\sigma_\phi}$$

and σ_ϕ is the mixture standard deviation in Ø units ($Ø = -\log_2 D$, where D is grain size in mm). The variation of P with σ_ϕ for a range of D_i/D_m, shown for lognormal size distributions in Figure 1.1, illustrates the potential need for considering more than one relative-size parameter. Following the curve for $D_i/D_m = 2$ in Figure 1.1, $\sigma_\phi = 0.5$ corresponds to P = 98 percent finer than; at $\sigma_\phi = 2.0$, a value common for gravel-bed streams, P = 68 percent finer than, representing a substantial change in the relative position of the same fraction. It is not clear that the transport rates for the fraction $D_i/D_m = 2$ would be the

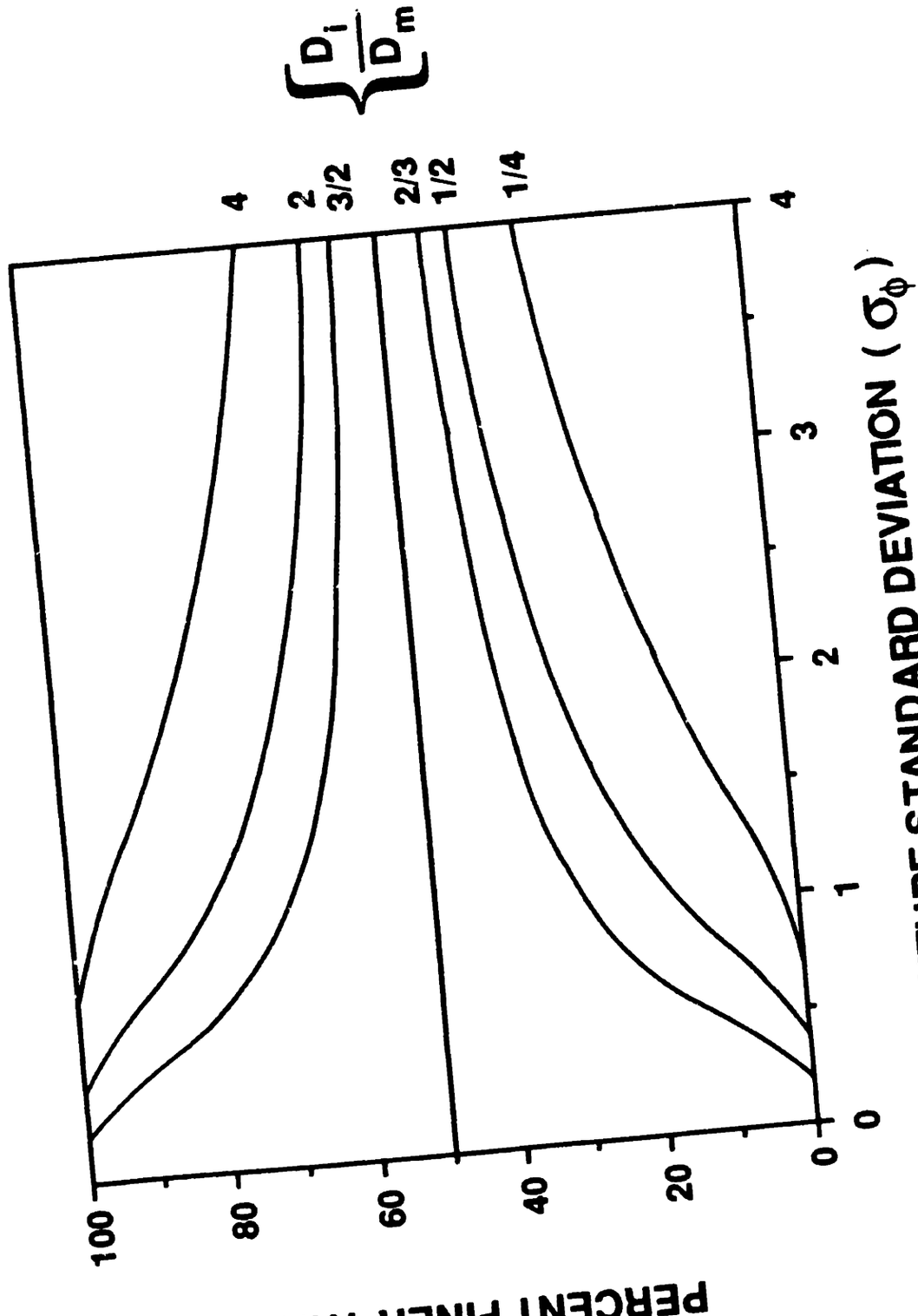

Figure 1.1. General relation between D_i/D_m, percent finer than, and mixture sorting

same for both mixtures. Because most studies on initial motion have represented relative grain size by one or the other of D_i/D_{50} or P, a direct test of this approximation was a goal of this work.

PREVIOUS WORK

Prior to the seminal work of Einstein (1950), the effect of relative grain size was not included in mixed-size sediment transport models. Most models computed only the total transport rate, using a a single grain size (commonly D_{50}; e.g., Meyer-Peter and Müller, 1948) to represent the transport rate of the mixture. Some transport models did operate on a fractional basis, but did not incorporate relative grain size into the computation of the transport rate of each fraction. Rather, the fractional transport rate was computed as if that fraction formed a uni-size bed; the total transport rate was then computed as a sum of the fractional transport rates weighted by the proportion of each fraction present in the bed. Surprisingly, even though the effect of relative grain size on fractional transport rates has been demonstrated for decades, recent models of mixed-size sediment transport have continued to use a fractional approach based on the sum of uni-size transport computations (e.g., Borah et al., 1982; Li and Fullerton, 1985).

The first major attempt to incorporate the effect of relative grain size on fractional transport rates was made by Einstein (1950). Einstein defined several empirical correction functions in terms of mixture properties, but only one of these, the hiding factor ξ, was defined as a function of relative grain size. Although the exact derivation of ξ is not clear, it was apparently computed as a final empirical correction between predicted and measured fractional transport rates. The hiding factor is defined as a function of D_i/X, where X is an empirical quantity intended to represent the largest grain size in a mixture that experiences hiding effects. The hiding factor is included in the transport model as a multiplicative correction term

$$W_i^* = f(\xi \tau_i^*)$$

where W^*_i and τ^*_i are dimensionless fractional transport rate and shear stress, respectively, and will be defined below. The hiding factor decreases in value for $D_i < X$ and takes on a constant value at $D_i \geq X$ (Figure 1.2). The form of the hiding function reveals the root of its name: it expresses a decrease in transportability (hiding) for fractions smaller than X, but not an increase in transportability for fractions coarser than X.

In later applications (e.g., Parker et al., 1982), the Einstein hiding function has been found to be inaccurate. One major reason for this is related to the experimental data from which Einstein derived the function (Einstein, 1950; Einstein and Chien, 1953). Most of these experiments involved very high transport rates in which large amounts of sediment were imposed on the flow and the bed was actively eroding or aggrading during the run. Furthermore, only the total load was measured in the experiments, even though the flow strengths in many runs were high and suspended sediment transport dominated the bed load. The bed-load fractional transport rates were computed by subtracting an estimated value of the suspended load from the total load. Both the unsteady, nonequilibrium flow conditions and the approximate method used to measure the bed load contribute to an apparently large error in fractional transport rates computed with the hiding function.

Egiazaroff (1965) also developed a mixed-size sediment transport model that incorporates relative-size effects. In this case, the relative-size variation was introduced in terms of the flow velocity acting on different fractions. Egiazaroff assumed, as did Einstein, that a logarithmic velocity profile could be extended down among the grains on the bed. This assumption operates mostly as a necessary but artificial constraint on the problem, because it is unlikely that a logarithmic velocity profile represents even some mean velocity acting on the smaller fractions on the bed, due to momentum defects arising from form drag on the coarser bed sizes. In contrast to Einstein, who used a single characteristic velocity for all fractions in the bed, Egiazaroff defined the velocity acting on each fraction as the velocity at a distance above the bed equal to a constant times the grain diameter of each

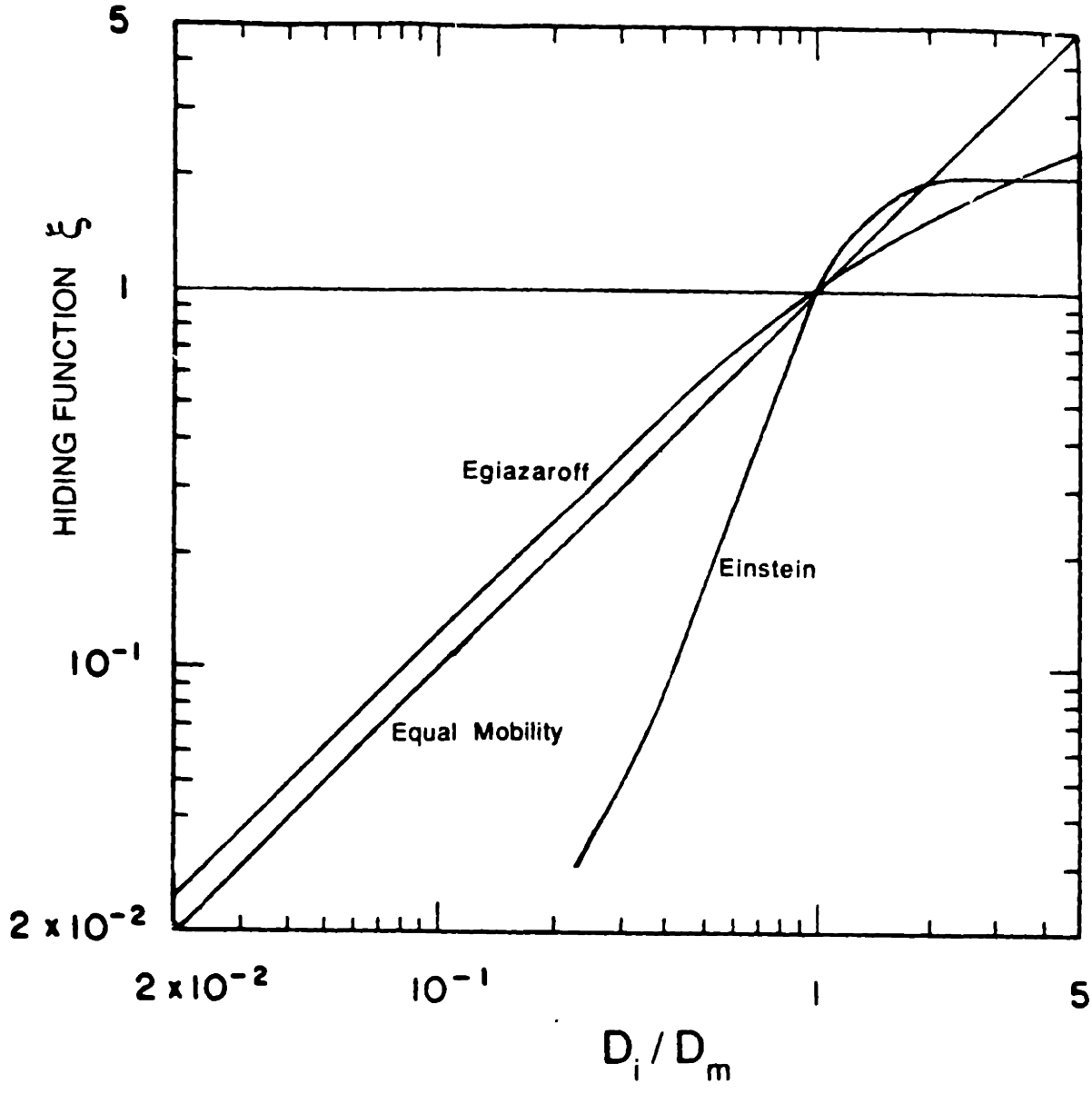

Figure 1.2. Hiding functions of Einstein and Egiazaroff (after Andrews and Parker, 1985). The Einstein Hiding Function assumes rough flow, $X = D_{65}$, and $D_{65}/D_m = 2$. The Egiazaroff relation is from Ashida and Michue (1972).

fraction. Because the drag coefficient was assumed to be a constant for each fraction, the velocity (and drag force) increases with grain size. The Egiazaroff model may be modified slightly and put in the form of a multiplicative correction function (Ashida and Michue, 1972). It is much less curved than the Einstein hiding function and shows a relative-size correction that extends to the coarsest fractions in the mixture (Figure 1.2).

Several recent empirical studies of mixed-size sediment transport have determined the value of bed shear stress necessary to produce a small, constant value of transport rate for each fraction. This is an analogue for the critical shear stress and will be discussed in detail in Chapter Three. At this point, it is worth comparing with the Einstein and Egiazaroff hiding functions a result common to some of these studies (Andrews, 1983; Parker et al., 1982) which we essentially confirm in Chapter Three: all fractions in a mixture begin moving (or are transported at the same, low transport rate) at nearly the same bed shear stress. This result has been termed equal mobility (Parker et al., 1982) and may be expressed as a hiding function with a slope of -1.0 in Figure 1.2. The Egiazaroff hiding function is quite close to equal mobility, except at high values of D_i/D_{50}, where equal mobility is somewhat greater than the Egiazaroff hiding function. It is surprising that an assumption as simple as Egiazaroff's concerning the form of the velocity profile down among the bed grains would produce a result so close to that measured in a variety of different sediments.

The mixed-size sediment transport models discussed to this point provide only a one-dimensional correction for the relative size effect on fractional transport rates. The size ratio D_i/D_{50}, but not the mixture sorting (or P), can be accounted for in predicting the fractional transport rates. In addition, the same correction function applies at all values of bed shear stress (and transport rate), so the form of the transport function is a constant for each fraction. Attempts to incorporate other parameters have not been particularly successful or applicable beyond the data from which they were derived. White and Day (1981) defined the grain size within a mixture whose reference shear stress was equivalent to its uni-size value, D_A. They attempted to relate the ratio

D_A/D_{50} to the mixture sorting, but found the physically incorrect result that the ratio did not approach unity as the sorting went to uni-size. Both Parker et al. (1982) and Diplas (1987) examined the the field data of Milhous (1973) and investigated the change in the form of the fractional transport function with relative grain size, thus including the magnitude of the bed shear stress as an additional parameter. As will be discussed in Chapter Four, the resulting empirical relations are not applicable to our fractional-transport data or those of others, and so do not appear to have an application beyond the stream from which the data were collected.

DIMENSIONAL ANALYSIS

A dimensional analysis of the fractional-transport problem serves several purposes. It provides a useful basis for thinking about the important physical aspects of the problem, and it provides a framework for an experimental program in which the effects of particular independent variables are isolated in carefully controlled experiments. Which variables can reasonably be considered to govern the bed-load transport of a given size fraction (denoted by q_{bi}) in steady uniform flow in a rectangular channel? The flow may be characterized by the boundary shear stress τ_o, flow depth d, and the flow width b; the fluid, by density ρ and viscosity, μ; and the sediment, by density ρ_s, grain shape, grain-size distribution, distribution standard deviation σ, relative grain size D_i/D_m or P, and the size of a particular fraction D_i. The acceleration of gravity g is also needed. Other commonly used variables, such as mean flow velocity or sediment fall velocity, could also have been chosen, but these should be largely determined by the variables in the above list.

We can begin to constrain the problem by choosing values for some of the variables above that represent common natural conditions, and then holding these variables constant for all our experiments. Grain-size distribution may be eliminated from the list because only a single size-distribution shape was used for our sediment mixtures. For comparisons of transport rates among fractions of the same size in different mixtures, grain shape was held

essentially constant in our experiments. Furthermore, we can reasonably eliminate the effect of flow width (which was a constant for all runs) on the bed shear stress and the sediment transport by using a sidewall correction procedure. Details on this procedure and the means by which we held grain shape and size distribution constant will be given where appropriate in later sections of the thesis. Even with these simplifications, ten variables remain:

$$q_{bi} = f(\tau_o, d, \rho, \mu, \rho_s, g, D_i, \{\frac{D_i}{D_m}, P\}, \sigma) \qquad (1.1)$$

Because these involve three dimensional units (mass, length, and time), there are seven independent dimensionless groups upon which a suitably nondimensionalized version of q_{bi} should depend. Among the many equivalent possibilities, the following functional relation derived from Equation 1.1 will be used here:

$$\frac{(s-1)gq_{bi}}{f_i\rho_s u_*^3} = f\left(\frac{\tau_o}{(s-1)\rho g D_i}, \frac{d}{D_i}, \frac{D_i^{3/2}\sqrt{(s-1)g}}{\nu}, s, \{\frac{D_i}{D_m}, P\}, \sigma_\phi \right) \qquad (1.2)$$

where, for convenience, the following substitutions have been made: $s = \rho_s/\rho$ is the relative grain density; $\nu = \mu/\rho$ is the kinematic fluid viscosity, and $u_* = (\tau_o/\rho)^{1/2}$ is the bed shear velocity.

The fractional transport rate q_{bi} is taken to have the dimensions of sediment mass transported per unit time and unit channel width. It is computed as the product of the total transport rate q_b and the proportion p_i of fraction i in the transport load. For reasonable comparison among different fractions in a mixture, q_{bi} is appropriately normalized by f_i, the proportion of fraction i present in the bed mixture. The dependent variable in Equation 1.2, here denoted as W^*_i, is formed without the grain size. This allows the transport rates of different fractions to be compared without distortion arising from the variation in grain size from fraction to fraction. W^*_i also has the convenient property that it approaches a constant value at high transport rates (q_{bi} is

generally found to approach a constant function of u_*^3 at high transport rates; Ashida and Michue, 1972; Parker et al., 1982).

The first independent variable, denoted here by τ^*_i, is the Shields parameter formed with the fraction grain size. The second independent variable, denoted by d^*, expresses the grain roughness relative to the flow depth. The next variable, denoted by S^*, represents the effect of fluid viscosity on the near-bed flow structure. S^* is commonly substituted for the grain Reynolds Number u_*D/ν (which has typically been used to express the ratio of viscous forces to inertial forces), because S^* does not contain u_* and permits more direct interpretation of the viscous effect on the fractional transport rates. The two relative-size parameters are grouped together because our sediment mixtures have nearly exact lognormal distributions, so that only one of D_i/D_m or P, along with σ_ϕ, is necessary to specify the relative size of a given fraction. The mixture standard deviation σ_ϕ is dimensionless. With the variables in their shorthand form, Equation 1.2 becomes

$$W_i^* = f(\tau_i^*, d^*, S^*, s, \{\frac{D_i}{D_m}, P\}, \sigma_\phi) \qquad (1.3)$$

EXPERIMENTAL PROGRAM

The physics of mixed-size sediment transport is sufficiently complex that empirical results are an unavoidable component of our understanding of the problem. If the leading independent variables of the problem are experimentally isolated, and their effect on fractional transport rates are accurately measured, inferences drawn from the results may be applicable beyond the specific set of experimental conditions used. The leading variables that make mixed-size sediment transport different from the better understood uni-size case are those that determine the size of each grain relative to the others in the mixture: D_i/D_m, P, and σ_ϕ. The objective of the experimental program of this thesis is to isolate experimentally the effect of these variables on the transport rates of individual fractions in a mixed-size sediment, thereby permitting the definition

of empirical relations that may be used in a general mixed-size sediment transport model.

Equation 1.2 provides a basis for the experimental control that allows us to focus on the relative size parameters. Flow depth was held within a narrow range in all our experimental runs, thereby making d^* a constant for fractions of the same size in different mixtures. If d^* is formed with D_m, the value of d^* is then also a constant for all runs with sediment mixtures of the same mean grain size. The water temperature was held nearly constant during all runs, so that the water viscosity and S^* were nearly constant for a given value of D_i. Again, if S^* is formed with D_m, S^* remains nearly constant for all runs with sediment mixtures of the same mean size. Fluid density was a constant in all our runs and grain density was nearly constant for all fractions in the sediments, so the ratio s is also a constant.

The remaining independent variables in Equation 1.2 are τ^*_i, the relative-size parameters, and σ_ϕ. Because τ^*_i is clearly the leading independent variable of the problem — it represents the force driving the transport — it was not held constant but was varied from run to run over as wide a range as was feasible. Thus, we are not examining the relative-size effect on fractional transport rates for a constant value of τ^*_i; instead, we will investigate the relative-size effect on the relations between W^*_i and τ^*_i.

At the heart of our experimental design are three sediment mixtures that have the same mean size and the same size-distribution shape but values of mixture standard deviation that vary from well sorted to poorly sorted (σ_ϕ = 0.2 to 1). Because the same sediment sources were used for each mixture (providing reasonable control over grain shape, density, etc.) and because d^* and S^* were held nearly constant, we are able to isolate the effect of the three relative-size parameters on fractional transport rates. For example, the value of P for the same fraction in the mixtures (and hence the same value of D_i/D_m) changes systematically with the change in mixture sorting from mixture to mixture. The three mixtures may also be used to test the effect of only mixture sorting on the transport rates of the central fractions of the size mixtures (for

which D_i/D_m and P are identical), or on the total transport rates of the sediments.

In addition to the three primary sediments with the same mean size, the transport rates of two other sediments were measured. These sediments were well sorted and had values of D_m chosen to fall toward the fine and coarse ends of the most poorly sorted sediment mixture. These two sediments permit a direct examination of the effect of relative grain size on the transport rates of particular fractions in the fine and coarse portions of a poorly sorted sediment. Because both D_i/D_m and P vary between the corresponding fine and coarse fractions, only the total relative size effect on the fractional transport rates may be examined.

CHAPTER TWO

EXPERIMENTAL METHODS

This chapter presents the details of the experimental apparatus and procedure, as well as the sampling and data-analysis methods used to produce the basic flow and transport parameters. The methods used to investigate the fractional transport rates in terms of these fundamental parameters are discussed where appropriate in later chapters. The experimental design is discussed in Chapter One.

APPARATUS

The experiments were conducted in a laboratory flume with a channel 23 m long, 0.6 m wide, and 0.3 m deep (Figures 2.1, 2.2). Both water and sediment were recirculated, but in separate systems. The water passed without overfall into a large tailbox and was recirculated via a large vertical propeller pump through a single line of 15.2 cm (6") and 20.3 cm (8") pipes located beneath the channel. Discharge was controlled with a 15.2 cm (6") gate valve located at the centrifugal pump outlet. At the head of the flume, the recirculated water passed through a vertical section and then directly down into the headbox, where a curved vertical wall was installed to prevent stagnation and sediment deposition. To suppress the largest-scale turbulence, the flow passed immediately through a acrylic plastic grid with 8-cm square openings extending 10 cm in the flow direction. To spread the flow across the channel, a 4 cm blade was placed transverse to the flow 4 cm above the bed. The blade served as an undershot weir that backed the flow into the headbox and distributed it evenly across the flow-straightening grid. Downstream of the weir, two flat plywood plates 1.0 m long and as wide as the channel were suspended so that they just touched the water surface to eliminate surface waves.

The upstream 6 m of the flume contained a acrylic plastic false bottom at the same elevation as the sediment bed. Sand grains 1.83-2.00 mm in diameter (the mean size of the sediment mixtures used in the study) were glued to the

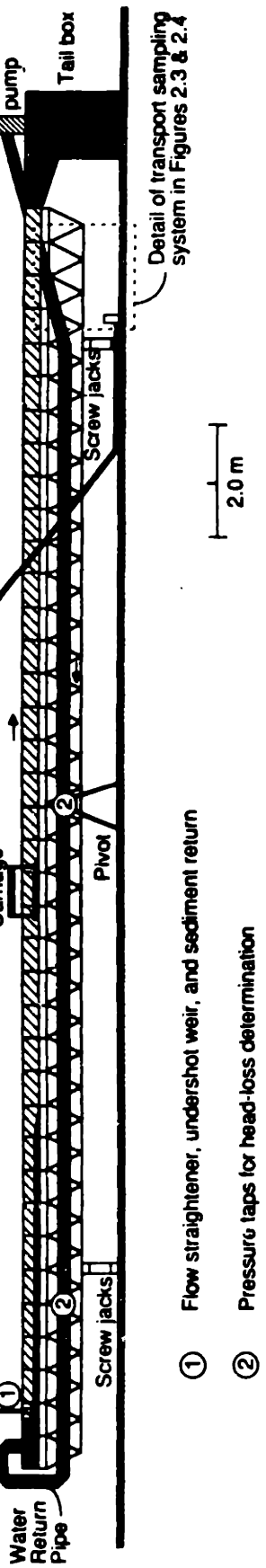

Figure 2.1. Diagram of flume in which all of the experiments were made

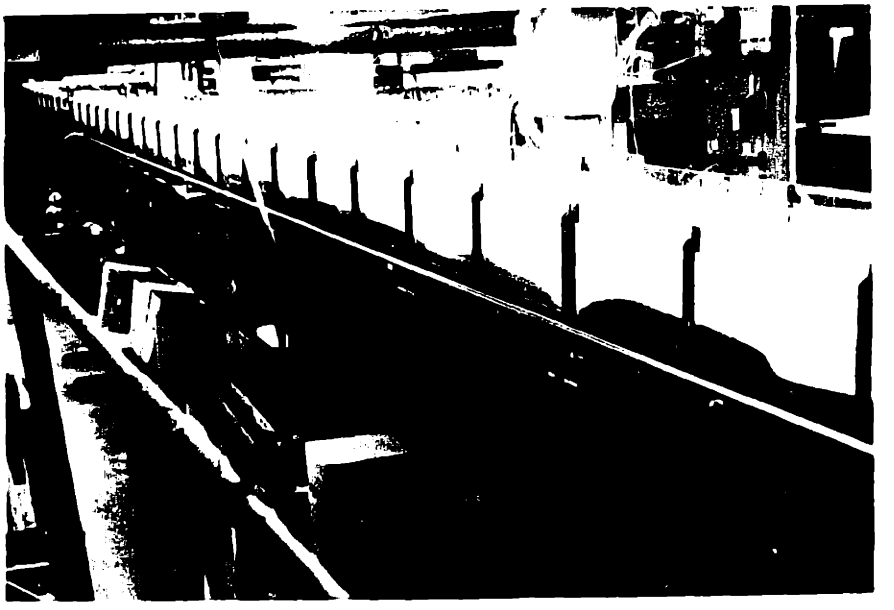

Figure 2.2. Photograph of Flume. View is upstream from vicinity of sediment trap.

Figure 2.3. Photograph of transport sampling arrangement. Flow left to right at top. Sediment trap at top right. Diversion valve, sampling hose, and sampling funnel also visible.

downstream 4.9 m of the false bottom to allow the boundary layer to develop before it reached the movable bed. This section of the flume was also long enough to allow any grains traveling in suspension in the return flow to settle to the channel bottom before reaching the bed. A sloping transition to the bed was made with a plastic plate with a sand-roughened surface that dropped 6 cm in elevation from the bed surface over a distance of 60 cm. The sediment was screeded onto the transition section to make a smooth surface with the grains on the false bottom. The transition section provided a very sensitive indicator of nonuniform flow conditions, because scour or deposition could be easily detected where the bed tapered to zero thickness at the boundary between the false bottom and the bed.

A sediment bed 7 cm thick was used in all runs. The working section of the bed was 16.2 m long and ended in a sediment trap constructed across the full width of the flume (Figures 2.3 and 2.4). All the transported sediment fell into the trap and was returned to the headbox by a small air-driven double-diaphragm pump through a flexible, clear 2.5 cm (1") tube. At the headbox, the recirculated sediment was split into four lines and discharged downward into the channel immediately downstream of the flow-straightening grid and undershot weir. Although the flow and sediment were never perfectly divided between the four discharge tubes — the sediment discharge varied between the tubes, although there was always some discharge in each tube — the spacing of the tubes was sufficiently small (12.5 cm) that any inequalities between the tubes were evened out within a few centimeters of transport in the highly turbulent flow leaving the headbox. No cross-sream nonuniformity of transport was evident along the false bottom during the runs.

The sediment trap was 25 cm long in the flow direction. Its upstream wall was vertical; the other three sloped downward to bring the trap to a 2.5 cm (1") tube outlet. A small retaining wall extended above the upstream side of the trap to minimize the length of the sediment slip face. The upper surface of the wall was set to a level just below the deepest bed-form troughs that were expected in a given run. With some experience, it was possible to set the height

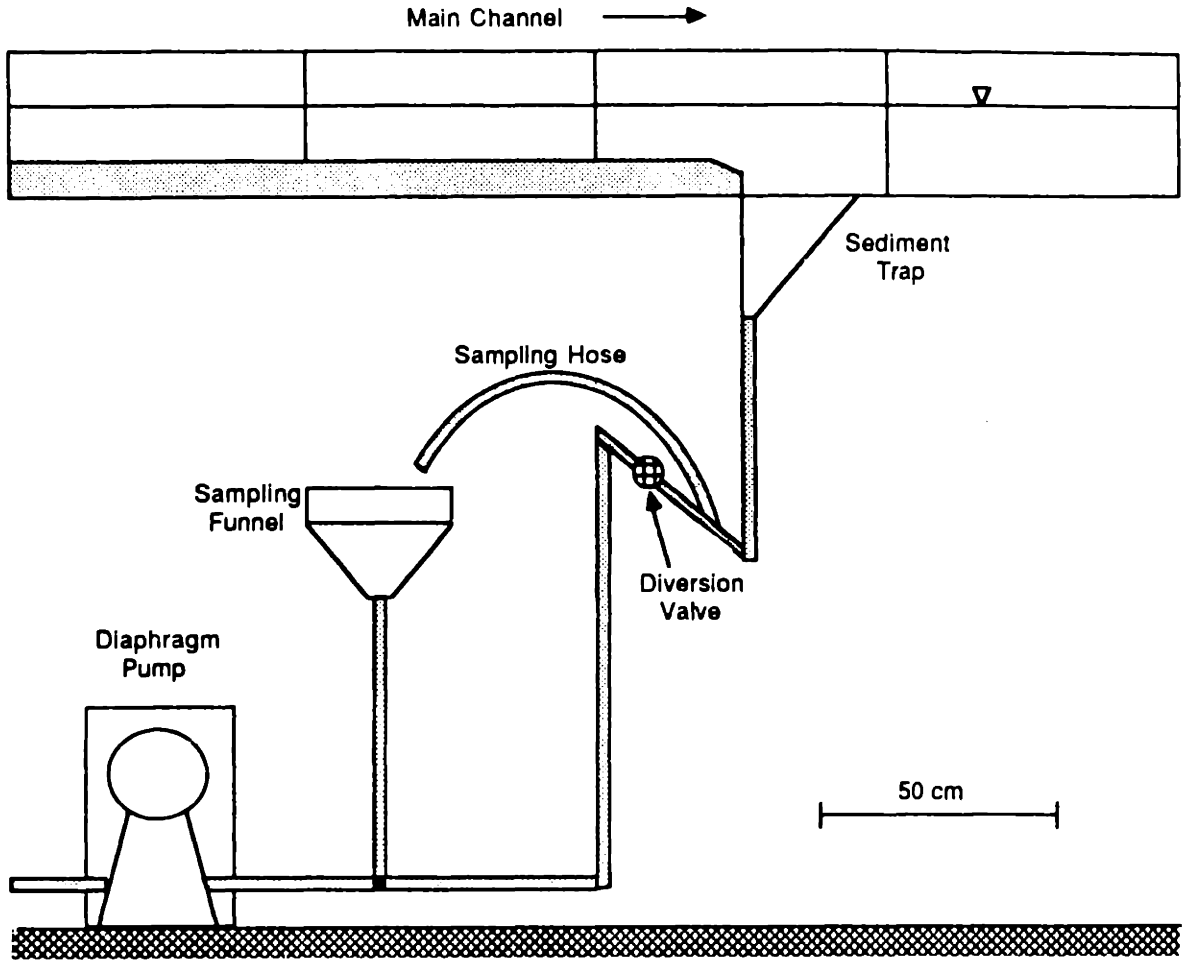

Figure 2.4. Schematic diagram of sediment trap and transport sampling arrangement

of the wall so that transported sediment moved into the trap without a substantial period spent traversing the slip face. No periodic buildup and release of the sediment on the slip face was noticed during the experiments. The efficiency of the trap was nearly 100%. A transition section between the trap and the tailbox increased flow depth from 20 cm to 40 cm (roughly two to four times the depth above the sediment bed) over a length of 1.5 m and served to catch any sediment that bypassed the trap. No sediment was found in the transition during most runs. During the highest-velocity runs, on the order of tens of grams were recovered from the tailbox for runs lasting 25-30 hours and involving the transport of 10,000 to 40,000 kg of sediment. Much of the sediment found in the transition section was transported, before the run began, as isolated clusters of grains picked off the bed surface when the flume was filled and was carried at the water surface by surface tension.

The slope of the flume channel was fully adjustable by two coupled sets of screw jacks that tilted the flume about a pivot at its midpoint. The flow passed into the tailbox with no free overfall, so that the volume of water in the flume determined the mean depth of flow. Uniform flow was maintained by adjusting the flume slope. To minimize head loss in the return system, the discharge was determined directly from the head loss in a straight 9.15 m section of 20.3 cm (8") return pipe (Figure 2.1). The head-loss section was located downstream of 9.0 m (49 pipe diameters) of straight pipe and 6.0 m (29 pipe diameters) downstream of an abrupt pipe expansion from 15.2 cm (6") to 20.3 cm (8"). The head-loss section was located upstream of 3.2 m (16 diameters) of straight 20.3 cm (8") pipe. The head loss was determined via two pressure taps connected to an open air-water manometer inclined 1:13 to enable the reading of the small head loss (1 to 9 cm of water).

The sediment recirculation system contributed a small and known part of the total discharge. This part of the discharge was not measured during the experiments, because direct measurement showed it to be nearly constant for most transport rates used in the experiments. The contribution of the diaphragm pump decreased slightly at higher sediment transport rates, but at

these flow rates the contribution of the diaphragm pump represented 2.5% or less of the total discharge. Hence, even a substantial error in estimating the discharge of the diaphragm pump would produce an error smaller than that with which the main discharge could be measured.

The elevations of the water surface and bed surface were measured using a point gauge mounted on a cart that traversed rails parallel to the flume bottom. A datum for each run (and flume-slope setting) was determined by reading the elevation of a still water surface at every water-surface and bed-surface location.

Sediment transport was sampled by passing the entire water-sediment mixture in the return system through a 20.3 cm (8") sieve that trapped the sediment and allowed the water to return to the headbox through the diaphragm pump. This was achieved by closing a valve in the sediment return line between the trap and the pump and allowing the water-sediment mixture to flow under gravity through a flexible tube into a large funnel that was itself connected to the sediment return system between the diversion valve and the pump (Figures 2.3 and 2.4). An open-air, gravity-driven sampling system was chosen to provide maximum flexibility in sampling methods and periods (sample intervals from 10 seconds to 4 hours were used during the experiments, depending on the transport rate, which itself varied by almost five orders of magnitude) and to allow convenient removal of samples of the entire sediment load for size analysis. Sediment could also be returned to the return system via the sample funnel, so that sampled sediment could be replaced.

SEDIMENT

The sediments form the heart of the experimental control and the scientific basis of this work. Essential to the experimental plan was the use of several sediment mixtures with different values of standard deviation of the grain-size distribution. To maintain constant values of the dimensionless variables d^* (d/D_i) and S^* ($[(s\text{-}1gD_i^3]^{1/2}/v$) for particular size fractions, and to allow direct comparison of the transport rates of the same fractions, the

mean size of the principal mixtures used was held constant. The choice of this mean size was constrained by several considerations. The minimum mean grain size of the mixtures was constrained by the focus of this study on bed-load motion and the need to measure a range of transport rates for each size fraction in order to define a relation between transport rate and shear stress. Hence, it was necessary that the mean size of the sediment mixtures be coarse enough so that the smallest fractions in the most poorly sorted mixture would move only as bed load for at least a twofold range in bed shear stress. The maximum mean grain size that could be used was limited mainly by the flow depth, which was itself constrained to be no more than 12.5 cm by the fixed flume width of 60 cm and the desire to keep the width-depth ratio of the flow in excess of five. With this maximum depth, it was necessary that the mean grain size be small enough that the maximum size in the mixture met the following constraints: (1) a d^* value for the coarsest fractions no less than 12 or 13; (2) a Froudenumber not greater than about 0.8 for flows that would exceed the critical shear stress for the coarsest fractions by a factor of two; and (3) a 2:1 clearance in the sediment return system (with its 25 cm inner diameter), to prohibit clogging by rare, oblong grains with a largest dimension considerably greater than the sieve size (an intermediate diameter) of the fraction. The d^* constraint was chosen to ensure that all grains would be at least one order of magnitude smaller than the flow depth, giving a conservative assurance that no grain would individually influence the overall flow structure. The Froudenumber constraint was chosen to ensure that the flow did not become critical, at which point standing waves appear on the water surface and the relation between the mean flow properties and the bed shear stress might differ from the subcritical flow conditions used.

To some extent these criteria could not be met with certainty, because some involved the experimental results we were seeking. The best compromise between the experimental criteria (calculated or estimated) and the availability of sediments involved three sediments with a mean size in the 1.68 mm to 2.00 mm fraction. The standard deviations of these mixtures were chosen to be 0.20, 0.50, and 0.99 when the grain size is expressed in Ø units. These will be termed

the MUNI, 1/2Ø, and 1Ø sediments, respectively. In the classification of Folk (1980), these sorting values correspond to very well sorted, the boundary between well sorted and moderately well sorted, and the boundary between moderately sorted and poorly sorted. The sorting values were chosen to provide a transition between the relatively common and well understood uni-size transport case and the published fractional-transport data already available, all of which have sorting values in excess of 1 Ø. Cumulative grain-size distributions for these mixtures are shown in Figure 2.5. Percentile values for each fraction are given in Table 2.1.

To effectively isolate the effects of the relative-size parameters, the shape of the grain-size distribution was held constant. A lognormal distribution was chosen because it is a well defined distribution that approximates many natural sediments.

Two other well sorted sediments were used to provide a direct comparison of transport rates between the well sorted and poorly sorted cases for fractions in the fine and coarse portions of the mixed-size sediment. These are termined FUNI and CUNI, respectively. Although these other two sediments (Figure 2.5) were unimodal and were contained primarily within only three 1/4-Ø fractions, they did not have lognormal (in this case, merely symmetrical) distributions because of the limited quantities of sediment available for processing and the lack of sufficient sieve grades to process the sediment more precisely.

The sediment was obtained from two sources, both Pleistocene outwash deposits. The finer fractions came predominantly from a large outwash deposit in Rhode Island (distributed by Holliston Sand Co. of Holliston, Massachusetts). The coarser fractions were mined from an outwash channel in New Jersey (distributed by New England Silica of South Windsor, Connecticut). All the sediment was washed of fine material and processed to produce submixtures that could be blended in the flume to produce the desired experimental mixture. Most of the processing was done in a large rotating-barrel sieve with an automatic feed and 2.2 m^2 screen area. Towards the end of the bulk sediment

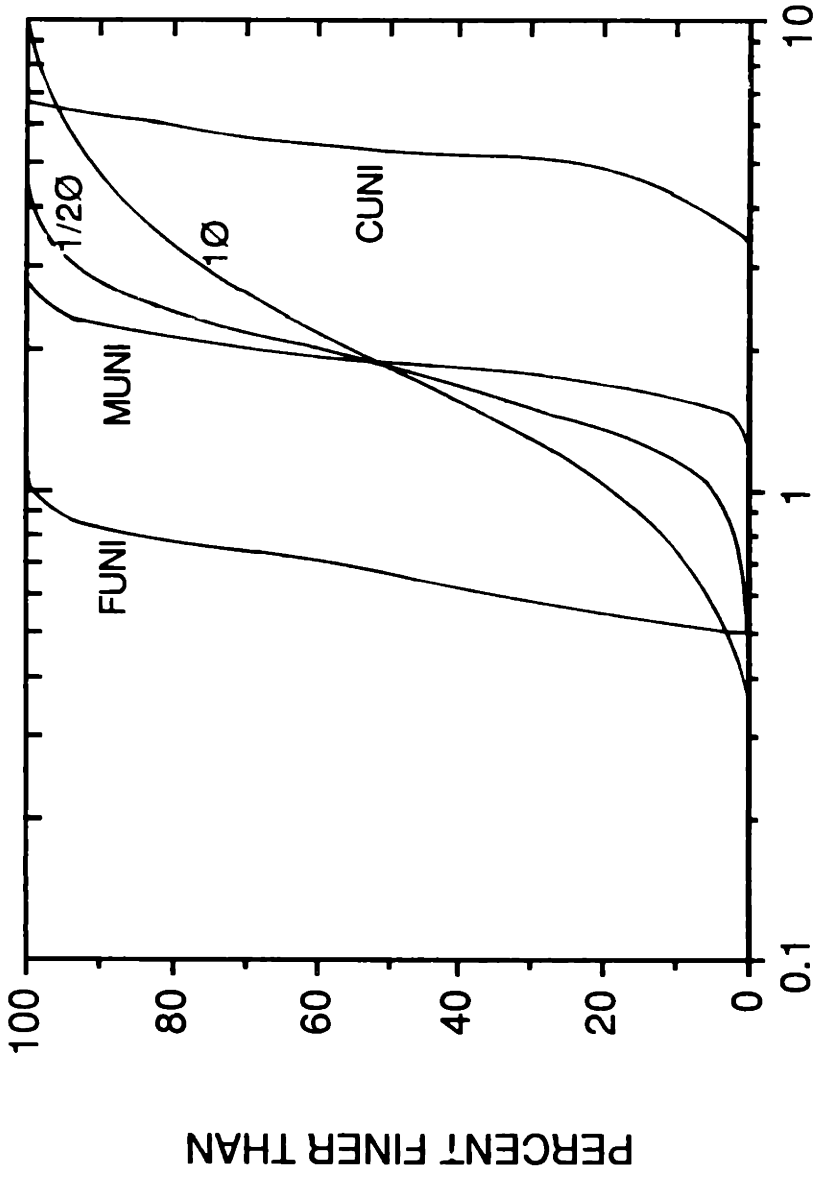

Figure 2.5. Cumulative grain-size distributions for sediment mixtures

TABLE 2.1 GRAIN-SIZE DISTRIBUTIONS OF SEDIMENT MIXTURES

SIEVE SIZE (mm)	MUNI	CUNI	FUNI	1/2 PHI	1 PHI
8.00					1.67
6.73		0.30			1.93
5.66		30.55			2.66
4.76		52.32		0.30	3.29
4.00		15.69		0.62	4.47
3.36		1.14		2.44	5.38
2.83	0.17			5.89	7.47
2.38	3.86			12.95	8.07
2.00	24.93			17.94	9.93
1.68	51.59			19.06	10.23
1.41	18.35			17.23	9.73
1.19	0.85			11.92	8.52
1.00	0.27		0.71	7.34	7.62
0.841			5.69	2.72	6.20
0.707			33.58	0.61	4.60
0.595			27.89	0.39	2.95
0.500			29.15	0.28	2.48
0.420			2.63	0.14	1.71
0.354			0.35	0.16	1.10

processing, when a sediment mixture was close to specifications, a substantial amount of processing was done using a standard laboratory sieve shaker and 20.3 cm (8") sieves.

Experimental control is more difficult to achieve for grain shape and density than for grain size. Although near-perfect control could be obtained using artificial sediments, it has been found that natural grains and spheres with the same size distribution have significantly different transport mechanics (Meland and Norrman, 1969). Hence, it seemed preferable to use natural sediment and exert as much control over grain shape and density as practicable, primarily by using the same source sediments for the same fractions in each mixture.

Control of grain shape and density was virtually exact for comparisons of the transport rates of the same fractions among the three principal sediments, and hence relative size expressed as D_i/D_m. This was achieved by using various combinations of the same sediment sources for each mixture. Comparison among different mixtures of the the same percentile fractions (i.e., the same percentile position in the mixture and hence different D_i/D_m and D_i) could not be controlled as closely, although the shape and size variations were small because the difference in fraction size for the same percentile never exceeded a factor of 2.

The shape and mineralogy of the sediments can be described in terms of the three well sorted sediments. The appropriate portions of the two mixed-size sediments were made from the same source sediments.

The mean well sorted sediment (MUNI) consisted of 97% primary quartz grains and quartzite, 2.3% siliceous chalk, and 1.6% lithic fragments composed primarily of quartz and quartz-density minerals (point count of 257 grains). 99.6% of the sediment was of quartz density. The grains were predominantly subangular and of low sphericity.

The coarse well sorted sediment (CUNI) was composed of 74.8% primary quartz grains with a small amount of chert, 22.3% siliceous chalk, and 2.9% quartz-rich rock fragments (point count of 278 grains). All grains in the point

count were of quartz density. The grains have a large range of roundness and sphericity, although the majority of the quartz grains (and hence the sediment) were subrounded to subangular with moderate sphericity. Some of the chalk grains were soft and could be abraded somewhat during flume runs. The majority, however, were quite hard and could be expected to undergo little or no modification during the relatively small amount of transport any individual grain might experience during the experiments.

The fine well sorted sediment (FUNI) was composed of 69.3% primary quartz grains, 13.9% feldspar (ρ_s = 2.57 g/cm^3), and 16.4% rock fragments. The rock fragments were composed predominantly of quartz, although roughly one quarter of them (4.4% of the entire mixture) contained some chalcopyrite (ρ_s = 4.2 g/cm^3 to 2.72 g/cm^3), which would increase the density of these grains. The grains were subrounded and of moderate sphericity.

A constant value of quartz grain density (2.65 g/cm^3) is used in the transport computations. Because virtually all of the sediment consists of quartz and near-quartz-density minerals, little error should be associated with such an assumption. The MUNI sediment and the middle portions of the sediment mixtures appear to be slightly more angular (subangular vs. subrounded) and of lower sphericity than either CUNI, FUNI, or the tails of the sediment mixtures.

EXPERIMENTAL PROCEDURE

The experimental procedure was essentially the same for all the sediment mixtures, although the size-homogenization program was not as stringent for the well sorted sediments as for the mixed-size sediment.

Each sediment mixture was loaded into the flume and mixed by hand following a precise methodology. The vertical channel-wall supports located every 60 cm along the length of the flume provided natural boundaries for mixing cells. Homogenization always involved mixing by hand within each cell, followed by an exchange of roughly one-half the sediment in each cell with that in another cell according to a predetermined pattern. The sediment in each cell was then rehomogenized by hand. The sediment bed was entirely remixed at

least once following every run involving any sediment transport. The mixing procedure was followed only once after low-transport-rate runs with the well sorted sediments because little size sorting of the sediment was produced during these runs. After higher-transport-rate runs, particularly with the mixed-size sediment, the bed was mixed twice using a different recipe for between-cell exchanges each time. When a sediment was initially loaded into the flume, the entire double-exchange mixing process was performed twice. Six bulk samples of the 1/2Ø and 1Ø sediment mixtures were taken after the initial loading and mixing. For fractions constituting at least 2.5% of the bed (which are the only ones considered later in the thesis), the coefficient of variation (standard deviation as a percent of the mean) for each fraction varied from 2% to 28% for the 1/2Ø mixture, and from 4% to 31% for the 1Ø mixture, with most of the scatter occurring in the fine and coarse fractions containing smaller amounts of sediment. The mean coefficient of variation (weighted by the amount in each fraction) was 9.3% for the 1/2Ø mixture and 12.3% for the 1Ø mixture. An accuracy of about 10% is assumed for the grain-size distribution of these sediments, as well as for the efficiency of homogenization.

Following homogenization of the sediment, a plane bed 7 cm thick was formed using a vertical template mounted on the flume cart. The screeding was done in air for all sediments except for the fine well sorted sediment, for which a plane bed with only grain-scale roughness was more easily created by screeding under water.

Following the bed preparation, the flume was filled slowly with a combination of hot and cold tap water to achieve a temperature between 24°C and 26°C, depending on the air temperature in the laboratory. The water temperature was generally held within this 2° range during runs, although during some particularly hot days the temperature would creep higher for periods of an hour or two. The temperature never varied beyond 22°C to 28°C during any run. The temperature was between 23.6°C and 26.4°C during all measurements of transport, water discharge, and water-surface slope and between 24.1°C and 25.9°C for all but two of these measurements. Temperature

control was maintained by adding small quantities of hot or cold water to the flume. A constant water volume (and hence flow depth) was maintained with an open standpipe placed in the flume tailbox.

With experience developed with the flume and each sediment mixture, it was possible to preset the flume slope for a given water discharge very close to that needed for uniform flow. When a particular run was begun, the flow depths at the upstream and downstream ends of the flume were closely monitored (with an accuracy of a few mm) to ensure uniform flow conditions from the start of each run. After the run had progressed an hour or so, a water-surface profile was taken. The flume was then turned off, a bed-surface profile taken, and the flow depth computed, so that any changes in the flume slope necessary for uniform flow could be made. Although water-surface and bed-surface profiles were sometimes measured during a run, it was found that observations of the water-surface elevation through the transparent flume sidewalls afforded an accurate check on the uniformity of the flow. In addition, observations of the thickness of the sediment bed at the transition between the upstream false bottom of the live bed and at the small retaining wall at the trap provided a second, very sensitive indicator of flow uniformity.

The goal of the experiments was to measure transport rates not only for steady, uniform flow conditions but also for conditions of equilibrium bed-load transport. It was found that the flow tended towards equilibrium (long-term steady) conditions after about four to eight hours, the period necessary for the bed forms to reach a stable configuration. At that point, the hydrodynamic roughness of the system no longer changed with any long-term trend, although it continued to vary about some stable mean with changing details of the bed configuration.

The transport rates of different fractions in the bed can also vary with time, particularly in response to any size sorting of the bed surface. It was not clear at the outset of this work whether the bed surface and transport grain-size distribution would reach a steady state over the same time period in which the bed configuration and flow achieved an equilibrium state. As a consequence,

small transport samples were taken throughout each run so that any long-term trends in the transport grain-size distribution could be detected. Because transport samples were not taken during the first few hours of the run, and because a number of samples are necessary to detect any long-term trends for a somewhat variable quantity such as the transport grain-size distribution, and because a lag of at least a few hours exists between sampling and determining the grain-size distribution of the sample, the equilibrium criterion that the transport grain-size distribution be without long-term trends always determined the length of the run. Often, though, this reflected procedural requirements rather than physical bed processes. In most instances, little change in the transport grain-size distribution was noted, suggesting that it reached equilibrium within roughly the same time period as the bed forms.

As soon as no clear trend in the transport grain-size distribution could be found, the transport sampling procedure was begun. Sampling the fractional transport rate involves both determining the total transport rate and obtaining samples for grain-size analysis. The sampling procedure involved a combination of volumetric and mass samples. Most of the transport was measured volumetrically by emptying the sample from the sampling sieve into a graduated cylinder. While a second sampling sieve was filling, the volume of the sediment in the cylinder could be determined and then returned to the slurry.system. During the sample period, all of the transport was sampled except in cases with very high transport rates, when we were not able to keep pace and could sample only 10 or 15 out of every 30 seconds of transport. The duration of the individual samples varied from 10-second subsamples to a single 4-hour sample of a very small transport rate.

Some volumetric transport samples were not returned, but saved to be dried, weighed, and sieved. When a sample was retained, it was replaced with an equal volume of additional sediment. In general, this replacement sediment was material sampled earlier in the same run or during the previous run, so its grain-size distribution would not be substantially different from the sampled sediment. At low flow strengths, however, the replacement sediment was

simply that of the original mix. In hindsight, we know that at low transport rates both the fine and coarse ends of the grain-size distribution are underrepresented in the transport load. This discrepancy is primarily present in the tails of the grain-size distribution; the bulk of the grain-size distribution is fairly closely represented by the original mix. This factor, along with the fact that the amount of sediment removed for samples during these low-transport runs is on the order of a few tens to hundreds of grams out of a bed containing roughly 1250 kg of sediment, suggests that the impact of the sample on the bed should be minute. Nonetheless, to avoid biasing the measured transport rates, transport sampling (other than the small samples taken to check for trends in the transport size distribution) was conducted only at the end of a transport run.

While the transport sampling was underway, the water-surface elevation was read and the head loss in the return pipe was determined for later conversion to water discharge. After this and the transport sampling were completed, the flume was shut down and bed-surface and still-water-surface profiles were taken.

The duration of the mixed-size runs varied between 20 and 40 hours, with the longer durations corresponding to runs at lower transport rates. One exception is the highest-transport run with the 1/2Ø mixture, which involved transport rates well in excess of what the sediment return system could pump continuously without clogging. Through intense monitoring of the return system, a run slightly longer than 6 hours was completed, which included transport sampling for nearly one hour. Because of the high transport rates in this run, the quantity of sediment transported during 6 hours was the same as, or greater than, that in the lower-transport runs, so the evolution of the bed-surface size distribution and transport size distribution is likely to be the same. Runs with the well sorted sediments were conducted over 5 to 17 hours. With these mixtures, only hydraulic equilibrium was used as the duration criterion.

SAMPLING METHODS AND DATA ANALYSIS

The mean hydraulic and transport parameters for all experimental runs are given in Tables 2.2 through 2.5. Twenty-nine runs with sediment transport were completed in 1986 and are reported here. Additional runs were carried out with each sediment at flow rates below that sufficient to transport any sediment; these runs were conducted primarily to ensure that very low values of transport rate were measured for each sediment and to develop hydraulic relations that could be used to predict initial uniform flow conditions at higher flow rates for that sediment.

FLOW DEPTH AND WATER-SURFACE SLOPE

The mean flow depth and water-surface slope for each run are given in Table 2.2. The experimental plan called for flow depths within 0.5 cm of 11.25 cm. This was achieved for all runs, with the exception of the highest-discharge MUNI runs. In those runs, the standpipe in the tailbox was not lowered to compensate for the lower elevation of the downstream end of the flume (resulting from the greater flume slope), so the mean flow depths fell outside of the planned experimental range. Because the depths were no more than 15% greater than the intended mean depth (and less than 10% outside of the planned depth range), the effect of the greater flow depth on the transport rates for these runs is likely to be small.

The locations of the point-gauge readings of the water surface and bed surface were varied with the strength of the flow. At low flow rates, the variability of the free surface was minimal, and accurate depth and slope measurements could be made using readings at 0.5 m or 0.2 m intervals (depending on the smoothness of the water surface) along two sections: 3.5 to 5.5 m and 13.5 to 15.5 m downstream of the false bottom. At higher transport rates, flow turbulence increased the short-period variability of the water surface, and bed forms produced a variation in the water-surface elevation of the same order as the height of the bed forms. The topography of the water surface and bed surface changed rapidly enough that the position of one bed

TABLE 2.2 MEASURED HYDRAULIC PARAMETERS

MIXTURE	RUN	MEAN DEPTH (cm)	DEPTH ERROR @90% (±%)	WATER SURFACE SLOPE ($\times 10^4$)	SLOPE ERROR @90% (±%)	WATER DISCHARGE ($\times 10^3$) (m^3/s)	DISCHARGE ERROR @90% (±%)	MEAN VELOCITY (cm/s)	WATER TEMPERATURE (°C)	RUN DURATION (hours)
MUNI	A2	11.4	0.3	9.6	-	30.6	1.5	44.8	25.1	7.2
	A3	11.4	0.4	12.4	2.6	35.3	1.5	51.8	25.5	5.5
	A4	11.5	0.6	14.2	13.1	39.7	1.4	57.6	24.5	16.5
	A5	11.8	1.0	21.5	6.5	43.6	1.4	61.8	25.9	13.2
	A6	12.0	1.1	24.2	12.5	48.8	1.3	67.5	24.1	5.9
	A7	12.8	1.4	29.3	14.9	55.7	1.3	72.4	25.0	7.1
1/2 Ø	B1	11.0	0.6	10.0	2.9	28.7	1.5	43.6	25.5	29.8
	B2	11.2	1.6	10.3	3.0	30.4	1.5	45.3	24.5	30.9
	B3	11.2	1.0	12.6	5.3	35.6	1.5	52.8	24.8	28.2
	B4	11.3	1.4	16.8	4.9	39.3	1.4	58.0	26.4	27.5
	B5	11.6	1.5	21.4	8.4	43.4	1.4	62.2	25.9	23.5
	B6	11.7	1.4	33.4	10.1	47.7	1.3	67.9	24.4	19.5
	B7	11.5	2.6	49.2	9.7	54.9	1.3	79.4	25.0	6.1
1 Ø	C1	11.1	0.8	10.4	4.0	28.6	1.5	43.1	25.4	39.2
	C2	10.9	0.4	11.1	1.8	30.3	1.5	46.5	24.7	38.5
	C3	11.2	2.1	18.2	3.2	35.0	1.5	52.4	24.7	34.4
	C4	11.2	1.7	21.4	5.9	39.1	1.4	58.0	24.9	31.3
	C5	11.0	2.0	28.0	9.9	43.4	1.4	65.5	23.6	27.3
	C6	10.9	2.2	33.0	11.8	47.8	1.3	72.9	25.2	20.4
CUNI	D1	11.1	0.7	25.5	3.3	39.2	1.4	59.1	24.6	4.5
	D2	11.0	0.8	31.0	2.2	43.2	1.4	65.4	25.0	5.5
	D3	10.8	0.6	38.2	2.1	47.7	1.3	73.3	24.5	8.4
	D4	11.1	0.6	49.1	1.6	54.8	1.3	82.6	24.5	7.8
FUNI	E1	10.8	0.1	2.9	10.6	17.8	1.8	27.5	25.1	8.1
	E2	10.8	0.2	3.2	11.6	19.6	1.8	30.2	25.2	8.1
	E3	10.8	0.4	3.6	4.5	21.7	1.8	33.4	24.6	6.0
	E4	11.2	1.3	5.8	4.3	25.2	1.7	37.7	24.3	11.4
	E5	11.4	2.0	14.1	7.8	27.7	1.6	40.4	25.6	9.0
	E6	11.2	2.8	17.5	6.3	30.2	1.6	44.9	24.8	7.1

form could change substantially over a period sufficiently long to permit a profile to be taken with the detail necessary (say 0.1 m intervals) to determine a reasonable mean trend. In addition, the short-period variability of the water surface was so large that a large number of readings were necessary to adequately determine the water-surface and bed-surface elevations. Because the flume has a finite length, it was simpler to increase the sample number by extending the sampling in time rather than in space. Both these considerations led to a change in sampling procedure at high transport rates, wherein the water-surface and bed-surface elevations were taken simultaneously at two locations, 9 m and 14 m downstream of the false bottom. A small wire probe was attached to the point gage to allow the bed-surface elevation to be read without disturbing the bed. Readings of both water and bed elevations at both locations were taken roughly every minute over a period from 30 to 90 minutes to provide a time series of elevations that covered the passage of several bed forms. The mean water and bed elevations were then determined for whole numbers of bed forms at each location. The mean flow depth and water-surface slope were computed from these mean values.

The point gauge used to measure water-surface and bed-surface elevations could be read to 0.05 mm. The precision of the measurements of flow depth and slope was considerably less than this, however, because the water surface was not still and because there is an inherent inaccuracy in measuring the elevation of a granular bed. The error in these terms is given in Table 2.2 as a percentage of the mean value at a 90% confidence interval determined from the variance in the sample data. At low transport rates with very low bed forms or a plane bed, the flow depth was measured with a precision of about 1% or better by computing the mean of either 10 or 22 direct measurements along the channel. The water-surface slope for these runs was measured with a precision of about 2% to 12% by fitting least-squares lines to plots of water-surface elevation versus downchannel position after the water-surface elevations had been corrected for their difference from the horizontal datum. The two-point time-series method for the higher transport rates

provided a precision of about 1% to 3% for the depth, which was computed as the mean of the direct depth measurements over whole numbers of bed forms. The difference in mean water-surface elevation over the 5 m between the two time-series points varied from 1.0 cm to 2.5 cm, and the accuracy of the resulting slope computation was about 5% to 15%.

BED PROFILES

A profile of bed-surface elevations was taken following each run. The profiles were taken in the downstream 8 m of the flume over a distance of at least 5 m. A 20 cm interval was used for the profiles and supplemented by additional readings at any point where there was a visible change in slope of the bed surface. The type of bed configuration and the mean bed-form spacing and height for each run are given in Table 2.3. The mean height of the bed forms was determined by fitting two parallel best-fit (by eye) lines through the mean crest and trough elevations. The difference between these two lines was taken to be the mean bed-form height. The bed-form spacing was determined as the mean trough-to-trough distance observed for each profile.

WATER DISCHARGE AND FLOW VELOCITY

The water discharges determined from the head-loss calibration of the return pipe are given for each run in Table 2.2. The relationship between discharge and head loss was determined using 17 calibration runs in which a volume of water was pumped from the downstream end of the flume to the upstream end. (A temporary dam was constructed halfway down the channel for this purpose.) The volume of water pumped (1.1 to 1.8 m^3 of water) and the pumping time (30 to 160 seconds) were measured to determine the flow rate. The head loss in the return pipe was also measured at these flow rates to provide a calibration curve between flow rate and head loss. The range of discharges used in the calibration runs encompassed all the discharge values used in the experiments. The maximum residual from the fitted calibration curve was 2% at the lowest discharges and 0.7% at the higher discharges. The

TABLE 2.3 BED CONFIGURATIONS

MIXTURE	RUN	BED CONFIGURATION	MEAN BED-FORM SPACING (cm)	MEAN BED-FORM HEIGHT (cm)	SPACING/ HEIGHT RATIO
MUNI	A2	Plane	-	-	-
	A3	Plane	-	-	-
	A4	2D Large Ripples	450	0.9	500
	A5	2D Large Ripples	110	1.2	92
	A6	2D Large Ripples	60	1.9	32
	A7	2D-3D Large Ripples	60	3.6	17
1/2 Ø	B1	Plane	-	-	-
	B2	Incipient 2D Large Ripples	450	0.7	640
	B3	2D Large Ripples	500	0.9	550
	B4	2D Large Ripples	115	1.0	115
	B5	2D Large Ripples	80	1.2	70
	B6	2D Large Ripples	73	1.7	43
	B7	2D-3D Large Ripples	66	2.6	25
1 Ø	C1	Plane	-	-	-
	C2	Plane	-	-	-
	C3	Incipient 2D Large Ripples	100	0.5	200
	C4	2D Large Ripples	110	1.2	92
	C5	2D Large Ripples	115	1.4	82
	C6	2D-3D Large Ripples	80	1.5	55
CUNI	D1	Plane	-	-	-
	D2	Plane	-	-	-
	D3	Plane	-	-	-
	D4	Plane	-	-	-
FUNI	E1	Plane	-	-	-
	E2	Plane	-	-	-
	E3	Plane	-	-	-
	E4	2D Large Ripples	90	1.3	69
	E5	3D Large Ripples	85	4.5	19
	E6	3D Large Ripples	52	2.1	25

error in computing the discharge during a run could result from error in this curve itself, error in reading the curve, or error in reading the manometer. Conservatively combining the maximum residuals along the discharge-head loss curve with estimates of the possible reading errors gives a range in discharge measurement error from 1.8% to 1.3% for the experimental runs. These errors are given in Table 2.2 as a percentage of the mean discharge at a 90% confidence interval. Although not a directly measured quantity, the mean flow velocity (water discharge divided by flow area) is included in Table 2.2 for convenience.

SEDIMENT TRANSPORT RATES

Transport samples were taken at the end of each run. The sample period varied from 35 to 540 minutes. If bed forms were present, an effort was made to ensure that the transport rates were measured during the passage of at least three bed forms. Transport rates were computed only for whole numbers of bed forms. At high flow strengths this presented no problem because three or more bed forms would pass into the trap in less than half an hour. For some runs of intermediate strength, however, the passage of a single long bed form could take well over an hour. At least two bed forms were sampled in all runs where they were present. An attempt to sample more bed forms in these cases by using a longer sampling period was not attempted because the sampling procedure interrupts the sediment recirculation (sampled sediment is replaced by volume, but may have a slightly different grain-size distribution) and could alter the characteristics of the bed or, in time, the nature of the sampled load. At low flow strengths a plane bed was stable for all sediments. In these cases the sampling problem became one of simply collecting enough sediment to gain an accurate estimate of the transport rate. At these flow strengths, transport samples were taken over a period of 1 to 5 hours.

The samples retained for drying and weighing were taken regularly during the passage of a single bed form and occasionally at other times. Because the transport rate tended to vary widely during the passage of a bed form, these samples allow a representative mass to be determined for a wide range of

volumetric transport measurements. The mass/volume ratio of the samples was then used to convert the complete volumetric record of the transport rates into a mass transport rate. Once the pattern of total transport was determined, samples for size analysis were chosen to represent different characteristic transport rates over the bed form. The grain-size distributions for the samples were then weighted by transport rate to provide a mean transport grain-size distribution. In general, this weighting procedure gave only minor adjustments. As found in a preliminary study (Wilcock and Southard, 1985), the transported load showed remarkably little grain-size variation during the passage of a bed form.

TOTAL TRANSPORT RATE. Data on the total transport rate are given in Table 2.4. The mean transport rate was determined for only whole numbers of bed forms. The minimum number of bed forms sampled was two (for two runs), although these represent continuous sampling for 122 and 195 minutes. Despite the accuracy with which we could sample the total load at a given time, it is difficult to estimate the accuracy of the mean transport calculations because they are strongly dependent on the number, size, and shape of bed forms sampled. The standard deviation of all the individual transport samples does not provide a reliable estimate of the error in the overall mean transport rate, because the transport rate varies systematically over a bed form and the individual transport samples are in no way independent of each other, nor are they necessarily representative of the overall mean transport rate. A highly accurate mean transport rate would require the total sampling of many bed forms (perhaps a few dozen). This type of sampling was not possible with our experimental setup because the sediment system would change from a recirculating one to essentially a feed one for a long period of time. A relative estimate of the accuracy of the transport samples may be obtained from the number of bed forms sampled (Table 2.4), which varied from 2 to 23. In lieu of a confidence interval for the transport measurements, the minimum and maximum transport rates observed are given. The sample period given in Table 2.4 represents the length of sampling actually used to compute the mean transport

TABLE 2.4 TRANSPORT RATES

MIXTURE	RUN	MEAN TRANSPORT RATE (g/ms)	MAXIMUM TRANSPORT RATE (g/ms)	MINIMUM TRANSPORT RATE (g/ms)	NUMBER OF BED FORMS SAMPLED	SAMPLE INTERVAL (seconds)	SAMPLE PERIOD (Minutes)
MUNI	A2	0.00185	-	-	-	3600	60
	A3	0.359	0.44	0.30	-	180	66
	A4	3.19	4.93	1.95	2	120	122
	A5	8.91	19.63	0.62	5	90	111
	A6	23.0	85.3	0.426	11	60	90
	A7	46.4	109.9	2.66	15	30	75
1/2 Ø	B1	0.0144	0.0162	0.0126	-	10,800	540
	B2	0.037	0.0429	0.0304	-	1,800	300
	B3	1.12	2.85	0.493	3	300	120
	B4	5.98	15.2	0.242	4	90	82
	B5	13.7	41.4	2.34	11	60	48
	B6	25.8	88.7	1.27	10	30	47
	B7	97.0	238.0	16.5	23	30	56
1 Ø	C1	0.0231	0.0238	0.0224	-	14,400	240
	C2	0.0330	0.0424	0.0195	-	1,800	495
	C3	2.32	5.63	0.595	3	180	117
	C4	10.7	26.8	0.218	4	60	35
	C5	29.7	87.2	0.45	10	30	58
	C6	59.4	145.8	11.4	17	30	58
CUNI	D1	0.00335	-	-	-	4,380	73
	D2	0.0345	0.0363	0.0323	-	3,600	180
	D3	0.555	0.686	0.489	-	1,200	60
	D4	9.55	13.1	7.5	-	120	94
FUNI	E1	0.00247	-	-	-	14,400	240
	E2	0.0245	0.0254	0.0237	-	7,200	120
	E3	0.189	0.207	0.180	-	900	60
	E4	1.75	3.12	0.60	2	600	195
	E5	4.12	26.8	1.09	3	120	130
	E6	6.31	13.4	0.349	4	120	86

rate (representing whole numbers of bed forms). The actual sampling period was longer in each case.

TRANSPORT GRAIN-SIZE DISTRIBUTION. The mean grain-size distributions of the transported load in each run are given in Tables A1 through A4 in Appendix A. The size distributions were determined using sieves at a 1/4-Ø interval on a Cenco vibrating sieve shaker. Size analyses were not conducted for the mean well sorted sediment. In general, 6 to 10 size analyses were performed for the end-of-run transport sampling. These size data were also compared with the transport samples taken during the run to ensure that there were no long-term trends in the transport grain-size distribution.

BED SHEAR STRESS

In addition to the mixture sorting, the only parameter varied in our principal experiments is the bed shear stress. Considerable effort is spent in this section in an attempt to compute the best estimate of the bed shear stress. The motivation for this work is that the transport rate is a very strong and nonlinear function of the shear stress driving the transport. This is particularly true for shear stresses near incipient motion — a range covered with all of our sediments — where an error in the shear stress on the order of 10 percent can produce order-of-magnitude scatter in the transport rate. Unfortunately, no single, reliable means of estimating the bed shear stress in the presence of considerable transport and bed forms is available. The estimate of the bed shear stress made in the following section is that which most reduces the scatter in the transport-rate data.

TOTAL BED SHEAR STRESS

The total shear stress acting on the wetted boundary of a steady, uniform, open-channel flow may be computed as the resistance the flow boundary offers to the downstream component of the weight of the water, or

$$\tau_o = \rho g R S \qquad (2.1)$$

where ρ is the water density, g the acceleration of gravity, R the flow hydraulic radius, and S the free-surface slope. The total bed shear stress can also be expressed in the dimensions of a velocity

$$u_{*o} = \sqrt{\frac{\tau_o}{\rho}} = \sqrt{gRS}$$

where u_{*o} is termed the total bed shear velocity. Values of u_{*o} are given in Table 2.5 for all our experimental runs. To determine the shear stress acting only on the sediment bed, τ_o computed in (2.1) must be corrected for the fact that the walls of the flume are hydraulically smooth and make a smaller contribution per unit area to the total resistance in (2.1) than the sediment bed. Because the roughness of the bed can vary from run to run while the roughness of the flume walls is constant, it is necessary to use a correction method that permits a variable allocation of the total shear stress in (2.1) between the bed and the sidewalls. Vanoni and Brooks (1957) modified a method developed by Johnson (1942) that divides the cross-sectional area of the flow into two fictitious parts, one for the bed and one for the walls. By assuming that the flow resistance of each section is a function of the mean channel velocity and the water-surface slope, the total shear stress can be broken up as

$$(b\tau_b + 2d\tau_w) / (b + 2d) = \tau_o \qquad (2.2)$$

where b is the flow width, d is the flow depth, and the subsrcripts b and w represent the bed and wall sections, respectively. Equation (2.2) clearly presents an interpretation of the divided-radius approximation as two separate shear stresses acting on the appropriate portions of the flow boundary. The shear stress acting on the sidewalls may be estimated using the same assumptions that led to (2.2), which permit the sidewall flow resistance to be computed using mean flow properties in a standard resistance relationship for hydraulically smooth surfaces. All quantities other than τ_b in (2.2) are then known and the bed shear stress can be computed directly. Throughout the

TABLE 2.5 BED SHEAR VELOCITY

MIXTURE	RUN	TOTAL BED SHEAR VELOCITY (cm/s)	SIDEWALL-CORRECTED TOTAL BED SHEAR VELOCITY (cm/s)	SKIN-FRICTION SHEAR VELOCITY (cm/s)	SKIN-FRICTION/TOTAL SHEAR VELOCITY RATIO
MUNI	A2	2.79	2.99	-	-
	A3	3.17	3.40	-	-
	A4	3.40	3.64	3.70	1.02
	A5	4.22	4.63	4.16	0.90
	A6	4.52	4.96	4.57	0.92
	A7	5.08	5.65	5.03	0.89
1/2 Ø	B1	2.81	3.02	-	-
	B2	2.87	3.09	2.95	0.96
	B3	3.18	3.41	3.43	1.01
	B4	3.68	3.98	3.84	0.97
	B5	4.20	4.60	4.22	0.92
	B6	5.25	5.85	4.88	0.84
	B7	6.34	7.08	6.12	0.87
1 Ø	C1	2.87	3.11	-	-
	C2	2.95	3.17	-	-
	C3	3.81	4.19	3.63	0.87
	C4	4.14	4.55	4.04	0.89
	C5	4.71	5.18	4.66	0.90
	C6	5.09	5.58	5.28	0.95
CUNI	D1	4.50	4.97	-	-
	D2	4.95	5.47	-	-
	D3	5.47	6.03	-	-
	D4	6.24	6.91	-	-
FUNI	E1	1.51	1.57	-	-
	E2	1.58	1.62	-	-
	E3	1.68	1.72	-	-
	E4	2.15	2.27	1.94	0.86
	E5	3.38	3.77	2.33	0.62
	E6	3.75	4.17	2.68	0.64

remainder of this work, these estimates of the bed shear stress are used as the total bed shear stress. The sidewall-corrected shear stresses, expressed as shear velocities u_{*b}, are given in Table 2.5. The sidewall-corrected bed shear velocities are consistently about 10% greater than the uncorrected values for all runs and sediments.

SKIN-FRICTION MODELS

It is well known that in the presence of bed forms only a portion of the total bed shear stress acts directly on the grains at the bed surface and thus drives the sediment transport. The remainder of the total bed shear stress is accounted for by the spatially variable pressure over the bed forms, which exerts a flow resistance that is termed form drag. The shear stress acting on the grains, or, more appropriately, on an area of the bed with a length scale of tens of grain diameters, is termed skin friction. This quantity is extremely difficult to measure directly in the presence of substantial transport on a bed whose topography is varying on a time scale similar to that necessary to make reasonable time-averaged measurements. Thus, skin-friction estimates must be made using models that predict the skin friction from either flow or bed-form parameters. Although considerable effort has been made in this area, no general and reliable model is available that can determine the skin friction for the range of bed configurations measured in our experiments.

Einstein (1950) developed a method for estimating the skin friction from the mean flow velocity U, the water-surface slope S, and the characteristic roughness length of the sediment bed. In a manner analogous to the sidewall correction method used above and the similar correction method developed by Einstein (1942), the hydraulic radius is divided into two portions, one for the skin friction and the other for the form drag. Einstein then postulated that the mean channel velocity may be estimated by inserting R', the portion of the hydraulic radius due to skin friction, in the vertically integrated logarithmic velocity profile:

$$\frac{U}{u_{*b}} = \frac{1}{\kappa} \ln\left(\frac{d}{2.718\, z_o}\right) \tag{2.3}$$

where κ is von Karman's constant, taken to be 0.4 here, and z_o is the roughness length characteristic of the sediment bed. If R' is used to replace both the flow depth d and the hydraulic radius term in u_{*b}, (2.3) becomes:

$$\frac{U}{\sqrt{gR'S}} = \frac{1}{\kappa} \ln\left(\frac{R'}{2.718\, z_o}\right) \tag{2.4}$$

When both S and U are known, R' may be determined iteratively from (2.4), if z_o is known. Engelund and Hansen (1972) interpret R' in (2.4) as the height of an internal boundary layer that develops on the back of each bed form, although for this to be strictly true, a velocity appropriate to the internal boundary layer, which would be smaller than U, would have to be used. Although the skin-friction method of Einstein is not rigorously derived, it has been heavily used and has provided a useful approximation for the skin friction in many studies. In one case where the skin friction was measured directly over fixed-bed ripples, Einstein's method gave estimates of the skin friction within 10% (Paola, 1983).

In contrast to estimating the skin friction directly, Smith and McLean (1977) have developed a model for spatially averaged velocity profiles over bed forms that can be used to estimate the form drag. Following the work of Arya (1975), Smith and McLean (1977) used a drag equation for the force acting on each bed form:

$$F_D = \rho\left(\frac{C_D}{2}\right) U_r^2 H = (\tau'' - \tau')\lambda \tag{2.5}$$

where C_D is the drag coefficient for the bed form, U_r is the appropriate reference velocity, H is the bed-form height, τ'' is the form drag, τ' is the skin friction, and λ is the bed-form spacing. Assuming that the velocity in the vicinity of the bed can be approximated by a logarithmic velocity profile and

that this profile connects with an upper logarithmic velocity profile that reflects the integrated total bed roughness (grain roughness plus bed-form roughness), the reference velocity in (2.5) can be estimated if the matching height z_* of the two profiles is known. Smith (1976) provides an expression for estimating z_* that is slightly different from that given in Smith and McLean (1977) but more appropriate for the smaller bed forms encountered in the laboratory:

$$z_* = 0.0931\, z_o \left(\frac{\lambda}{z_o}\right)^{.834} \tag{2.6}$$

Inserting (2.6) into (2.5) and considerable rearranging yields

$$\frac{(u_*)'}{(u_*)_t} = \left\{1 + \frac{C_D}{2\kappa^2}\left(\frac{H}{\lambda}\right)\left[\ln\left(\frac{(z_*)}{(z_o)}\right)\right]^2\right\}^{-0.5} \tag{2.7}$$

Equations (2.6) and (2.7) allow the skin friction $(u_*)'$ to be computed in terms of the total shear velocity, the bed-form height and spacing, and the roughness length appropriate to the sediment bed and state of transport.

Two major problems stand in the way of unquestioned application of the Smith and McLean model to our laboratory data. First, a value for the drag coefficient is needed, but values have been determined previously only for a few bed forms and flows, all of which are at a scale considerably greater than those in our experiments. Second, using the model implies that the spatially averaged velocity field over the bed forms may be well approximated by two connecting logarithmic velocity profiles. This is strictly true only for bed forms with a spacing-to-height ratio well in excess of 100, and becomes especially questionable when the ratio becomes smaller than 25 or 30. At lower λ/H values, the effect of the turbulent wake in the lee of the bed form — which has not been included in the model — becomes increasingly important as a larger portion of the bed form experiences flow with a wake component (Paola, 1983). Although 5 of our runs with bed forms had a λ/H value of 32 or less, the

remaining 12 runs with bed forms had λ/H values greater than 40, which is within or greater than the range of λ/H used by Smith and McLean to calibrate their model. Their model may then provide reasonable estimates of u_*' for the majority of our runs, provided that their C_D value is appropriate to our sediment and bed forms. The Smith and McLean model does provide at least an alternative estimate of $(u_*)'$ that can be used as a comparison with the more standard Einstein method.

ROUGNESS-LENGTH MODELS

Either of the skin-friction models discussed above requires an estimate of the bed roughness length, or z_o, in the logarithmic velocity profile used by both. The value of z_o is easily estimated when no bed forms are present, because only the total bed shear velocity is needed and all quantities other than z_o in (2.3) are known. Values of z_o were computed using (2.3) for our zero-transport and lower-plane-bed runs and are shown in Figure 2.6. Because these runs had grain Reynolds numbers in the transitionally rough range, the values of z_o for these runs were computed using the Colebrook approximation, which modifies (2.3) for both fully rough and transitionally rough flow (Colebrook, 1938). The computed z_o values for each mixture show higher values at flow strengths which move little or no sediment and a drop near the onset of sediment transport (marked as u_{*c} on Figure 2.6). This change in z_o presumably reflects an artificial over-roughening of the bed from the screeding performed prior to each run. Diplas and Parker (1985) also noted that a freshly screeded surface of mixed-size sediment appears to have an artificially coarser surface. The data of Figure 2.6 suggest that the over-roughening also applies to sediment close to uni-size. The smooth curves on Figure 2.6 are drawn for each sediment mixture from the mean value of z_o for the no-transport runs to the value of $D_{65}/30$, which is the roughness length originally suggested by Einstein (1950) for mixed-size sediments. Although there are insufficient data to define accurately any minimum value of z_o in Figure 2.6, D_{65} appears to be a reasonably good approximation. Because z_o is present in a log term in both skin-friction models,

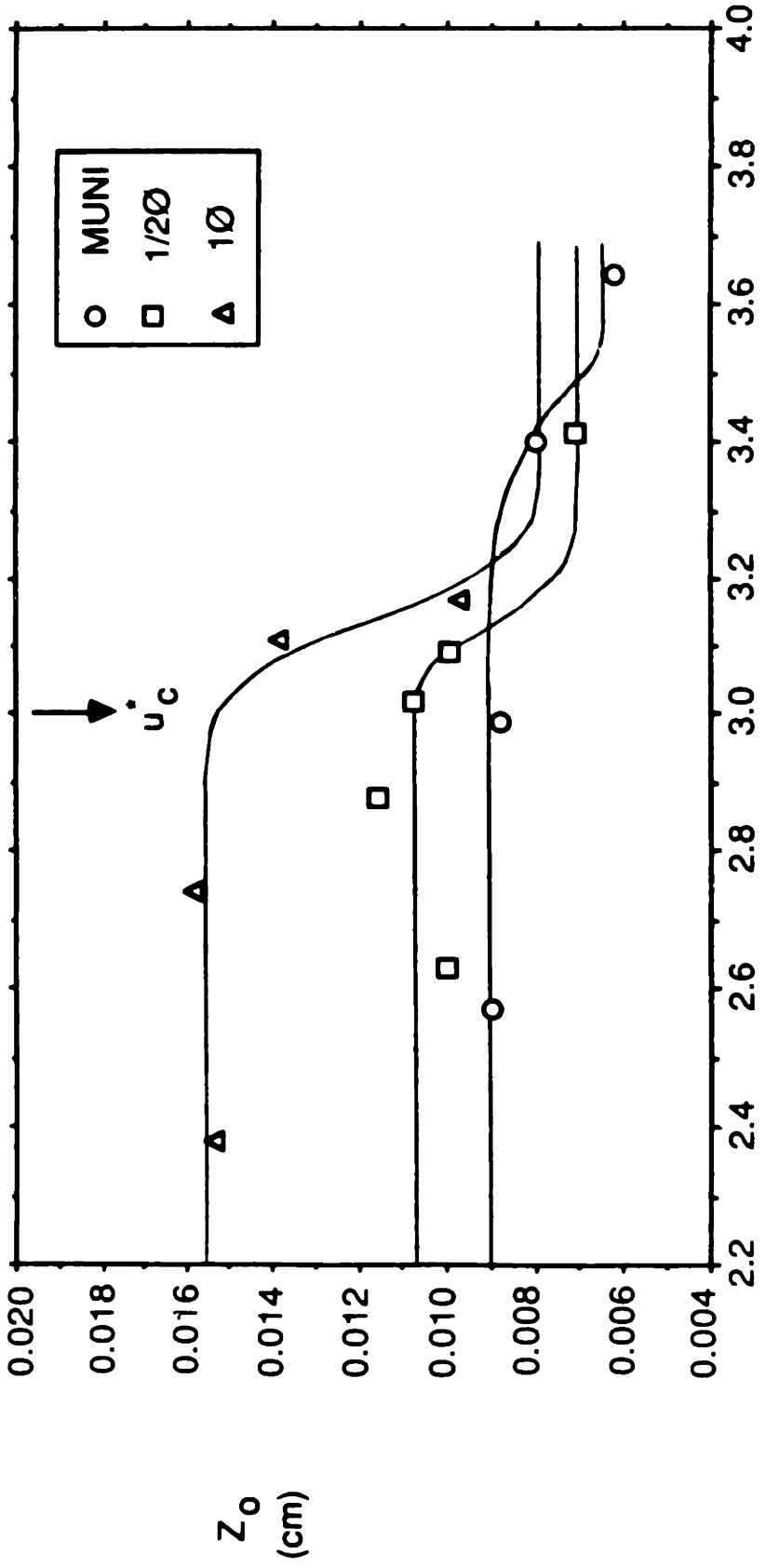

Figure 2.6. Rougness length $(z_o)_o$ as a function of bed shear velocity for zero-transport and lower-plane-bed runs. Critical shear velocity for all three sediments is 3.0 cm/s.

the estimated skin-friction values are relatively insensitive to the choice of z_o, so $D_{65}/30$ for each mixture can be used as the roughness length with sufficient accuracy for the purpose at hand.

At higher values of sediment transport rate, the apparent roughness length of the sediment bed will be the sum of the roughness length of the bed grains, $(z_o)_o$, evident when no sediment is in transport, and the apparent roughness length due to the wakes shed by the moving grains, $(z_o)_{st}$. Bed forms appear in our sediments with the onset of significant transport rates. In these cases, an independent estimate of z_o is necessary because both the skin friction and z_o are unknown and z_o can no longer be directly computed from (2.3). Einstein (1950) used $D_{65}/30$ as the roughness length regardless of the transport rate. Engelund (1966) suggested that a value of twice $D_{65}/30$ accounts for the contribution to z_o of the sediment transport and provides better correlation with lab data. Smith and McLean (1977) modified the ideas of Owen (1964) and estimated the roughness length as a proportion of the height of the layer of moving sediment. However, values of $(z_o)_{st}$ calculated using their method were more than an order of magnitude too large to give reasonable skin-friction values for our data using either skin-friction model. This discrepancy is presumably because in the analysis of their velocity-profile data, Smith and McLean were unable to separate the hydraulic roughness due to small ripples present on the backs of the bed forms from the grain and transport roughness. Hence, the fitted coefficient in their z_o model reflects the added roughness of the small ripples and is apparently not appropriate for bed forms different from the ones they studied. Because there is no independent way to calibrate their z_o model for our data, it is not used here.

Wiberg (1986, personal communication) has also developed a z_o model using a proportion of the transport-layer height as the roughness length. In this case, the hop height of a saltating grain is estimated using the saltation model of Wiberg and Smith (1985). Using velocity profile data taken by the Waterways Experiment Station (U.S.W.E.S., 1938), Wiberg (1986, personal communication) found the roughness length to be given by

$$z_o = (z_o)_o + \frac{2}{30}\delta_B \qquad (2.8)$$

The second term in (2.8) represents $(z_o)_{st}$, and δ_B is the mean hop height of saltating grains computed by

$$\delta_B = 0.68D\frac{(\tau'/\tau_c)}{1 + a(\tau'/\tau_c)} \qquad (2.9)$$

where D is a characteristic grain size, τ_c is the critical shear stress, and *a* is a coefficient that takes a value of 0.09 for a grain size of 1.85 mm and 0.16 for a grain size of 0.66 mm. Although developed for uni-size sediment, this model, like that of Smith and McLean, has the advantage that it permits the roughness length to increase as the number of moving grains and their hop height increases with increasing transport.

Wiberg's model appears to give z_o values somewhat too high, however, particularly for flows with little or no transport. At τ_c, her model predicts a $(z_o)_{st}$ of roughly D/24 for 1.85 mm sediment — a value greater than $(z_o)_o$ = D/30 -- even though there are presumably few, if any, grains moving and hence increasing the apparent roughness. It seems more appropriate to allow $(z_o)_{st}$ to go to zero at τ_c as the number of moving grains vanishes. A simple way of doing this is provided by the transport model of Engelund and Fredsøe (1976), which includes a term *p* which represents the proportion of grains of the bed surface layer in motion. This proportion is estimated by equating the excess shear stress $(\tau - \tau_c)$ with the drag force acting on all the grains in motion per unit area. Approximating the drag force as the grain weight times a friction coefficient, the proportion of grains in motion becomes

$$p = \frac{\tau - \tau_c}{\frac{\pi}{6}\tan\phi(s-1)\rho g D} \qquad (2.10)$$

where ϕ is a friction angle taken equal to 27° (Fernandez Luque and van Beek, 1976) and s is the relative density of the sediment, ρ_s/ρ. The parameter p may be combined with the Wiberg model in (2.8) to give an alternative method of estimating z_o, which we will term Reduced Wiberg:

$$z_o = (z_o)_o + \frac{2}{30} p\delta_B \qquad (2.11)$$

with δ_B determined by (2.9) and p determined by (2.10).

The Wiberg and Reduced Wiberg models are physically more realistic estimates of z_o than using the constant values of either D_{65} or twice D_{65} because they allow $(z_o)_{st}$ to vary with transport rate. They have not, however, been sufficiently tested with a wide range of data to allow their unquestioned application in a skin-friction model. Consequently, all four methods for predicting z_o were used for the skin-friction estimates, so that a clearly superior estimate of z_o, if one exists, could be selected. The four z_o estimates also provided a reasonably wide range of z_o values that could be used to evaluate the sensitivity of the skin-friction estimates to error in the z_o estimate. Figure 2.7 presents the computed values of z_o using the Wiberg and Reduced-Wiberg methods. To facilitate comparison with the fixed z_o estimates, Figure 2.7 presents the variable z_o as a ratio with $D_{65}/30$. The variable-z_o estimates presuppose the results of the next section in that they require τ' for the computation of z_o. This requires an iterative procedure wherein an initial τ' estimate is used to compute z_o, which is then used in the skin-friction model to refine the τ' estimate, which is then used to recompute z_o, etc. The z_o values in Figure 2.7 are computed using the Einstein skin-friction model; the Smith and McLean skin-friction model produces similar z_o values, which are not shown here.

It may be seen in Figure 2.7 that the Reduced Wiberg z_o values for all mixtures proceed from the minimum z_o value of $D_{65}/30$ near incipient motion to maximum values between 1.5 and 2.5 times $D_{65}/30$. The Wiberg z_o values are

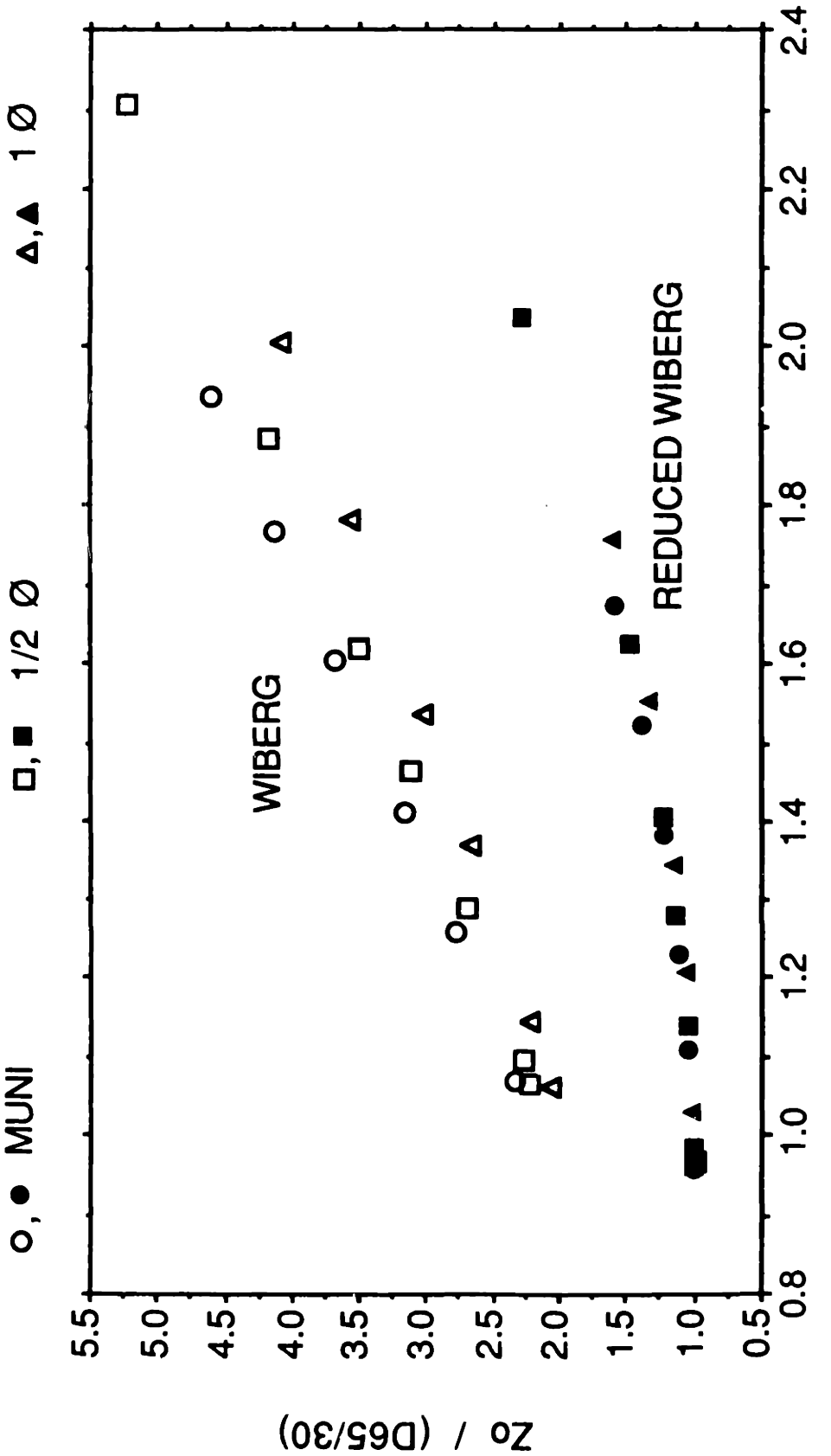

Figure 2.7. Roughness-length estimates using Einstein skin-friction model and two z_o models: Wiberg and Reduced Wiberg. Roughness length scaled by $D_{65}/30$; skin-friction shear velocity scaled by the critical shear velocity.

significantly higher than the others, starting at a value just greater than $2(D_{65}/30)$ and proceeding to a maximum three times greater than $2(D_{65}/30)$.

SKIN-FRICTION ESTIMATES

A major problem with computing estimates of skin friction with either of the models discussed above is that only very limited means exist to evaluate their accuracy or adjust the various empirical coefficients in the models. The total bed shear stress provides a general constraint that the skin friction cannot exceed. The Smith and McLean model may be integrated to obtain a mean velocity for the entire flow depth, which can then be compared with the mean channel velocity computed as the flow discharge divided by flow area. Unfortunately, the integrated velocity is only a weak function of the skin-friction shear stress, so this test was found to be insufficiently sensitive to permit the choice of either z_o or skin-friction models. The only remaining test we can make of the accuracy of the skin-friction estimate is to evaluate the reduction in scatter in the measured transport rates when plotted against the total bed shear stress and against the estimated values of skin friction. Although this is a crude approach that directly uses the physical relationship we are most interested in to evaluate the accuracy in estimating the independent variable, it only requires the assumption that the transport rate should be a monotonic, and preferably strong, function of the driving force. That this is indeed the case is well known, and the strong power relation between transport and skin friction provides a relatively sensitive test of the accuracy of the skin-friction estimates.

Because of the sensitivity of the transport rate to the skin friction, the accuracy of the skin-friction models will be discussed before the appropriate choice of the z_o values used within them. To provide a basis for comparison with the skin-friction results, Figure 2.8 presents the mean transport rate for the MUNI, 1/2Ø, and 1Ø mixtures plotted against the total bed shear velocity. It is striking that there is little data scatter in Figure 2.8, even though the three sediments have different values of mixture sorting and no correction for form

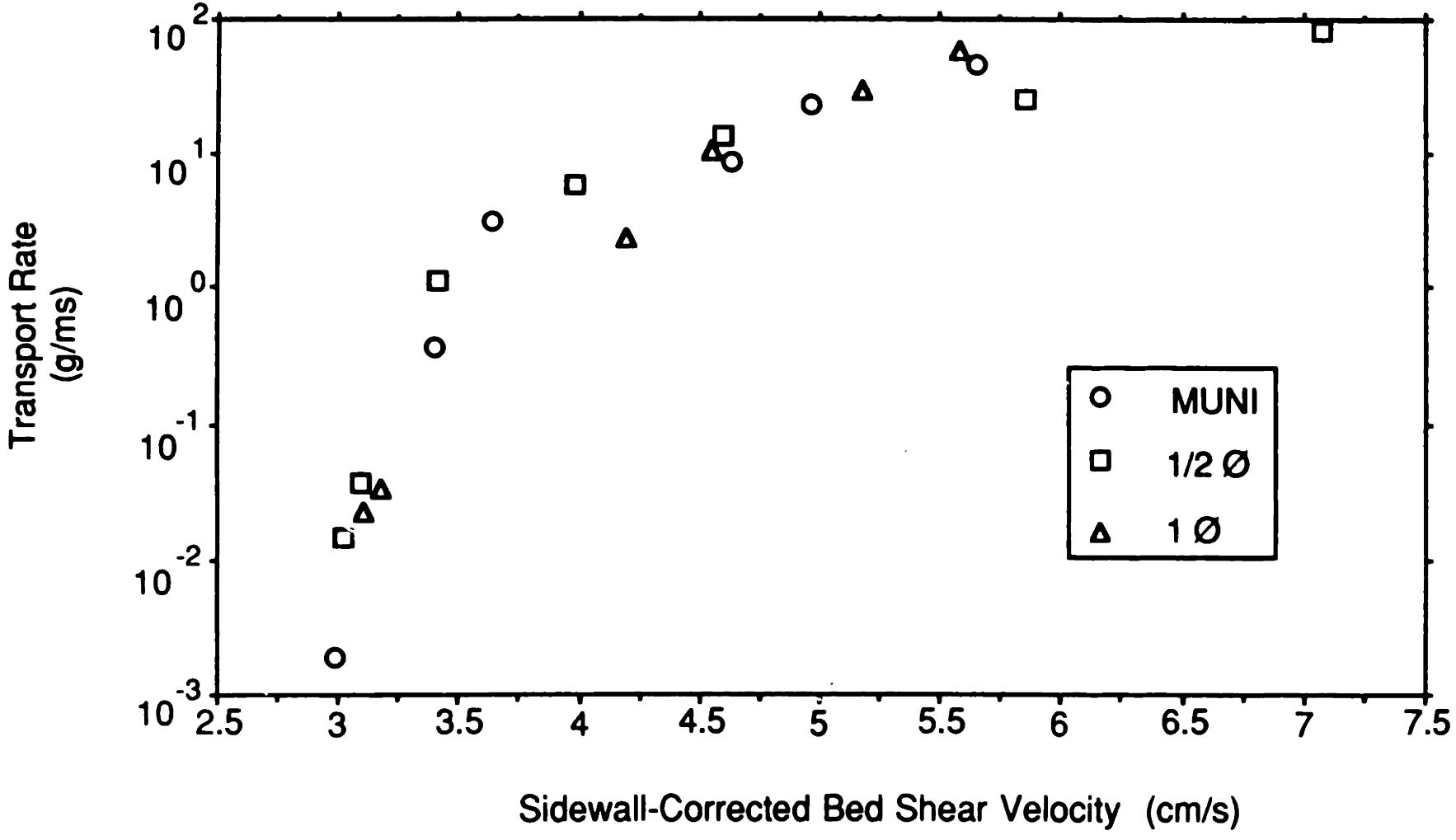

Figure 2.8. Mean transport rate vs. sidewall-corrected bed shear velocity

drag has been made. This immediately suggests the important result that mixture sorting plays little role in producing variation in the total transport rates. It also suggests that the form-drag correction may be relatively small for these sediments, bed forms, and flows.

Figure 2.9 presents the same transport rates plotted against u_{*b}, the skin-friction shear velocity, estimated using both the Einstein and the Smith and McLean methods. The skin-friction estimates in both cases used the Reduced Wiberg values of z_o. The skin friction is plotted for all runs, including those with lower-plane-bed transport. Although the lower-plane-bed skin-friction estimates are not used in the later analysis of fractional transport rates — u_{*b} is appropriate for these runs — they do provide a useful check here because the estimates of the skin-friction should be very close to the measured total bed shear stresses for these runs. The equivalent plots for the other z_o estimates are virtually indistinguishable from those in Figure 2.9 and are not shown here. In evaluating the accuracy of the skin-friction estimates, only the reduction in scatter for each individual mixture is significant, because it is not neccesary that the total transport rates of mixtures with widely varying values of mixture sorting collapse to a single curve. In this regard, the data collapse using the Einstein skin-friction estimate in Figure 2.9.a is superior to that of Smith and McLean in Figure 2.9.b. On this basis alone it appears likely that the Einstein method in some way gives a more accurate estimate of the forces driving the transport, so we will use the Einstein skin-friction estimate in the remainder of this work. The degree of data collapse among sediment mixtures using the Einstein method is also striking, there being practically no difference among mixtures in the relation between total transport and skin friction.

It is curious that the Einstein method appears to give results superior to those of Smith and McLean, even though Einstein's approach is derived only in a heuristic fashion and its assumptions are difficult to explicitly understand or evaluate compared to the more modern and carefully derived Smith and McLean method. Several factors contribute to the apparently poorer estimates produced by the Smith and McLean model. Two, mentioned earlier, concern the necessity

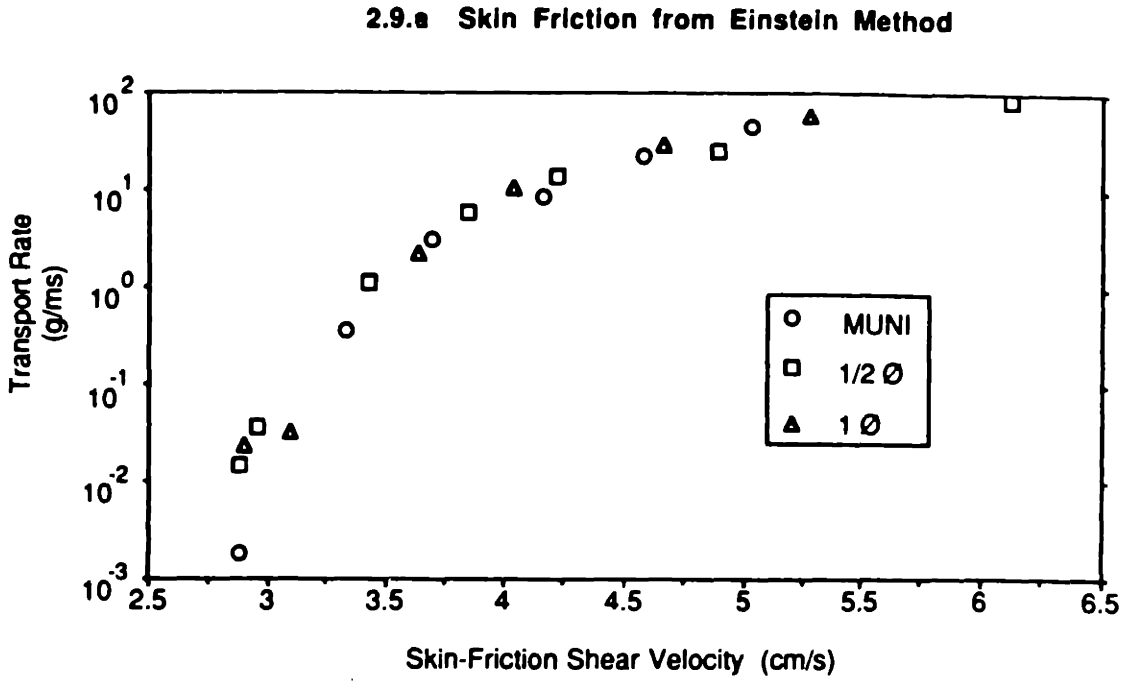

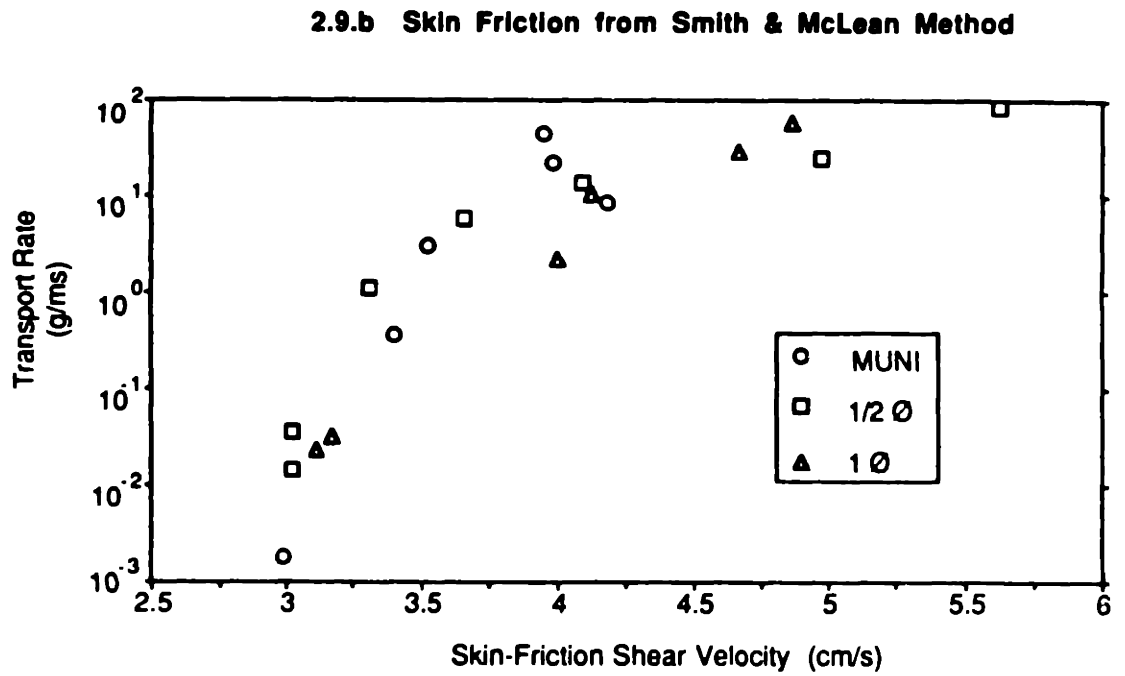

Figure 2.9. Mean transport rate vs. Einstein and Smith-McLean estimates of skin-friction bed shear velocty

of using a C_D value derived for bed forms very different from the ones we are studying, and the exclusion of the wake portion of the flow field in the model. Improvement of the model in this respect may become possible with the development of a spatially averaged flow model that incorporates the wake (McLean and Smith, 1985). An even greater problem exists with any application of the Smith and McLean method, which cannot be addressed by more appropriate empirical coefficients or more sophisticated modeling. This problem results from the uncertainty with which the mean spacing and height of the bed forms can be determined. Even for well controlled flume studies, the natural variation in bed-form size limits the accuracy with which the mean bed-form parameters can be estimated to perhaps $\pm$ 20 to 50%. In cases where the bed forms become relatively high or short, which is often when their dimensions are most variable, this inaccuracy can be directly translated into an equal error in estimating the skin friction because the ratio H/λ is present to the power of unity in the expression used to estimate τ_*'. The apparent inaccuracy of the method is particularly evident in the three MUNI runs with the highest transport rate, which also have the smallest and third smallest λ/H ratio of all the mixed-size runs. Figure 2.9.b shows that the Smith and McLean skin-friction estimate decreases from one run to the next, even though the transport rate increases twofold or more between the runs.

The choice of the appropriate z_o value to insert in the skin-friction model is both more difficult and less significant than the choice of which skin-friction model to use. Although the different z_o estimates give different skin-friction estimates, all choices of z_o gave a collapse of the transport data similar to that shown for the Reduced Wiberg method in Figure 2.9. In this circumstance, the only remaining constraint that could allow the selection of the most reasonable z_o estimate is that the computed skin friction not exceed the total bed shear stress. The skin-friction estimates produced by the Einstein formula and the four z_o estimates are given in Figure 2.10 as a proportion of the total bed shear velocity plotted against the total bed shear velocity. Figures 2.10.b and 2.10.c show that both the Wiberg and $2(D_{65}/30)$ estimates produce

Figure 2.10. Skin-friction proportion of the total bed shear velocity for all roughness-length estimates

(A) $D_{65}/30$
(B) $2(D_{65}/30)$
(C) Wiberg
(D) Reduced Wiberg

2.10.A: Zo = D65/30

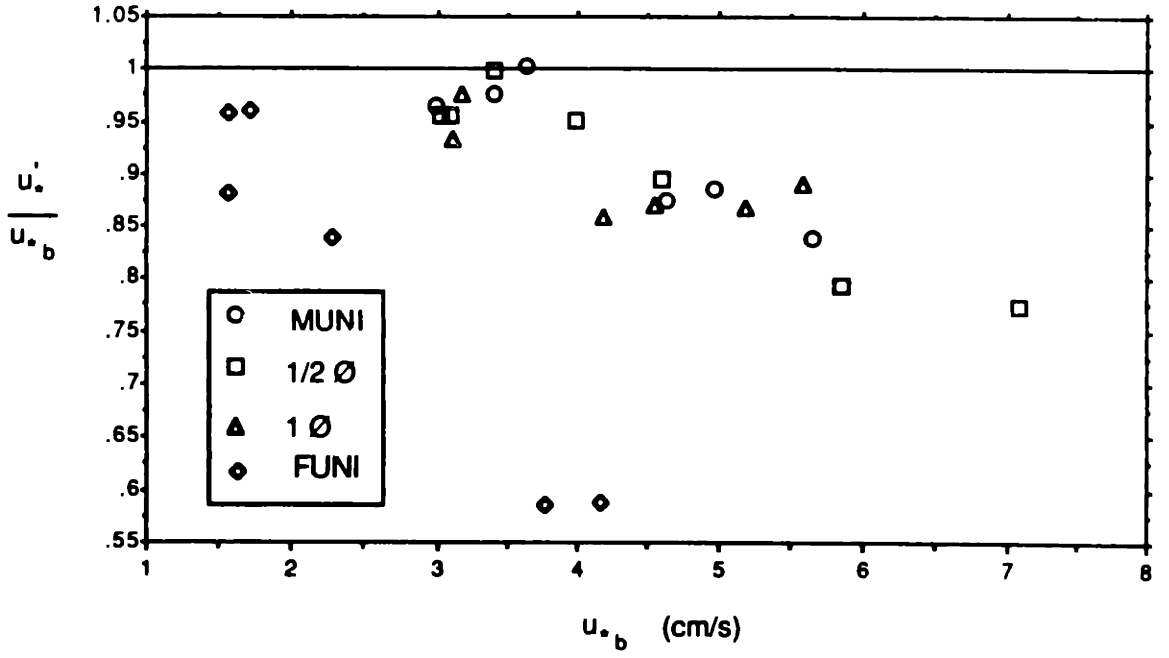

2.10.B: Zo = 2(D65/30)

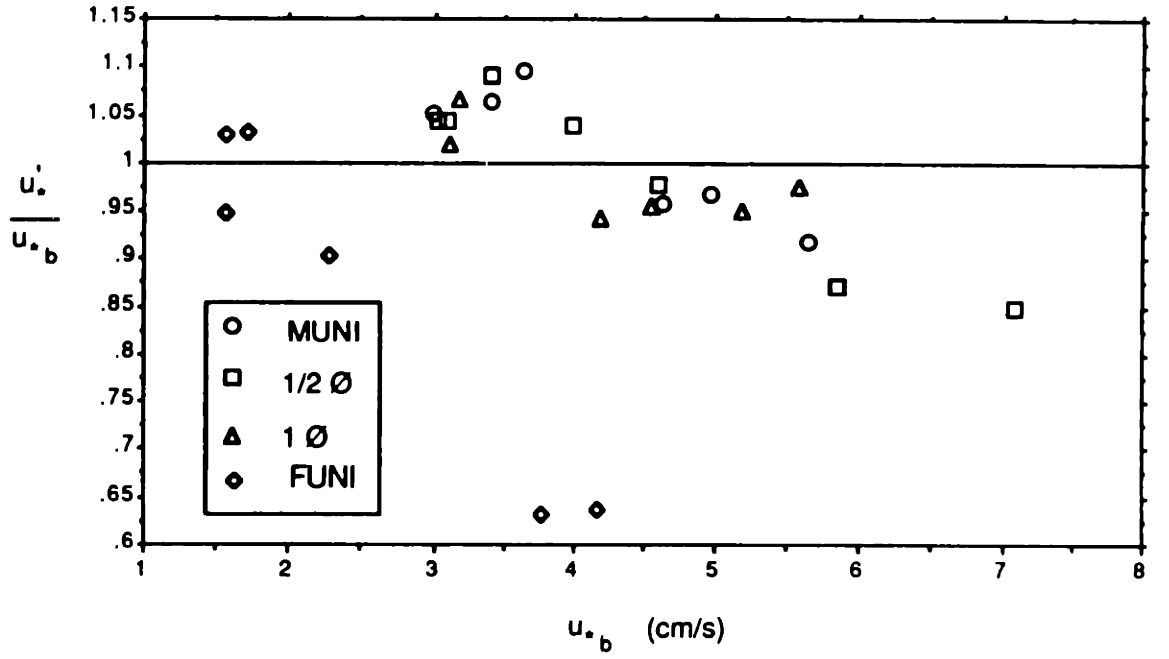

2.10.C: Zo by Wiberg Method

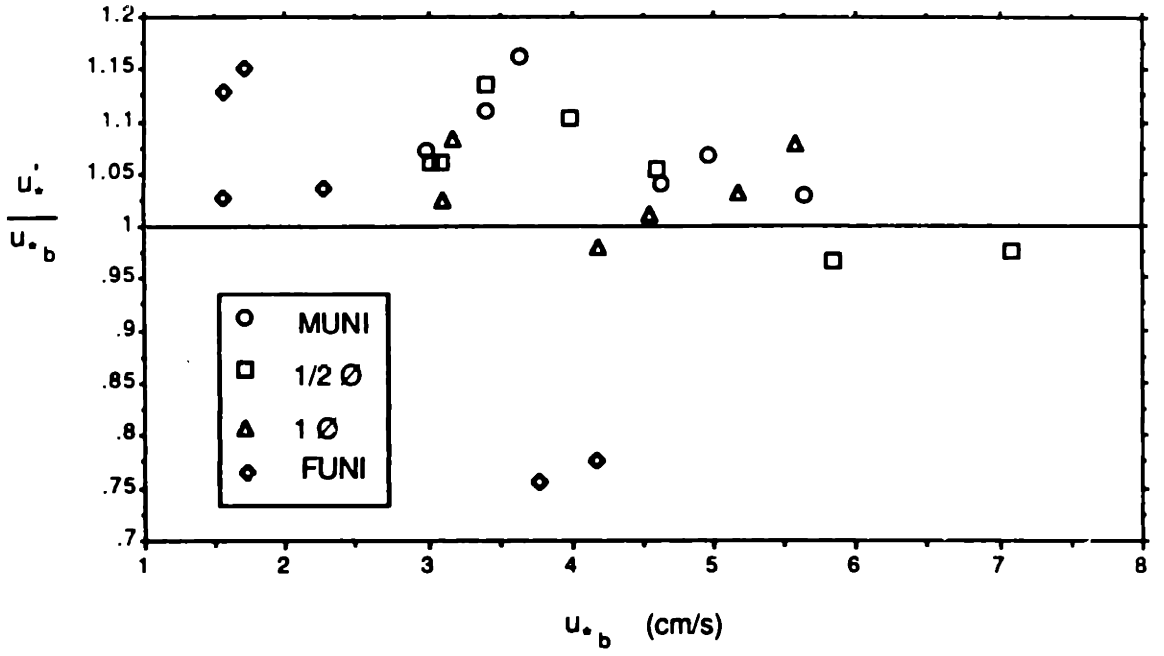

2.10.D: Zo by Reduced Wiberg Method

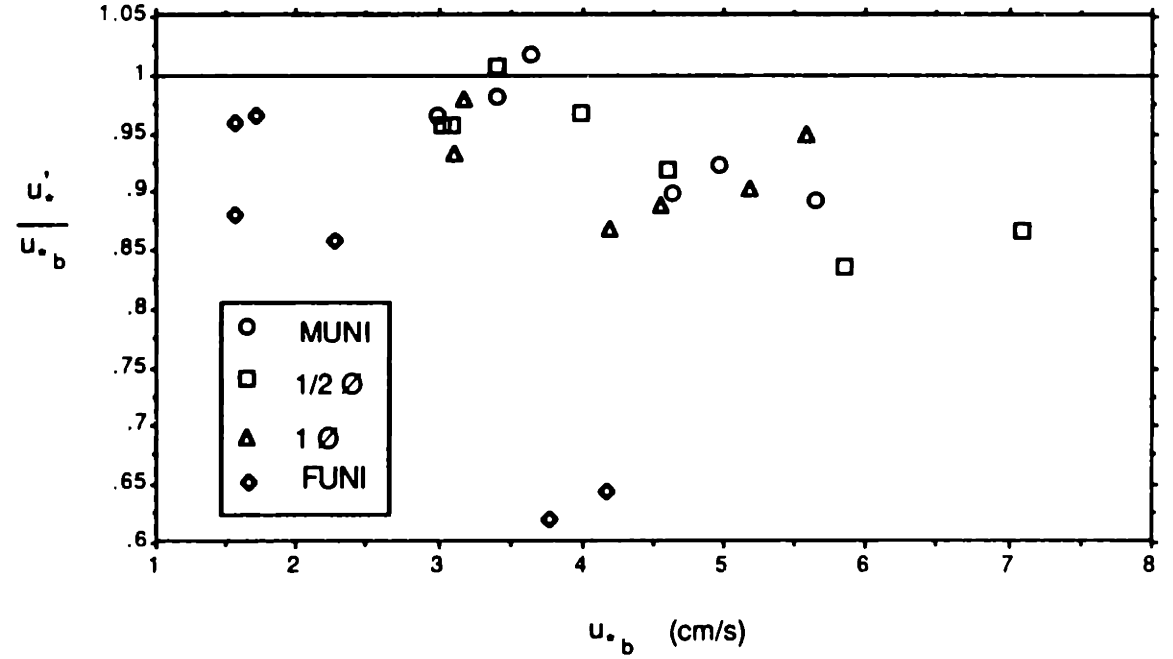

skin-friction estimates 10 to 15% too large at the lowest runs, a result that could be anticipated by the fact that these z_o values are larger than $D_{65}/30$, which gives a good approximation of the roughness for zero-transport and lower-plane-bed runs. In addition, the Wiberg z_o estimates are sufficiently large that only three of the mixed-size runs have estimated skin-friction values less than the total, so these z_o values are significantly too large for either low-transport or high-transport runs. $D_{65}/30$ gives the correct roughness length at incipient motion, but it is difficult to imagine that the roughness of the bed should remain unchanged as the transport rate increases to the relatively high levels measured in our experiments. Hence, at high transport rates the only remaining choices among the z_o estimates we have examined are $2(D_{65}/30)$ and the compromise Reduced Wiberg z_o method, which have similar values of u_*'/u_{*b} at the higher transport rates. Because $2(D_{65}/30)$ gives skin-friction values that are clearly too large at low transport rates, the Reduced Wiberg method appears to give the most reasonable z_o estimate for our sediment and flows, when used with the Einstein skin-friction method.

The skin friction used in the remainder of this work is that computed using the Einstein Formula (2.4) with the Reduced Wiberg Formula of (2.11) used to estimate z_o. These values of skin friction are given in Table 2.5 along with the ratio of skin-friction shear velocity to total, sidewall-corrected bed shear velocity.

It should be pointed out that, within the accuracy with which z_o values can be evaluated with our data, a method simpler than the Reduced Wiberg method, such as one that uses p from (2.10) to make a simple transition between $D_{65}/30$ at incipient motion to $2(D_{65}/30)$ at high transport rates,

$$z_o = (1 + p)\frac{D_{65}}{30} \qquad (2.12)$$

would work equally well.

Figure 2.11 gives the variation of the Einstein-Reduced Wiberg skin-friction estimate (expressed as a proportion of the total bed shear velocity)

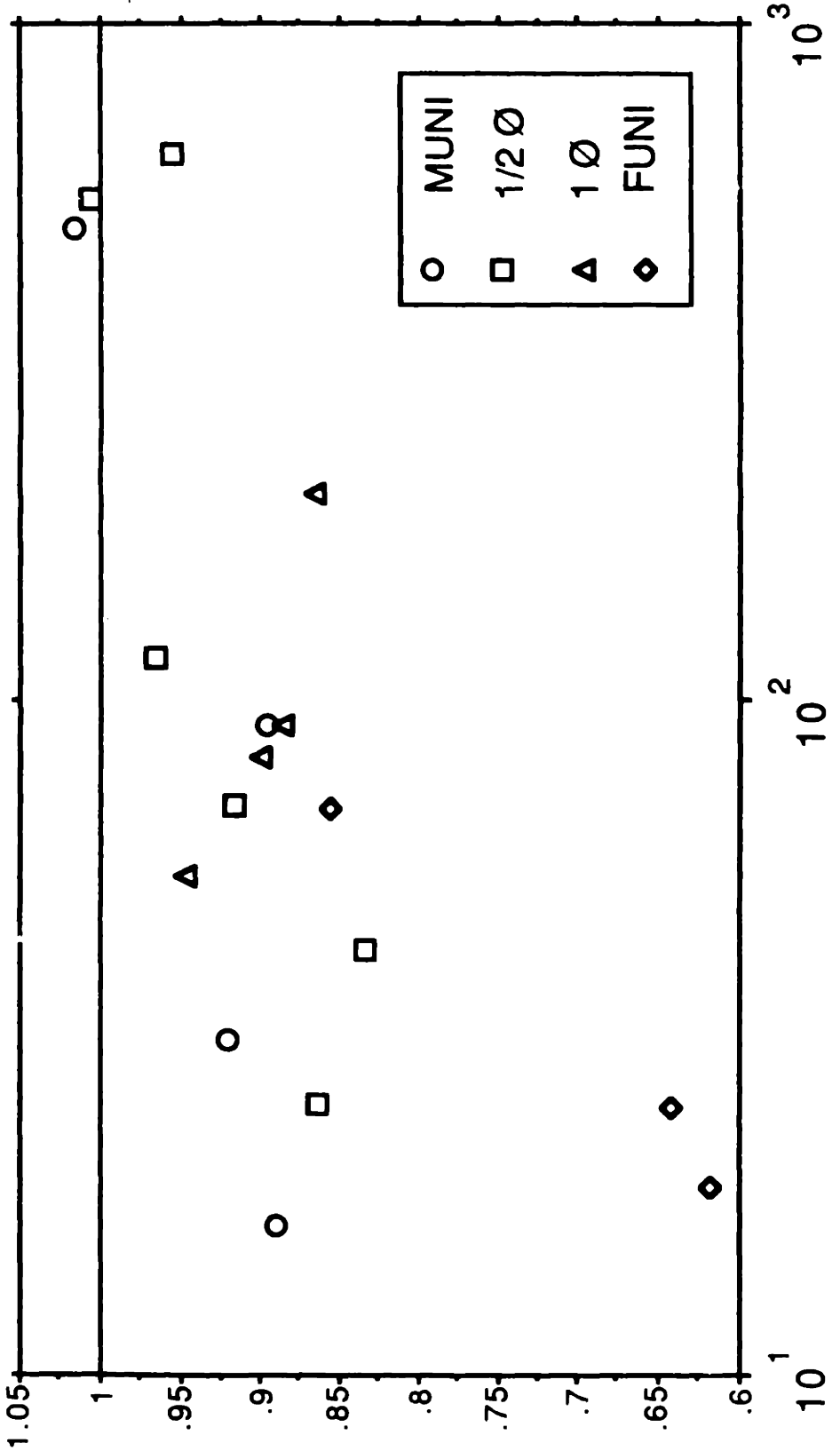

Figure 2.11. Skin-friction proportion of the total bed shear velocity vs. bed-form spacing-to-height ratio

with the bed-form height-to-spacing ratio. There are distinct trends in this figure that vary from sediment to sediment. The MUNI and FUNI mixtures both show a more or less continuous drop in the skin-friction proportion of the total shear velocity as the flow becomes stronger and the bed forms steeper. A similar pattern is evident in the 1/2Ø mixture except for one point representing the highest flow strength. The 1Ø mixture shows a consistent increase in the skin-friction proportion of the shear stress for all four runs with bed forms, even though the bed-form height and steepness increase consistently. This counterintuitive result may result from the development of subtle alternate-bar topography in these runs. Although this topography was not evident in the bed profiles taken following each run, which were taken only along the channel centerline, incipient alternate-bar topography was evident following some runs. Hence, the flow could presumably follow a distinctly smoother, slightly curved path that was not well represented by the flow-parallel bed profile.

COMPARISON WITH ENGELUND DRAG-PARTITION MODEL

It is of interest to compare the skin-friction computations from our mixed-size sediments with previous results. One of the most commonly used flow-resistance models is that developed by Engelund (1966, 1968), which presents a relationship between the dimensionless total shear stress τ^*_t and the dimensionless skin friction $\tau^{*\prime}$. The principal use of this model is to estimate the skin friction given only the total bed shear stress, a situation common in many field studies. Figure 2.12 presents our results in $\tau^*_t - \tau^{*\prime}$ space along with the relationship fitted by Engelund to the flume data of Guy et al. (1966). It may be seen that while the Engelund curve intersects our data, there is little similarity in the trends between the two. Figure 2.13 presents the same data as Figure 2.12, along with the Guy et al. data for the same portion of the Figure (labeled Fort Collins and representing the 0.93 mm Fort Collins runs). Also included are data generated by Williams (1970) for 1.35 mm sand. All data in Figure 2.13 represent dune bed configurations. It may be seen in Figure 2.13 that while the uppermost four points of Guy et al. follow the Engelund curve

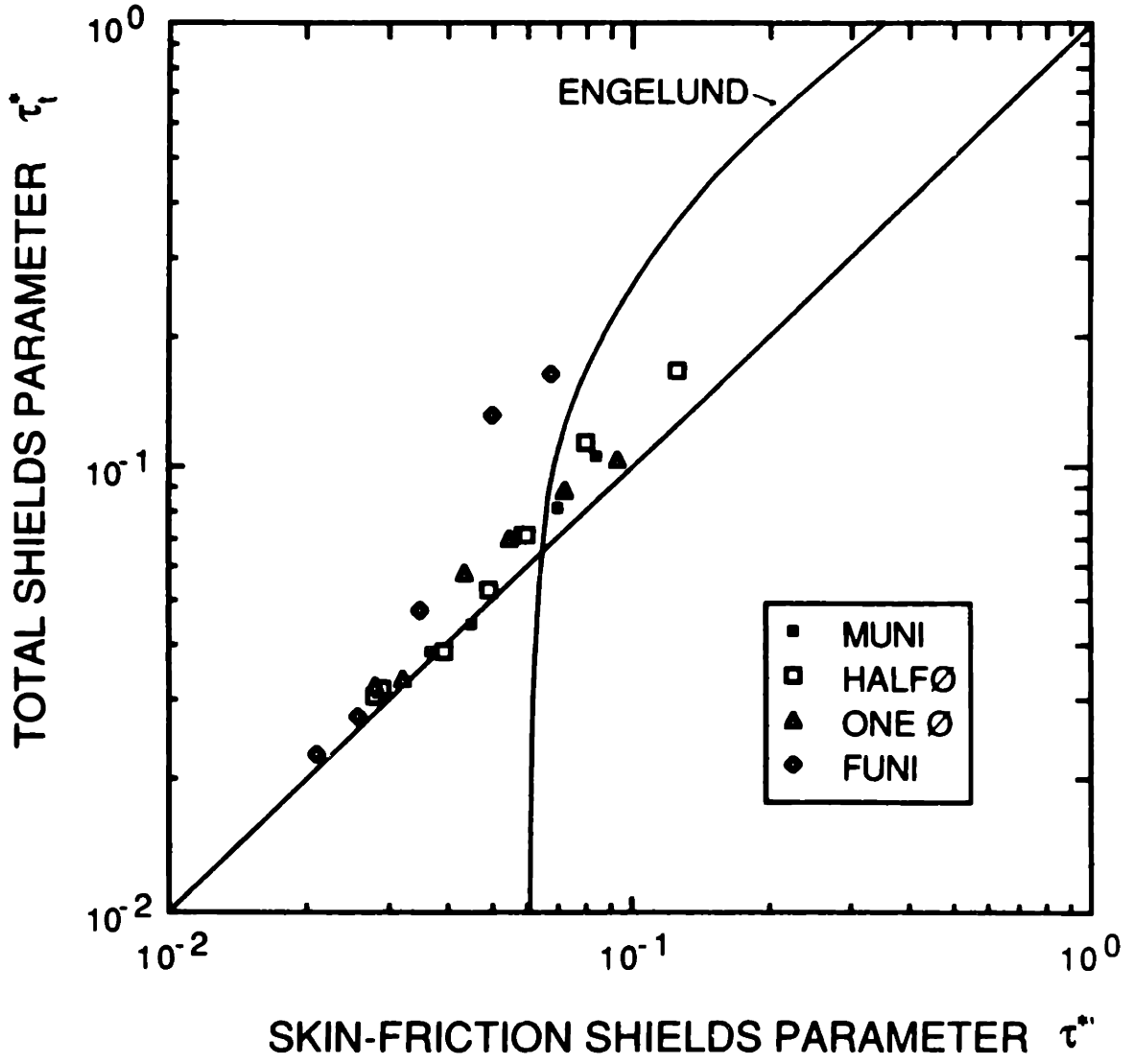

Figure 2.12. Total-shear-stress Shields Parameter vs. skin-friction Shields parameter: MIT data

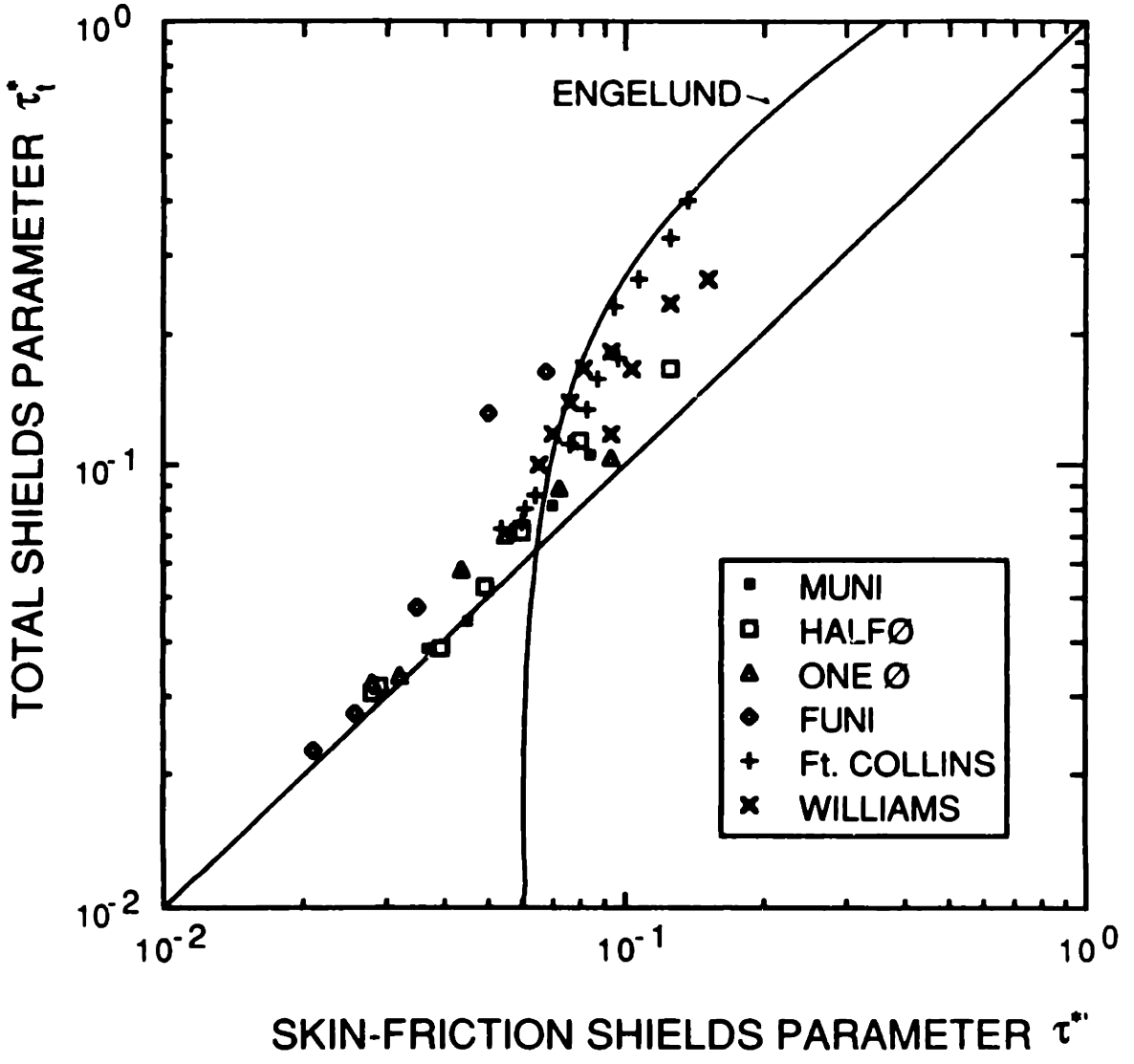

Figure 2.13. Total-shear-stress Shields Parameter vs. skin-friction Shields parameter: MIT, Guy et al., and Williams data

quite well, the lowermost eight fall within the range of, and follow the trend of, our data. The same may be said for the Williams data. The trend of these data is not surprising, however, because they all represent sediment that is sufficiently coarse that a lower-plane-bed configuration exists between incipient motion and the dune stability region (Harms et al., 1985). In lower-plane-bed conditions, the skin friction must equal the total shear stress, so the appropriate resistance curve in Figure 2.13 for such coarse-grained sediments must approach the line of slope one, as shown by the trend of the data. It should also be pointed out that substantial differences in the skin-friction estimates — such as those evident in Figures 2.10 and 2.11 — are largely masked by the two-cycle log-log plot in Figure 2.13. For example, the loss of detail masks what may be real differences in the trends of the different sediments as a function of mean grain size, mixture sorting, and the geometry of the dune bed configurations.

CHAPTER THREE

INITIAL MOTION

INTRODUCTION

In recent years much effort has been spent on the critical shear stress at which individual size fractions in mixed-size sediments begin to move. In field studies the critical shear stress has been determined from the largest grain observed in motion (Andrews, 1983; Carling, 1983; and Hammond et al., 1984). Mixed-size sediment transport rates — from which incipient motion may be estimated — have been measured in several laboratory studies (Day, 1980a, 1980b; Dhamotharan et al., 1981; Misri et al., 1984) and in the field (Milhous, 1973; Parker et al., 1982). Experiments on part of the problem — the pivoting angle of individual size fractions — have been made by Li and Komar (1986). Wiberg and Smith (1987) have used the earlier pivoting-angle results of Miller and Byrne (1966) in developing a semianalytical model of critical shear stress. All this work is motivated in part by the importance of the problem: the critical shear stress for individual size fractions is an integral component of mixed-size sediment transport models. It is also important in problems like static armoring and channel stability. The recent work has also been motivated by the realization, supported by a growing body of data, that the critical shear stress of individual fractions in mixed-size sediment is considerably different from that of uni-size sediments and from many earlier attempts to model it.

In all of the recent work, the initial-motion results for size mixtures are compared to the better understood case of uni-size sediment. Although it is natural to compare a new relation to a better known existing one, this is also a necessary first step in defining general relations for initial motion which must hold for all mixtures, including the limiting case of uni-size sediment. Attempts to define general initial-motion relations for all mixtures have not been particularly successful (e.g., White and Day, 1981) and suffer in large part from the absence of data that fall between well sorted and poorly sorted

sediments. One goal of this thesis is to bridge this gap by computing initial-motion results for our sediments whose sorting varied from well sorted to poorly sorted (0.18 Ø to 0.99 Ø). These new data and the existing initial-motion data for mixed-size sediments cover a sorting range of 1.0 Ø to 2.1 Ø, which includes most natural sediments (Table 3.1). The data now available provide fairly even coverage of a broad range of sorting values, which should permit a good definition of initial-motion relations.

In addition to comparing initial-motion relations for uni-size and poorly sorted sediments, it is of interest to test whether the mixture sorting itself has a direct and consistent influence on initial-motion values for individual size fractions. The motivation for such a test is the fact that the relative size of a fraction — which along with its absolute size largely controls its initial motion — is completely described for a given reasonably smooth distribution by three variables: the size ratio of the fraction (e.g. D_i/D_m), the percentile position of the fraction (e.g. percent finer than) and the mixture standard deviation. To date, only one of the relative-size parameters (D_i/D_m or percent finer than) has been used to model the initial motion of a size fraction. To test whether more than one of these parameters is needed to explain the variation in initial motion, three of the sediment mixtures in our experiments were made with the same mean size (1.85 mm) and grain-size distribution shape (lognormal) but with sorting equal to 0.20, 0.50, and 0.99 Ø. By also holding the flow depth and water temperature within a narrow range, we can isolate the effect of one size-distribution variable (e.g. mixture sorting or the percentile position of a fraction in the mixture) on the initial motion of an individual fraction (specified by a particular value of D_i/D_m).

A second important topic of this paper concerns the methodological problems that have always haunted the study of incipient motion of sediments. In the case of sediments that are nearly uniform in size it has long been realized that different methods for determining the critical shear stress, and even different variations of the same method, can produce different results (e.g. Neill, 1968; Miller et al., 1977). The same problems have been carried over to

TABLE 3.1. SIZE-DISTRIBUTION PARAMETERS FOR BED SEDIMENTS

SEDIMENT	REFERENCE	D_m (mm)	D_{15} (mm)	D_{50} (mm)	D_{85} (mm)	σ_ϕ [1]	σ_g [2]
MIT MUNI		1.87	1.63	1.86	2.20	0.20	1.15
MIT 1/2Ø		1.82	1.25	1.83	2.59	0.50	1.41
MIT 1Ø		1.85	0.893	1.83	3.88	0.99	1.99
MIT FUNI		0.662	0.538	0.670	0.807	0.26	1.20
MIT CUNI		5.31	4.68	5.28	6.17	0.18	1.13
DAY A		1.50	0.336	1.82	6.05	1.77	3.41
DAY B		1.17	0.318	1.57	3.49	1.45	2.73
MISRI N1	Misri et al. (1984)	2.37	1.15	2.36	4.91	1.00	2.00
MISRI N2	Misri et al. (1984)	3.78	1.21	3.81	11.9	1.44	2.71
MISRI N3	Misri et al. (1984)	4.09	1.70	4.00	10.1	1.18	2.27
SAF	Dhamotharan et al. (1980)	2.10	0.828	2.16	6.04	1.29	2.45
OAK CREEK	Milhous (1973)	13.1	2.37	19.5	56.6	2.10	4.29

[1] σ_ϕ is the standard deviation of the size distribution when expressed in ϕ units

[2] $\sigma_g = 2^{(\sigma_\phi)}$ σ_g is the geometric standard deviation of the size distribution in mm

the case of mixed-size sediment and are combined with additional problems unique to mixed-size sediment. Although the recent work is in general agreement that relatively smaller sizes show greater resistance to movement and relatively larger sizes show less resistance to movement in a mixture than in a uni-size sediment bed, there is considerable discrepancy in the published results. These discrepancies are not random, however, but fall into two groups that may be associated with two broad classes of methods for determining initial motion. Initial-motion results determined by one of these classes of methods — wherein the critical shear stress for individual fractions τ_{ci} is associated with the largest grain moved by that bed shear stress — show a variation of τ_{ci} with roughly the square root of D_i/D_{50} (see Komar, 1987, for review). On the other hand, when τ_{ci} is determined as the bed shear stress that produces a low, constant value of transport rate, τ_{ci} is found to have little, if any, dependence on D_i/D_{50} (Parker et al., 1982; analysis later in this paper). Unfortunately, most of the data appropriate to one type of initial-motion analysis are not appropriate to the other, with one important exception discussed in this chapter. This leaves open the question of whether differences in initial-motion results between different sediments and flow conditions are real or merely reflect the different methods used to determine the initial motion. An important goal of this chapter is to demonstrate how the different methods can give very different initial-motion results and to advocate that a consistent initial-motion criterion be adopted (or, at a minimum, that the differences between the various methods be clearly understood), so that future work may focus on the physics of the problem rather than the methodology. Where possible, this paper will combine the best available data into the same analyses, so that the existence of general initial-motion relations for mixed-size sediments can be discussed.

INITIAL-MOTION METHODOLOGY

DEFINING INITIAL MOTION FOR MIXED-SIZE SEDIMENTS

The different methods used to measure initial motion of individual fractions are appropriately applied to very different kinds of data. Can the critical shear stress determined from direct observation of the bed be compared with that determined from the largest grain in a transport deposit, or with the shear stress that produces a small value of transport rate? Is there an appropriate means for comparing the initial-motion values for grains of a different size in the same mixture? Which method, if any, can be compared with critical shear stresses estimated from theoretical models? The following section presents a rational definition of initial motion in mixed-size sediment that can serve as a basis for comparison, and can also serve to guide future attempts to collect or interpret data.

It has been long been recognized that a basic problem encountered when determining the critical shear stress is that it can be estimated only with data from flows with some grain motion, for which the bed shear stress already exceeds critical. A second and more fundamental problem is that the bed shear stress is a fluctuating quantity, and one cannot precisely define a value below which there is no motion. Both problems lead naturally to a definition of τ_c in terms of a small but finite number of grains in motion. But if the bed shear stress is varying in space and time, and the force necessary to initiate motion varies from grain to grain, the area of the bed observed and/or the time period during which the bed is observed must be adjusted so that grains of different size have an equal opportunity to move. This adjustment is essential if the critical shear stress determined for different sediments, or for different fractions in a sediment mixture, are to be comparable, and it is also necessary if empirical data on critical shear stress are to be combined into a general model or compared to theoretical models.

Neill and Yalin (1969) defined a set of scaling relations for uni-size sediment using the argument that the area of the bed observed and the period of

observation must be scaled by the sediment grain size. They argued that geometrically similar bed areas for two different grain sizes D_1 and D_2 are related as

$$\frac{A_1}{D_1^2} = \frac{A_2}{D_2^2}$$

and kinematically similar sample periods are related as

$$\frac{t_1 u_{*1}}{D_1} = \frac{t_2 u_{*2}}{D_2}$$

where u_* is the bed shear velocity $u_* = [\tau_0/\rho]^{1/2}$. Defining n as the number of grains observed moving per unit bed area and unit time, the requirement that the same number of grains be observed in motion is

$$n_1 A_1 t_1 = n_2 A_2 t_2$$

Inserting the similarity ratios into this requirement produces the initial-motion criterion

$$\frac{nD^3}{u_*} = \text{constant} \qquad (1)$$

Neill and Yalin (1969) suggest a value of 10^{-6} for the constant in (1), because it is close to the lower limit that can be practically observed in open-channel flow. Equation 1 is not the only initial-motion criterion possible. Yalin (1977) introduced another criterion

$$\frac{nD^3}{\sqrt{(s-1)gD}} = \text{constant} \qquad (2)$$

Although derived only in part using similarity arguments, Equation 2 can be presented in terms of the scaling arguments that led to Equation 1. In this case, if the similarity ratio for the bed area is the same, kinematic similarity of sample periods would be defined as

$$t_1 \left(\frac{g}{D_1}\right)^{1/2} = t_2 \left(\frac{g}{D_2}\right)^{1/2}$$

Still other similarity ratios could be used, and these would produce other initial-motion criteria. Alternative ratios are more reasonably defined for the sample period than for the sample area, for which an intuitive argument can be made that the size of the bed area observed must be increased for the larger grains in the mixture. The two sample-period similarity ratios presented above are the simplest possible using a dimensional analysis of the relevant physical parameters.

The initial-motion criteria of Equations 1 or 2 are defined for uni-size sediments, but may be extended to mixed-size sediments. The exact initial-motion criterion, or the specific value of the constant used in that criterion, is not as relevant to this discussion as the scaling implications of Equations 1 or 2 for individual fractions in mixed-size sediment. Equation 2 may be used as an example. For constant values of s and g, the initial-motion criterion varies only with D and n. To achieve a constant value of this criterion for each fraction in the mixture, the value of n that must be observed for each fraction is

$$n = \text{constant}\,(D)^{-2.5}$$

If, for example, one is directly observing grain motion over a fixed area of the bed for a fixed length of time, Equation 2 states that the number of grains observed moving must vary with the -2.5 power of grain size. If the mixture has the relatively modest range of sizes such that the coarsest fraction is 16 times the size of the finest, Equation 2 requires that 1024 of the fine grains

must be observed moving for every one of the coarsest grains, if the bed area and observation time are the same for each fraction. This scaling can present a difficult practical problem, although tractable compared with the second part of the scaling problem for initial motion of mixed-size sediments: for representative sampling of different sizes in a mixed-size sediment, the observation area or sample size must also be scaled with the proportion f_{ai} of each particular fraction present on the bed surface. Geometrically similar bed areas for individual fractions in mixed-size sediments must be defined as

$$f_{a1}\frac{A_1}{D_1^2} = f_{a2}\frac{A_2}{D_2^2}$$

Inserting this similarity ratio into the Yalin requirement (Equation 2) yields

$$\frac{nD_i^3}{f_{ai}\sqrt{(s-1)gD_i}} = \text{constant} \qquad (3)$$

If the bed surface grain-size distribution is described in terms of the proportion of each fraction by weight, a conversion to an areal proportion must be made:

$$\frac{f_{a1}}{f_{a2}} = \frac{f_{m1}}{f_{m2}}\left(\frac{D_2}{D_1}\right)$$

and Equation 3 becomes

$$\frac{nD_i^4}{f_{mi}\sqrt{(s-1)gD_i}} = \text{constant} \qquad (4)$$

The practical problems associated with satisfying the initial-motion criterion of Equations 3 or 4 are extreme. If the two fractions with a 16-fold difference in grain size contain an equal percentage of the mixture by weight, and a constant observation area and period are used, Equation 4 requires that

16,384 of the fine grains be observed moving for each of the coarse grains. Or, for a constant observation period and the same number of grains observed in motion (say, one grain in each fraction), the observation area for the coarse grains would have to be 16,384 times the size of the area for the fine grains to produce a constant value of the initial-motion criterion in Equation 4.

In addition to the sample scaling problems embodied in Equation 3 or 4, it must be recognized that the proportion f_{ai} is both a scaling parameter and a dependent variable of the problem. Because the proportion of a given fraction on the bed can change during the sampling period, or from one sample period to the next, it is difficult to imagine how a truly representative initial-motion sample could be obtained.

INITIAL-MOTION TECHNIQUES

The scaling problems associated with Equations 3 or 4 are sufficiently extreme that no direct observation of initial motion of mixed-size sediment has been made that can be scaled properly. Indeed, just the direct observation of mixed-size sediment transport is itself a difficult task and has only been attempted in a few cases (Drake and Shreve, 1985; Hammond et al., 1984). Other measurements of the the initial motion of individual fractions in mixed-size sediment have used approximations of the initial-motion criteria given above. These can be broadly divided into two categories. The first involves determining the largest clast in a sediment mixture that is moved by a given bed shear stress. This quantity may be measured directly using the largest clast found in a transport sample (Andrews, 1983; Carling, 1983) or measured visually by observing the largest grain moving over an area of the bed (Hammond et al., 1984). The largest mobile grain is assumed to represent initial-motion conditions if coarser grains are available in the bed. The second general initial-motion method involves measuring the transport rates of individual fractions in the mixture and determining from a fitted relation between shear stress and transport rate a reference shear stress that produces a very small, constant transport rate (Parker et al., 1982; Day, 1980b). The two general classes of

initial-motion methods will be termed here the largest-grain method and the reference-transport method.

Because the two initial-motion methods involve measurements of entirely different quantities, it is not clear *a priori* that results obtained from the different methods can be directly compared. Because initial-motion data from both methods are commonly combined without distinction, and because it is not clear which, if either, of the methods should be used to calibrate semianalytical initial-motion models, it is worth pursuing a direct comparison of the two methods. We will make a comparison in a general, abstract fashion, as well as in terms of the only data set that allows computation of τ_{ci} from both methods. The implications of the scaling problems embodied in Equations 3 or 4 will be also examined in the context of both initial-motion methods.

In principle the two initial-motion methods should give identical results in all but one special case. The ideal conditions for identical results include a sediment bed with a smooth, continuous grain-size distribution and a very large number of samples from a broad range of flows with a very small increment in bed shear stress from one to the next. Assuming that scaling requirements have been met, complete comparability between the two methods requires several conditions: (1) the flows must not exceed the shear stress necessary to move the coarsest grain in the bed; (2) the samples must be of sufficient duration to ensure that all sizes have a representative chance of moving; (3) initial-motion conditions for individual fractions in a mixture must increase continuously with grain size; and (4) the reference transport rate must be chosen so that the reference shear stress is close to that at the true initial motion of the various grain sizes in the bed.

In practice the two methods appear to give very different results. The problems associated with the two methods are entirely different. The largest-grain method suffers primarily from sampling problems associated with measurements made when the bed shear stress is greater than that necessary to move any fraction in the mixture and with the scaling problems implicit in determining the critical shear stress for different sizes in a mixture. In

contrast, the reference shear stress can be measured much more accurately, and the necessary grain-size scaling may be incorporated in the reference-transport criterion. However, the relation of the existing reference-shear-stress criteria to the true critical shear stress is unclear. As will be discussed below, it is functionally possible to equate the reference shear stress with an initial-motion criterion like Equations 3 or 4, although the actual function that would perform such a transformation is currently not available. The problems associated with the two initial-motion methods are considered in order.

LARGEST-GRAIN METHOD. The most common departure of the largest-grain method from the ideal involves sampling problems that arise when samples are taken in flows that exceed the shear stress necessary to move the coarsest grain in the bed, or when there are so few of the coarsest grains available that the sampling period or bed area sampled is insufficient to give the coarse grains a representative opportunity to be sampled. The effect of these sampling and scaling problems is illustrated schematically in Figures 3.1 and 3.2 in terms of a set of 'true' initial-motion relations and the related largest-grain results. The comparison is made in terms of a variety of relations between the critical shear stress τ_{ci} and D_i/D_{50} that are chosen to include the natural range of relations between these two variables. These range from $\tau_{ci} \propto D$ (no relative-size effect on the initial motion of individual grains) to $\tau_{ci} \propto$ constant (relative-size effects exactly balance the difference in mass between different fractions — the equal mobility hypothesis of Parker et al. (1982).

Figure 3.1 expresses the initial-motion relations in terms of

$$\frac{\tau_{ci}}{\tau_{c50}} = \left[\frac{D_i}{D_{50}}\right]^a \qquad (5)$$

The subscript *c* in Equation 5 represents the critical shear stress for the fraction i. The subscript *lg* in Figure 3.1 represents the largest-grain estimate of τ_{ci}. The 'true' initial-motion relations, shown in Figure 3.1.a, are simple

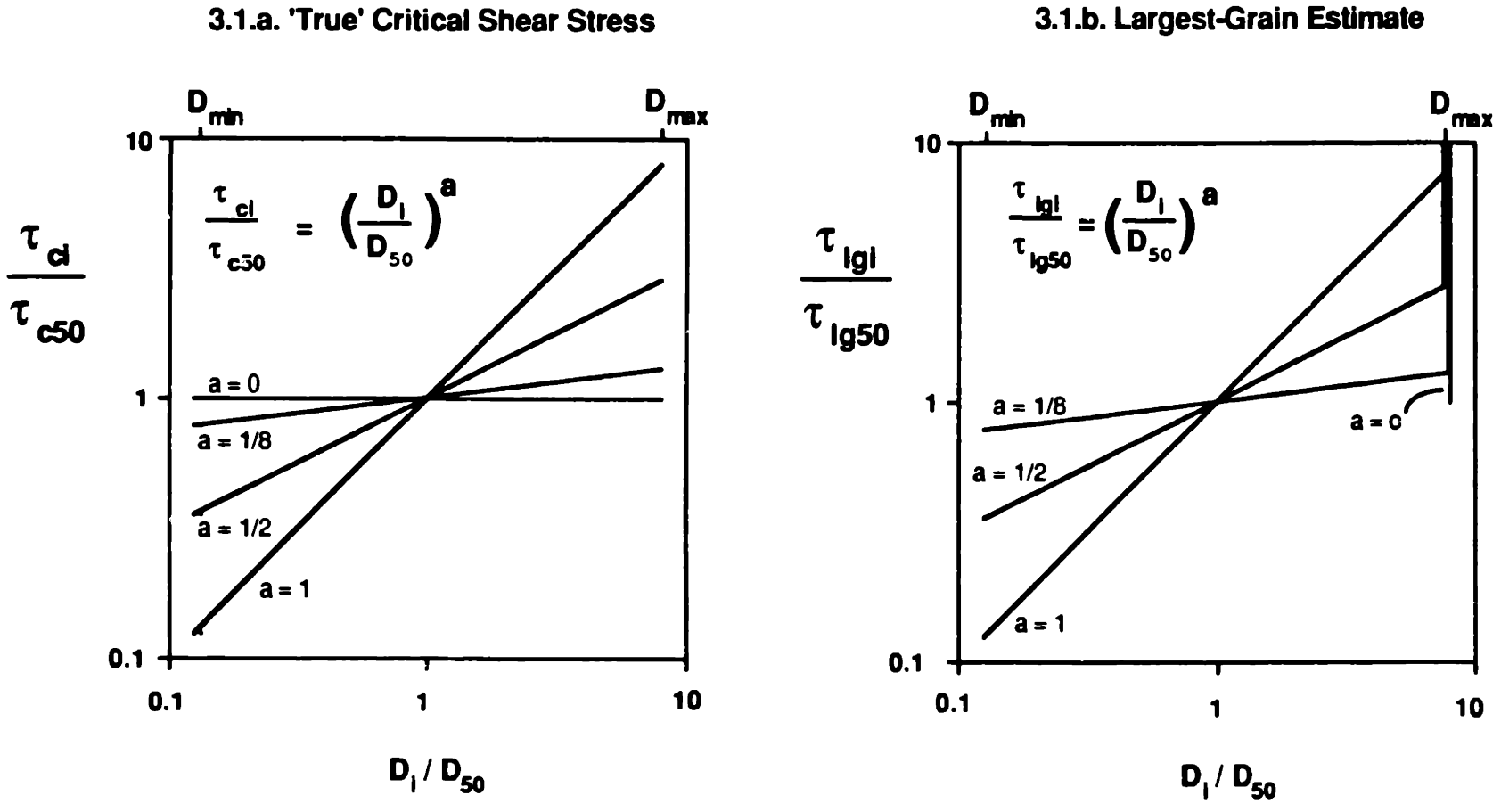

Figure 3.1. Schematic initial-motion relations for the largest-grain estimate of the critical shear stress See text for discussion.

straight lines with a log slope of *a* in Equation 5. The lines for the largest-grain method, shown in Figure 3.1.b, each consist of two parts: one is identical to its counterpart in Figure 3.1.a, and the other follows a vertical trend at D_{max} as the bed shear stress exceeds that necessary to move the largest grain on the bed. One line in Figure 3.1.b is exceptional: the case of equal mobility, for which the exponent *a* in Equation 5 is zero. In this case the largest grain on the bed should be found in all samples when the bed shear stress is large enough to move any sediment, and the appropriate line in Figure 3.1.b is a vertical line segment beginning at the point (D_{max}/D_{50}, 1). In this special case the largest-grain method gives results opposite to the true relation.

Figure 3.2 illustrates the dimensionless version of Figure 3.1, using

$$\frac{\tau^*_{ci}}{\tau^*_{c50}} \equiv \frac{\dfrac{\tau_{ci}}{(s-1)\rho g D_i}}{\dfrac{\tau_{c50}}{(s-1)\rho g D_{50}}} = \frac{\tau_{ci}}{\tau_{c50}}\frac{D_{50}}{D_i} = \left[\frac{D_i}{D_{50}}\right]^b \qquad (6)$$

From Equations 5 and 6, b = a - 1, except when $\tau_o > \tau_{cmax}$, for which D_{lg} is invariant with τ. Figure 3.2.a shows the true initial-motion relations and Figure 3.2.b shows the largest-grain estimates of these relations. As in Figure 3.1.b the largest-grain lines in Figure 3.2.b have two segments: one is identical to those in Figure 3.2.a, and the other is a vertical line segment at $D = D_{max}$, for which the bed shear stress exceeds that needed to move the coarsest grain. The special case of equal mobility corresponds to an exponent b = -1 in Equation 6 and is represented on Figure 3.2.b by a vertical line segment begining at (D_{max}/D_{50}, D_{50}/D_{max}). Again this line contrasts strongly with that determined using the reference method in Figure 3.2.a.

The second sampling problem associated with the largest-grain method — that large, scarce grains have a diminished chance of being observed in motion — is only part of the more fundamental problem of scale, for which Equations 3 or 4 can serve as a guide. This problem may be illustrated best with an example.

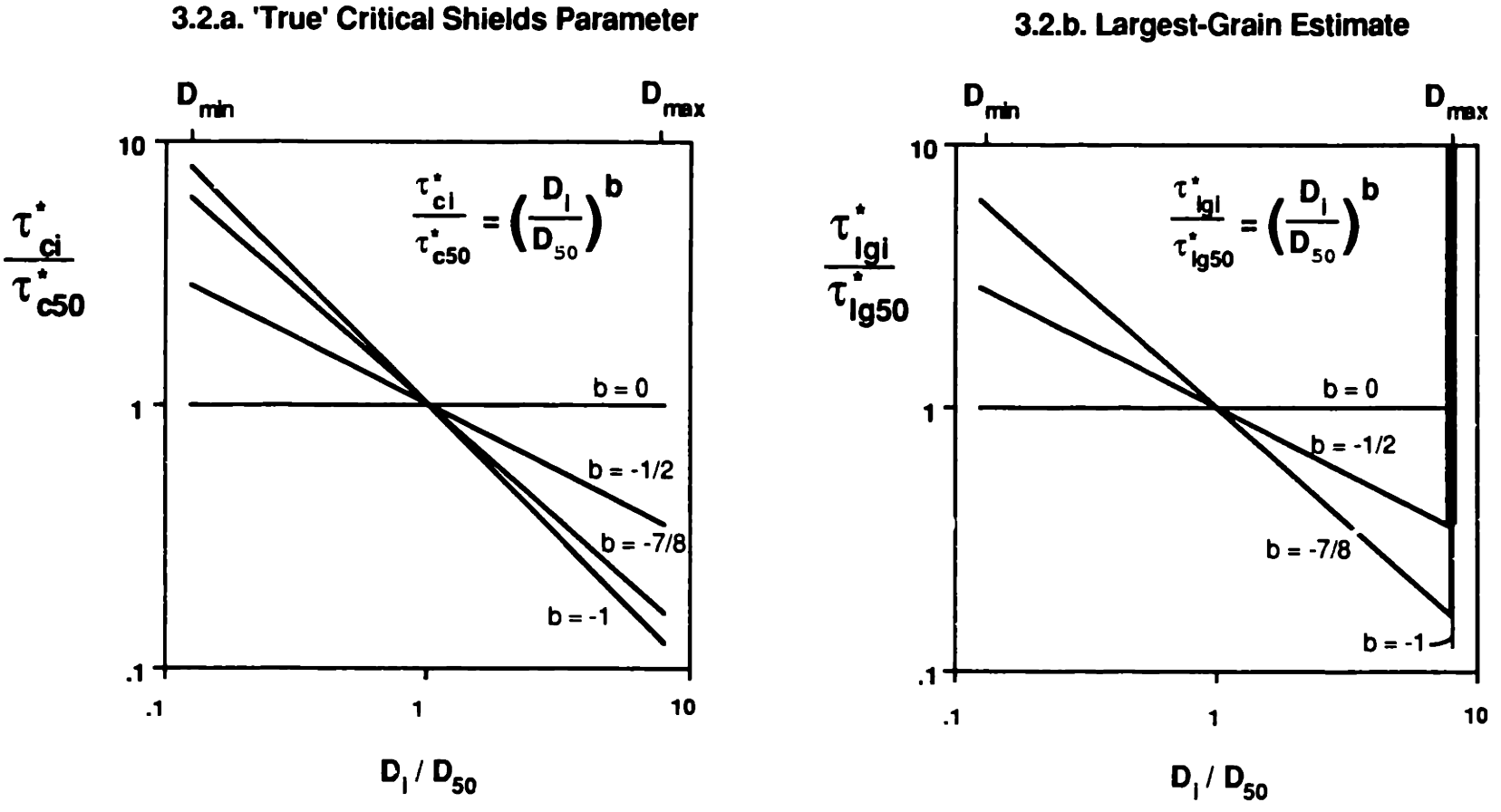

Figure 3.2. Schematic initial-motion relations for the largest-grain estimate of the critical Shields parameter See text for discussion.

Hammond et al. (1984) used the largest-grain method with video observations of initial motion of gravel by a tidal current. Although aware of the scaling principles behind Equation 2, they were unable to alter the viewing area used. The viewing period could not be varied because it was gradually varying over the tidal cycle. Hence, the value of n in Equation 2 was essentially constant, because the number of grains observed moving, the bed area, and the sample period were not varied from fraction to fraction. The coarsest particle they observed moving was 4.82 cm in size, compared with a mean size observed moving of 1.7 cm and a minimum size of 0.3 cm. Approximately 4.5% by weight of the coarsest size was present in grab samples of the surface material, compared with 10.5% of the mean size and 1% of the finest size. The scaling provided by Equation 4 requires that, for dynamic and kinematic similarity and for the constant viewing area and period used by Hammond et al., 3694 of the finest grains and 90 of the mean-sized grains would have to be observed moving for each of the coarsest grains observed moving.

Similar scaling problems exist when the critical shear stress is estimated from the largest grain found in a transport sample. In this case, however, the problem may be crudely addressed by examining transport samples of the same size at each flow strength (although this would require very long sampling periods at the lower transport rates). This approach at least provides an equal chance for a grain of a given fraction (say a very large one) to be found in any sample, although it obviously does not provide equal chances for grains of different sizes to be sampled.

If truly similar observation areas or sample sizes are not achieved, how do deviations from similarity in the observation technique affect initial-motion results? The degree to which initial-motion results would vary between similar and nonsimilar samples cannot be exactly determined, although the different trends of the results are fairly clear. For a given bed shear stress and a nonsimilar sampling technique, the size of the largest grain sampled will, in general, be smaller than that obtained with a sampling technique that meets a similarity criterion such as Equation 4. (For example, the probability of

observing a coarser grain moving will increase if the viewing area and/or sample period are increased.) On Figure 3.1.b, nonsimilar sampling techniques will result in a point falling above the true initial-motion line. Because grains larger than the mean size are predominantly observed using the largest-grain method, and because the scaling problems become particularly extreme for rare, very large grains, one can expect that a nonsimilar technique would produce points that fall above the right-hand part of the true line on Figure 3.1.b and that these points would follow a trend that is steeper than the true initial-motion line. This tendency would be reinforced by any samples that were taken for values of bed shear stress that exceeded that necessary to move all fractions in the mixture.

Both sampling and scaling problems in the largest-grain method can produce trends in Figure 3.1 that are steeper than the true initial-motion line. It is well worth noting that this is exactly the direction in which the published largest-grain initial-motion results ($\tau_{lgl} \approx \alpha[D_i/D_{50}]^{1/2}$) differ from results determined with the reference-transport method ($\tau_{ri} \neq f[D_i/D_{50}]$).

REFERENCE-TRANSPORT METHOD. Although the reference-transport method does not measure directly the true instant of initial motion for each fraction in a mixture, it has the distinct advantage that it may be used far more reliably than the largest-grain method. It is a relatively simple matter to determine the reference shear stress. The basic requirement is that accurate transport samples be obtained for enough flows (perhaps on the order of ten) that the relation between shear stress and transport rate is well defined for all fractions in the vicinity of the reference transport rate. The problems of sample duration and sample area important to the largest-grain method are not as restrictive for determining the fractional transport rate, which is naturally expressed as a percentage of the entire transport and scaled by the proportion of each fraction present in the bed. Thus, the absence of a rare, very large grain in the sample will not strongly affect the results. If a sufficiently large transport sample is taken, the proper scaling for determining the reference

shear stress may be directly incorporated when computing the fractional transport rates.

A number of different reference-transport criteria have been suggested. Parker et al. (1982; hereafter PKM) define the reference transport rate in terms of a constant value of the transport parameter W^*,

$$W^* = \frac{(s-1)g\, q_b}{(u_*)^3}$$

where q_b is the transport rate in terms of volume transport per unit width and time. The PKM reference transport rate ($W^* = 0.002$) is shown in Figure 3.3, along with the other reference-transport criteria and, for illustration, the fractional-transport data for three fractions of our 1Ø mixture.

Day (1980b) defines the reference transport rate using the Ackers and White (1973; hereafter AW) transport model, in which the transport parameter Ggr is defined as

$$Ggr = \frac{q_b}{VD}\left[\frac{u_*}{V}\right]^n$$

and V is mean flow velocity, D is a representative grain size, and the exponent n varies with a dimensionless measure of grain size from 1.0 for silt-sized grains to 0.0 for grains coarser than about 2.0 to 3.0 mm. The reference transport rate is assigned the essentially arbitrary value $Ggr = 10^4$. The AW reference-transport criterion may be expressed in terms of W^* and τ^* as

$$W^* = \frac{10^{-4}}{\tau_*}\left[\frac{V}{u_*}\right]^{n+1} \qquad (7)$$

An exact comparison between the PKM and AW transport parameters is possible only for specific combinations of grain size, fluid viscosity, flow velocity, and

bed shear velocity. However, a general comparison can be made by using the flow-resistance formula contained in the AW model to substitute for V/u_* in Equation 7:

$$\frac{V}{u_*} = \sqrt{32}\ \log_{10}\left[\frac{10d}{D}\right] \tag{8}$$

Because flow depth d is virtually constant in our experiments, a value of 11 cm can be used in Equation 8 to produce reference-transport criteria for the three fractions shown in Figure 3.3.

The values chosen for the PKM and AW reference-transport criteria are, within a range of low transport rates, essentially arbitrary. Because each is given in terms of a constant value of a particular dimensionless transport parameter, they share the advantages and disadvantages of that parameter, and are appropriately applied as reference values for transport rates described using that parameter — which is the use for which they were originally derived. For example, PKM used their reference-transport criterion (which does not include D_i) to provide a collapse of the transport-rate data for individual fractions that was undistorted with respect to grain size. The scaling arguments presented earlier suggest, however, that for the purpose of defining a general initial-motion criterion — and by extension a reference transport rate — grain size should be included in the initial-motion criterion. Because initial-motion relations have significance beyond serving as a reference level for analysis of transport-rate data, it is worth considering whether the scaling arguments presented earlier can be used to provide a rational basis for selecting a reference-transport criterion.

The relation between the number of grains moving per unit bed area and unit time (n) and the transport rate is

$$n\forall_g l = q_b \tag{9}$$

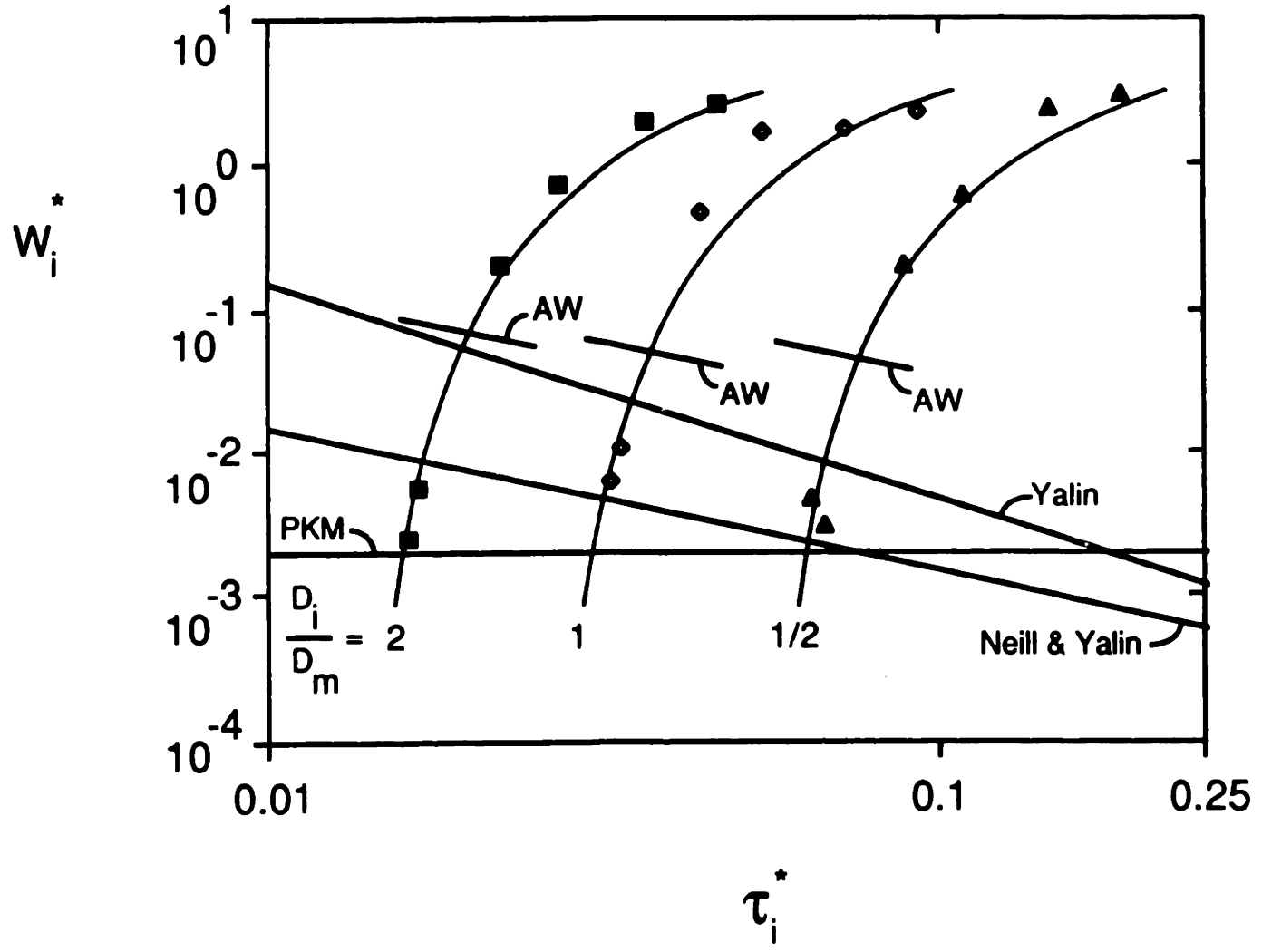

Figure 3.3. Reference-transport criteria of Parker et al. (1982; PKM) and Ackers/White (1971;AW) and approximate presentation as transport rates of the initial-motion criteria of Neill/Yalin (1969) and Yalin (1977). Fractional transport data for three fractions from the 1Ø mixture are shown for reference.

where $\forall_g$ is grain volume and l is mean excursion length of a grain in motion. $\forall_g$ can be described without serious error as $\forall_g = \alpha D^3$ ($\alpha = \pi/6$ for spheres). The expression for l is more problematic. Einstein (1950) used $l = 100D$, although the basis for this is unclear. Fernandez Luque and van Beek (1976) measured $l = 288D$ experimentally for several different uni-size sediments. If this result, $\alpha = \pi/6$, Equation 9, and Neill and Yalin's suggested constant of 10^{-6} are substituted into Equation 2, the Neill and Yalin initial-motion criterion becomes

$$q_b = (1.51 \times 10^{-4})(u_* D)$$

which is equivalent to

$$W^* = \frac{1.51 \times 10^{-4}}{\tau^*} \qquad (10)$$

This relation is plotted in Figure 3.3. It has the same slope as the AW criterion, but is lower in magnitude. Similar substitution into Equation 3 converts the Yalin criterion to

$$W^* = \frac{1.51 \times 10^{-4}}{(\tau^*)^{3/2}} \qquad (11)$$

The form of Equation 11 is the same as that which would be produced by holding constant the Einstein transport parameter, which is equal to $[W^*][\tau^*]^{3/2}$.

It may be seen in Figure 3.3 that the different reference-transport criteria will give different reference shear stresses. Because the fractional-transport data tend to follow a steep, concave-downward trend in this graph, the reference shear stresses will differ not only in magnitude but also in variation of the measured τ^*_{rl} with relative grain size. The exact differences in the measured τ^*_{rl} will be discussed later; the difference in results is mentioned here to motivate the argument for the use of a consistent reference-transport

criterion and to emphasize the importance of distinguishing clearly between reference shear stresses determined using different methods.

Reference-transport criteria such as Equations 10 and 11 have the advantage that they are based on similarity arguments that provide each fraction on the bed a representative chance of being observed or sampled. Unfortunately, their transformation into a transport rate is very inexact at present. Most critical to the transformation is the relation between l and grain size. The value of β used in $l = \beta D$ is based on the experiments with uni-size sediment of Fernandez-Luque and van Beek (1976). It is entirely unknown at present whether any constant would hold for all fractions in a size mixture, or even whether the relation between l and D is linear. This does not, however, reflect a fundamental problem with the initial-motion criteria. If a rational relation between excursion length and grain size for mixed-size sediment were available, a rational reference-transport criterion could be defined.

COMPARISON OF INITIAL-MOTION METHODS

The Oak Creek data collected by Milhous (1973) are particularly valuable here because they are the only data we know that include both extensive transport measurements and largest-grain measurements for conditions where grains coarser than those measured were available in the sediment bed. Thus, identical initial-motion results should be obtainable from these data, if an appropriate reference transport rate is selected and if sampling problems are not serious. Strikingly different initial-motion relations, however, have been found. Komar (1987) found $\tau_{lgi} \propto D_i^{0.57}$ using the largest-grain method, whereas PKM found essentially no dependence of τ_{ri} on D_i using the reference-transport method. These two relations are not directly comparable, because Komar examined all 66 samples from the best data set of Milhous whereas PKM examined a subset of these data, using the 22 samples with the highest transport rate. (It is worth noting that the lowest transport rate used by PKM, 0.28 g/ms, is fairly small.) Figure 3.4 compares the reference-transport and largest-grain results for only the uppermost 22 points. The largest-grain data

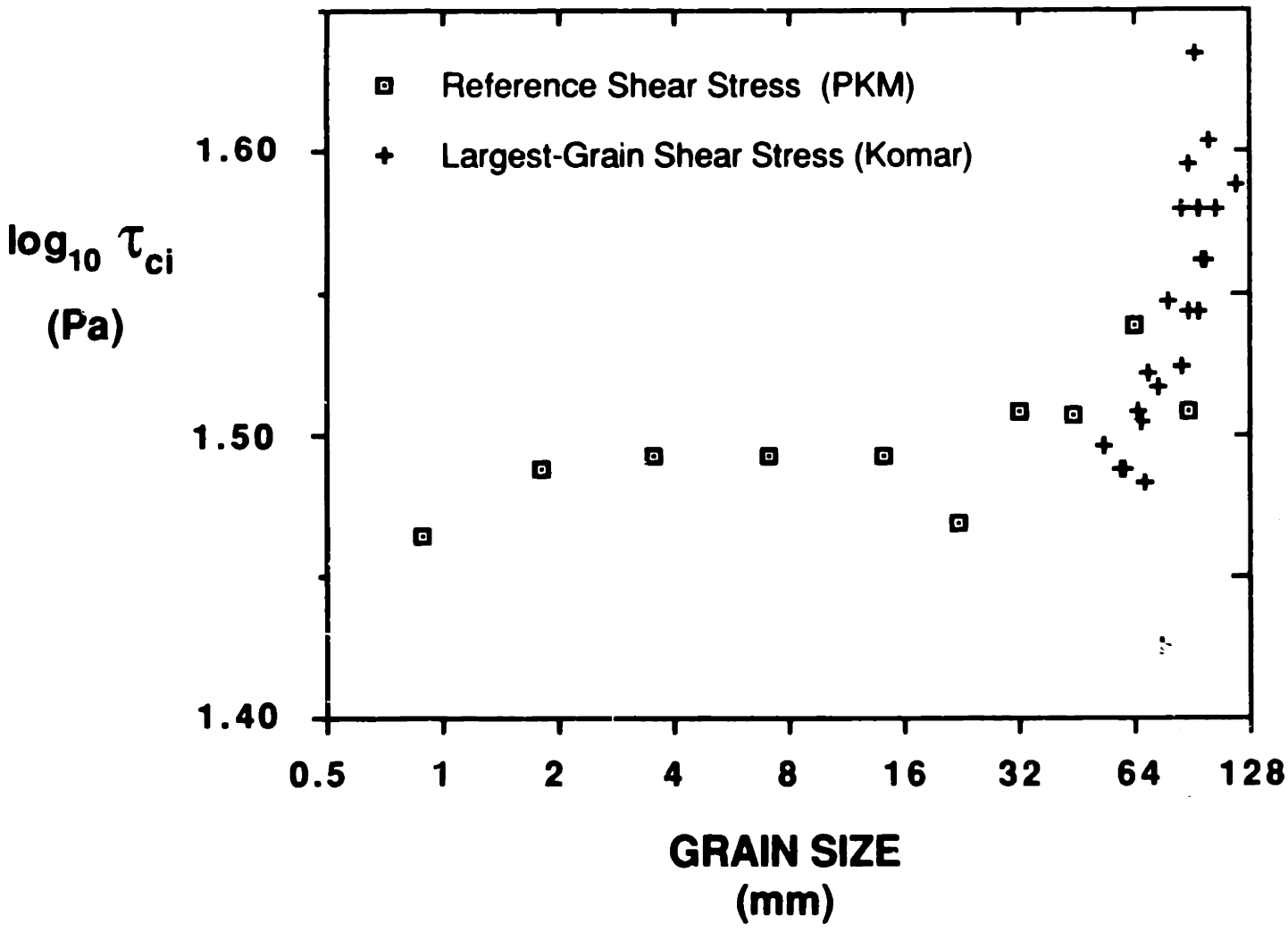

Figure 3.4. Initial-motion results for the Oak Creek data of Milhous (1973). Data labeled 'Komar' from largest-grain method; data labeled 'PKM' from reference-transport method

are identical to the appropriate data subset in Komar, and the reference-transport data are those fitted by PKM. Note that the scales of log axes in Figure 3.4 are unequal in order to show the data points clearly.

The most important point concerning Figure 3.4 is that — even for the same transport samples — the initial-motion results found with different methods are strikingly different. The largest-grain data show τ_{lgi} to vary with D_i/D_{50} to the power 0.405; PKM found τ_{ri} to vary with D_i/D_{50} to the power 0.018. An even larger exponent for the largest-grain method would be obtained if the line is fitted only to the points farthest to the right on Figure 3.4, a procedure that would appear reasonable given the sampling problems inherent in this method. An additional obvious difference between the initial-motion results is that the largest-grain data represent only the coarsest part of the bed mixture. The smallest grain measured is coarser than more than 80% of the bed mixture. Both the preponderance of coarse grains and the difference in the τ_{ci} — D_i/D_{50} relations produced by the two methods are about what one would expect if the true initial-motion relation for this sediment is close to equal mobility ($a = 0$ in Equation 3), particularly given the sampling problems inherent in the largest-grain determinations. Such problems appear to be important with the Oak Creek data. The availability of coarser grains in the Oak Creek sediment bed may have been strongly limited. Although grains coarser than those sampled are found in the bed, their percentage of the total bed material (all of which is assumed available for motion for the subset of the Milhous data examined by PKM) is vanishingly small (reported as 0% for $D_i > 102$ mm in PKM). In addition, there is a strong positive correlation between the size of the coarsest grain trapped and the total quantity of sediment collected. Hence, there is a relatively lower probability for a coarse grain to be found in the smaller transport samples, which were taken at the lower values of bed shear stress, than in the larger samples at higher flows and greater transport rates. Because the total shear stress and sample size are highly correlated, it is difficult to assess the relative importance of each in determining the variation with bed shear stress of the largest grain sampled. If all samples had been equal in size to the

largest, some of the lower-shear-stress samples would have included coarser grains, although it is not clear whether this would have produced a vertical τ_{cl} - D relation that would be in agreement with the reference-transport results.

The Milhous data illustrate that strikingly different results are obtained from the same data by using different initial-motion methods. Clearly, the results produced by one method cannot be used to confirm or deny those produced by the other. It is worth emphasizing, however, that the difference in the results may be understood in terms of the sampling problems associated with the largest-grain method. Even if the largest-grain results could be scaled to match an initial-motion criterion such as Equation 3 or 4, it is not clear that the two methods would give similar results, because the two methods give such fundamentally different results when the special case of equal mobility is approached.

APPLICATION OF INITIAL-MOTION METHODS

Without an accurate conversion between the initial-motion results determined by the different methods available, care must be taken to compare initial-motion data only with previous results determined with the same method and with the same type of data. For situations where only a transport deposit is available, as in paleohydraulic interpretation of a fluvial deposit, the largest-grain method is clearly appropriate. Indeed, because the sampling and scaling problems associated with the largest-grain method can produce initial-motion results that are strikingly different from either theoretical or reference-transport results, it appears that *only* initial-motion results determined with the largest-grain method would be applicable to the paleohydraulic analysis of a transport deposit. Unfortunately, if many natural rivers are found to operate at conditions near equal mobility, it is not clear how useful the largest-grain method would be for making any hydraulic interpretations, because most, if not all, flows would involve the transport of all grains (including the coarsest).

The reference-transport method is clearly appropriate for scaling the transport rate of individual fractions, provided that the same transport parameter is used for both the transport analysis and the reference-shear-stress calculations. Unless properly scaled, neither initial-motion method will give results that are generally interpretable or are comparable with results computed using a different method. Properly scaled initial-motion results are also necessary for verification of theoretical computations or comparison with experimental data on the pivoting angle of individual sizes in mixed-size sediment. For such applications a truly general and properly scaled initial-motion methodology is needed. Equations 10 or 11 provide a practical basis for such a criterion, if an accurate method can be found to relate the mean excursion length of a fraction to its relative grain size.

OTHER FRACTIONAL-TRANSPORT DATA

Fractional transport rates have been measured for a variety of different sediments in recent years. These data provide an opportunity to compare our results with other sediments and flows, although at the expense of control over other potentially important independent variables. Data examined here are from the laboratory experiments of Day (1980a), Misri et al. (1984), and Dhamotharan et al. (1981) and the Oak Creek field data of Milhous (1973). These data are all for steady, uniform flow and involve bed preparation and run times (for the laboratory data) and sampling methods of a nature that permit reasonable estimates of the accuracy of the transport rates of individual fractions in the mixtures. The mean hydraulic parameters for these studies, as well as for ours, are given in Table 3.2. Cumulative plots of the bed grain-size distributions are given in Figure 3.5. In addition to a wide range in mean size and sorting, the size-distributions of these sediments show a marked variation in size-distribution shape. Three sediments are distinctly bimodal. These are (with the location of the modes expressed as D_i/D_m) Day Bed A (0.30, 4.0), Day Bed B (0.30, 2.4), and Dhamotharan et al. (0.84, 3.3). Sediments N1 and N3 of Misri et al. are close to lognormal, and sediment N2 has a nearly rectangular

TABLE 3.2. MEAN HYDRAULIC AND TRANSPORT PARAMETERS FOR ALL MIXED-SIZE TRANSPORT DATA

SEDIMENT	VELOCITY (cm/s)	DEPTH (cm)	SLOPE ($\times 10^3$)	TOTAL BED SHEAR VELOCITY (cm/s)	TRANSPORT RATES (g/ms)
MIT MUNI	44.8 - 72.4	11.4 - 12.8	0.96 - 2.93	2.99 - 5.65	0.00185 - 46.4
MIT 1/2Ø	43.6 - 79.4	11.0 - 11.7	1.00 - 4.92	3.02 - 7.08	0.0144 - 97.0
MIT 1Ø	43.1 - 72.9	10.9 - 11.2	1.04 - 3.30	3.11 - 5.58	0.0231 - 59.4
MIT FUNI	27.5 - 44.9	10.8 - 11.4	0.29 - 1.75	1.57 - 4.17	0.00247 - 6.31
MIT CUNI	59.1 - 82.6	10.8 - 11.1	2.55 - 4.91	4.97 - 6.91	0.00335 - 9.55
DAY A	47.9 - 74.5	10.7 - 16.9	0.660 - 3.67	3.20 - 6.11	0.711 - 65.4
DAY B	44.1 - 72.2	11.5 - 18.9	0.445 - 2.99	2.72 - 5.70	0.134 - 90.3
MISRI N1	49.9 - 73.4	5.9 - 11.7	3.30 - 4.24	4.26 - 6.69	0.0642 - 68.5
MISRI N2	55.8 - 80.8	7.8 - 13.5	3.78 - 4.75	5.30 - 76.1	0.494 - 16.9
MISRI N3	58.7 - 82.6	8.4 - 13.3	3.45 - 4.31	5.14 - 7.14	0.627 - 29.7
SAF	44.3 - 65.8	4.0 - 6.7	6.8 - 8.2	5.58 - 6.46	0.333 - 26.7
OAK CREEK	84.2 - 116.3	27.4 - 44.5	9.7 - 10.8	16.3 - 20.8	0.281 - 111.0

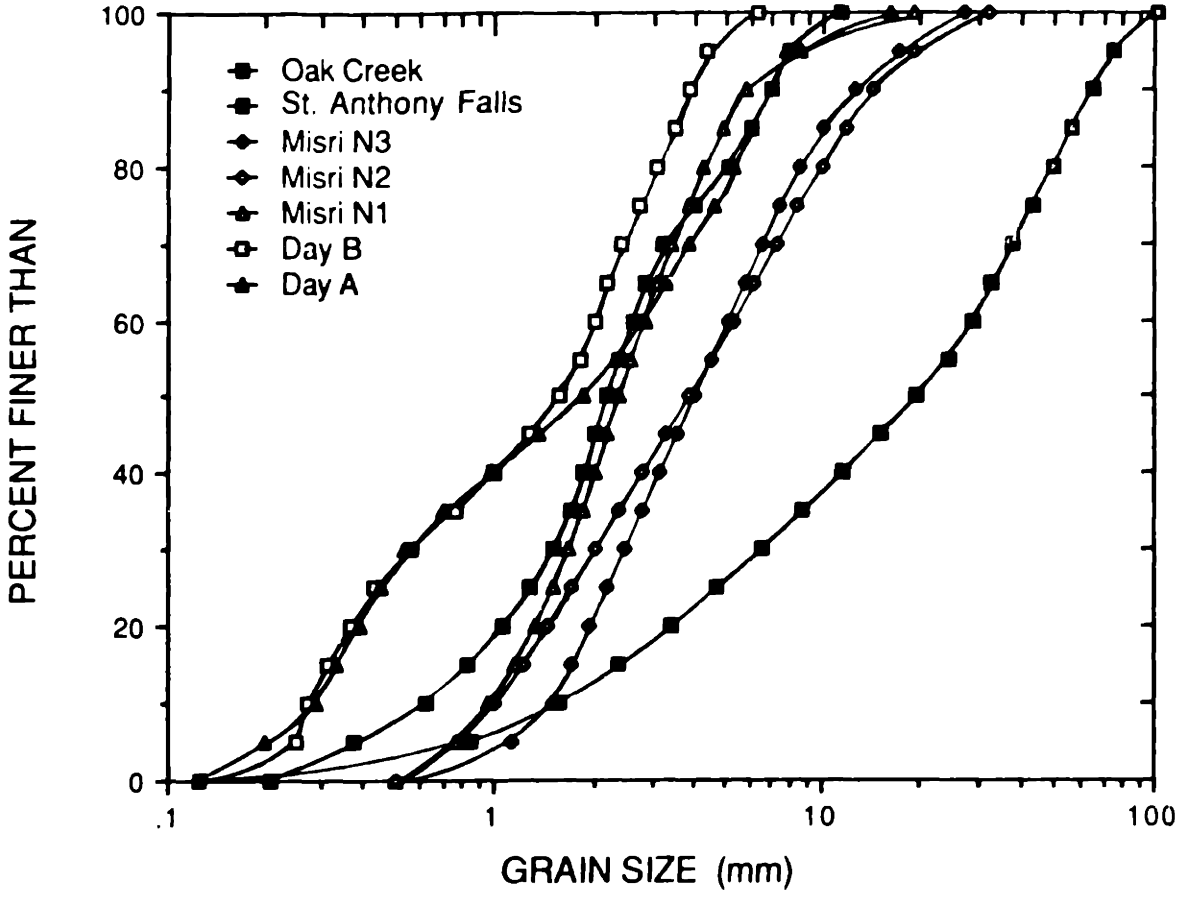

Figure 3.5. Cumulative grain-size distributions for other sediments

distribution. The Oak Creek bed size distribution has a very long fine tail ($D_5/D_{50} = 6[D_{95}/D_{50}]$).

INITIAL-MOTION RESULTS

FITTING TECHNIQUE

Although conceptually simple, computation of the reference shear stress for individual fractions requires a number of choices concerning the appropriate techniques for fitting the data. Not only must a reference-transport criterion be chosen, but also an appropriate curve of transport rate versus shear stress must be fitted to the data, and the method of fitting the curve to the data must be chosen.

Values of τ^*_{ri} were computed with all the reference-transport criteria in Figure 3.3, although the discussion here will focus primarily on the PKM reference-transport criterion ($W_i^* = 0.002$). This is because the τ^*_{ri} values measured at constant W^* are undistorted with respect to grain size, a considerable convenience when comparing the reference shear stresses for different sizes in a mixture. The PKM criterion is also of interest because it was used with the Oak Creek data to produce the distinctive and important result that all grains begin moving at nearly the same bed shear stress (Parker et al., 1982). Initial-motion results computed with different reference-transport criteria are directly convertible from the PKM values of τ^*_{ri}; the results computed with the other methods will be discussed in comparison with the PKM results.

The form of the relation between transport rate and shear stress fitted to the data was determined largely by the trend of the data. The fractional transport rates of every third fraction in the MIT 1Ø mixture are presented in Figure 3.6 in terms of W^*_i and τ^*_i. The separation of the data along the τ^*_i axis results solely from the presence of the fraction size in the denominator of τ^*_i. Because grain size is not present in W^*_i, the dimensional transport rates of the different fractions may be seen to be comparable at the same level of τ_o. This

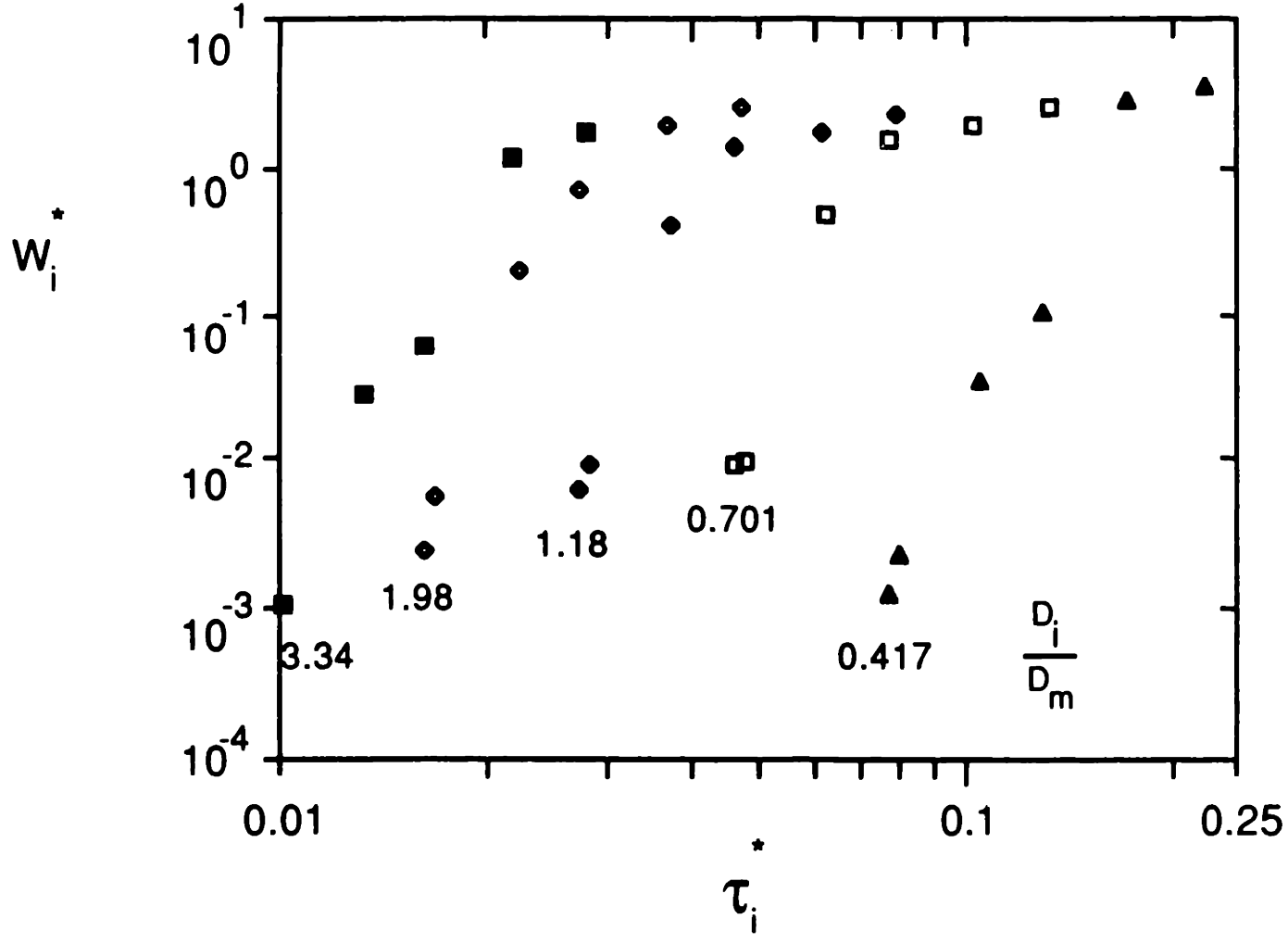

Figure 3.6. Fractional transport rates for the 1Ø MIT sediment mixture (every third fraction shown)

observation, combined with the similarity in form of the $W^*_i - \tau^*_i$ relations for each fraction, leads directly to the conclusion that all fractions begin moving at about the same bed shear stress. Hence, the reference-transport procedure is essentially a means of documenting this observation consistently. The data in Figure 3.6 show a strong concave-downward trend. To obtain a good fit to these data, and hence a good estimate of the reference shear stress, a similarly curved transport function is needed. The relation chosen is a power approximation of the Einstein (1950) bed-load function at low stresses derived by Parker (1979),

$$W_i^* = 11.2 \left(1 - \frac{0.8531\tau_{ri}^*}{\tau_i^*}\right)^{4.5}$$

This curve is shown in Figure 3.3. Other transport functions could have been chosen, although they would not have produced significant differences in the measured τ^*_{ri} because the transport function was primarily used to simply extrapolate or interpolate to W^*_r from points near W^*_r, and because transport functions that provide a reasonable fit to the data have about the same slope near W^*_r.

Placement of the curve was determined largely from the data points near W^*_r. The curve was fitted by eye as a convenient means of giving added weight to points near the reference-transport value. Nonlinear least-squares fitting was initially used, but did not always give the best visual match to the data because it was overly influenced by small errors in the shear-stress term for points near initial motion, where the transport function is very steep. The fitting was done as follows. If two or more points fell close to W^*_r (within approximately a factor of two), the curve was placed so as to match those points most closely. When only one point was found near W^*_r, this point was still given added weight, but placement was also influenced by the fit of the curve to the rest of the data points for that fraction. In these cases, and when no points were close to W^*_r, the importance of using a curved line to fit the

data was obvious, because it gives an extrapolation to W^*_r that is more reasonable than the loglinear extrapolations used previously (e.g. Parker et al., 1982). To preserve the grain-size independence of the fitting procedure, the transport curve was translated only parallel to the τ^*_r axis.

Because the curve-fitting was to some extent subjective, a conservative estimate of the error in the measured values of τ^*_{ri} is necessary. This error was estimated by reading the values of τ^*_r when the curve was placed as far as possible to the right and left of the measured τ^*_{ri} while still giving a reasonable fit to at least some of the transport data for each fraction. This error estimate is analogous to a confidence interval for an estimated intercept in that the true τ^*_{ri} is highly likely to fall within the error bounds, but is different from a standard confidence interval in that (i) it is fitted by eye, (ii) it has only a subjective dependence on the number of data points fitted, and (iii) the measured data point generally does not fall at the midpoint of the error bounds. The fitted τ^*_{ri} and the associated error bounds are given in Table 3.3.

The τ^*_{ri} fitted to our data generally involved at least two points near W^*_{ri} because we clustered some runs for each sediment near initial-motion conditions. Although these points determined the placement of the curve, the fit of the curve to our data at higher transport rates was also usually very good. The fit of the transport function to the other data was in some cases less accurate than the fit to our data, owing to the absence of points near W^*_{ri} (DAY A), data scatter (MISRI N1), or trends that were significantly different from the fitting curve (DAY A). Although cases where the fit was poor increased the error in estimating τ^*_{ri} for any given fraction (which is reflected in the error bounds of Table 3.3), the poor fit does not lead to a similar uncertainty in the variation of τ^*_{ri} from fraction to fraction, which is more central to understanding the relative-size effect on τ^*_{ri}. This is because plots of W^*_i against τ^*_i were in most cases clearly translated from fraction to fraction with little change in the form of the scatter. Thus, the transport function could be fitted consistently to each fraction, so that the variation of τ^*_{ri} with relative

TABLE 3.3. VALUES OF τ^*_{ri} FITTED BY PKM REFERENCE-TRANSPORT CRITERION

MIT 1Ø			MIT 1/2Ø			MIT FUNI			MIT CUNI		
D_l	τ^*_{ri}	Error Bounds	D_l	τ^*_{ri}	Error Bounds	D_l	τ^*_{ri}	Error Bounds	D_l	τ^*_{ri}	Error Bounds
0.595	0.105	.100 - .129	0.771	0.0794	.0759 - .0955	0.545	0.0275	.0240 - .0275	4.36	0.0457	.0437 - .0501
0.771	0.0794	.0708 - .0871	0.917	0.0603	.0589 - .0724	0.648	0.0229	.0186 - .0229	5.19	0.0380	.0363 - .0398
0.917	0.0631	.0575 - .0661	1.09	0.0501	.0479 - .0562	0.771	0.0191	.0162 - .0195	6.17	0.0316	.0302 - .0339
1.09	0.0501	.0457 - .0525	1.30	0.0427	.0398 - .0479	0.917	0.0166	.0138 - .0170			
1.30	0.0417	.0389 - .0437	1.54	0.0355	.0331 - .0380						
1.54	0.0363	.0324 - .0372	1.83	0.0295	.0263 - .0316						
1.83	0.0309	.0275 - .0309	2.18	0.0251	.0234 - .0269						
2.18	0.0257	.0240 - .0269	2.59	0.0209	.0200 - .0229						
2.59	0.0224	.0200 - .0229	3.08	0.0178	.0174 - .0191						
3.08	0.0191	.0170 - .0191									
3.67	0.0158	.0151 - .0162									
4.36	0.0141	.0138 - .0148									
5.19	0.0123	.0117 - .0132									
6.17	0.0105	.0105 - .0123									

TABLE 3.3. VALUES OF τ^*_{ri} FITTED BY PKM REFERENCE-TRANSPORT CRITERION (CONTINUED)

DAY A			DAY B			MISRI N1			MISRI N2		
D_l	τ^*_{ri}	Error Bounds	D_l	τ^*_{ri}	Error Bounds	D_l	τ^*_{ri}	Error Bounds	D_l	τ^*_{ri}	Error Bounds
0.288	0.162	.155 - .170	0.275	0.158	.151 - .174	0.957	0.120	.105 - .132	0.997	0.186	.186 - .224
0.336	0.129	.129 - .158	0.318	0.135	.135 - .151	1.15	0.102	.0794 - .107	1.21	0.132	.132 - .159
0.393	0.107	.107 - .145	0.369	0.110	.110 - .135	1.33	0.0832	.0631 - .0871	1.45	0.110	.110 - .129
0.455	0.0955	.0955 - .166	0.438	0.0933	.0933 - .107	1.49	0.0741	.0537 - .0741	1.70	0.0871	.0871 - .112
0.537	0.0813	.0813 - .123	0.559	0.0692	.0692 - .0851	1.66	0.0676	.0479 - .0692	2.00	0.0724	.0724 - .0851
0.694	0.0617	.0617 - .0912	0.758	0.0537	.0490 - .0575	1.82	0.0603	.0437 - .0646	2.35	0.0603	.0603 - .0724
0.971	0.0490	.0490 - .0813	0.997	0.0398	.0380 - .0417	2.00	0.0562	.0380 - .0562	2.76	0.0513	.0501 - .0603
1.36	0.0372	.0372 - .0550	1.27	0.0324	.0309 - .0363	2.18	0.0513	.0372 - .0525	3.24	0.0427	.0427 - .0490
1.82	0.0324	.0309 - .0389	1.57	0.0269	.0263 - .0324	2.36	0.0457	.0331 - .0490	3.81	0.0363	.0347 - .0407
2.29	0.0263	.0263 - .0347	1.81	0.0240	.0240 - .0295	2.57	0.0437	.0309 - .0447	4.51	0.0324	.0316 - .0372
2.74	0.0229	.0219 - .0275	1.99	0.0229	.0229 - .0295	2.80	0.0398	.0288 - .0398	5.31	0.0288	.0288 - .0347
3.25	0.0191	.0186 - .0219	2.17	0.0204	.0200 - .0240	3.09	0.0363	.0275 - .0372	6.20	0.0251	.0245 - .0282
3.87	0.0170	.0162 - .0191	2.40	0.0191	.0178 - .0214	3.43	0.0331	.0240 - .0331	7.20	0.0219	.0209 - .0251
4.59	0.0151	.0145 - .0186	2.72	0.0158	.0148 - .0195	3.83	0.0295	.0209 - .0295	8.43	0.0195	.0186 - 0.209
5.32	0.0138	.0129 - .0166	3.09	0.0145	.0129 - .0182	4.30	0.0257	.0166 - .0257	10.0	0.0178	.0174 - .0200
6.05	0.0120	.0117 - .0141	3.49	0.0135	.0126 - .0158	4.91	0.0229	.0162 - .0229	11.9	0.0155	.0151 - .0170
6.95	0.0110	.0105 - .0132	3.88	0.0126	.0120 - .0151	5.83	0.0204	.0138 - .0204	14.40	0.0132	.0129 - .0148

TABLE 3.3. VALUES OF τ^*_{ri} FITTED BY PKM REFERENCE-TRANSPORT CRITERION (CONTINUED)

MISRI N3			SAF			OAK CREEK		
D_l	τ^*_{ri}	Error Bounds	D_l	τ^*_{ri}	Error Bounds	D_l	τ^*_{ri}	Error Bounds
1.48	0.112	.112 - .132	0.616	0.309	.288 - .347	1.57	0.575	.575 - .631
1.70	0.0955	.0851 - .100	0.828	0.204	.204 - .246	2.37	0.380	.380 - .427
1.93	0.0794	.0759 - .0871	1.05	0.166	.159 - .191	3.40	0.282	.269 - .302
2.18	0.0646	.0646 - .0813	1.28	0.126	.120 - .132	4.75	0.200	.195 - .214
2.45	0.0562	.0562 - .0676	1.49	0.0977	.0933 - .1023	6.48	0.148	.145 - .158
2.77	0.0490	.0479 - .0525	1.68	0.0851	.0794 - .0933	8.72	0.107	.100 - .117
3.12	0.0407	.0389 - .0447	1.83	0.0776	.0741 - .0851	11.5	0.0832	.0794 - .0891
3.52	0.0380	.0347 - .0398	1.98	0.0692	.0646 - .0724	15.1	0.0646	.0589 - .0692
4.00	0.0331	.0295 - .0347	2.16	0.0646	.0575 - .0692	19.5	0.0490	.0447 - .0525
4.56	0.0324	.0324 - .0355	2.36	0.0589	.0537 - .0617	24.3	0.0389	.0372 - .0417
5.17	0.0295	.0288 - .0331	2.58	0.0525	.0513 - .0575	28.4	0.0339	.0316 - .0380
5.81	0.0263	.0257 - .0288	2.84	0.0479	.0457 - .0513	32.5	0.0302	.0288 - .0331
6.54	0.0234	.0224 - .0251	3.19	0.0447	.0417 - .0490	37.1	0.0257	.0251 - .0288
7.41	0.0219	.0209 - .0229	3.96	0.0355	.0316 - .0380	42.8	0.0234	.0214 - .0251
8.50	0.0200	.0186 - .0214	5.07	0.0288	.0269 - .0295	49.3	0.0200	.0186 - .0209
10.1	0.0178	.0170 - .0182	6.04	0.0240	.0234 - .0257	56.6	0.0170	.0170 - .0186
12.7	0.0145	.0141 - .0151	6.94	0.0219	.0200 - .0229	64.6	0.0158	.0151 - .0170
						74.4	0.0141	.0126 - .0148

size is of a higher precision than that with which individual values of τ^*_{ri} can be determined.

RELATIVE-SIZE EFFECT

One of the primary goals of this work is to determine whether a single relative-size parameter, like D_i/D_{50}, is sufficient to describe the effect of relative grain size on τ^*_{ri}. By holding the mean size and size-distribution shape constant in our experiments, as well as flow depth and water temperature, we isolated the effect on τ^*_{ri} of percent finer than (or mixture sorting) for particular fractions (values of D_i/D_{50}). The fitted τ^*_{ri} for our data are plotted against D_i/D_{50} in Figure 3.7. The error bounds are shown as cross-hatching in the figure; the error bounds for the 1Ø and 1/2Ø mixtures essentially overlap and are shown as only one pattern representing the outermost error bounds for either mixture. The coefficients and expcnents of straight lines fitted to the data in Figure 3.7 are given in Table 3.4.

The data in Figure 3.7 suggest clearly that only a single relative-size parameter — in this case D_i/D_{50} — is needed to characterize the relative-size effect on τ^*_{ri}. This may be illustrated in two complementary ways. First, the τ^*_{ri} for the same fractions (and hence, the same grain sizes) in the 1/2Ø and 1Ø mixtures may be compared. Only the percentile position within the mixture varies between these fractions, yet the τ^*_{ri} values for each D_i/D_{50} are nearly identical. Alternatively, it may be seen that the τ^*_{ri} — D_i/D_{50} trends for all four sediments in Figure 3.7 are very similar, even though mixture sorting varies from 0.19 Ø to 0.99 Ø. The trends for these sediments fall in the narrow range of -0.97 to -1.06. Only the trend of the CUNI mixture (-1.06) is significantly different from the other mixtures at the 95% level. Both views of the problem provide a well controlled demonstration that when the effect of D_i/D_{50} on τ^*_{ri} is taken into account, the mixture sorting (or percent finer than) does not affect τ^*_{ri} appreciably .

The data in Figure 3.7 also show, for the first time, that consistent initial-motion relations appear to hold for sediments with a broad range of

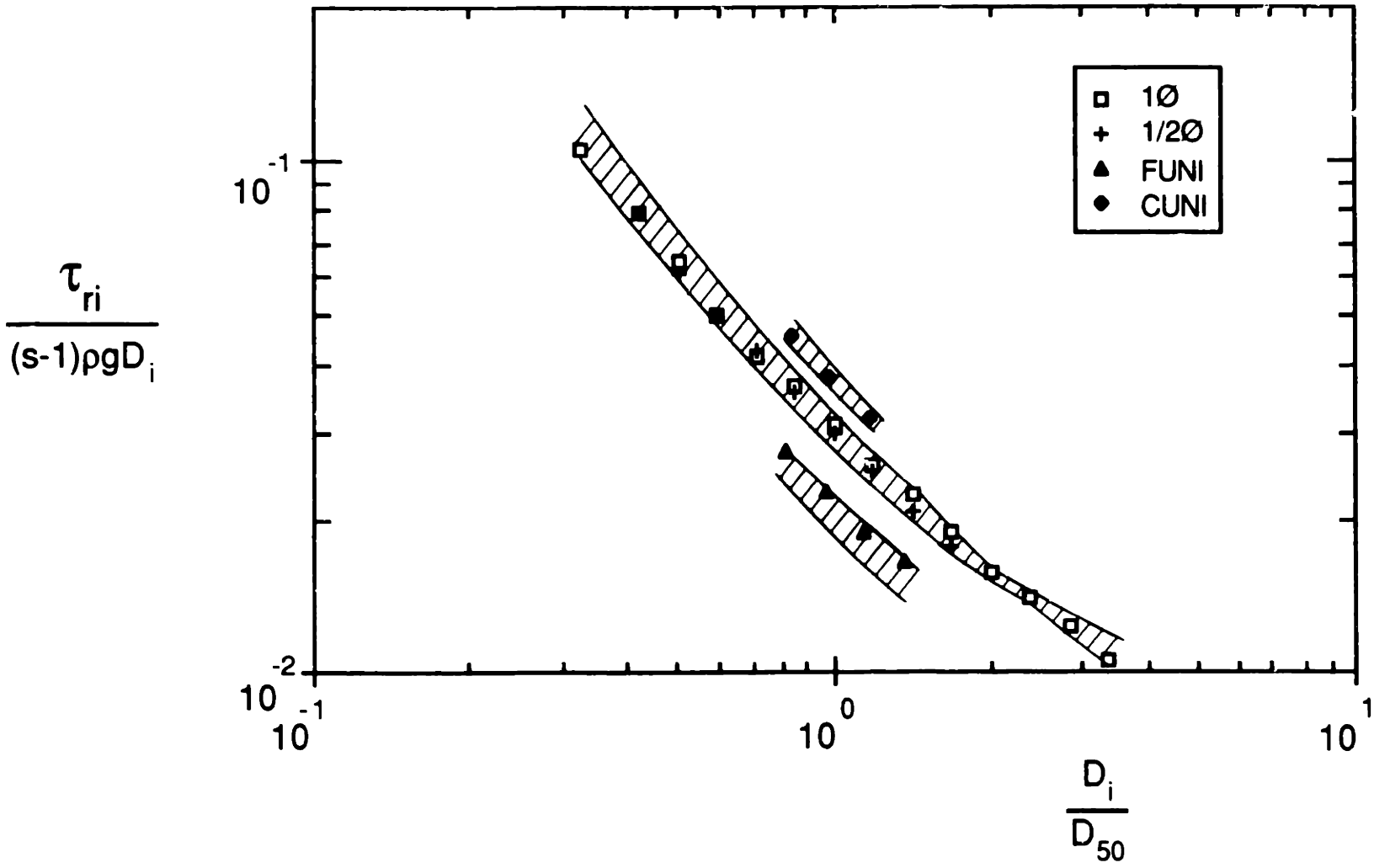

Figure 3.7. τ^*_{ri} as a function of D_i/D_{50} for the MIT sediments. Error bounds shown as cross-hatching

TABLE 3.4. LEAST-SQUARES FIT TO $\tau^*_{ri} = \alpha(D_i/D_{50})^{\beta}$

SEDIMENT	α	β	β error (@ 95%)
MIT1/2Ø	0.0301	-1.006	0.0158
MIT1Ø	0.0356	-0.970	0.0447
MIT FUNI	0.0226	-0.984	0.1986
MIT CUNI	0.0371	-1.064	0.0150
DAY A	0.0368	-0.809	0.0286
DAY B	0.0368	-0.953	0.0292
MISRI N1	0.0475	-0.997	0.0255
MISRI N2	0.0415	-0.953	0.0653
MISRI N3	0.0371	-0.920	0.0806
SAF	0.0708	-1.091	0.0610
OAK CREEK	0.0732	-0.979	0.0093

grain sizes and for sediments very close to uni-size. Such a result is necessary for any generally valid model for initial motion of mixed-size sediments, which must include the limiting case of uni-size sediment. As we will show later, the actual τ^*_{ri} for our well sorted sediments fall within the range one would expect for uni-size sediments. Both the consistency of τ^*_{ri} — D_i/D_{50} relations over a wide range of sorting and the fact that the τ^*_{ri} converge to reasonable uni-size critical shear stresses lend credence to our specific τ^*_{ri} results and the methodology used to compute them.

Figure 3.8 presents τ^*_{ri} against D_i/D_{50} for the other, previously published, transport data. Error bounds for these data (given in Table 3.3 but omitted from Figure 3.8 for clarity) tend to be of the same order as those for our sediments, but are slightly larger. The coefficients and exponents of straight lines fitted to the data in Figure 3.8 are given in Table 3.4. Again, the slopes of the τ^*_{ri} — D_i/D_{50} relations fall within a fairly small range of -0.81 to -1.09. This result is striking, because the experimental control behind our data in Figure 3.7 is lacking in Figure 3.8. Although the mixture sorting of the sediments in Figures 3.7 and 3.8 varies from 0.19 Ø to 2.1 Ø, there is no consistent trend between mixture sorting and the form of the τ^*_{ri} — D_i/D_{50} relations. This provides more general, empirical, support for our controlled experimental result that, once the effect of D_i/D_{50} is accounted for, mixture sorting (or percent finer than) does not contribute significantly to variation in τ^*_{ri}.

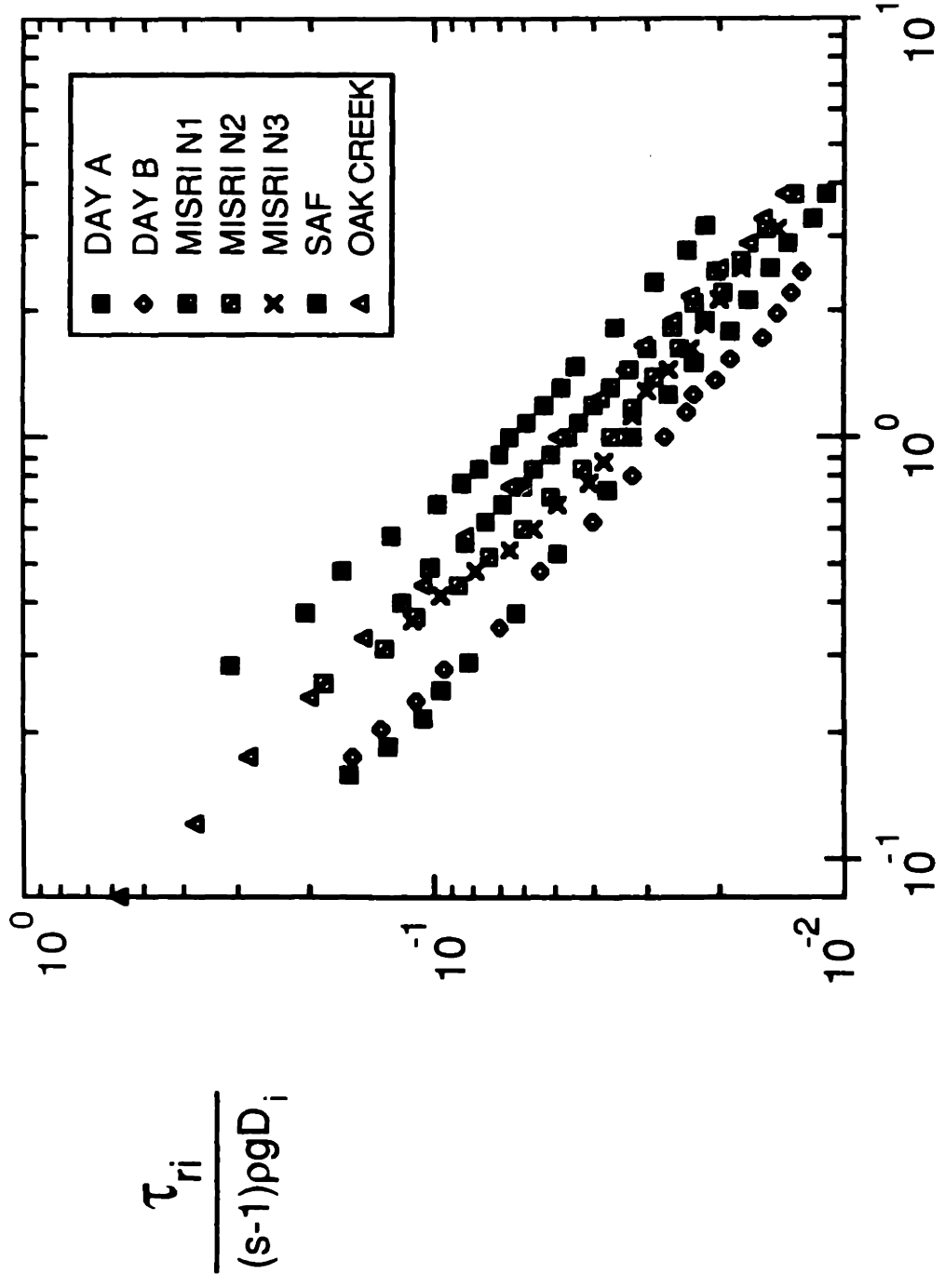

Figure 3.8. τ^*_{ri} as a function of D_i/D_{50} for other sediments

The variation in τ^*_{ri} can also be examined with respect to the percentile position of the individual fractions. This has the advantage of an obvious limit for τ^*_{ri}, providing a chance to evaluate the reasonableness of our measured τ^*_{ri}. When a mixture is close to uni-size, τ^*_{ri} should not depend on P, percent finer than, because all fractions are nearly the same size. Plots of τ^*_{ri} against P also have the advantage of not shrinking to a single point as the mixture approaches uni-size, a considerable advantage when the variation of τ^*_{ri} with relative grain size is of interest. Figure 3.9, τ^*_{ri} as a function of P for our data, clearly shows the trends to decrease in slope as sorting approaches uni-size. This change in slope is illustrated in Figure 3.10, which presents the slopes b_1 of straight lines fitted to the central parts of τ^*_{ri} — P relations for all the sediment mixtures. The slopes, graphed as a function of mixture sorting, show a trend that is remarkably consistent over the entire range of sorting and approaches the appropriate limiting value of zero at uni-size. Although Figure 3.9 shows no new physical information beyond Figure 3.7, it does establish that the measured τ^*_{ri} values conform to a physically reasonable limit.

Although only one of D_i/D_{50} or P is sufficient to describe the effect of relative size on τ^*_{ri} for sediments investigated here, D_i/D_{50} appears to be preferable for practical use because τ^*_{ri} — D_i/D_{50} relations are simpler in form and allow physical conclusions on initial motion to be drawn directly from the data.

The lack of variation in the τ^*_{ri} — D_i/D_{50} relations of Figures 3.7 and 3.8 is striking because, in addition to a broad variation in the mean size, sorting, and shape of the mixture size distributions, other potentially important independent variables, like relative depth and grain Reynolds number, show considerable variation both within each mixture and from mixture to mixture. Figure 3.11 presents the τ^*_{ri} for all mixtures plotted against S^* ($=[D_i^3(s-1)g]^{1/2} / \nu$), a convenient surrogate for grain Reynolds number. Also shown is the classic Shields curve for incipient motion of uni-size sediments (Shields, 1936; version of Miller et al., 1977, plotted here). Even though the

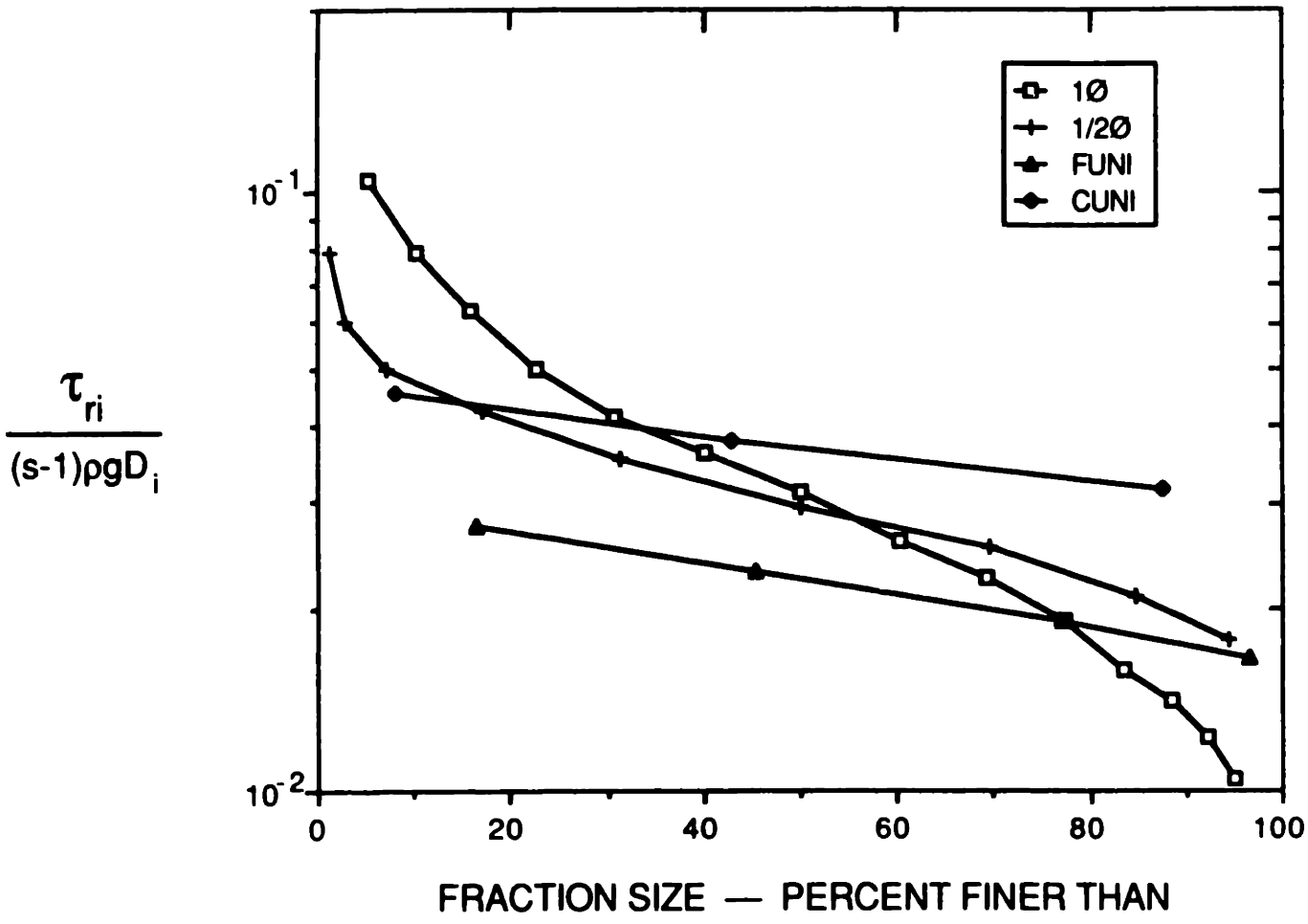

Figure 3.9. τ^*_{ri} as a function of percent finer than for MIT sediments

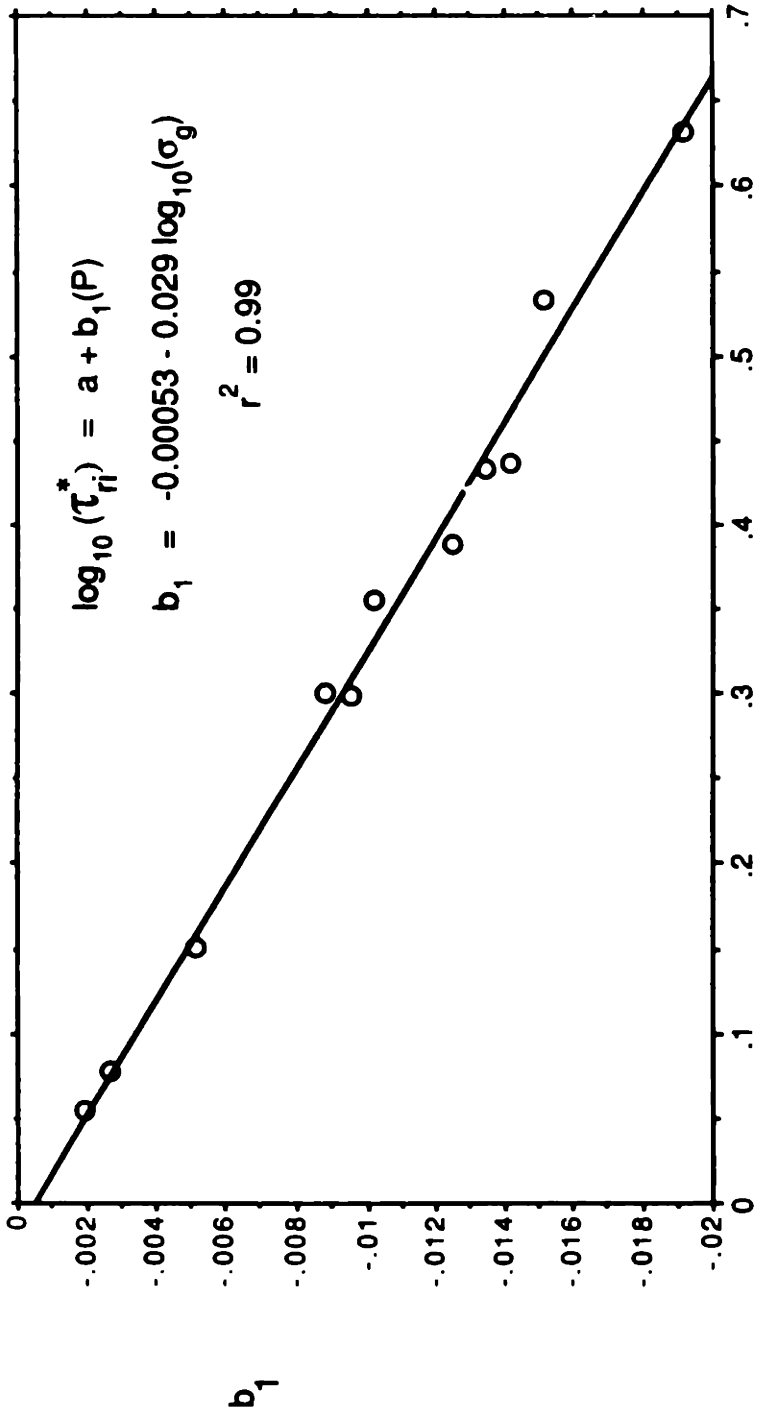

Figure 3.10. τ^*_{ri} — P slopes b_1 as a function of mixture sorting

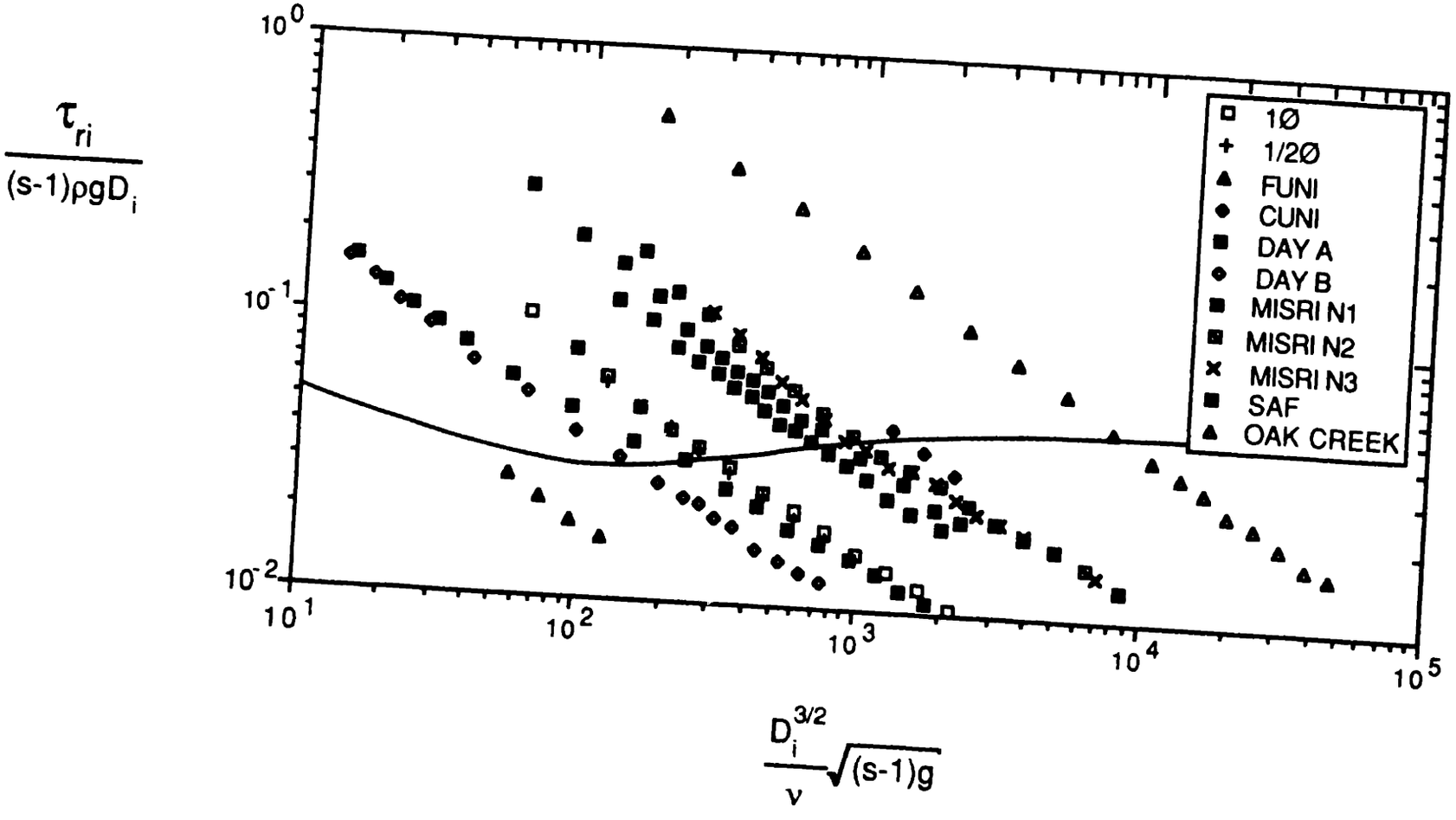

Figure 3.11. τ^*_{ri} as a function of S^* for all fractions and sediments

sediment mixtures are broadly distributed across the figure and extend to varying degrees into the transitionally rough and smooth turbulent ranges, the form of the τ^*_{ri} plots (in this case, as functions of $D_i^{-3/2}$) are remarkably consistent. The consistent trends in Figures 3.7, 3.8, and 3.11 are an important result that is independent of methodological problems. When the best available data on mixed-size sediment transport are combined into the same reference-transport analysis, there is virtually no variation in the relative-size effect on τ^*_{ri}, even though flow and sediment conditions vary from mixture to mixture. Although there are far from enough data to support an absolute and general conclusion, the consistency evident in these figures suggests that the relative-size effect on the initial motion of individual fractions is dominant and consistent for a broad range of flows and sediments.

An additional important result is that the slopes of the τ^*_{ri} — D_i/D_{50} relations all fall in the vicinity of the special value -1.0, although to some extent this depends on the use of the PKM reference-transport criterion. Other reference-transport criteria produce slightly different relations, to be discussed in a later section of this chapter. Using the PKM reference-transport criterion, six of the eleven sediments have slopes not significantly different from -1.0 at a 95% confidence level. Of the remaining five, two have slopes actually smaller than -1.0. Of the three that have slopes greater than -1.0, only sediment A of Day (1980a) has a value of β considerably different from -1.0 (Table 3.3). This is also the only sediment for which no points fall close to W^*_r, making it the least certain of the sets of τ^*_{ri} values. A τ^*_{ri} — D_i/D_{50} slope of -1.0 means that all fractions in the mixture cross the reference-transport level at the same dimensional bed shear stress τ_o. If the reference transport rate is analogous to the critical shear stress for each fraction, a slope of -1.0 signifies that all fractions begin moving — at least, at any appreciable transport rate — at the same dimensional bed shear stress. If this is so, the relative-grain-size effect exactly balances the absolute-grain-size effect on the critical shear stress. This is the result PKM found using their reference-transport criterion on the Oak Creek data, which they termed the

equal-mobility hypothesis. The trends in Figures 3.7 and 3.8 suggest that this result may not be particular to that stream, but may have a broader application for equilibrium transport by steady, uniform flows.

The cause of the size independence of τ_{ri} in the data examined here is worth considering. Parker and Klingeman (1982) point out that equal mobility is the natural state towards which equilibrium transporting systems evolve, although this is in fact true only for transporting systems in which the mixed-size transport rate is *imposed* on the system (sediment-feed flumes and perhaps some rivers, including Oak Creek). In these cases, the slope and grain-size distribution of the bed surface must become adjusted to an equilibrium state of equal transportability of all fractions imposed on the system. All of the data used here, however, with the exception of Oak Creek, involved recirculation of the transported sediment. There is no apparent reason why all fractions should be equally transportable in a recirculating, equilibrium transport system. For example, some fractions could simply be immobile at bed shear stresses for which other fractions are in motion. Equal mobility in a recirculating system is an empirical result that happens to be the same as when the fractional transport rates are imposed on the system; it is both important and convenient that recirculating transport systems appear to have the same initial-motion relations that are a requirement for sediment-feed systems. Natural rivers contain aspects of both systems to a degree that is not entirely understood, but depends to some extent on the time and space scales appropriate to a given problem. The modeling of mixed-size sediment transport in natural situations is considerably simplified if initial-motion conditions are similar for both types of transport systems.

Equal-mobility conditions in both types of system result from two processes. The first is the direct effect of relative grain size on the mobility of the various fractions in the mixture. The second is a natural sorting process in which the bed surface becomes coarser, making the larger grains proportionately more exposed to the flow and thus more available for movement. This sorting occurs simply because finer grains can fall into positions vacated

by coarser grains, while coarser grains do not fit into positions vacated by finer grains. With time this process can lead to a vertical size segregation at the bed surface and an increase in the transportability of the coarser grains. This is a natural process with a simple, geometric cause. In combination with other relative-size effects, the bed-surface sorting contributes to what is apparently a fairly consistent relation between the reference shear stress and the relative grain size.

CONTROLS ON τ^*_{r50}

Although the relative-size effect on τ^*_{ri} is well described by only one of D_i/D_{50} or percent finer than, there is also variation in the absolute values of τ^*_{ri}, as shown by the separation of the fractional plots in Figure 3.11. Because the τ^*_{ri} — D_i/D_{50} curves are quite consistent in form, this displacement can be approximated by the position of only one value of τ^*_{ri} for each mixture. Figure 3.12 presents the reference shear stresses for D_{35}, D_{50}, and D_{65} in each mixture as a function of S^*; the Shields curve is also plotted. The reference shear stresses corresponding to D_{50} give the closest fit to the Shields curve. Except for one point (SAF), all of these data fall within a factor of 1.4 of the Shields curve, which is the approximate width of data scatter typically found in equivalent uni-size plots, including the original diagram by Shields (1936). Except for two points (SAF and Misri N1), the scatter in the D_{50} points is actually considerably less; these points also follow the trend of the Shields curve reasonably closely, and fall mainly below the Shields curve. That these results are slightly and consistently different from the Shields curve is not surprising, in that the method used here to estimate the reference shear stress is different from that used by Shields (1936). It has often been noted (e.g. Taylor and Vanoni, 1972) that the Shields curve frequently corresponds to a finite transport rate in uni-size sediments This transport rate is presumably somewhat different from the $W^*_i = 0.002$ criterion used here. The reason why two points (representing the SAF and Misri N1 mixtures) fall well outside the trend defined by the others could not be determined, but is apparently not a

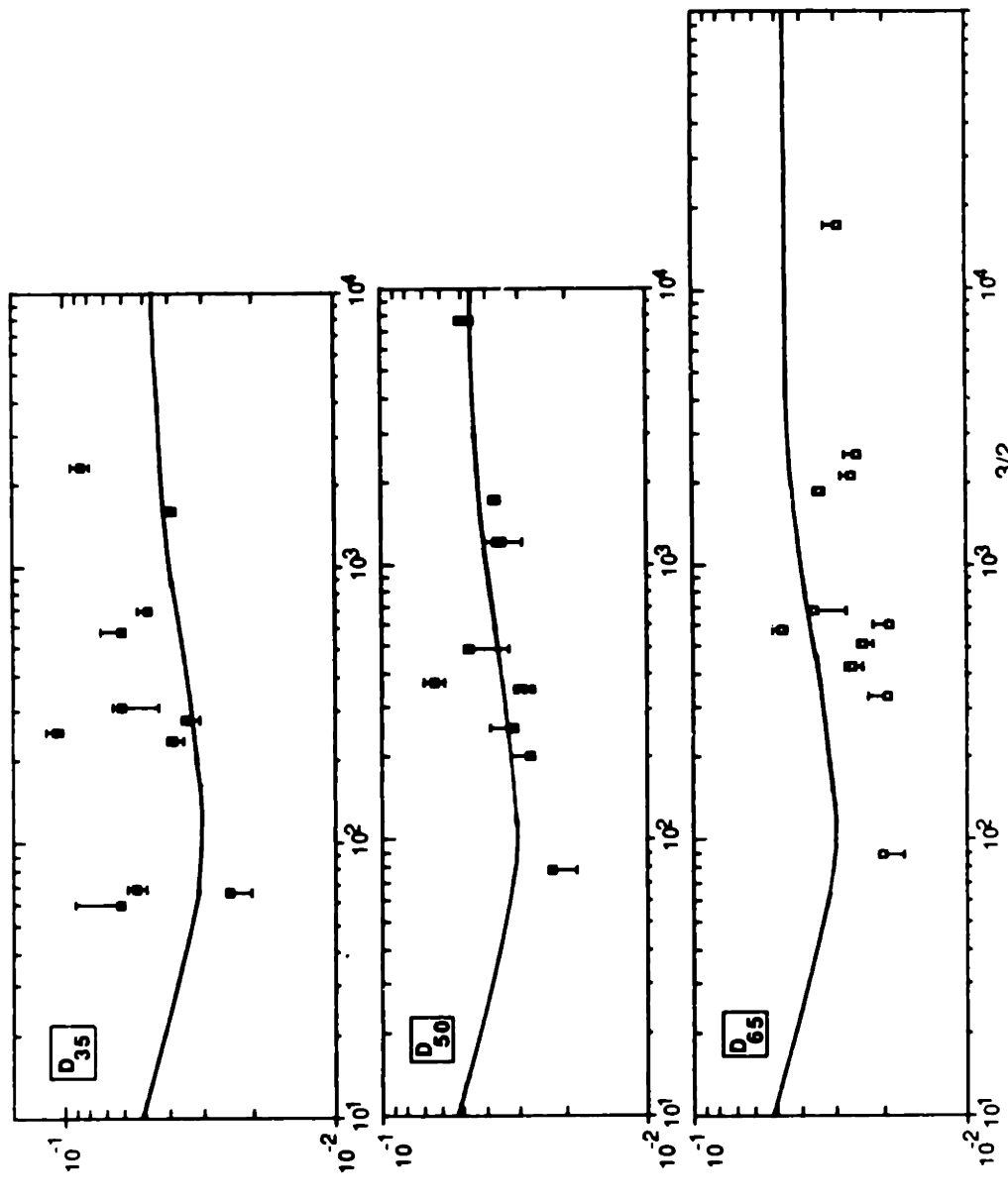

Figure 3.12. τ^*_{ri} as a function of S^* for D_{35}, D_{50}, and D_{65} and all sediments

function of D_{50}, size-distribution sorting or shape, relative depth, grain shape or density, or grain Reynolds number. If the two outlying points are ignored, the trend of the remaining points in Figure 3.12 could be described reasonably well by either a slightly lower position (≈12%) of the Shields curve or by a simple loglinear trend between τ^*_{r50} and S^*. The choice of a loglinear trend depends primarily on only the two extreme points on Figure 3.12 (representing FUNI and Oak Creek), and could simply be the result of data scatter.

τ^*_{ri} FITTED WITH OTHER REFERENCE-TRANSPORT CRITERIA

Plots of τ^*_{ri} — D_i/D_{50} made with τ^*_{ri} computed with our reference-transport approximations of the Neill/Yalin and Yalin initial-motion criteria (Equations 10 and 11) are similar to those of Figures 3.7 and 3.8, although the plots for some sediments show a slight concave-upward curvature. The exponents β in $\tau^*_{ri} = \alpha(D_i/D_{50})^\beta$ are slightly greater than the PKM results. These are shown in Figure 3.13 for the PKM, Neill/Yalin, and Yalin criteria. Error limits on the fitted slopes at a 95% confidence interval are shown for the PKM fit; error bars for the other two are virtually the same and are omitted for clarity. The decrease in β is large enough that the β values for seven of the eleven mixtures are significantly different from -1.0 with the Neill and Yalin criterion; nine are significantly different from -1.0 with the Yalin technique. One of the remaining (FUNI) is not significantly different from -1.0 only because it has an unusually large error bar.

The Ackers and White reference-transport criterion produces reference shear stresses that are somewhat more different from the PKM values than those from Neill/Yalin and Yalin criteria. Because the AW transport model directly incorporates parameters not in the PKM model, the reference shear stresses from each method may be compared only approximately. If one assumes that the sediment bed is planar at incipient motion, so that the total bed shear stress and skin-friction shear stress (computed with the AW model) are equal, the square of the AW reference shear stress parameter A' may be taken to be equal to τ^*_{ri}. The square of the A' values fitted by Day (1980b) to

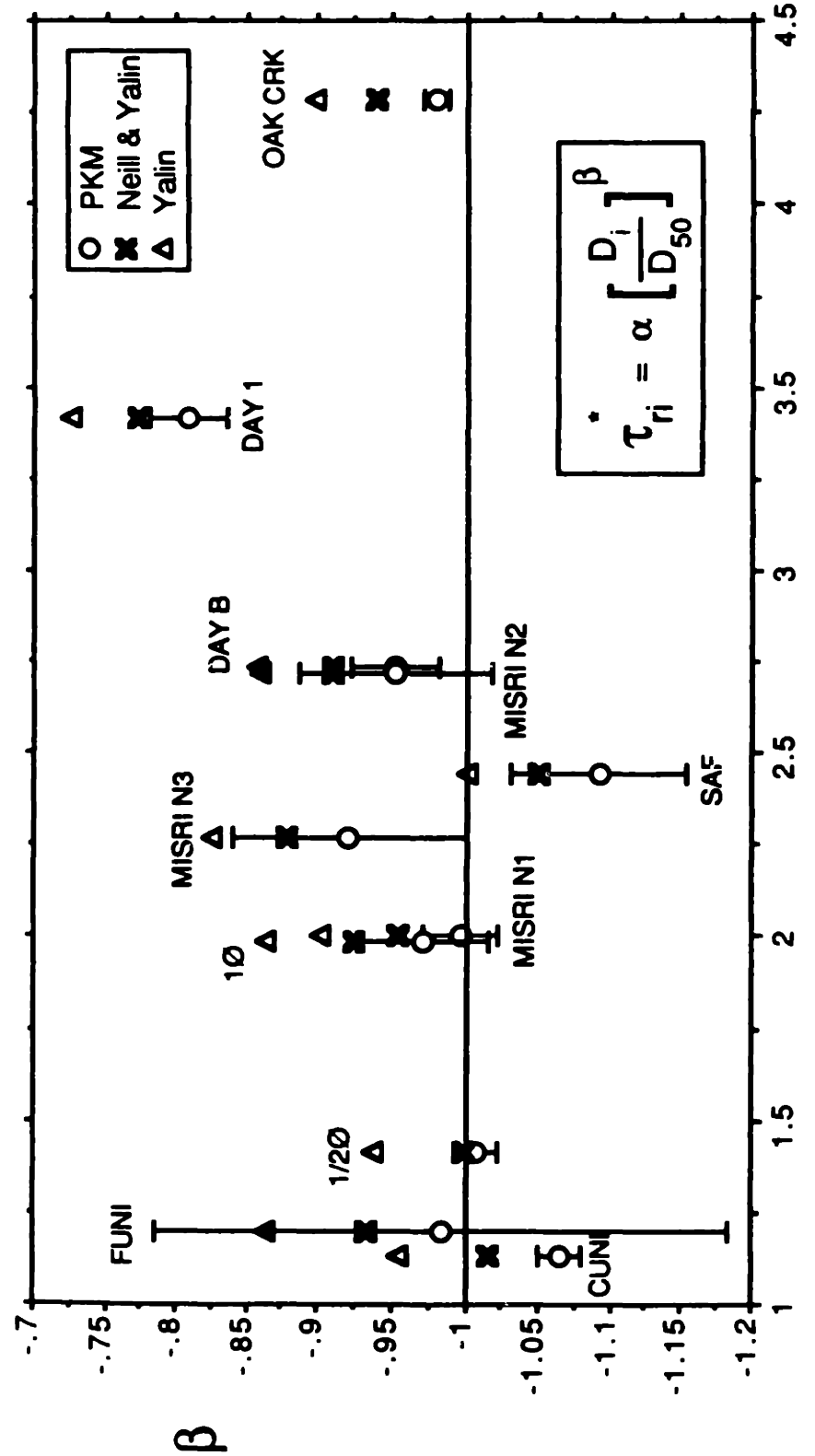

Figure 3.13. Exponent β from $\tau^*_{ri} = \alpha(D_i/D_{50})^{\beta}$ as a function of geometric standard deviation for all sediments and three reference-transport criteria

his data are given in Figure 3.14 as a plot of τ^*_{ri} against D_i/D_{50}. For comparison the PKM values of τ^*_{ri} for the same data are also plotted. The $(A')^2$ values for Bed A are distinctly curved and gentler in slope than the PKM fit (straight-line slopes of -0.56 and -0.81). The $(A')^2$ values for Bed B are more nearly loglinear, although still gentler in slope than the PKM fit (slopes of -0.84 and -0.96). It is worth recalling that the transport data for Bed A of Day (1980a) had very few values near the PKM reference-transport value of $W^*_i = 0.002$, making the τ^*_{ri} values for this mixture the least certain of all those fitted. Because the AW reference-transport criterion falls considerably above the PKM criterion, transport rates for both beds of Day (1980a) extend to the AW reference-transport criterion.

CONCLUSIONS

METHODOLOGY

There are two general methods for determining the critical shear stress for individual fractions in mixed-size sediment. One associates the critical shear stress with the largest grain in the mixture that can be moved by a given flow. The other approximates the critical shear stress as that shear stress that produces a certain small transport rate of a given fraction. In principle, the two classes of methods should give identical results except for the special case in which all fractions begin moving at the same bed shear stress. In practice, the two methods do not give the same results, partly because of sampling and scaling problems associated with the largest-grain method and partly because a general and properly scaled reference-transport criterion has not been developed.

Because the same data can only seldom be analyzed with both initial-motion methods, there is little basis for comparing results from the two methods. Although the results are not comparable, the nature of the differences can be understood in terms of the difficult scaling problems associated with measuring initial-motion conditions for individual fractions in mixed-size

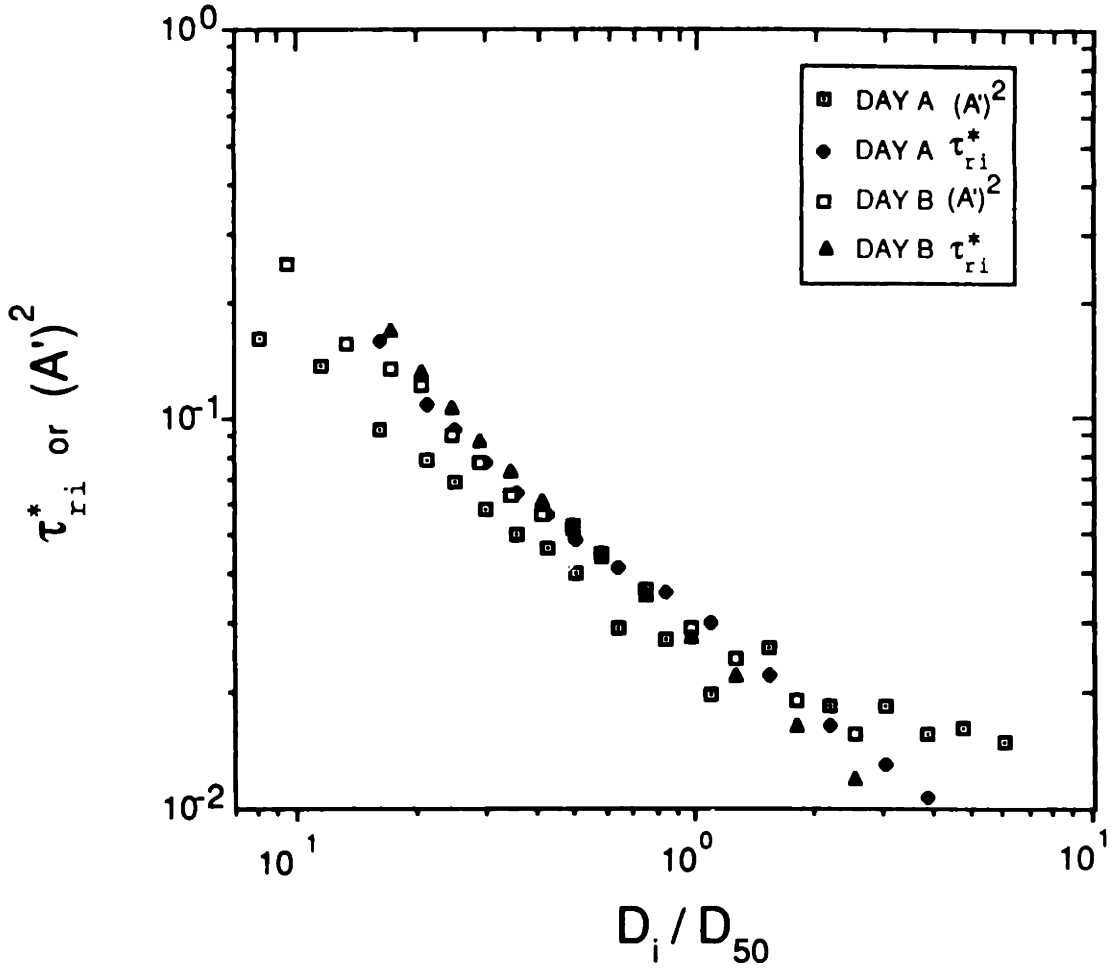

Figure 3.14. Initial-motion results for data of Day (1980a) using the Ackers/White (1971; A') and Parker et al. (1982; τ^*_{ri}) reference-transport criteria

sediment. This understanding is important, because it suggests that there is little basis for concluding that initial-motion relations determined for one sediment with one method reflect a truly different physical situation when compared with initial-motion relations determined for a different sediment with the other method. The methodological influence on initial-motion results is well illustrated by the one known case for which identical data may be analyzed with both methods.

The practical considerations involved in determining initial motion for mixed-size sediment suggest strongly that the reference-transport method is preferable to the largest-grain method. Unfortunately, a generally accepted and properly scaled reference-transport criterion is not now available. Such a criterion is definable but requires an unknown relationship between the size and excursion length of grains in individual fractions, so that an initial-motion criterion can be converted to a transport rate. Existing reference-transport criteria are necessarily arbitrary and tied to a particular dimensionless transport variable. We have demonstrated that different reference-transport criteria produce different initial-motion results, with the clear implication that models of mixed-size sediment transport that use a particular dimensionless transport-rate parameter must also use a reference value of the same transport-rate parameter in determining the reference shear stress for each fraction.

Even if a reference-transport criterion and a largest-grain criterion could be derived from the same general initial-motion criterion, and properly scaled measurements were made with each method, the initial-motion results would still be considerably different for cases where all sizes begin moving at nearly the same bed shear stress. In these cases, the largest grain in the mixture would be present in most, if not all, of the largest-grain samples, and would give a vertical τ^*_{ci} — D_i/D_{50} relation that would be perpendicular to the reference-transport relation. Transport data from western U.S. rivers (Milhous, 1973, Andrews, 1983; Andrews and Erdman, 1986) and the experimental

transport data discussed in this paper show transport conditions to be close to equal mobility and suggest that these conditions may be relatively common.

INITIAL-MOTION RESULTS

An explicit experimental test was made of the effect of mixture sorting on the initial motion of individual fractions in a size mixture. Using two sediments in which the mixture sorting was the only flow or sediment parameter varied, we found that the reference shear stress — a critical shear stress analogue — is independent of mixture sorting if the effect of D_i/D_{50} is accounted for. This result was also found in experiments with sediments for which the mean size varied by a factor of 8 and the sorting varied from 0.2 Ø to 1.0 Ø. We can therefore hypothesize that mixture sorting has little effect on initial motion in other types of sediment mixtures as well. This hypothesis is supported by τ^*_{ri} — D_i/D_{50} trends in data from other sources that are essentially similar to our results. Mean grain size, sorting, and size-distribution shape for all the data examined in this chapter vary over a broad range, yet the form of the τ^*_{ri} — D_i/D_{50} trends show no dependence on sorting. In all of these cases, only one of the relative-grain-size parameters (D_i/D_{50} or percent finer than) is necessary for modeling the initial motion of individual fractions in mixed-size sediment. Of these, D_i/D_{50} is preferable because the variation of τ^*_{ri} with D_i/D_{50} is quite simple and because physical conclusions may be drawn directly from the relation.

The strong similarity in initial-motion conditions for a variety of different sediments and flows is an important physical (as opposed to methodological) conclusion. Very consistent, and surprisingly simple, initial-motion relations can be defined for eleven different sediments with a variety of grain-size distribution shapes and sorting values from 0.19 Ø to 2.1 Ø, a range that includes most natural sediments. These relations are also consistent with existing relations for the limiting case of uni-size sediment. This suggests that the initial-motion relations shown here (and the reference-transport methodology used to determine τ^*_{ri}) may be generally valid. Such a conclusion

is supported not only by a general empirical argument based on the consistent initial-motion results for eleven different sediment mixtures, but also by our controlled demonstration that mixture sorting has little effect on fractional initial-motion conditions, once the relative size of each fraction is described by D_i/D_{50}. If the mixture sorting, which has a clear influence on the percentile position of a given fraction in a mixture (Figure 1.1), has little demonstrated effect on fractional initial-motion conditions, it can be hypothesized that other grain-size parameters may have little effect as well. If so, initial-motion relations for individual fractions in most natural sediment mixtures may be adequately described by two general functions, one involving only the size ratio of each fraction and the other the median size of the sediment mixture.

The actual form of the τ^*_{ri} — D_i/D_{50} relations depends on the reference-transport method used. Other reference-transport criteria produce τ^*_{ri} — D_i/D_{50} relations slightly gentler in slope and, in some cases, somewhat more curved than those produced using the PKM reference-transport criterion. With the reference-transport criterion of Parker et al. (1982), the slope of τ_{ri} — D_i/D_{50} curves for all sediments examined here varies closely about the condition of equal mobility (no dependence of τ_{ri} on D_i). Although equal mobility is a necessary condition for equilibrium transporting systems which must carry an imposed mixed-size sediment transport rate (feed systems), all of the experimental data examined here are from recirculating systems, for which equal mobility is not a requirement for steady-state transport. Because natural transporting systems exhibit — to an unknown degree — features of both recirculating and sediment-feed transport conditions, it is an important and convenient result that recirculating systems appear to produce initial-motion conditions that are similar to those necessary for a feed system.

CHAPTER 4

ESTABLISHED MOTION

INTRODUCTION

This chapter examines the second part of the mixed-size sediment transport problem: the form of the relations between transport rate and shear stress (hereafter termed transport functions) for individual fractions in sediment mixtures. Once the shear stress necessary to initiate grain motion is exceeded, how does the transport rate vary with bed shear stress, and how does the form of this relation vary with relative size? With the recent exceptions of Parker et al. (1982) and Diplas (1987), mixed-size sediment transport models have incorporated the relative-size effect only with respect to conditions for initial motion. That is, once the shear stress is expressed as the excess above that necessary to initiate motion, the same transport function is assumed to hold for each fraction in the mixture. The goal of this chapter is to investigate what effect, if any, relative grain size has on the form of transport functions for individual fractions in our experimental mixtures. As in the previous chapter, the sediment mixtures used in the transport experiments allow us not only to examine the effect of D_i/D_m on fractional transport rates, but also to isolate the effect of percentile position in the mixture (or mixture sorting) on the transport rates of individual size fractions (and values of D_i/D_m).

The motivation for examining the relative-size effect on the form of the fractional transport functions is the same as that for examining the relative-size effect on the initial motion of individual fractions. In the preceding chapter, it was demonstrated that the relative size of a fraction has a strong effect on the reference shear stress for that fraction. This arises from the variation in flow exposure and bed roughness with relative grain size and is sufficiently strong that it apparently balances the effect of differential grain mass among the fractions of a mixture, so that all fractions begin moving at close to the same bed shear stress. The relative-size effect on fractional

transport rates is present, however, not only near initial-motion conditions but throughout the transport function of each fraction. This is evident in Figure 3.6, which shows that the fractional transport rates W^*_i of the 1Ø mixture are comparable at all flow strengths, even though the values of τ^*_i are separated by a factor of $1/D_i$. If there were no relative-size effect on fractional transport rates (that is, if the data in Figure 3.6 represented five different uni-size sediments of a grain size equivalent to those in the figure), the transport rates of each fraction would fall much closer to a single curve. The transport functions would be separated only by a relatively small Reynolds-number effect on the critical shear stress, such as shown by the uni-size Shields curve in Figure 3.11. The equivalence in fractional transport rates was in fact the predominant (and necessary) condition that produced the equal mobility (grain-size independence) of the reference shear stresses presented in the preceding chapter. If relative grain size can produce such a substantial translation of the transport function for each fraction, it is natural to examine whether relative grain size also influences the form of the transport function.

TOTAL TRANSPORT RATES

The fractional transport rate is computed as the product of the total transport rate and the proportion of each fraction in transport. The fractional transport rates for a given mixture and flow strength are the product of the total transport rate and the grain-size distribution of the transported sediment. In this thesis, the transported sediment is that sediment caught in the sediment trap over a period of time. This is distinct from the instantaneous sediment concentration, which, when multiplied by the mean velocity of each fraction, gives the transport yield that we sampled. Size-mixture effects on the fractional transport rates may be profitably examined in terms of both components of the fractional transport rate. The effect of mixture sorting on the total transport rates will be examined here; the effect of the relative size (D_i/D_m and percent finer than) on the grain-size distribution of the transported sediment will be examined in a later section.

Figure 4.1 presents the total transport rates for all five sediments in terms of W^* and the Shields parameter τ^*_m based on the mean grain size. The axes in Figure 4.1 are plotted with very different scales, as are all other plots of transport rate as a function of shear stress in this chapter. Transport rates in our experiments vary by three to five orders of magnitude, while the bed shear stress varies less than one order of magnitude. The focus of this chapter is the effect of relative grain size on the form of the fractional transport functions; any differences that may exist between different functions would not be observable if the same scale were used for both transport and shear stress axes.

The total transport rates for the fine and coarse well sorted mixtures (FUNI and CUNI) in Figure 4.1 are somewhat different from those for the three sediments with the same mean size and variable sorting (MUNI, 1/2Ø, and 1Ø, which will be termed here the 1.83 mm sediments). The differences are a function of both a difference in reference shear stress and a difference in the form of the transport function. The reference-shear-stress effect is eliminated in Figure 4.2, which shows W^* as a function of τ^*_m/τ^*_r, where τ^*_r is determined for the total transport rate. Figure 4.2 makes the different form of the transport function among FUNI, CUNI, and 1.83 mm sediments more apparent. There is a progressive decrease in the curvature of the transport function with increasing grain size. The FUNI mixture is clearly the most curved, with a steeper $W^* - \tau^*_m/\tau^*_r$ relation at lower transport rates and a relatively abrupt transition to a nearly horizontal $W^* - \tau^*_m/\tau^*_r$ relation above a W^* of around 1.0. The transport functions for the 1.83 mm sediments are relatively less curved, and the transport function for CUNI is nearly loglinear. Because FUNI, MUNI, and CUNI all have the same mixture sorting, the differences between the three classes of transport functions is apparently a result of the absolute grain size of the sediment mixture rather than other size properties of the sediments.

There is remarkably little difference in the total transport function among the three 1.83 mm sediments, despite a variation in sorting from 0.20 Ø to 0.99 Ø. Because mixture sorting is the only parameter that varies among

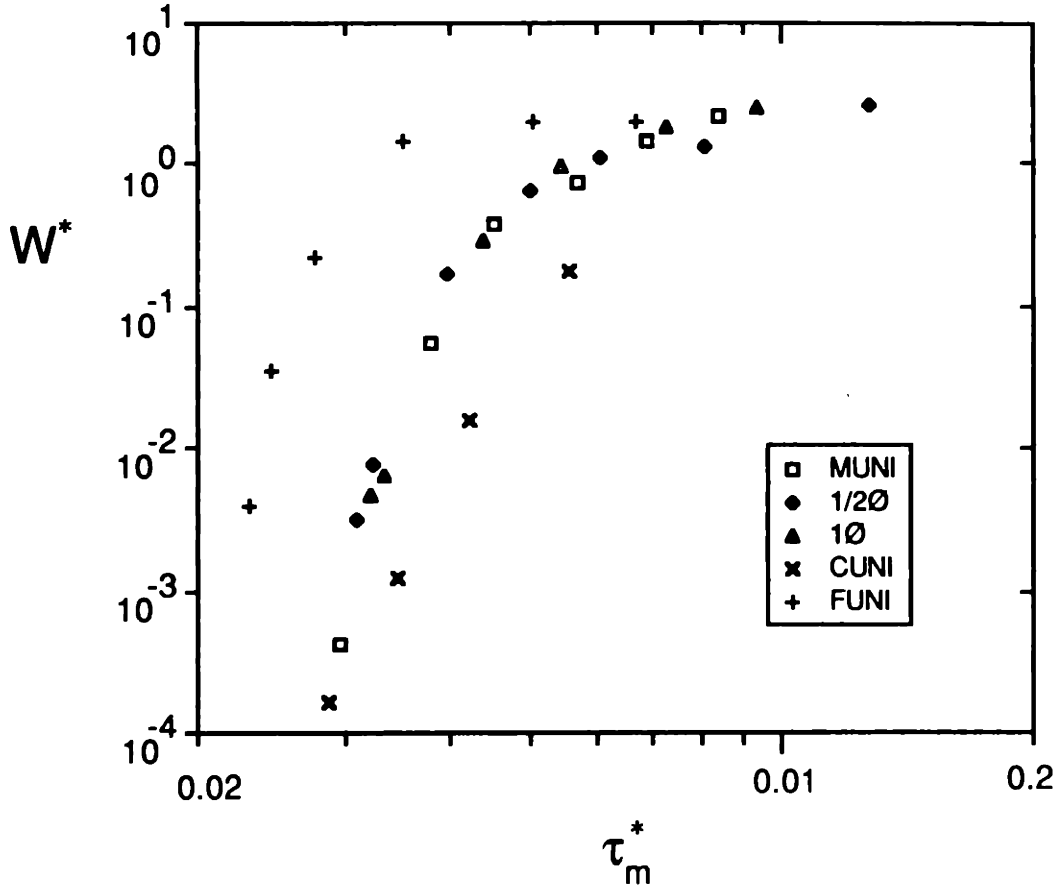

Figure 4.1. Total transport rates for MIT sediments: W* as a function of τ_m^*

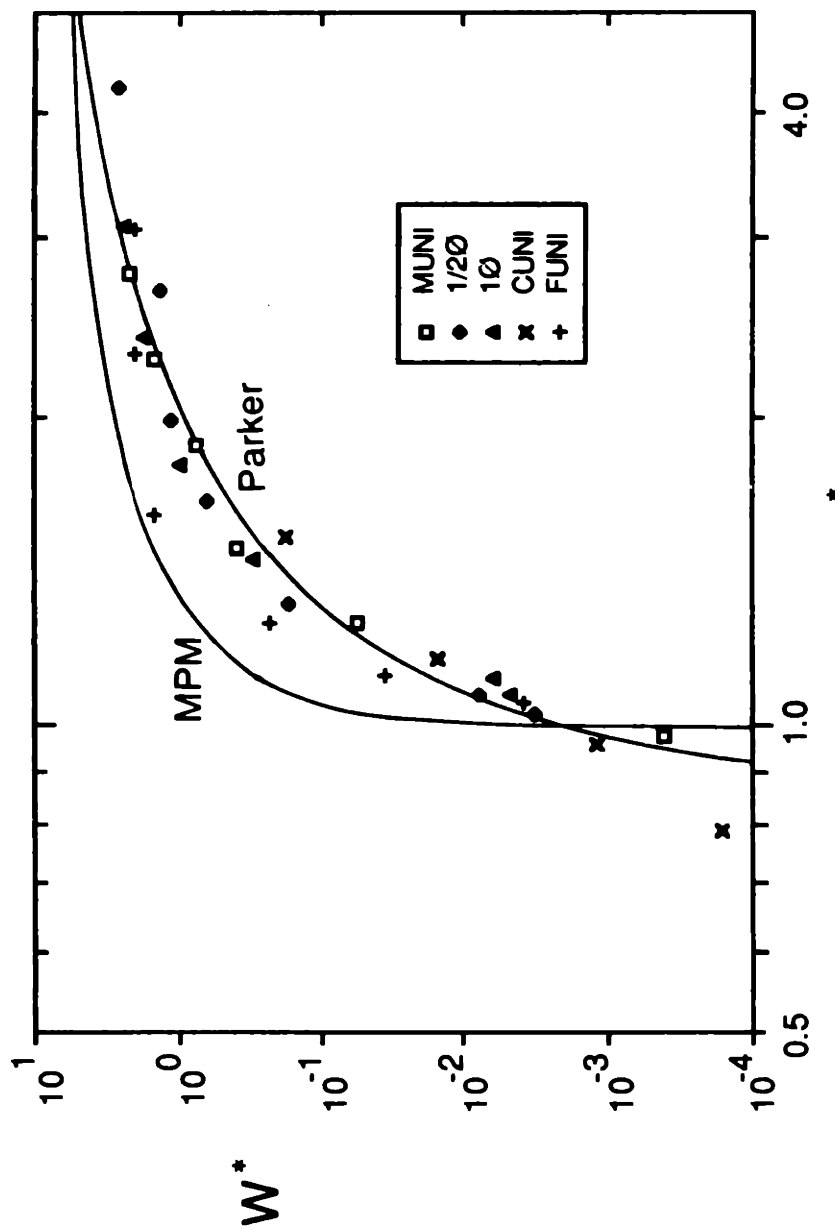

Figure 4.2. Total transport rates for all MIT sediments: W* as a function of τ^*_m/τ^*_r

these three mixtures, it is apparent that mixture sorting has little effect on the form of the total transport function. The similarity of the transport functions for the 1.83 mm sediments also suggests that the mean (or median) grain size does a satisfactory job of representing the total transport rate for these mixed-size sediments. Total-transport models for mixed-size sediment that use an alternative grain size for representing the total transport rate (e.g. D_{65}) would not give satisfactory results for these transport rates. Because the sorting varies among the 1.83 mm sediments, the grain size of a particular percentile position in these sediments diverges as the percentile becomes different from the median. Because D_i is present in τ^*, a grain size much different from D_{50} would cause an equivalent divergence in the total transport functions of these sediments. D_{65} for the 1Ø mixture is 22% greater than D_{65} for MUNI, a shear-stress differential that would produce a transport rate roughly 25 times lower for the MUNI mixture at conditions near incipient motion.

FRACTIONAL TRANSPORT RATES

The fractional transport rates for our experiments are given in Figures 4.3, 4.4, 4.5, and 4.6 for the 1/2Ø, 1Ø, FUNI, and CUNI sediments. The grain-size distribution of the transport was not determined for the MUNI sediment. Because the FUNI and CUNI transport grain-size distributions are nearly identical (as will be discussed below) and have nearly the same sorting and similar shape of grain-size distribution as MUNI, it is probable that a plot of the MUNI transport grain-size distribution would be much like those for FUNI and CUNI.

The line plots in these figures are presented in two different forms, although the actual data points are identical in each form. In Part a of Figures 4.3 through 4.6, lines connect the fractional transport rates for each fraction. To allow a visualization of the grain-size distribution of the transported sediment for each run, the lines in Part b of these figures connect the fractional transport rates of all the fractions for each run. Because the transport rate q_b

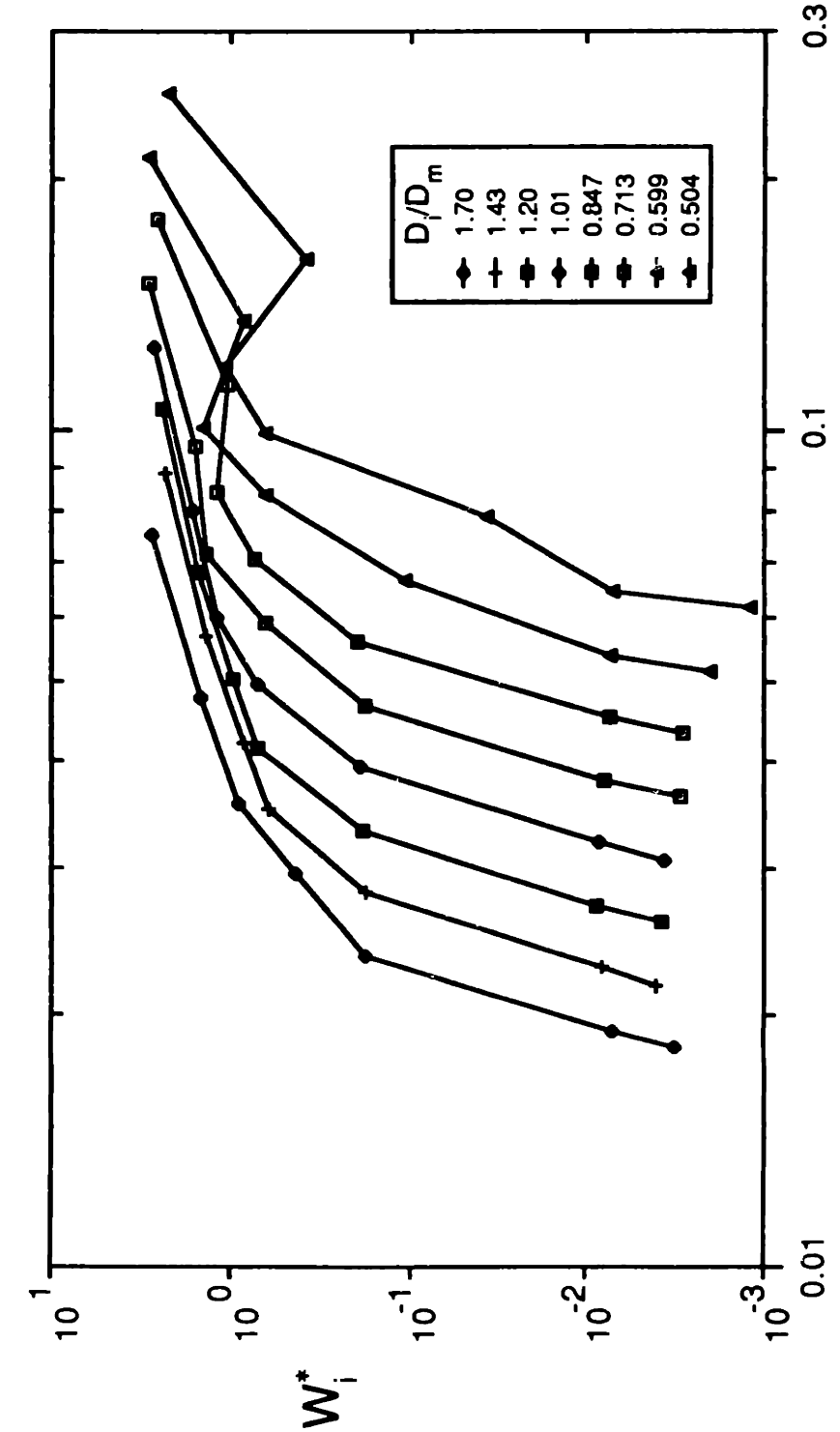

Figure 4.3.a. Fractional transport rates for the 1/2Ø mixture: W_i^* as a function of τ_i^*
(Lines connect transport rates of each fraction for all runs)

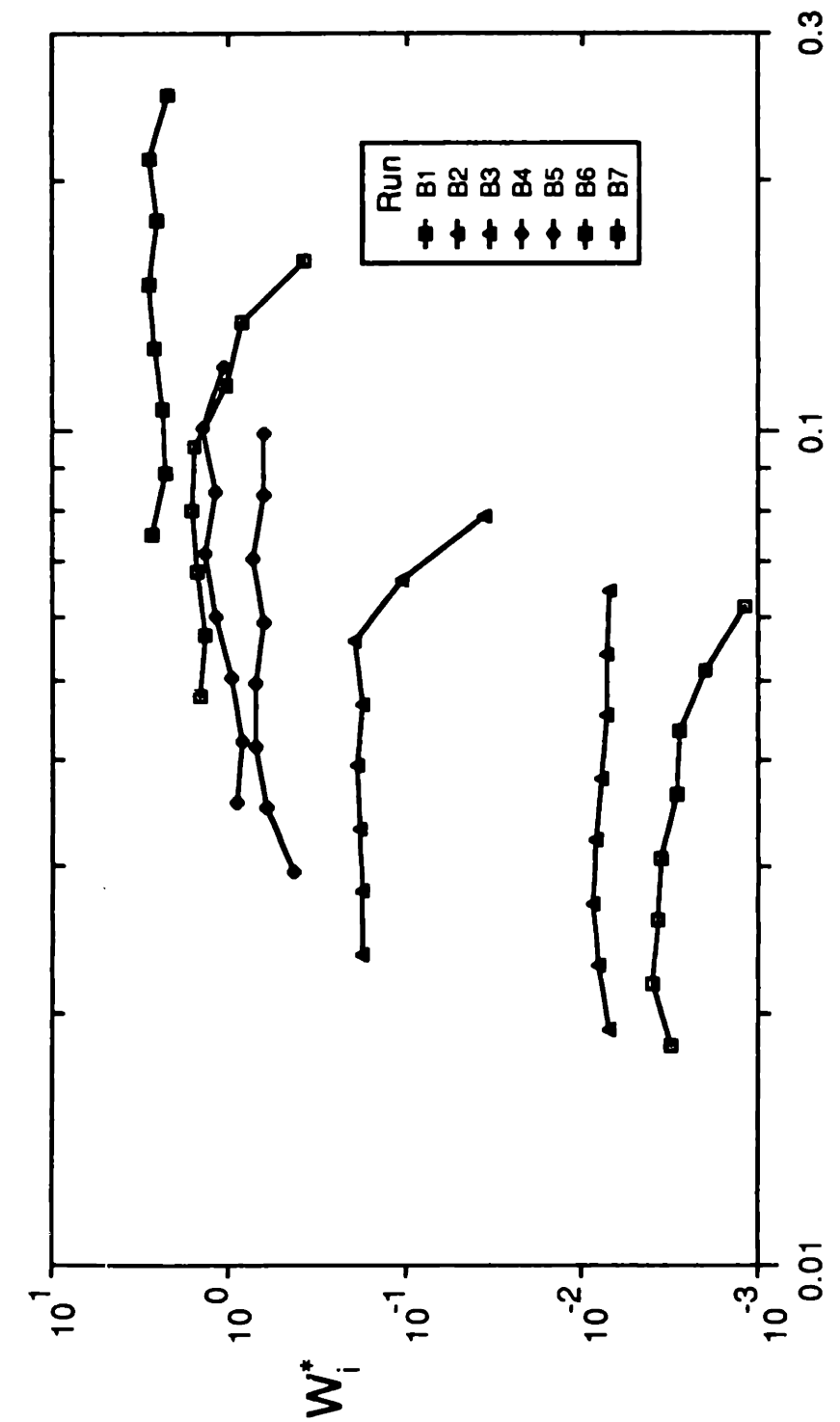

Figure 4.3.b. Fractional transport rates for the 1/2Ø mixture: W_i^* as a function of τ_i^* (lines connect transport rates of every fraction for each run, showing p_i/f_i as a function of $1/D_i$)

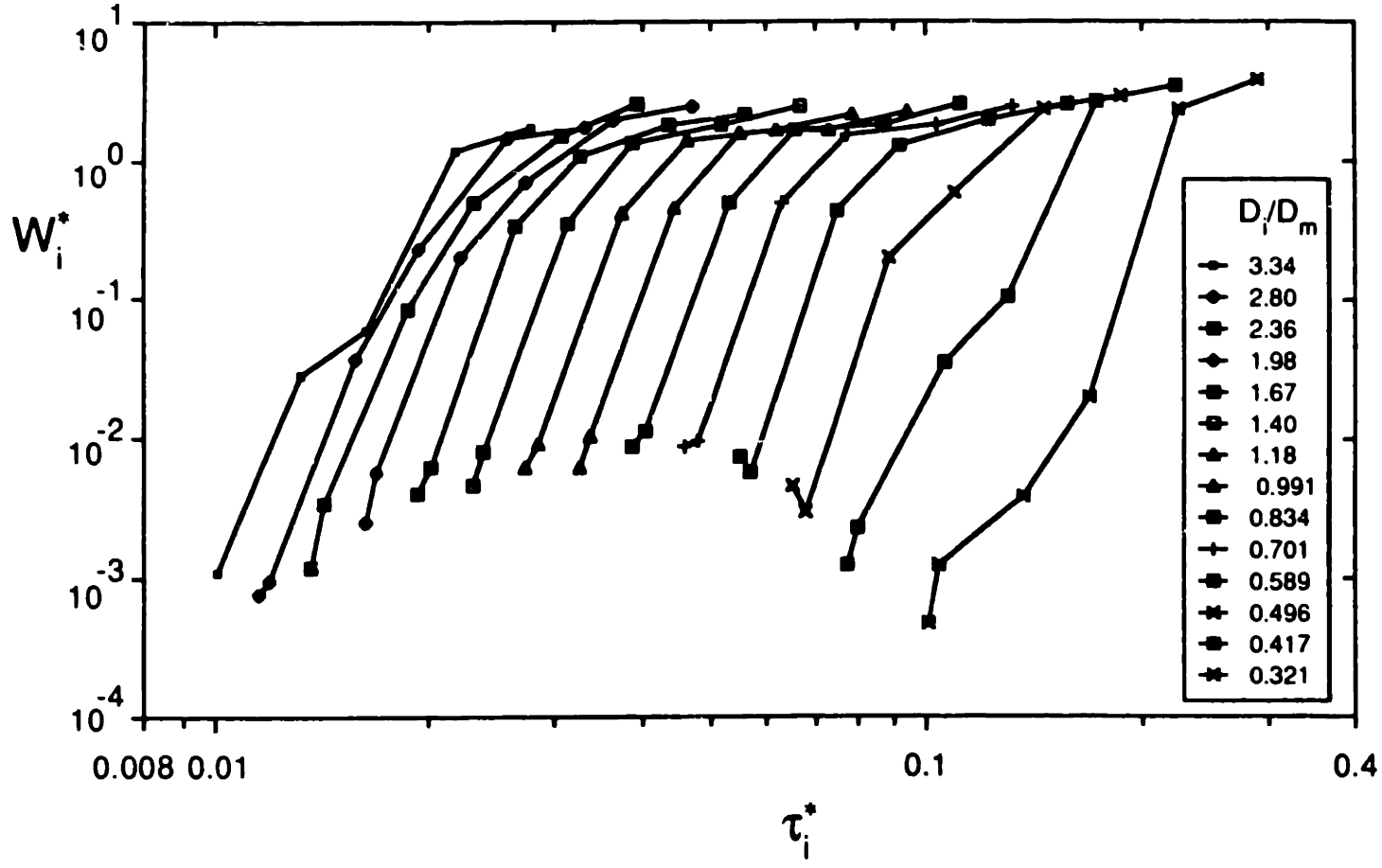

Figure 4.4.a. Fractional transport rates for the 1Ø mixture: W_i^* as a function of τ_i^*
(Lines connect transport rates of each fraction for all runs)

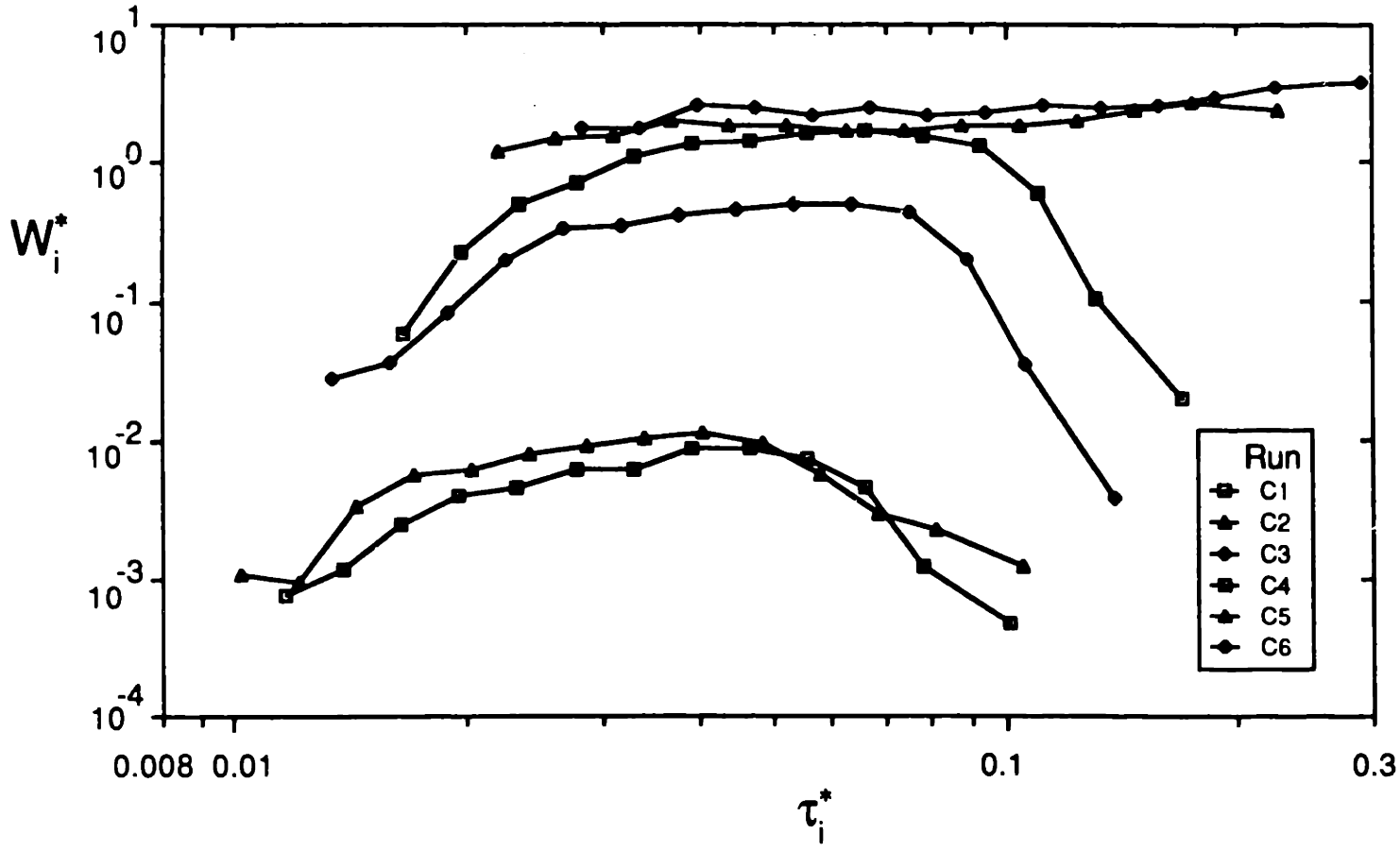

Figure 4.4.b. Fractional transport rates for the 1Ø mixture: W_i^* as a function of τ_i^* (lines connect transport rates of every fraction for each run, showing p_i/f_i as a function of $1/D_i$)

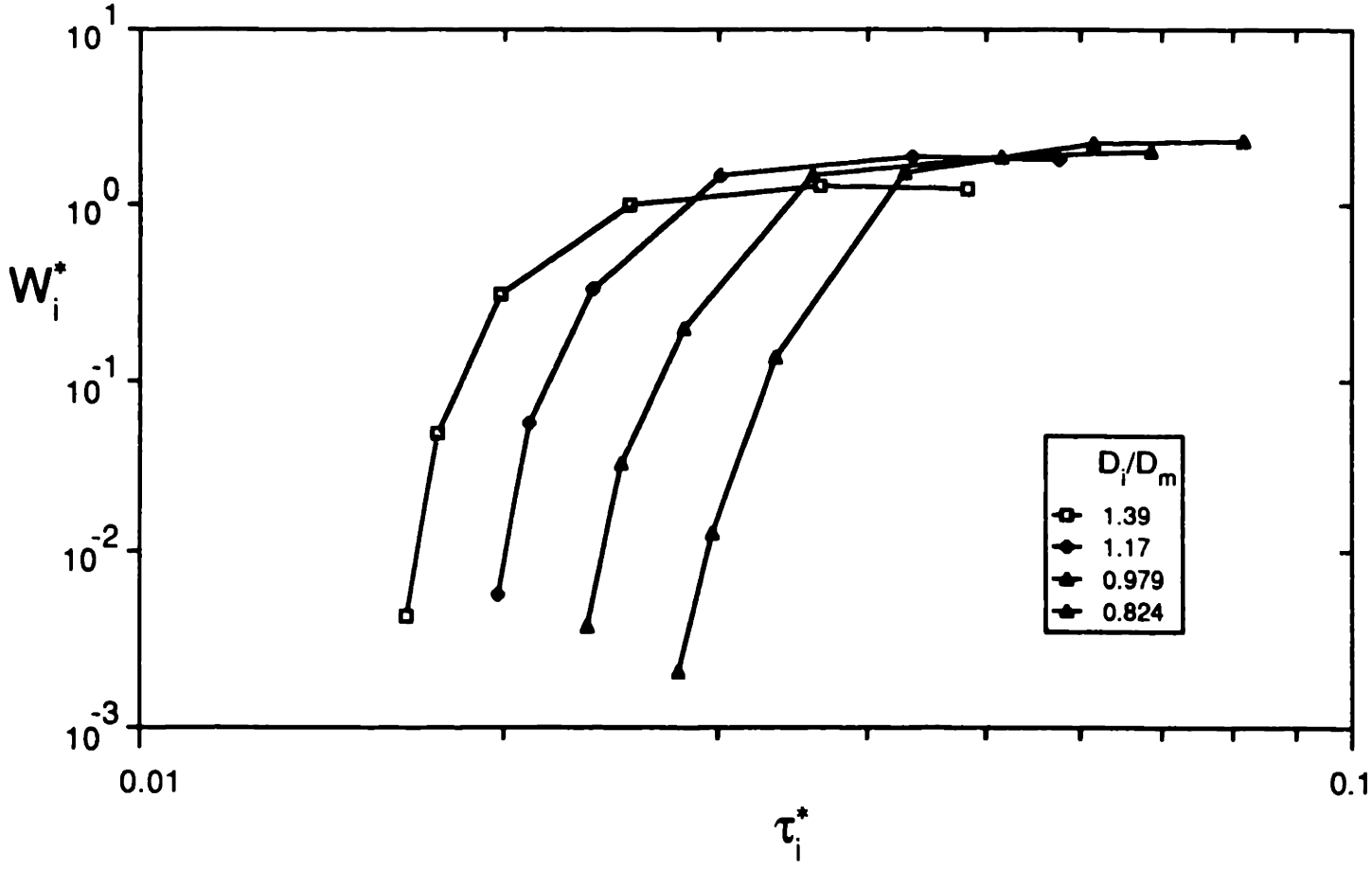

Figure 4.5.a. Fractional transport rates for the FUNI mixture: W_i^* as a function of τ_i^*
(Lines connect transport rates of each fraction for all runs)

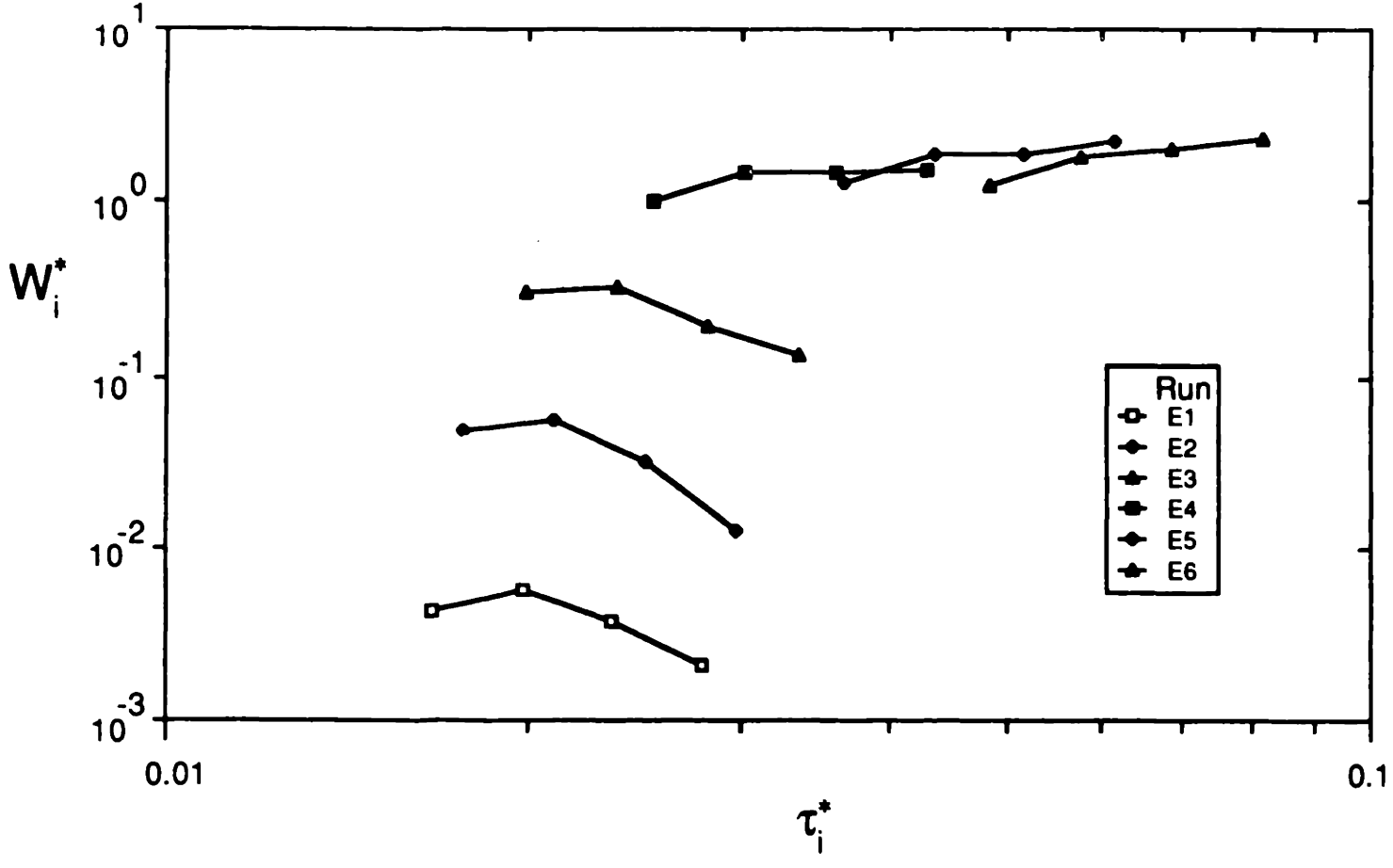

Figure 4.5.b. Fractional transport rates for the FUNI mixture: W_i^* as a function of τ_i^* (lines connect transport rates of every fraction for each run, showing p_i/f_i as a function of $1/D_i$)

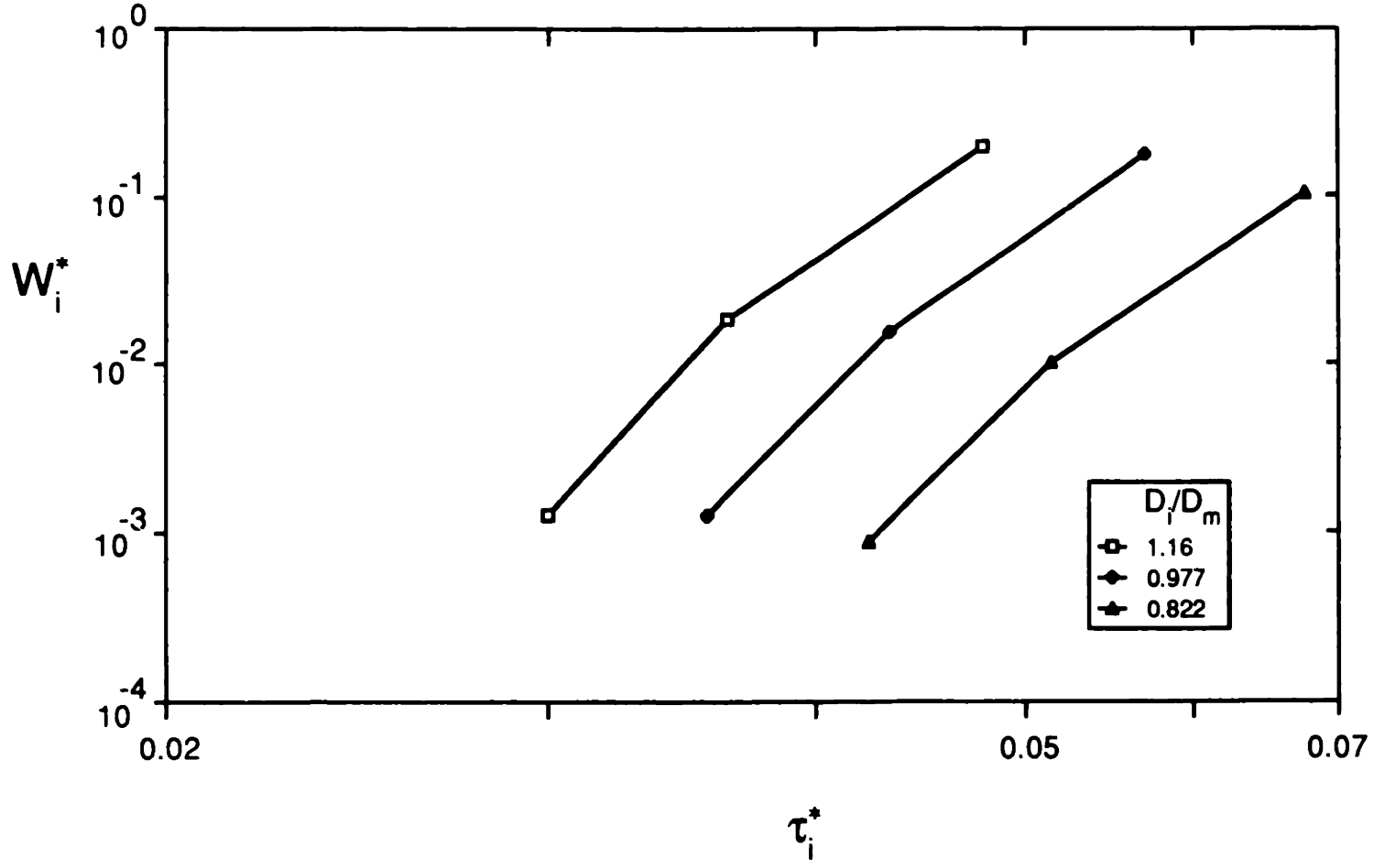

Figure 4.6.a. Fractional transport rates for the CUNI mixture: W_i^* as a function of τ_i^*
(Lines connect transport rates of each fraction for all runs)

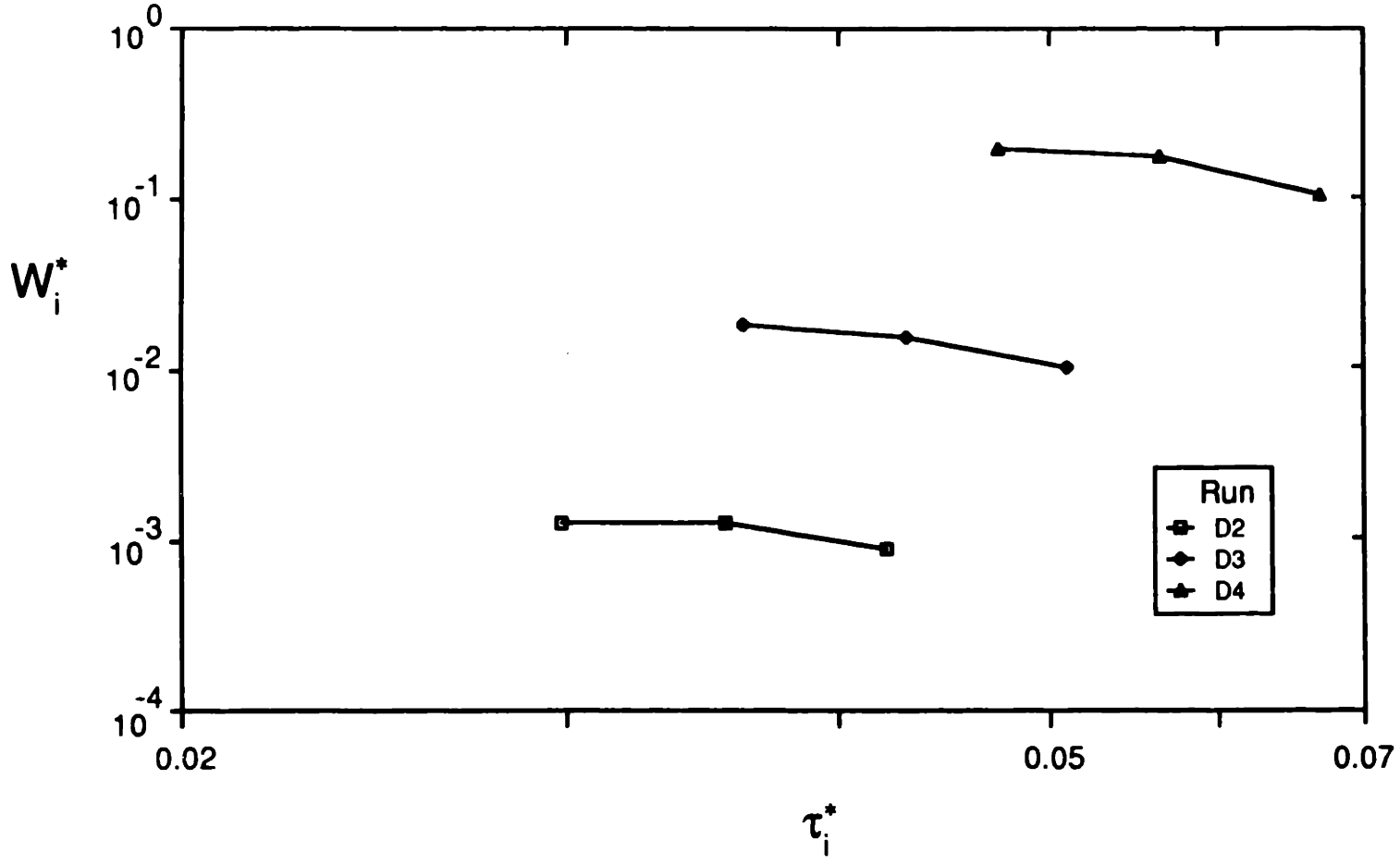

Figure 4.6.b. Fractional transport rates for the CUNI mixture: W_i^* as a function of τ_i^* (lines connect transport rates of every fraction for each run, showing p_i/f_i as a function of $1/D_i$)

and bed shear velocity u_* are the same for each fraction in a run, plots of W^*_i against τ^*_i for each run are an accurate representation of p_i/f_i against $1/D_i$, where p_i and f_i are the percentage of each fraction in the transport load and in the bed, respectively. Data for fractions with less than 2.5% in the bed grain-size distribution are not included in the plots of fractional transport rate or the following discussion. The availability of these grains for bed-load transport is deemed too limited to produce reliable results.

GRAIN-SIZE DISTRIBUTION OF THE TRANSPORTED SEDIMENT

An elementary way to evaluate the effect of relative grain size on the form of the fractional transport function is to examine directly the grain-size distribution of the transported sediment. If all fractions begin moving at close to the same bed shear stress (i.e., $\tau^*_{ri} \propto (D_i/D_{50})^{-1}$, the result of Chapter 3), and the form of the transport function is the same for each fraction in a mixture, the grain-size distribution of the transported load should be the same as that in the sediment bed. The most direct way to examine the relative-size effect on the transport grain-size distribution is as the ratio p_i/f_i, which gives the fractional transport as a convenient and interpretable proportion of that available for transport. It is also a practical form for modeling considerations, for which the bed grain-size distribution may be considered to be a given, and the transport grain-size distribution may be considered to be unknown. Grain-size distributions are given as fractional transport rates in Part b of Figures 4.3 through 4.6, allowing the variation of p_i/f_i (and the transport grain-size distribution) with τ^*_i and W^*_i to be observed.

Some variation of p_i/f_i with relative grain size is evident for all the mixtures. This is clearest with the 1Ø mixture (Figure 4.4.b), for which both the fine and coarse fractions are underrepresented in the transported load by one to two orders of magnitude for four of the six runs. These are the runs with the lowest transport rates; the two runs with the highest transport rates have a transport grain-size distribution much closer to that in the bed. The 1/2Ø mixture (Figure 4.3.b) shows much greater equivalence between p_i and f_i,

although three runs have an underepresentation of the finest two fractions by about half an order of magnitude. These, however, do not correspond to the lowest transport rates, but to the lowest, third-lowest, and second-highest transport rates.

The transport grain-size distributions of the FUNI (Figure 4.5.b) and CUNI (Figure 4.6.b) mixtures are very similar. The finer fractions in the three lowest FUNI transport rates, and in all CUNI runs, are underrepresented by a factor of about 1.75 to 3.0. At higher transport rates with the FUNI mixture (higher transport rates could not be achieved with the coarse-grained CUNI and our pumping capacity), the transport grain-size distribution is nearly equivalent to that in the bed, with a slight underrepresentation of the coarser fractions.

The most distinctive feature of the transport grain-size distributions is the change from nonequivalence with the bed size distribution to near equivalence as the transport rate increases. For the 1Ø and FUNI sediments this change is quite distinct. The CUNI sediment does not show a similar change because only relatively low transport rates could be achieved with it. The 1/2Ø mixture has two distinct transport grain-size distributions, but they are not as closely associated with the transport rate.

One explanation for the change in transport grain-size distribution with increasing flow strength is based on an analogy with similar behavior in uni-size sediment. Many authors (e.g. Yalin, 1977; Parker and Klingeman, 1982) have observed that most empirical uni-size transport formulas approach a limiting, constant value of W^*. Ashida and Michue (1972) give this constant a value of approximately 17. In dimensional form, a constant value of W^* is

$$q_b = \text{constant} \frac{\tau^{3/2}}{(s-1)g\rho^{3/2}}$$

which has no dependence on grain size. Thus, for the same values of τ, s, ρ, and g, the uni-size transport rates of all grain sizes approach the same constant value. If the transport rates of different grain sizes in uni-size beds approach a constant value at high values of bed shear stress, one may hypothesize that they

would also approach a constant transport rate in a sediment mixture. This would produce a transport grain-size distribution equivalent to that in the bed, which is essentially what we observe in all the sediments at the highest transport rates.

Figure 4.7, the same as Figure 4.2, presents the transport rates for the FUNI, CUNI, 1/2Ø, and 1Ø mixtures in terms of W^* and τ^*_m/τ^*_r. Points representing transport grain-size distributions close to that in the bed are circled, and points with nonequivalent grain-size distributions are enclosed in diamonds. There is a reasonably clear break between the two grain-size distributions at approximately $W^* = 1.0$. Three points from the 1/2Ø distribution provide the only scatter; of these, only one is significantly different from $W^* = 1.0$.

Although two transport grain-size distributions are evident in Figures 4.3 through 4.6, it is not clear whether the change in transport grain-size distribution with increasing transport rates is gradual, or an abrupt switch from one grain-size distribution to another. There is little in the data on fractional transport rate presented here to suggest that the transition is gradual, although this may result from the limited number of runs made with each mixture and the broad range of transport rates measured. There is a threefold difference in transport rate between 1Ø Runs C4 and C5, which are the pair that border on the shift in grain-size distribution in Figure 4.4.b. Although this is a significant change in transport rate, it is small relative to the 2,500-fold overall range in transport rates for the 1Ø mixture.

A second explanation that could account for the abrupt change in the p_i/f_i patterns is the corresponding onset of bed forms. If the bed forms are reasonably two-dimensional and the bed is not degrading or aggrading, one might expect that no grains would be exchanged from one bed form to another. If all the transported sediment merely cycles through each bed form, the mean transport grain-size distribution measured over several bed forms (as done here) would simply reproduce the bed grain-size distribution. This bed-form effect apparently does not happen. Two of the 1Ø runs with p_i/f_i distributions

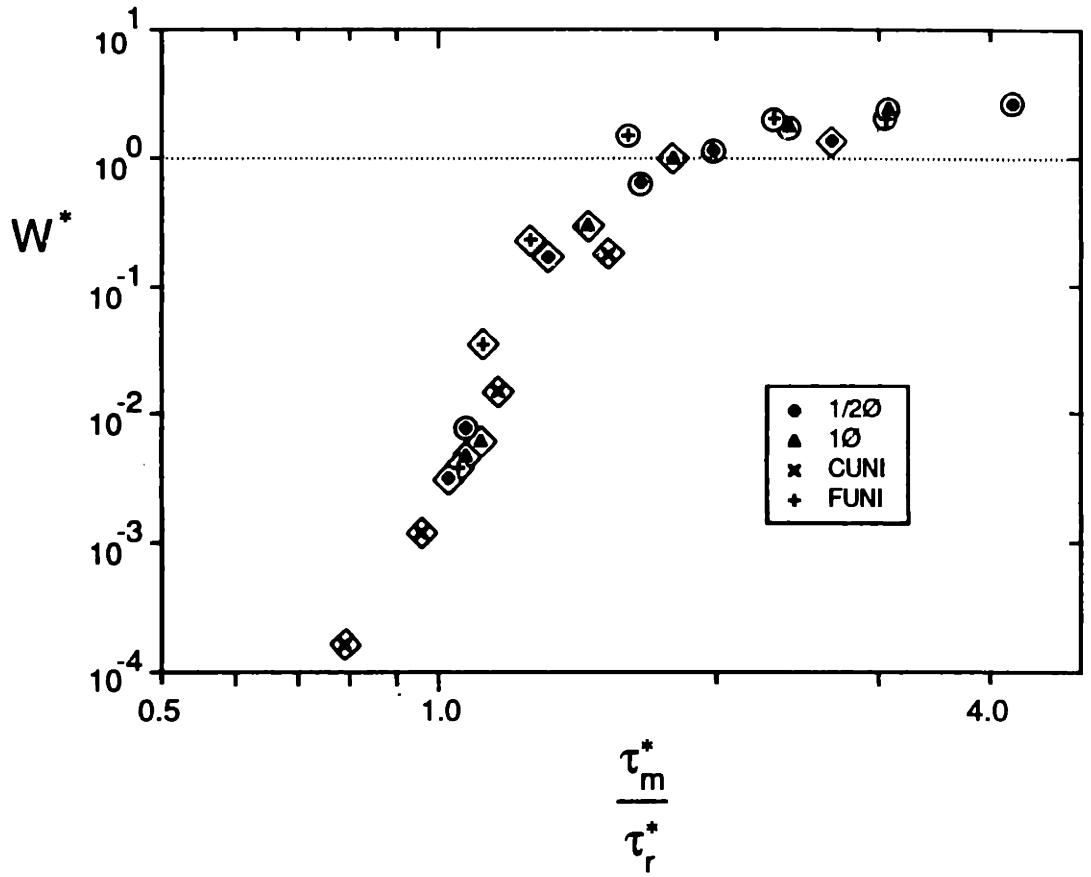

Figure 4.7. Total transport rates for all MIT sediments: W* as a function of τ^*_m/τ^*_r. Points enclosed in circles represent runs with a transport grain-size distribution close to that of the bed; points enclosed in diamonds represent runs with a transport grain-size distribution different from that of the bed.

different from unity had substantial and very regular bed forms. Two of the nonequivalent 1/2Ø transport grain-size distributions involved bed forms; one of the 1/2Ø runs with a transport grain-size distribution nearly equivalent to that of the bed had a planar bed configuration.

The reason why bed forms apparently do not have a dominant homogenizing effect on the transport grain-size distribution is that some size-dependent exchange of grains does occur between bed forms, even in cases where the bed forms are consistent in size, the bed is not degrading or aggrading, and no grains move forward (in suspension) from one bed form to the next. The size-dependent exchange occurs in the reverse direction, with some grains being left behind a particular bed form, and hence becoming underrepresented in the transport grain-size distribution. Figure 4.8 is a photograph of a bed-form trough for Run C4 with the 1Ø mixture. A coarse bed-surface layer is evident in the trough. It is certain that virtually all of these grains can no longer be moved in the separating flow behind the approaching bed form, but will instead stay in place while the approaching bed form (and possibly others) move over them.

The coarse surface layer not only provides evidence that some coarse grains move backwards with respect to the bed forms and hence become underrepresented in the transport load, but also serves to produce the same effect in finer sediments. The finer sediments may work their way beneath the coarser surface grains through a simple size-dependent sorting process in which smaller grains may fall into cavities vacated by larger grains, but larger grains cannot fit into positions vacated by smaller grains. It is a geometric necessity that finer grains become preferentially entrapped beneath coarser ones, if the coarser grains are moving at all and the finer grains periodically come to rest on the bed. We find that some coarse grains move at flow strengths involving at least some sediment transport, and that the finer grains do move in the classic stop-and-start motion characteristic of bed load.

Evidence of vertical size sorting is provided by samples of the bed surface and subsurface taken following the 1Ø runs. The samples were obtained by

Figure 4.8. Photograph of bed surface following Run C4 with the 1 ϕ mixture. Flow right to left. Bed-form crest at right. Scale = 15 cm.

Figure 4.9. Photograph of bed surface following Run C5 with the 1 ϕ mixture. Flow right to left. Bed-form crest at right. Scale = 15 cm.

pressing a circular cylinder containing moist kaolinite onto the bed surface. A layer of grains approximately equal in thickness to the coarsest grain on the surface was removed from the bed. After the surface layer was removed, a subsurface sample was obtained by repeating the sampling at the same location. Figure 4.10 presents the grain-size distribution of surface and subsurface samples taken in bed-form troughs following Runs C2 and C3 with the 1Ø mixture. The size distribution is presented as a ratio of that in the bed sample b_i to that in the bulk mixture f_i. The coarse fractions in the surface samples are substantially overrepresented with respect to the bulk of the distribution. The finer fractions in the subsurface samples are overrepresented, but to a smaller extent than the coarse grains in the surface samples. Vertical size sorting is also evident in Figure 4.8, in which the finer subsurface is visible at a location where a surface sample has been removed.

The vertical sorting at the bed surface decreases the availability of fine grains for transport and presumably acts at any flow strength that moves all the grains in a mixture. Along with the evident loss to a given bed form of coarse grains in the coarse surface layer, the entrapment of fine grains beneath the surface layer provides an explanation for the occurrence of a transport grain-size distribution not equivalent to that in the bed for those runs with regular two-dimensional bed forms.

The coarse surface layer is more poorly developed at higher flow strengths and transport rates. At the highest two flow strengths with the 1Ø mixture, no obvious coarse surface layer was observable. Figure 4.9 is a photograph of a bed-form trough following Run C5 with the 1Ø mixture. Figure 4.11 presents the bed-surface and subsurface grain-size distributions of samples taken from the troughs of bed forms following Runs C5 and C6 with the 1Ø mixture. An effort was made to find and sample the best-developed coarse surface layer following these runs. The results are given in Figures 4.10 and 4.11. At these higher transport rates, little difference between bed-surface and subsurface grain-size distribution could be found. The disappearance of the coarse surface layer is presumably related to the much larger and less regular

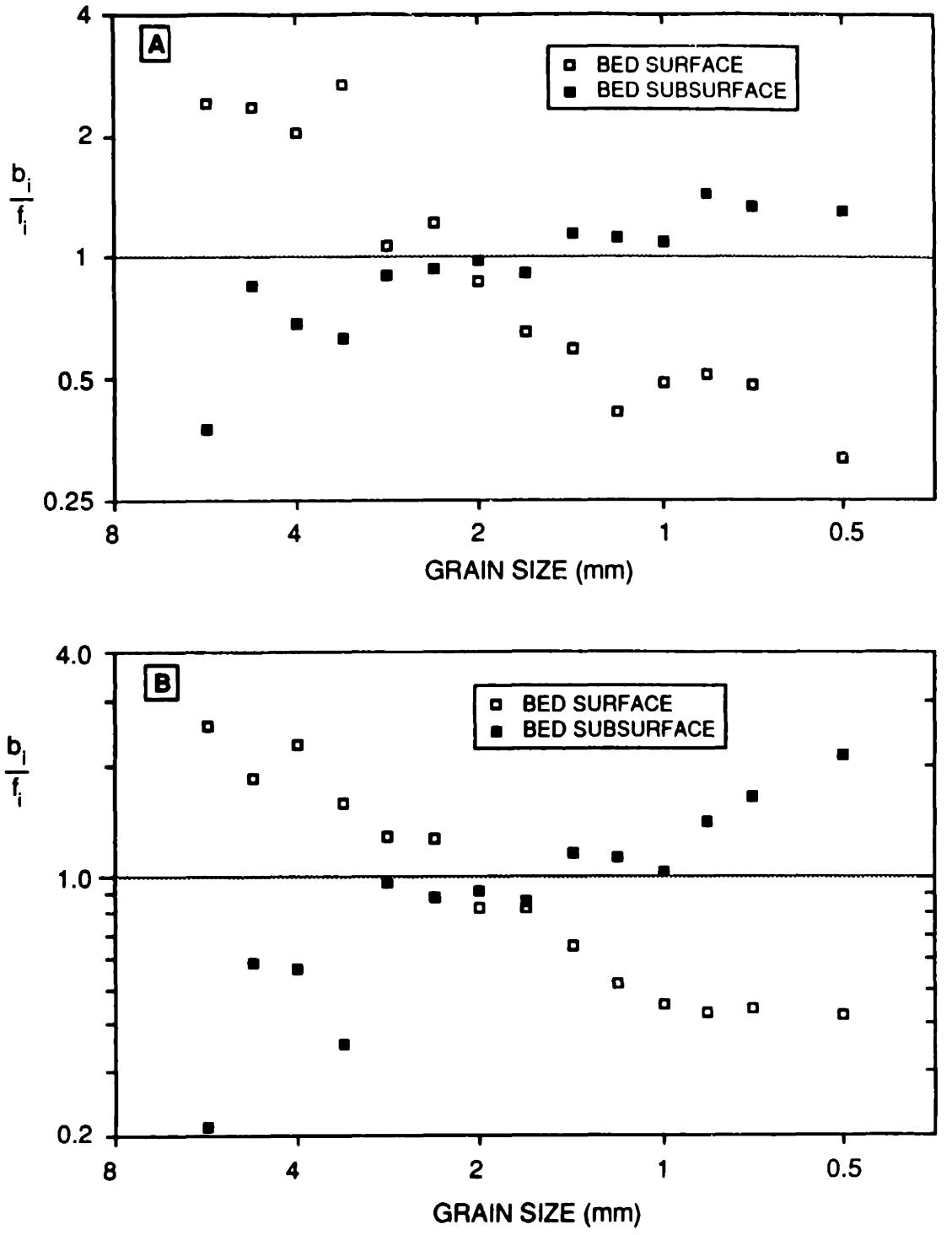

Figure 4.10. Grain-size distribution of bed surface and subsurface samples taken in bed-form troughs following Runs C2 (A) and C3 (B)

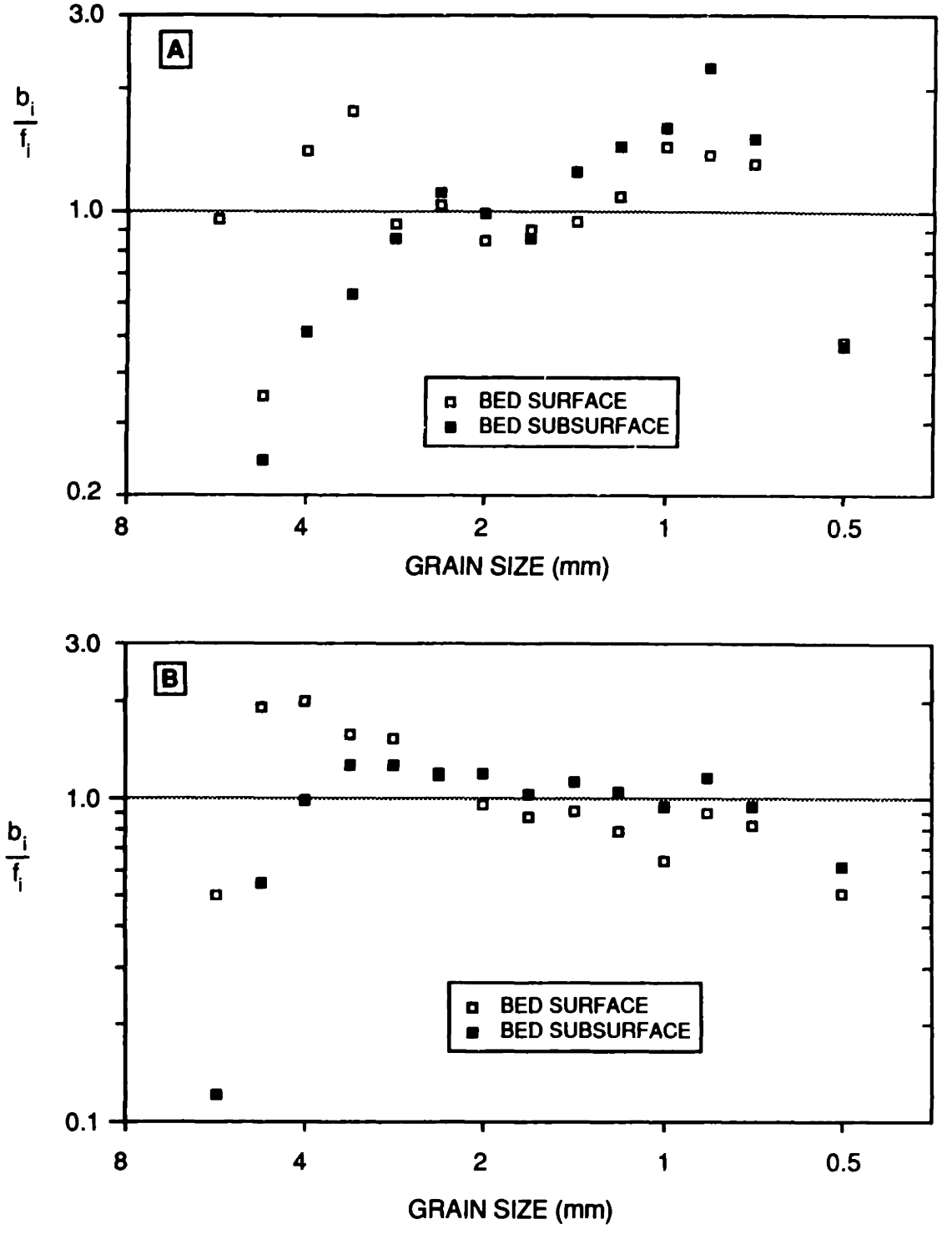

Figure 4.11. Grain-size distribution of bed surface and subsurface samples taken in bed-form troughs following Runs C5 (A) and C6 (B)

bed forms present at these transport rates (Table 2.3) With bed-form troughs of variable depth, and much more intense and spatially variable shear stress at the flow reattachment in the lee of the bed-form crests, a coarse surface layer cannot develop and thus cannot influence the transport grain-size distribution at these high transport rates, as evident in Figures 4.3 and 4.4.

The relative size of grains at the bed surface, the development of a coarse surface layer, and the effect of bed forms all play a role in determining the grain-size distribution of the transport load. The relative-size effects of variable exposure and bed roughness apparently balance the inherent variation in transportability with grain size due to grain mass and tend to make the transport grain-size distribution equivalent to that in the bed. The existence of a constant transport rate approached by all fractions at high excess shear stress would reinforce this effect. The development of a coarse surface layer can augment the relative-size effect for finer fractions by removing a portion of them from the actively transported sediment. The effect of the coarse surface layer on the transportability of the coarse fractions is less clear. The coarse surface layer should tend to increase the transportability of the coarse grains by increasing their representation on the bed surface. However, the increased roughness of the coarse surface layer also decreases the transportability of the coarse fractions by decreasing the relative-size "advantage" experienced by coarse fractions in a size mixture. The second effect apparently dominates, as suggested by the underrepresentation of the coarse fractions in the 1Ø transport load. The coarse surface layer apparently exerts a control on the transport grain-size distribution even in the presence of bed forms and works against the homogenizing effect that bed forms potentially have on the transport grain-size distribution. At high flow strengths the bed forms are sufficiently irregular in size, and the flow is sufficiently strong, that the coarse surface layer cannot develop. At these flow strengths the relative-size effect, the asymptotic constant high transport rates, and the homogenizing effect of bed forms can all contribute to the observed equivalence between the transport and bed grain-size distributions.

TEST OF MIXTURE SORTING

A mixture-sorting effect on the transport grain-size distribution would be manifested in Figures 4.3 to 4.6 as a variation in the *shape* of the p_i/f_i curves from mixture to mixture (and hence between sorting values of ≈0.2 Ø, 0.5 Ø, and 1 Ø). If the transport grain-size distribution is independent of mixture sorting, the shapes of the grain-size distributions in the figures would be identical; the mixtures with smaller values of sorting would simply be truncated at smaller deviations from the mean size.

To facilitate a comparison of the shapes of the transport grain-size distribution of all these sediments, the values of p_i/f_i for each sediment are plotted as a function of D_i/D_m in Figure 4.12. To reduce the complexity of this figure, runs with similar grain-size distributions are combined into a single line that represents the mean values of p_i/f_i for each fraction in those runs. The transport grain-size distributions for the CUNI sediment are combined with those for the three lowest-transport runswith the FUNI sediment. With this combination there are three pairs of curves, one for each sediment.

At the lower transport rates there are distinct variations in the transport grain-size distribution of the different mixtures. The well sorted mixtures show an underrepresentation of the finer fractions of roughly one half at $D_i/D_m = 0.84$. The 1/2Ø trend does not reach this value of p_i/f_i until $D_i/D_m = 0.6$, and the 1Ø mixture until D_i/D_m is less than 0.5. The coarse side of the low-transport grain-size distributions are roughly the same, however, and p_i/f_i remains close to unity in the grain-size range where the mixtures overlap (up to $D_i/D_m = 1.68$). At coarser sizes, the 1Ø mixture shows an underrepresentation of up to one order of magnitude. At higher transport rates the transport grain-size distributions for all sediments are quite similar, with all p_i/f_i values falling within a factor of 1.6 of unity.

The variation with size mixture of the fine end of the low-transport grain-size distributions suggests that mixture sorting has some influence on p_i/f_i. In other words, the low-transport trends in Figure 4.12 are not completely specified by D_i/D_m alone. Instead, the degree to which a fine

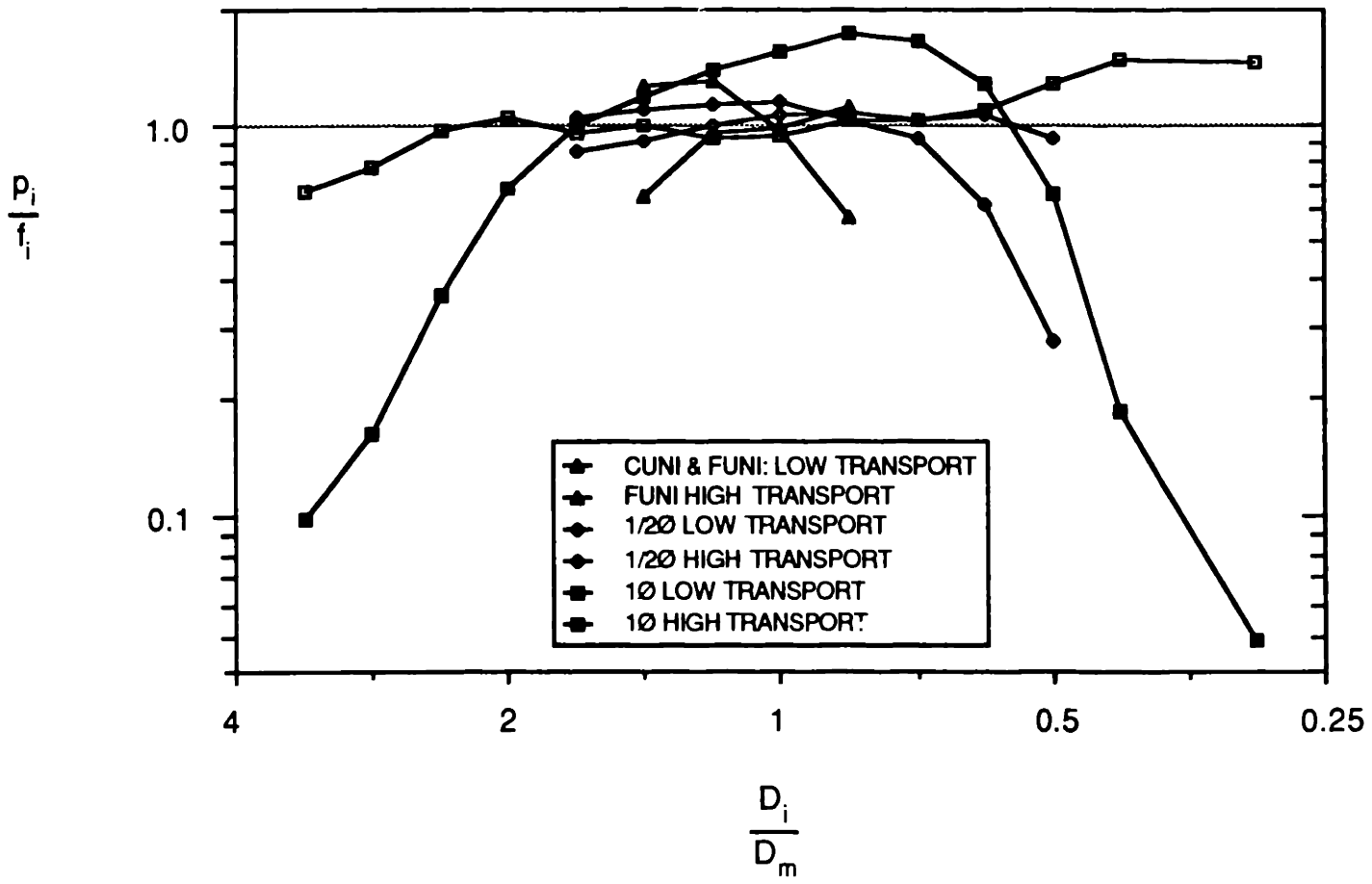

Figure 4.12. Normalized transport grain-size distributions for all MIT sediments: p_i/f_i as a function of D_i/D_m

fraction has a low value of p_i/f_i appears to depend also on its percentile position in the mixture, with larger p_i/f_i values associated with percentile positions closer to the mean grain size, as one would expect. It is difficult to draw any more than such a general, qualitative conclusion, however, because variation of p_i/f_i (or W^*_i) within a factor of 2.0 or so is difficult to distinguish from the scatter of the data at hand. It is also unlikely that such trends could be detected with other data, because both the total transport rate and the transport grain-size distribution are measured with a fairly low degree of precision. The degree of data scatter may actually be greater than that reflected in Figure 4.12. The lack of association between the transport grain-size distribution and the transport rate of the 1/2Ø mixture (Figure 4.33.b) suggests that, if a trend between the two exists, the threefold decrease in p_i/f_i for the fine 1/2Ø fractions in some runs may be a more representative example of the true error bounds on this type of data.

TEST OF PERCENTILE POSITION

The 1/2Ø and 1Ø mixtures have the same mean size and the same size-distribution shape. Because the mixture sorting of the 1Ø mixture is twice that of the 1/2Ø mixture, fractions of the same size (and same value of D_i/D_m) have different percentile positions within the mixtures. Because flow depth and water temperature were held within a narrow range for runs with both sediments, the percentile position P is the only parameter that varies for the same fractions in these two mixtures. The fractional transport rates for the same fractions in these mixtures are given in Figure 4.13. To allow the fractional transport rates to be distinguished, Figure 4.13 is split into two parts, each giving the fractional transport rates of every other fraction. The percentile position of each fraction is marked on the figure. There is a slight but consistent difference between the fractional transport functions for the two mixtures. The 1Ø curves all have slightly greater (5-7%) τ^*_i at low transport rates, then cross the 1/2Ø trend and have somewhat higher (10-60%) W^*_i at high τ^*_i.

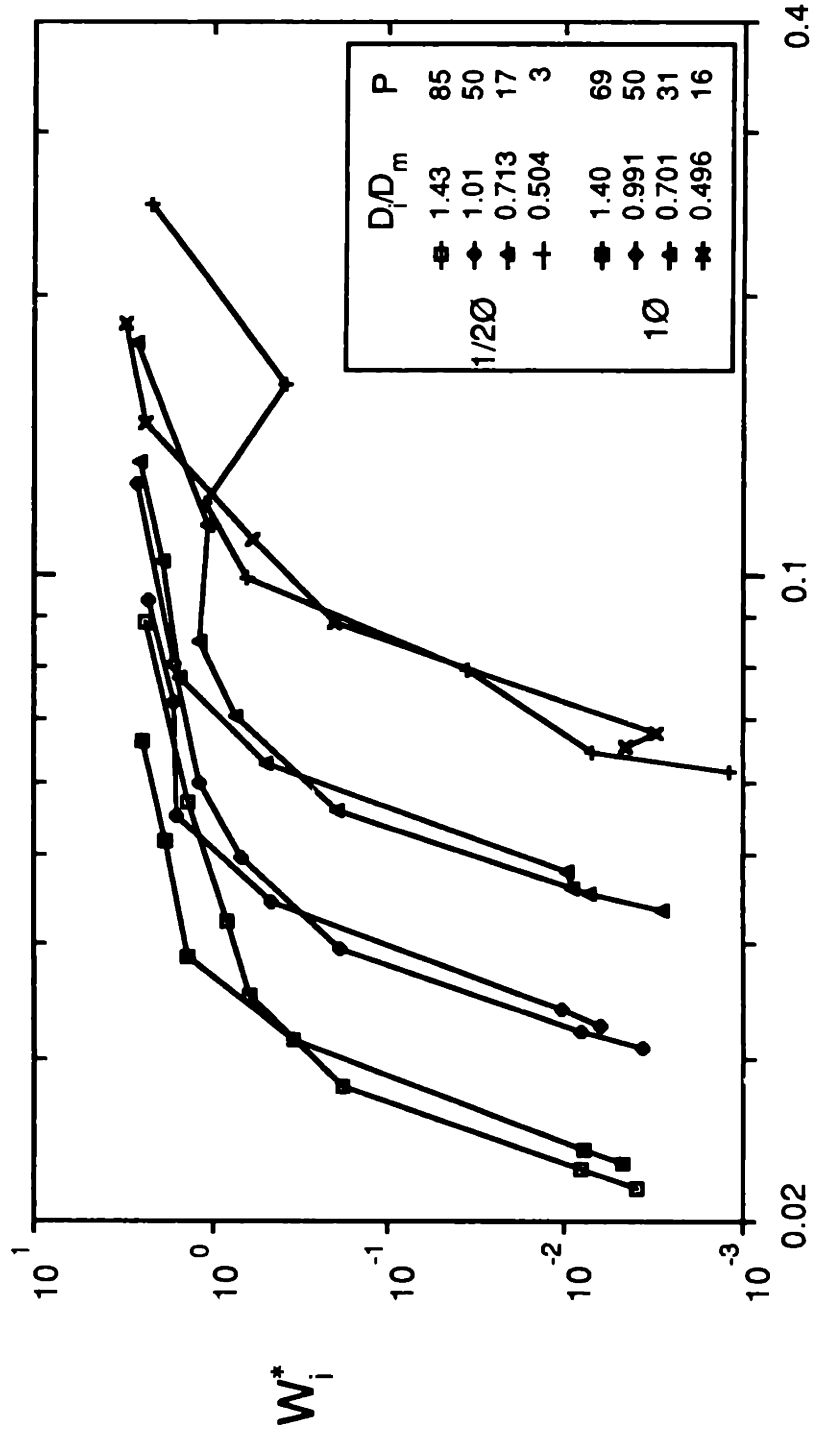

Figure 4.13.a. Comparison of fractional transport rates for the same fractions in the 1/2Ø and 1Ø mixtures: W_i^* as a function of τ_i^*

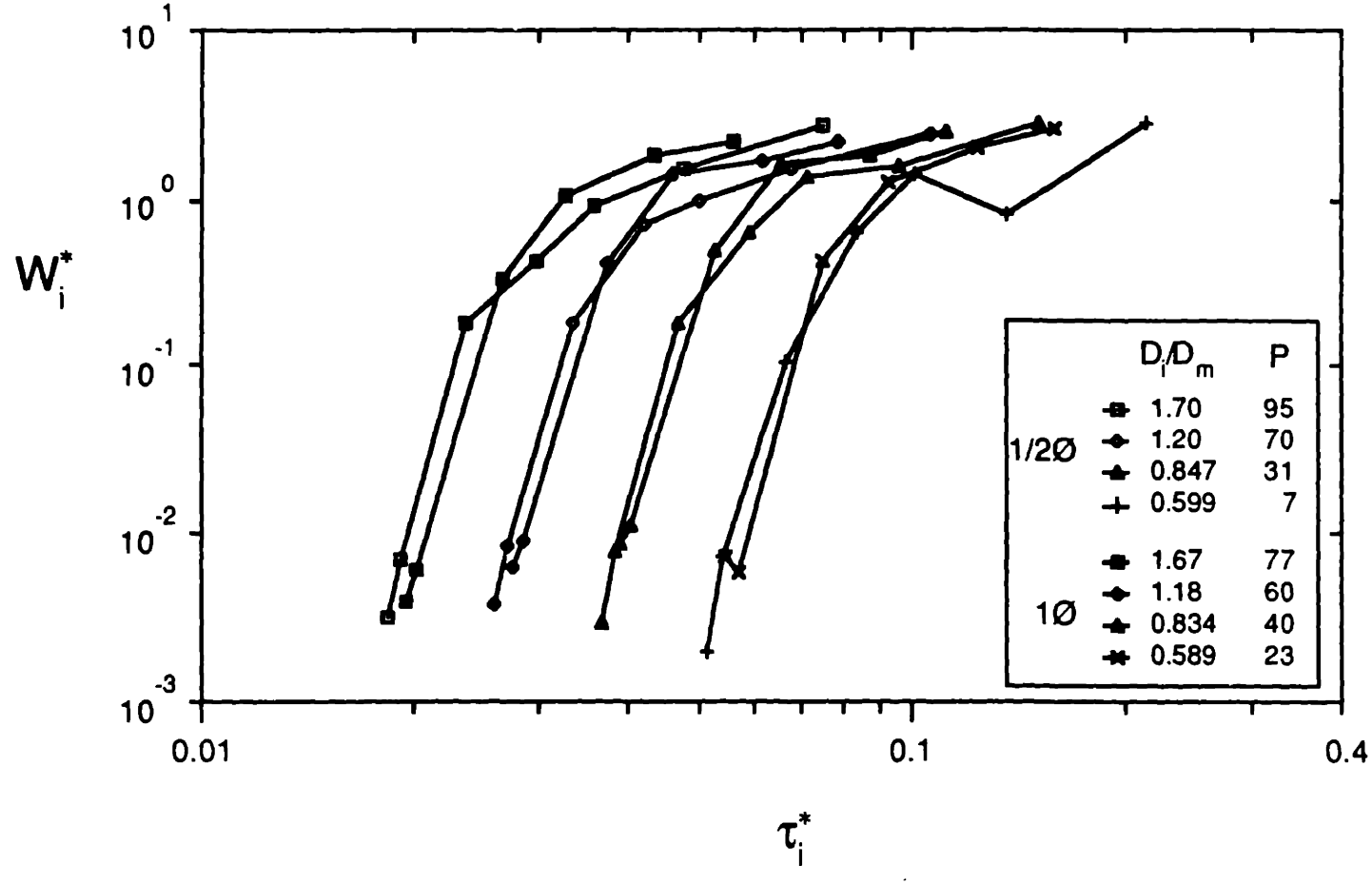

Figure 4.13.b. Comparison of fractional transport rates for the same fractions in the 1/2Ø and 1Ø mixtures: W_i^* as a function of τ_i^*

These slight differences between the same fractions in the two mixtures are apparently not a result of the different percentile positions in the mixture. If that were the case, it would be difficult to explain why the differences are consistent for both fine and coarse fractions. If percentile position were important one would expect that the closeness of the fraction to the mean size would determine the form of the transport function, and that any differences between the two would be symmetrical about the mean size. In addition, one would expect any differences to vanish at the mean size, for which the fractions in both mixtures have the same value of D_i/D_m and P. The consistency in the differences between the corresponding fractions of the two mixtures suggests that the differences result only from similar differences in the total transport rates for each fraction. This pattern is evident in Figures 4.1 and 4.2.

Thus it appears that, once the relative size of a grain is described by D_i/D_m, the percentile position adds no significant variation to the transport rate of that fraction. This result is the same as that found in Chapter 3 concerning the reference shear stress for these fractions. Figure 4.13 extends that conclusion from conditions near incipient motion to the entire fractional transport function.

TEST OF RELATIVE GRAIN SIZE BETWEEN UNI-SIZE AND MIXED-SIZE SEDIMENTS

Fractional transport rates for the central fractions in the FUNI and CUNI mixtures may be compared with the same fractions in the 1Ø mixture. This allows a direct demonstration of the effect of relative grain size on the transport rate of particular sizes. Because both D_i/D_m and P vary between the corresponding fractions in these mixtures, only the total relative-size effect may be determined; the individual effect of each of these relative-size parameters cannot be isolated. Figure 4.14 presents plots of the fractional transport rates of these fractions (D_i = 0.65 mm and 5.19 mm) in the 1Ø mixture and in the FUNI and CUNI sediments. Also shown are the same plots for D_i = 1.83 mm in the 1Ø mixture and for the central fraction in the MUNI sediment. The total-transport value of W^* is used for the MUNI sediment (which

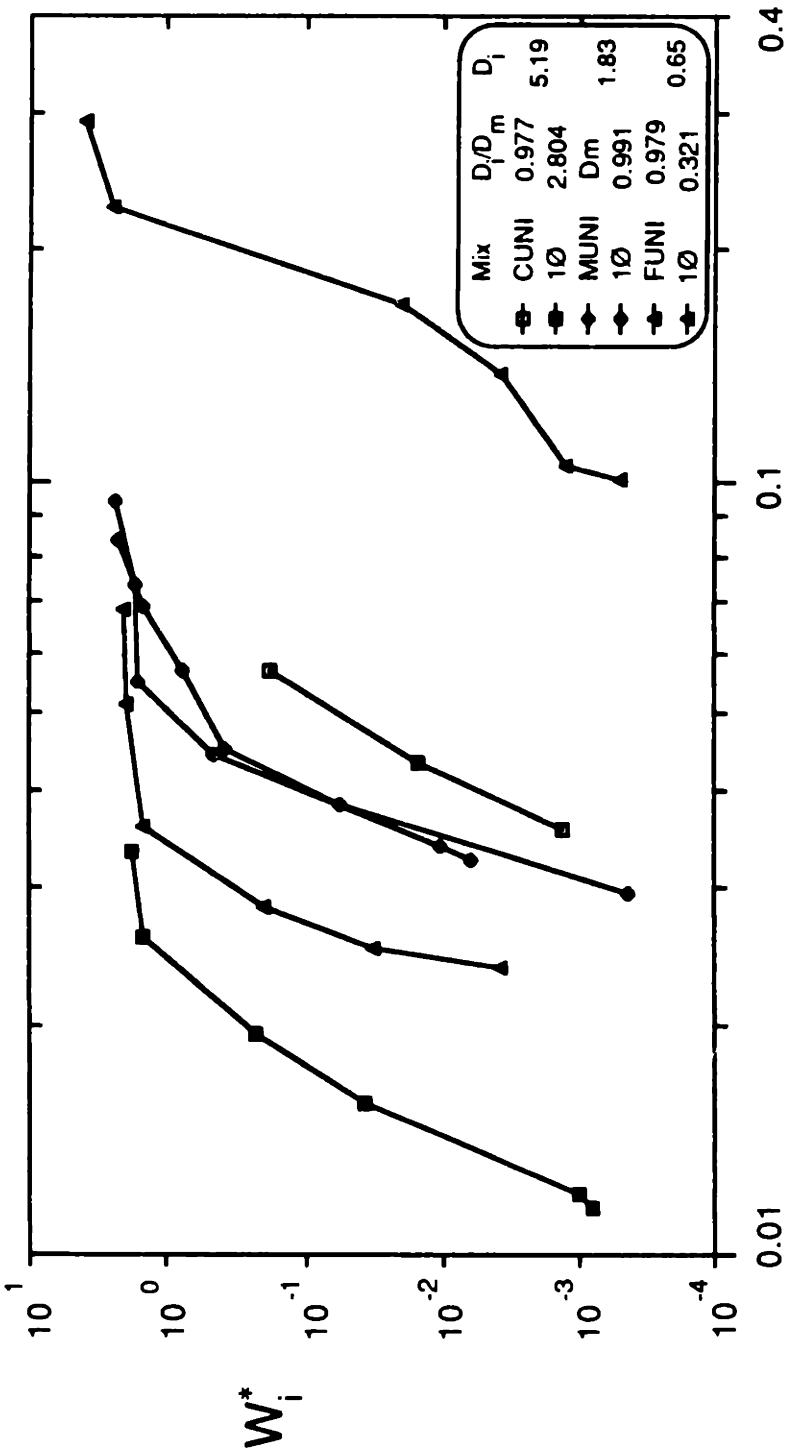

Figure 4.14. Comparison of fractional transport rates for the same fractions in the CUNI, MUNI, FUNI, and 1Ø mixtures: W_i^* as a function of τ_i^*

is the same as assuming $p_i = f_i$), because the grain-size distribution of the transport load for this sediment was not measured. This appears to be a very good approximation, because all runs with both the FUNI and CUNI sediments showed the central fraction of each to have p_i/f_i values very close to 1.0 (Figures 4.5b and 4.6b, Tables A3 and A4).

There is a striking separation in the transport rates for the 0.65 mm and 5.19 mm fractions. The transport functions for the 5.19 mm fractions are separated along the τ^*_i axis by a factor of about 3; the 0.65 mm fractions are separated by a factor of nearly ten. Given the steep dependence of transport rate on bed shear stress, the magnitude of this relative-size effect is enormous. The uni-size transport rate of the coarse fraction is clearly increased by orders of magnitude when placed in a mixture, and its motion begins at a bed shear stress some three times smaller. The transport rates for the fine fraction are changed in the opposite direction, and apparently to an even greater degree. There is a fivefold increase in τ^*_{ri}, and the differences in W^*_i are perhaps three orders of magnitude or more. The transport rates for the 1.83 mm fractions are roughly coincident, suggesting that the relative-size effect is symmetrical about the mean size of the sediment mixture.

These relative-size results are essentially those given in the preceding chapter; the separation in τ^*_i discussed here is analogous to the differences in τ^*_{ri} in Figure 3.13. The goal here is to investigate whether the form of the transport function varies between the corresponding fractions of the different mixtures. Because the fractional transport functions are so displaced in Figure 4.14, this comparison is more conveniently made in terms of W^*_i and τ^*_i/τ^*_{ri}, which are given in Figure 4.15. The transport rates for the 1.83 mm fraction are omitted because their relative positions are the same as in Figure 4.14. The form of the 5.19 mm transport functions is essentially the same for both sediments. Values of W^*_i for the 0.65 mm fraction are considerably smaller at intermediate transport rates when in the 1Ø mixture than when in the FUNI sediment. This is presumably a result of this fraction being partially removed from availability for transport by trapping beneath the

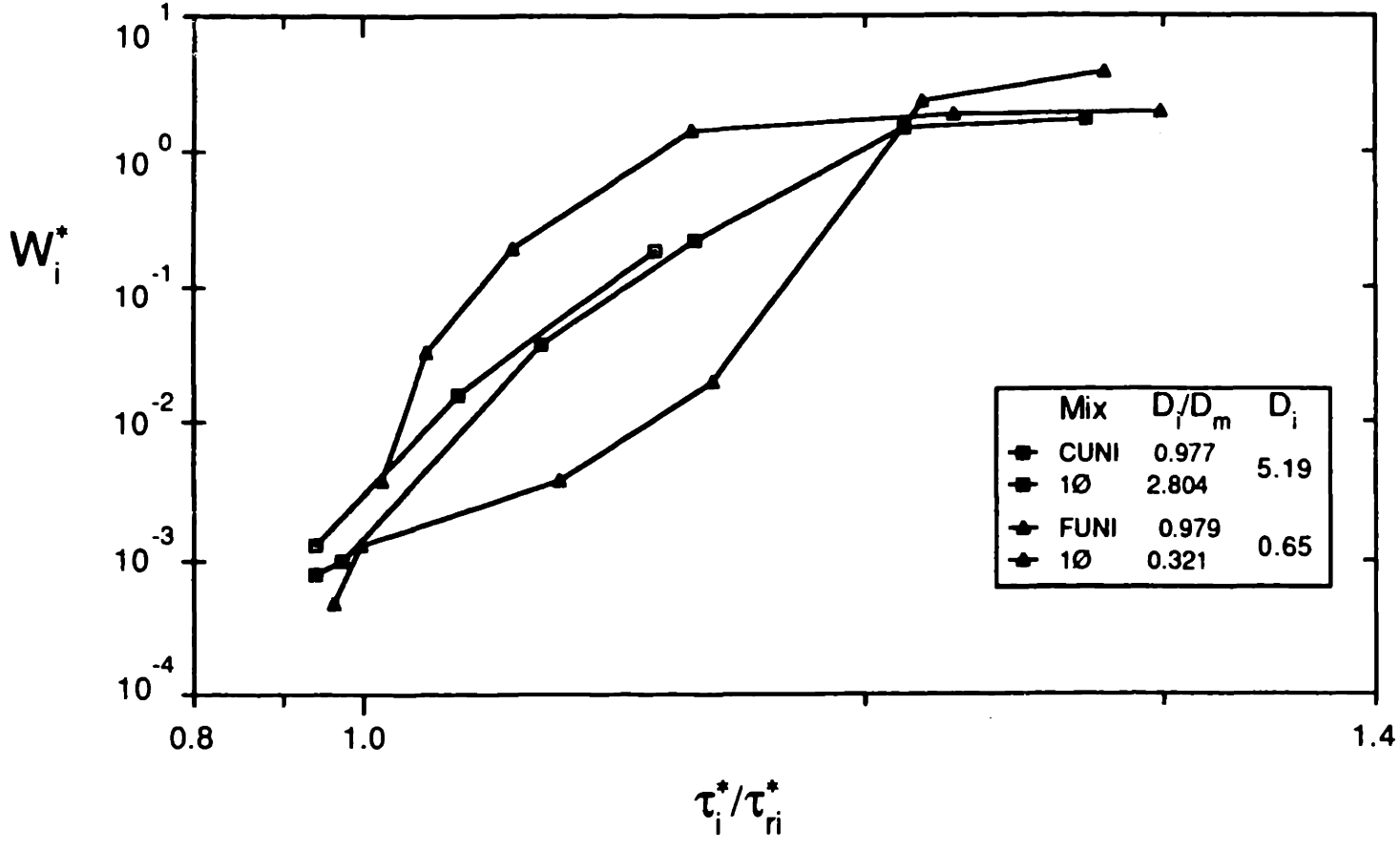

Figure 4.15. Comparison of fractional transport rates for the same fractions in the CUNI, FUNI, and 1Ø mixtures: W_i^* as a function of τ_i^*/τ_{ri}^*

coarse bed-surface layer. Values of W^*_i for this fraction are similar at the lowest transport rates, where the functions have been fitted to determine τ^*_{ri}. The W^*_i values are also similar at the highest transport rates, when the coarse surface layer is destroyed by the variable depths to which the bed forms scour.

FRACTIONAL TRANSPORT FUNCTIONS

PREVIOUS WORK

In their analysis of the Oak Creek data, Parker et al. (1982) considered the relative-size effect on fractional transport functions in a simple, three-part model. The bed size distribution was split into three parts: $D_i > 1.9D_{50}$, $1.9D_{50} > D_i > 0.48D_{50}$, and $D_i < 0.48D_{50}$. Because they found $\tau^*_{ri} \approx \tau^*_{r50} (D_i/D_{50})^{-1}$, the excess shear stress was computed as τ^*_{50}/τ^*_{r50}, which is a constant for each fraction for a particular flow. Figure 4.16 presents fractional transport functions fitted by eye to these three fractions in terms of W^*_i and τ^*_{50}/τ^*_{r50}. The coarsest and middle fractions are roughly similar in form, with the coarsest fractional transport function being slightly steeper. The transport function for the finest fraction is considerably less steep than the other two. The transport rates of the fine fraction are roughly one-half to one order of magnitude greater than those of the other two fractions at low excess shear stresses, and roughly half an order of magnitude smaller than the others at high excess shear stresses. The middle fraction has the highest fractional transport rates at the highest excess shear stresses, suggesting that the fine and coarse fractions are somewhat underrepresented, even at the highest flows sampled. However, the excess shear stress does not exceed 1.36 for any of the samples, a value considerably less than those we observed in our experimental data. In addition, a large part of the fine fraction may have not been sampled. The fine fraction includes sediment sizes down to less than a millimeter (D_5 = 0.7 mm), some of which, as noted by PKM, was probably moving as suspended load and would have escaped the sediment trap used by Milhous (1973) to collect the samples. In fact, at the higher flows

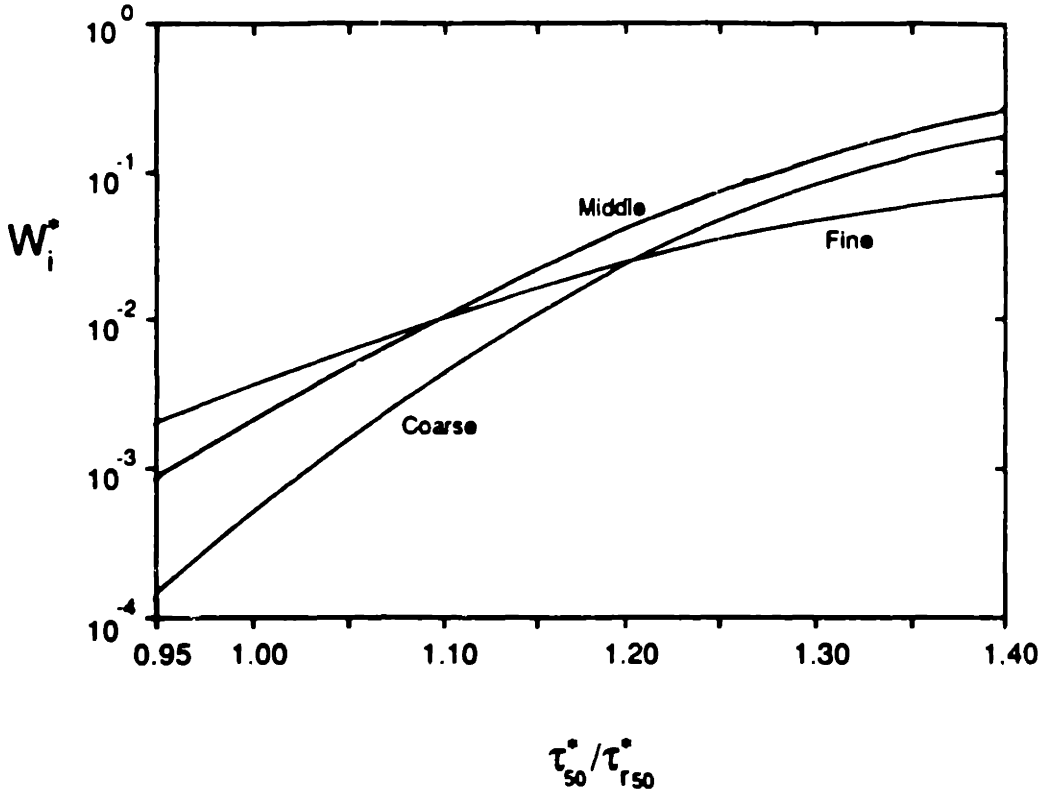

Figure 4.16. Empirical fractional transport functions for the Oak Creek data divided into three size fractions (after Parker et al., 1982)

sampled, the bed shear velocity exceeded the fall velocity of as much as 25% of this fine fraction, suggesting that there was considerable suspension transport.

In a later reanalysis of the Milhous (1973) Oak Creek data, Diplas (1987) developed a similarity function that incorporates the effect of relative grain size on the slope of loglinear fractional transport functions. He noted that log straight lines fit to the fractional transport rates of the Oak Creek data show a consistent increase in slope (m_1) from 5.51 at $D_i/D_{50} = 0.0457$ to 21.45 at $D_i/D_{50} = 3.26$. He found the variation of m_1 with relative size to be

$$m_1 = 13.71 \left(\frac{D_i}{D_{50}}\right)^{0.3214}$$

with a correlation coefficient r = 0.994. He then suggested representing the excess shear stress by the similarity function

$$\left(\frac{\tau_i^*}{\tau_{ri}^*}\right)^{\left(\frac{D_i}{D_{50}}\right)^{0.3214}}$$

which can be used to incorporate the effect of relative size on the form of the fractional transport functions. The form of this similarity parameter is somewhat dependent on the loglinear form of the fractional transport functions from which it was defined; its use in a fractional transport model also depends on a consistent variation in the slope of these functions with relative grain size. Neither of these approximations is found to hold true for fractional-transport rate data other than those of Oak Creek.

The fractional-transport data for our experiments are clearly curved in log-log space, and a loglinear transport function provides a poor representation. It is worth noting that this curvature is evident only when the data are presented on log-log plots with very different scales for each axis (as in Figures 4.3 to 4.6). If the τ^*_i axis is reduced to the same scale as the W^*_i axis, all the transport data fall indistinguishably on one curve, and appear loglinear.

Despite the curved nature of our fractional-transport data, there still could be a consistent change in the slope of the fractional transport functions with relative grain size. To check for such a trend, and to compare our data with the results of Diplas, loglinear curves were fitted to W^*_i and τ^*_i for the fractional transport rates of the 1/2Ø and 1Ø mixtures. The coefficients fitted by least squares to our data are given in Table 4.1. Although not providing a faithful representation of the fractional transport functions for our data (the data trends are all strongly concave downward with respect to the fitted straight lines), such a fit should nonetheless produce a consistent trend in slope with relative size, should the transport functions become steeper with relative grain size. No consistent trend is evident in Table 4.1, however. The values of m_1 are slightly greater for both the fine and coarse fractions in the 1/2Ø and 1Ø mixtures and decrease slightly for the central fractions. This trend results primarily from the fact that the extreme size fractions have slightly less curved fractional transport functions than the central fractions. Because of this change in the form of the transport functions, straight lines have a slightly better fit, and as a byproduct are slightly steeper than those fitted to the central fractions. The difference in slope is slight, however, and no overall trend is evident in the steepness of fractional transport functions with relative grain size (Figures 4.3 and 4.4).

Figure 4.17 presents the loglinear slopes of the fractional transport functions for the 1/2Ø and 1Ø mixtures, as well as for Oak Creek and the laboratory results of Day (1980a; beds A and B), Misri et al. 1984 (beds N1, N2, and N3), and Dhamotharan et al. (1980). No consistent trends in m_1 with relative size are evident. It appears that the approximation of Diplas (1987) is not general, but specific to the Oak Creek data.

MIT EXPERIMENTAL RESULTS

In order to examine the variation of the form of the fractional transport function with relative grain size, a transport function must be used as a reference standard. An existing function could be used (such as the Parker

1Ø MIXTURE

D_i/D_m	m_1	Confidence Interval (±95%)	R^2
3.34	7.32	3.11	0.949
2.80	7.85	3.03	0.929
2.36	7.29	3.17	0.911
1.98	6.60	3.50	0.873
1.67	6.14	3.99	0.820
1.40	6.02	3.92	0.820
1.18	5.69	3.92	0.803
0.991	5.63	4.02	0.790
0.834	5.54	3.83	0.801
0.701	5.59	3.86	0.802
0.589	5.98	3.95	0.815
0.496	6.75	3.32	0.889
0.417	7.87	2.00	0.968
0.321	8.89	2.79	0.951

1/2Ø MIXTURE

D_i/D_m	m_1	Confidence Interval (±95%)	R^2
1.70	4.57	2.78	0.781
1.43	4.32	2.79	0.760
1.20	4.37	2.91	0.748
1.01	4.47	2.98	0.749
0.847	4.62	3.07	0.750
0.713	4.46	3.18	0.723
0.599	4.69	3.15	0.746
0.504	4.73	3.28	0.734

Table 4.1 Exponent m_1 fitted by least squares to $W^*_i = a(\tau^*_i)^{m_1}$ for the 1Ø and 1/2Ø mixtures.

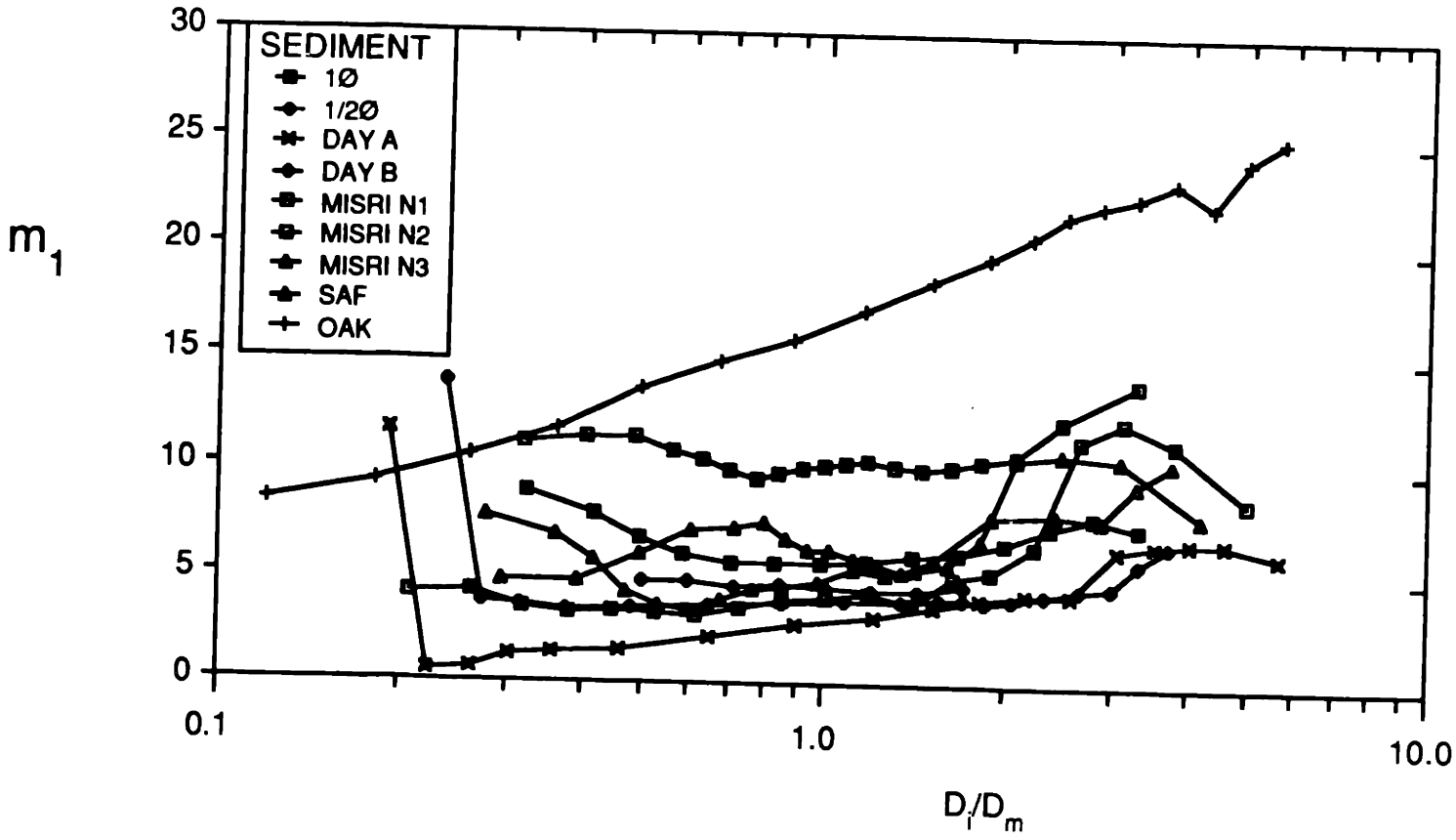

Figure 4.17. Exponent of the fractional transport function $W_i^* = a(\tau_i^*)^{m_1}$: m_1 as a function of D_i/D_m

(1979) function used to compute τ^*_{ri}), as long as it fits the data well and is based on W^*, a constant value of which was used as the reference-transport criterion. An existing function offers the advantages of having been correlated with transport data for other conditions (the Parker function is a power approximation of the Einstein (1950) transport function, probably the most widely used transport function), and of not adding to the proliferation of empirical transport functions fitted to individual data sets. A transport function fitted to our data could also be used as a reference, although its use beyond that application would require a markedly superior fit to the data relative to existing functions.

Figure 4.18 presents the 1Ø fractional-transport data in terms of W^*_i and τ^*_i/τ^*_r. Superimposed on the figure is the transport function of Parker (1979),

$$W_i^* = 11.2\left(1 - \frac{0.8531}{(\tau_i^* / \tau_r^*)}\right)^{4.5}$$

The Parker function is shown because it fits the total transport rates for our mixtures reasonably well (Figure 4.2) and because it was used to determine τ^*_{ri} in the preceding chapter. For comparison, the transport function of Meyer-Peter and Müller (1948) is also shown. To be comparable with the transport data expressed as a function of the excess shear stress above the measured reference value, the Meyer-Peter and Müller function (hereafter MPM) is expressed in a form that allows it to pass through $W^*_i = 0.002$ at $\tau^*_i = \tau^*_r$:

$$W_i^* = 8.0\left(1 - \frac{0.9960}{(\tau_i^* / \tau_r^*)}\right)^{1.5}$$

Because the MPM function is separated somewhat from the Parker function and from the fractional-transport data, a third transport function is included in Figure 4.16. This function was chosen to fall between the other two and is termed the Intermediate function. It is based on the Parker function but with an

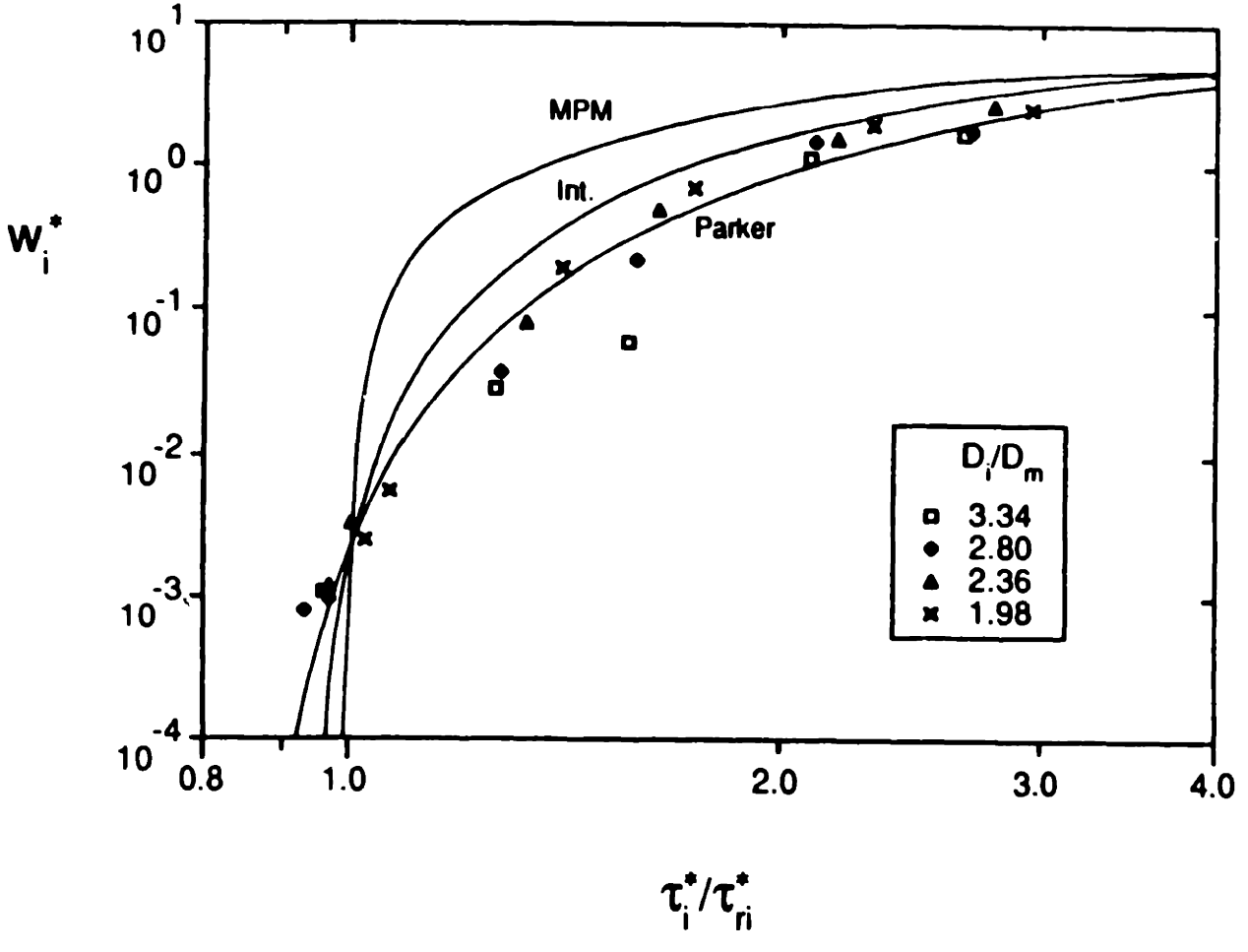

Figure 4.18.a 1Ø fractional transport rates: W_i^* as a function of τ_i^*/τ_{ri}^*
Lines represent Parker, Intermediate, and Meyer-Peter/Müller transport functions.
Part a: Coarsest four fractions

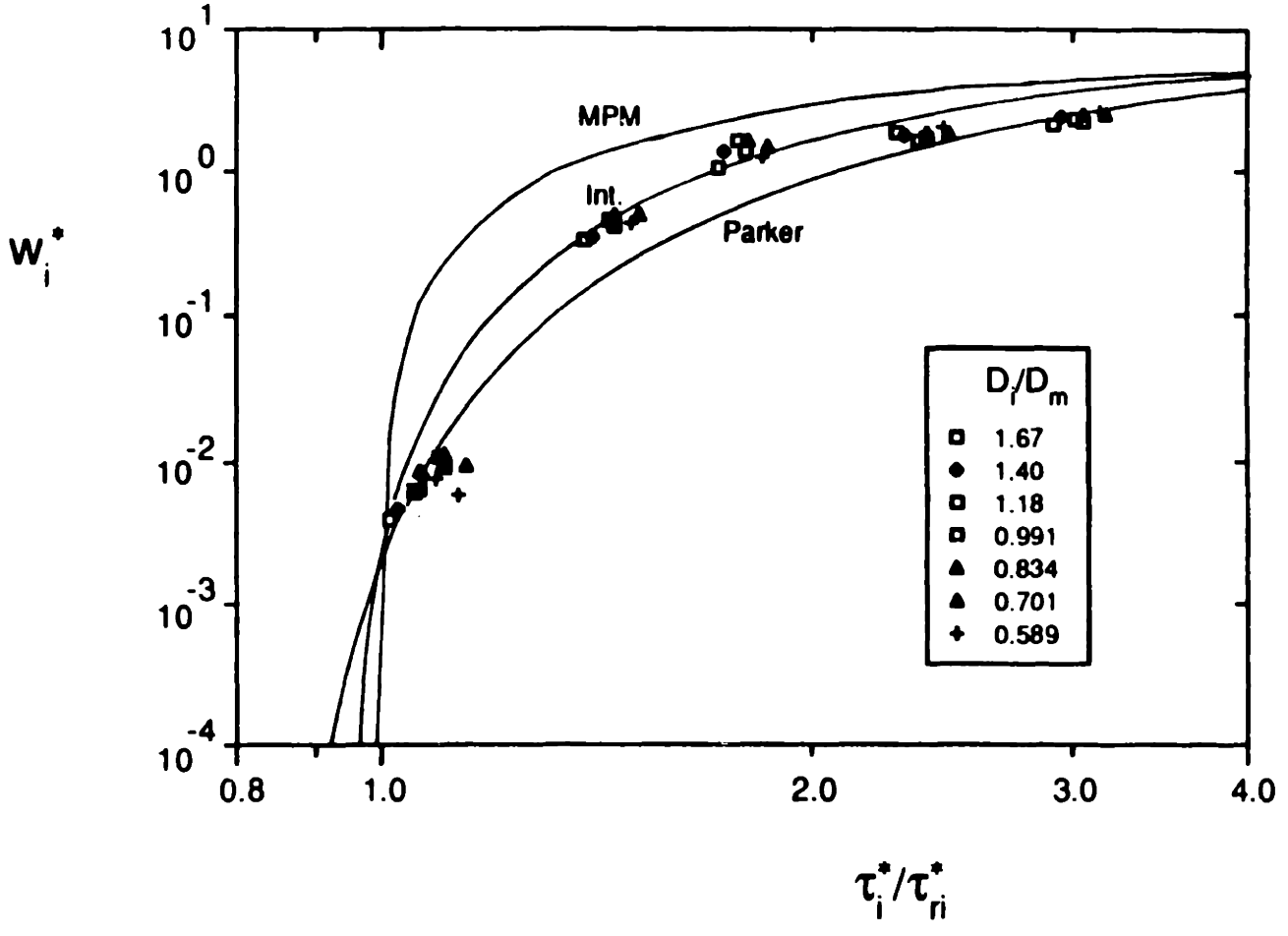

Figure 4.18.b 1Ø fractional transport rates: W_i^* as a function of τ_i^*/τ_{ri}^*
Lines represent Parker, Intermediate, and Meyer-Peter/Müller transport functions.
Part b: Seven middle fractions

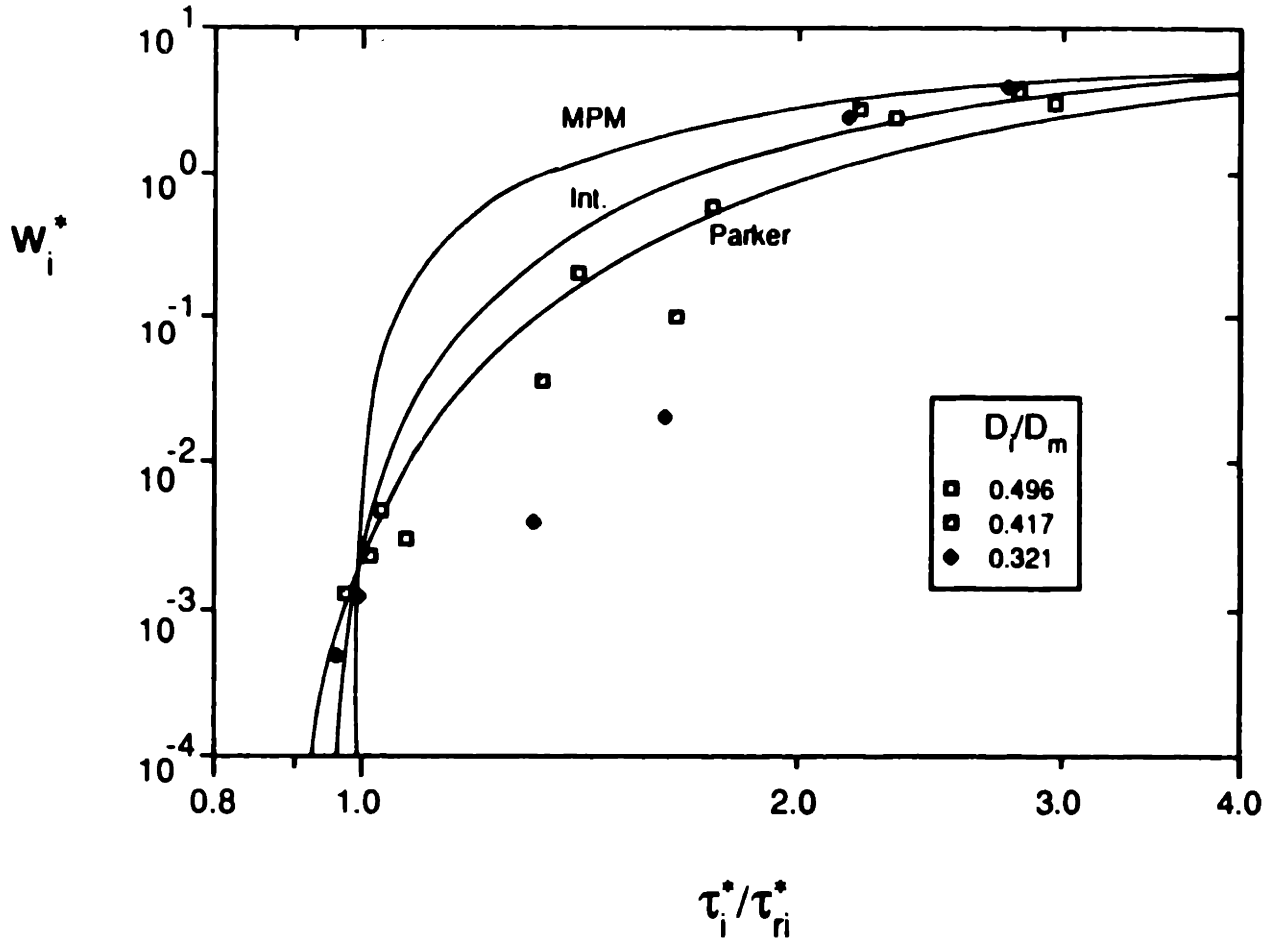

Figure 4.18.c 1Ø fractional transport rates: W_i^* as a function of τ_i^*/τ_{ri}^*
Lines represent Parker, Intermediate, and Meyer-Peter/Müller transport functions.
Part c: Three finest fractions

exponent of 3.0 and an adaptation in the excess-shear-stress term to allow it to pass also through the reference-transport rate at $\tau^*_i = \tau^*_r$:

$$W_i^* = 11.2\left(1 - \frac{0.9437}{(\tau_i^* / \tau_r^*)}\right)^{3.0}$$

The 1Ø fractional transport functions fall into three distinct forms, and Figure 4.18 is divided into three parts to match. The four coarsest fractions, plotted in Figure 4.18.a, follow the Parker function fairly closely, except for several points in the two coarsest fractions that are significantly lower than the Parker function at the intermediate transport rates. The middle seven fractions (representing 62% of the 1Ø mixture), plotted in Figure 4.18.b, fall close to the Parker relation at the low and high transport rates but fall above it and close to the Intermediate transport function, at intermediate transport rates. The finest three fractions of the 1Ø mixture show a transport pattern somewhat similar to that of the coarse fractions. The intermediate transport rates for the two smallest size fractions are considerably smaller than any of the transport functions

The 1Ø fractional-transport patterns in Figure 4.18 may be related to the transport grain-size distributions given in Figure 4.4.b. In Figure 4.4.b the four 1Ø runs with the lowest transport rates show an underrepresentation of the coarsest and finest fractions; values of p_i/f_i vary the most for the two intermediate transport rates, for which the differential in Figure 4.18 is also the greatest. The two runs at the lowest transport rates show little difference from the model transport functions, because they are close to the reference transport rate and were therefore closely fitted when determining τ^*_{ri}.

Because the term p_i in W^*_i is a percentage, if some fractions in a size mixture are underrepresented, then others must be overrepresented by a factor weighted by the amount of each fraction present in the bed. Hence, the two intermediate-transport runs, which have a distinct underrepresentation of the finest and coarsest fractions, also have a corresponding (but subdued, because

of the greater values of f_i) overrepresentation of the middle fractions. This appears in Figure 4.18b as fractional transport rates that fall above the Parker curve. The transport rates of all the fractions are reasonably close to the Parker curve at low and high transport rates. The result is somewhat flatter transport functions for the fine and coarse fractions, and more sharply curved transport functions for the central fractions.

The fractional transport functions for the 1Ø mixture vary with both bed shear stress and relative size. The details of this variation depend on the nature of the bed forms and the degree to which a coarse layer develops at the bed surface. Under conditions favorable to the development of a stable bed-surface layer (in the case of the 1Ø sediment, two-dimensional bed forms of consistent size developed at moderate flow strengths), the underrepresentation of the fine and coarse fractions will be much greater, and the transport functions of the fine and coarse fractions will be much flatter than those for the middle size fractions.

The Parker transport function gives a better overall fit to the fractional-transport data than the other two functions in Figure 4.18. The sum of squared errors,

$$\sum (\log_{10} W_i^* - \log_{10} W_i^{*\prime})^2$$

(where the second term is the value of the model transport function at τ^*_i) was computed for all three curves. The values are 8.81 for the Parker curve (7.0% of the total variation in W^*_i), 19.68 for the Intermediate transport function (15.6% of the total), and 61.46 for the MPM transport function (48.6% of the total). The mean deviation,

$$\frac{1}{n} \sum (\log_{10} W_i^* - \log_{10} W_i^{*\prime})$$

for the Parker curve was clearly superior to the others: 0.00249 for the Parker curve, -0.216 for the Intermediate, and -0.698 for MPM.

A best-fit curve could also be used as a standard to examine the variation of the fractional transport rates with relative size. To facilitate comparison with the Parker curve, which fits the data reasonably well, and because τ^*_{ri}, has been fitted by translating this function along the τ^*_i axis, the fitted function was allowed to vary only in its form (log slope) and position along the W^*_i axis (intercept) in the following form:

$$\log_{10} W_i^* = \log_{10} \alpha + \beta \log_{10} \left(1 - \frac{0.8531}{\tau_i^* / \tau_r^*}\right) \qquad (4.1)$$

The fitted values of α and β are given in Table 4.2. The values of α and β do not show much variation with relative size. None of the fitted curves is significantly different from the Parker curve in either slope or position at the intercept (log 11.2) or the reference-transport level (log 0.002). Virtually all of the slopes are significantly different from the MPM and Intermediate transport functions. Because a mean transport function determined from these fitted curves would not be much different from the Parker curve, there is little advantage in using an additional empirical transport function to investigate the effect of relative grain size on the form of the fractional transport function.

The fractional transport rates for the 1/2Ø mixture are presented in Figure 4.19. Also shown are the Parker transport function and the Intermediate transport function. The fractional transport functions are remarkably consistent, as could be anticipated by the near-equivalence of the transport and bed grain-size distributions in Figure 4.3.b. The 1/2Ø transport functions are closest to that of Parker, although slightly more curved. The sum of squared errors with respect to the Parker function is 2.43 (3.7% of the total variation in W^*_i); the equivalent error for the Intermediate function is 7.00 (10.6% of the total variation). The mean deviation from the Parker curve is -0.051 and from the Intermediate curve, -0.310.

Equation 4.1 was also fitted to the 1/2Ø fractional transport rates. The fitted values of α and β are given in Table 4.2. The best-fit values for both the

1Ø MIXTURE

D_l/D_m	α	β	Confidence Interval for β (±95%)	R^2
3.34	4.72	4.04	2.12	0.925
2.80	6.56	4.00	0.95	0.971
2.36	12.16	4.41	0.40	0.996
1.98	18.15	4.99	0.40	0.997
1.67	16.94	4.60	0.87	0.982
1.40	18.76	4.68	0.91	0.981
1.18	18.63	4.93	1.22	0.969
0.991	18.70	4.76	1.24	0.966
0.834	19.98	4.82	1.24	0.967
0.701	22.27	5.33	1.48	0.962
0.589	24.51	5.50	1.49	0.964
0.496	19.80	5.10	1.01	0.980
0.417	9.85	4.57	1.75	0.930
0.321	4.64	4.53	3.21	0.794

1/2Ø MIXTURE

D_l/D_m	α	β	Confidence Interval for β (±95%)	R^2
1.70	9.67	4.44	0.60	0.987
1.43	8.91	4.39	0.72	0.980
1.20	9.82	4.33	0.71	0.980
1.01	11.77	4.59	0.77	0.979
0.847	12.42	4.59	0.75	0.980
0.713	10.09	4.34	0.92	0.967
0.599	10.47	4.67	0.96	0.969
0.504	6.51	4.51	1.39	0.933

Table 4.2 Values of α and β fitted by least squares to:

$$\log_{10} W_i^* = \log_{10} \alpha + \beta \log_{10} \left(1 - \frac{0.8531}{\tau_i^* / \tau_r^*}\right)$$

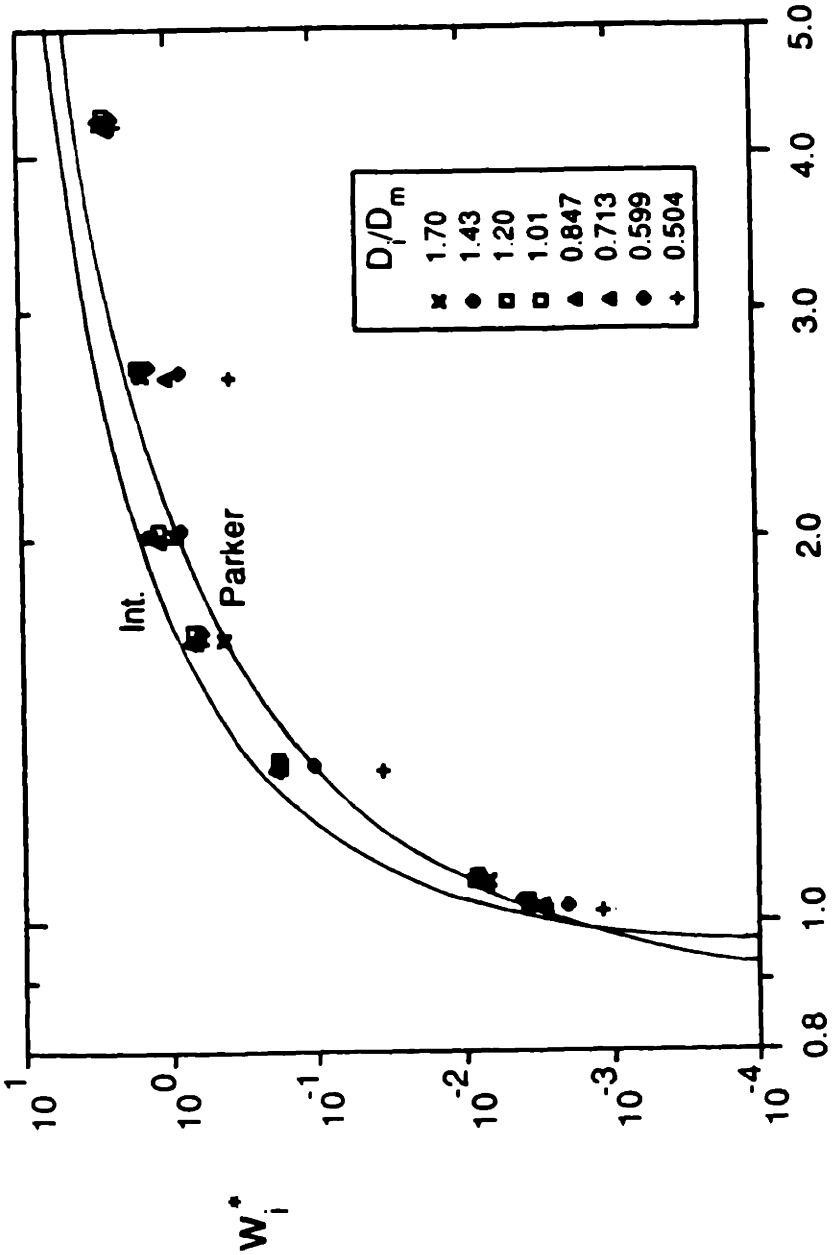

Figure 4.19. 1/2Ø fractional transport rates: W_i^* as a function of τ_i^*/τ_n^*
Lines represent Parker and Intermediate transport functions

slope and the intercept are remarkably close to the Parker values for all size fractions.

A SIMPLE FRACTIONAL-TRANSPORT MODEL

The central results of our fractional-transport experiments are that the reference shear stress (when measured with the PKM reference-transport criterion) is nearly independent of grain size, and that most of the fractional transport rates fall close to a common curve, suggesting that a single transport function may represent the fractional transport functions reasonably well. It is of interest to examine how much error is produced by using these very simple assumptions to predict the fractional transport rates.

Assume only that (1) the reference shear stress for D_{50} is given by a slightly reduced value of the Shields function, (2) $\tau^*_{ri} = (D_i/D_{50})^{-1}$, and (3) the Parker transport function represents the transport function for all fractions in a mixture. The reference shear stress used for D_{50} is $\tau^*_{r50} = 0.88\tau^*_{Shields}$, which is the best approximate fit of the Shields curve to the τ^*_{r50} values in Figure 3.11. The second assumption means that $\tau_{ri} = \tau_{r50}$, so that the excess shear stress, τ^*_i/τ^*_r, is identical for each fraction for a particular run. Although these are essentially empirical results, they are not best-fit values. Rather, they are the simplest approximations that may be made of the trends reported here.

Figures 4.20 and 4.21 present the results of this simple model for the 1/2Ø and 1Ø mixtures. Because the principal source of error for the model is error in the estimate of τ^*_{ri}, the ratio of actual to predicted values of W^*_i ($W^*_i/W^{*\prime}_i$) is presented as a function of the ratio of actual to predicted τ^*_r ($\tau^*_{ri}/\tau^{*\prime}_{ri}$) in Part b of each figure. Part a of each figure presents the variation of the τ^*_r ratio with D_i/D_m. The 1/2Ø model fits the data very well, with a sum of squared errors of 2.52 (3.8 % of the total variation in W^*_i for the 1/2Ø mixture). The mean deviation for the 1/2Ø mixture is -0.049, indicating that the predicted values of W^*_i are centered close to the actual values. This fit is

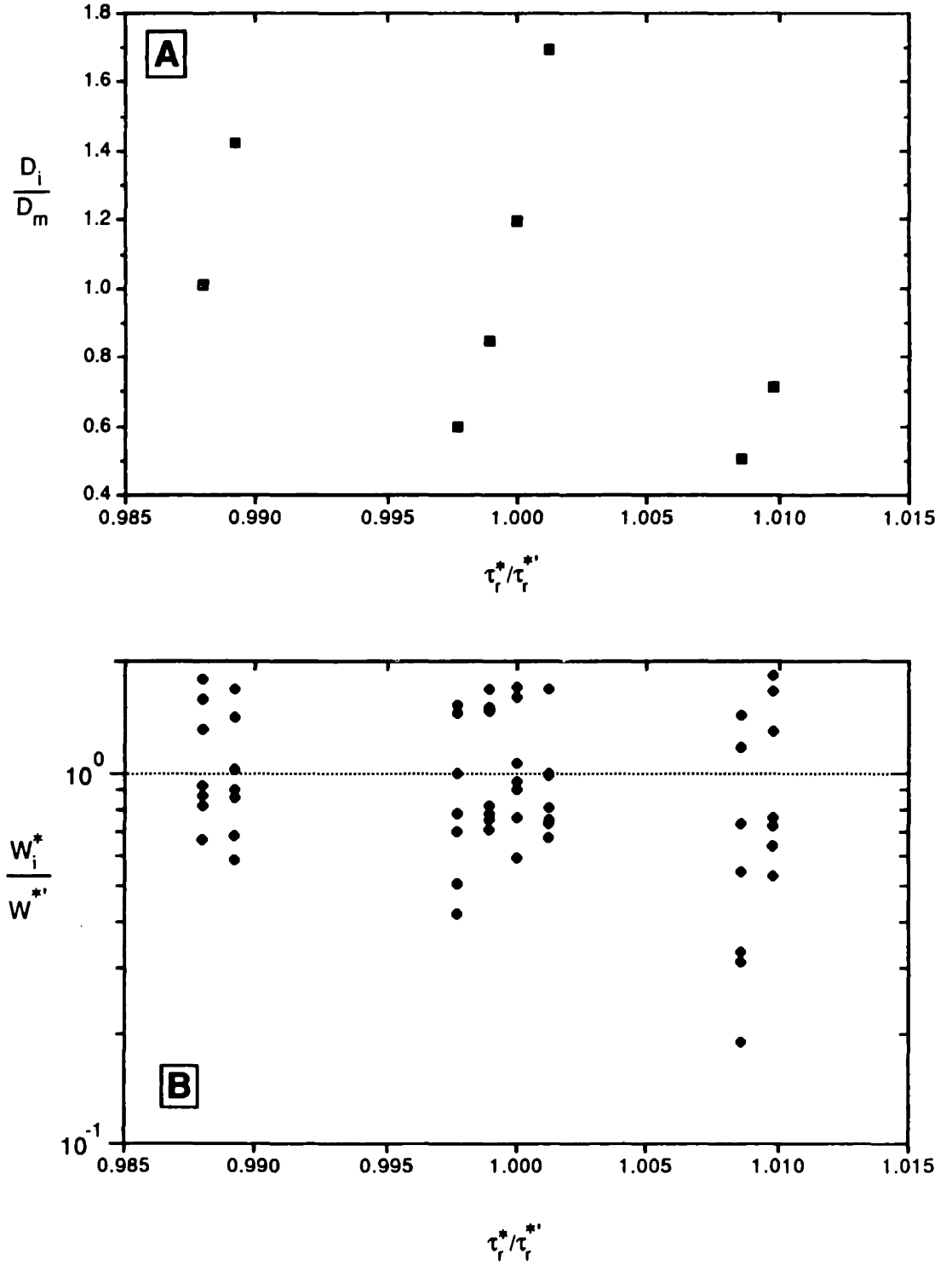

Figure 4.20: Residuals from simple fractional-transport model for 1/2Ø mixture.
A: Relative grain size as a function of error in the reference shear stress estimate
B: Error in W_i^* estimate as a function of error in reference shear stress estimate

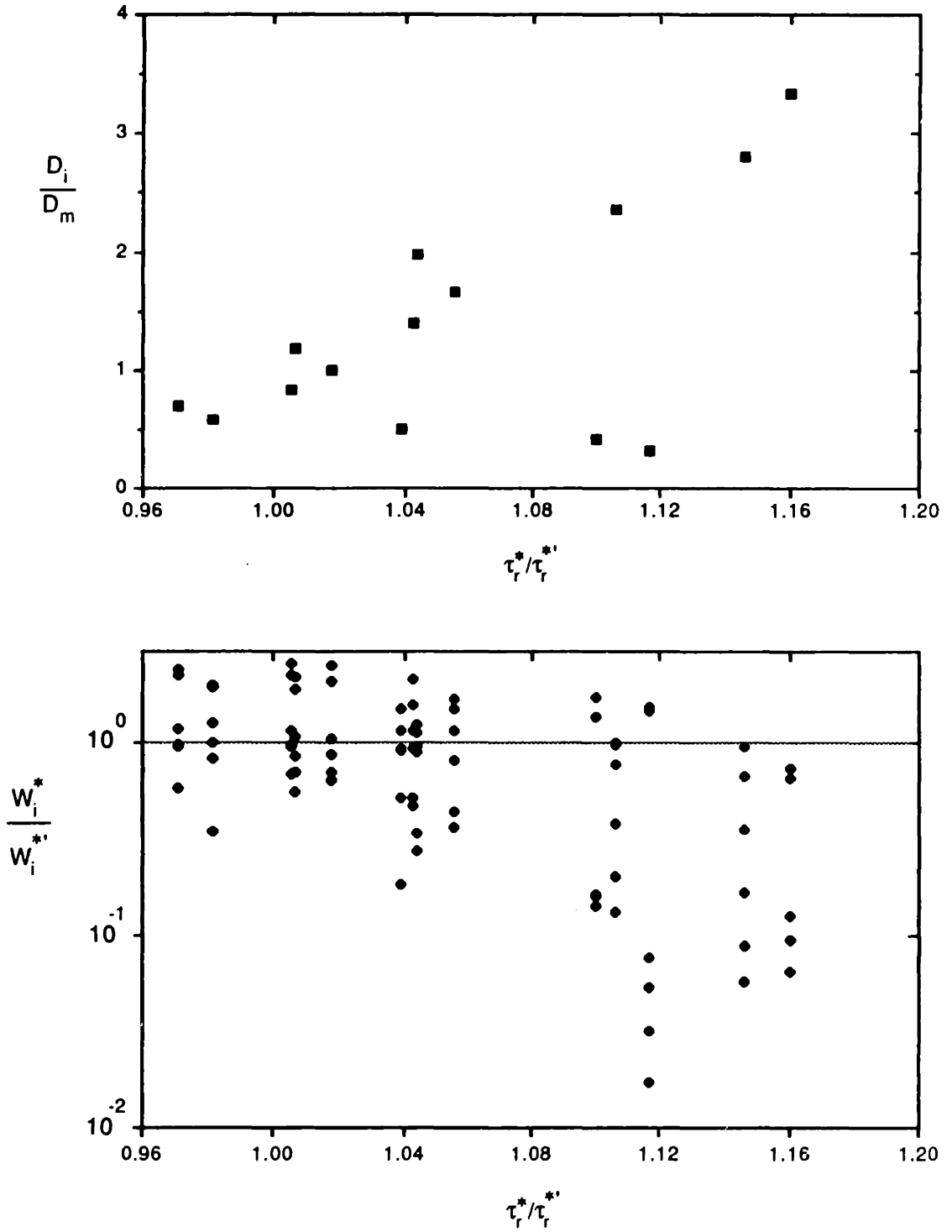

Figure 4.21: Residuals from simple fractional-transport model for the1Ø mixture.
A: Relative grain size as a function of error in the reference shear stress estimate
B: Error in W_i^* estimate as a function of error in reference shear stress estimate

essentially the same as that in Figure 4.19, because the predicted values of τ^*_{ri} are all within roughly 1% of the measured values.

The fit of the 1Ø model is considerably worse, with an error variation of 22.9 (18.1% of the total variation in W^*_i). The mean deviation for the 1Ø mixture is -0.213, indicating that the mean of the predicted values of W^*_i falls 40% below the mean of the actual values. In addition, the scatter of W^*_i in Figure 4.21 exceeds two orders of magnitude. Most of this error arises from much smaller errors in the predicted values of τ^*_{ri}. Five fractions in the 1Ø mixture (the three coarsest and the two finest) have errors in the τ^*_{ri} estimate of 10% or more. These fractions account for 84% of the model error; if they are removed from the model, the error variation decreases to 3.65 (2.9% of the total variation in W^*_i). This is a classic problem in sediment transport modeling: the steepness of the transport function magnifies any error in the value of bed shear stress. Even though τ^*_{ri} is relatively well estimated by $\tau^*_{ri} = \tau^*_{r50} (D_i/D_{50})^{-1}$, the remaining error is still too large to permit a reasonable estimate of the fractional transport rates.

CONCLUSIONS

Fractional transport functions show some variation with relative grain size for the 1Ø mixture, but not for the 1/2Ø mixture. The relative-size effect is evident only in the intermediate portions of the transport functions for the finest and coarsest fractions of the 1Ø mixture. The variation of the fractional transport functions with grain size depends not only on the variation in flow exposure and bed roughness with grain size but also on the development of a coarse layer at the bed surface and on the effect of bed forms on the stability of the coarse surface layer.

The variation in flow exposure and bed roughness with relative grain size balances the inherent variation in transportability with grain size and tends to make the transport rates of all fractions similar. This produces an equivalence of the transport grain-size distribution to that in the bed. Such an equivalence is particularly consistent for all our sediments at high transport rates. The

tendency of uni-size sediments of different sizes to approach a constant transport rate at high excess bed shear stress may also exist for different sizes in a mixture. This would reinforce the effects of relative exposure and relative roughness in producing the same fractional transport rates for all fractions at high transport rates.

The development of a coarse surface layer apparently decreases the transportability of both finer and coarser fractions in a mixture. This underrepresentation produces the observed variation of the fractional transport functions with relative grain size for the 1Ø mixture. A coarse surface layer augments the relative-exposure and relative-roughness effects on the finer fractions by removing a portion of these fractions from the actively transported sediment and thereby decreasing their availability for transport. The coarse surface layer competes with the relative-size effect on the transportability of the coarser fractions by increasing the roughness of the bed surface and decreasing the flow exposure these grains experience. The coarse surface layer exists, and influences the transport grain-size distribution, in the presence of stable, two-dimensional bed forms and defeats the potential homogenizing effect these bed forms have on the transport grain-size distribution. At high flow strengths the bed forms are sufficiently irregular in size and depth of scour, and the flow strength at reattachment is sufficiently strong, that the coarse surface layer apparently cannot develop. At these flow strengths the relative-exposure and relative-roughness effects, the constant high-transport-rate limit for each fraction, and the homogenizing effect of the bed forms may all act together to produce the observed relative-size independence of the transport grain-size distribution and fractional transport rates.

The transport functions of all size fractions in the 1/2Ø mixture are quite similar, as are those for the fractions representing most of the 1Ø mixture. The transport functions for the finest and coarsest fractions in the 1Ø mixture are somewhat flatter than the central fractions, although the transport rates of these extreme size fractions match those of the central fractions at low and high transport rates. Because only a portion of a minority of the transport

functions deviate significantly from a common trend, a very simple fractional-transport model may be made using only a slightly reduced version of the uni-size Shields curve to estimate τ^*_{r50}, an inverse relation between τ^*_{ri} and D_i/D_{50}, and a single transport function for all size fractions. The degree of explanation of our fractional-transport data is 82% for the 1Ø mixture and 96% for the 1/2Ø mixture The fit of the model for the 1Ø fraction is not as good as the coefficient of determination would suggest. The scatter in the W^*_i values exceeds two orders of magnitude, a problem that is primarily a result of small errors in the estimated reference shear stress for some fractions and the steep, nonlinear form of the fractional transport function.

CHAPTER FIVE

CONCLUSIONS

RELATIVE GRAIN-SIZE EFFECT ON FRACTIONAL TRANSPORT RATES

In the general case, three variables are necessary to describe the relative size of individual grains in a size mixture. The most convenient choices for these variables are the ratio of the fraction size to some central grain size (e.g. D_i/D_m), the percentile position of the size fraction (e.g. percent finer than, P), and the standard deviation of the mixture size distribution (the sorting, σ). For reasonably smooth and symmetrical size distributions, two of these parameters may be used to approximate the third. For perfectly lognormal sediments, which approximate many natural size distributions and which we have used in our experiments, two of the three parameters exactly determine the value of the third. The goal of the experimental work described in this thesis is to isolate the effect of these relative-size parameters on the transport rates of individual fractions in mixed-size sediments.

The experimental goal was achieved by measuring a wide range of transport rates for three sediment mixtures that had the same mean size and the same size-distribution shape, but values of mixture standard deviation that varied from well sorted to poorly sorted (σ = 0.2 Ø to 1.0 Ø). Because the same sediment sources were used for each mixture (providing reasonable control on grain shape, density, etc.) and because flow depth and water temperature were held nearly constant in all the runs, we were able to isolate the effect of the three relative-size parameters on fractional transport rates. For example, the fractional transport rates of the same fraction in two mixtures (and hence the same value of D_i/D_m) can be examined as a function of the change in only the percentile position of that fraction. Similarly, the effect of only mixture sorting may be tested for the central fractions of the size mixtures (for which D_i/D_m and P are identical), or for the total transport rates of the sediments.

In addition to the three primary sediments with the same mean size, the transport rates of two other well sorted sediments were measured. The mean sizes of these sediments were chosen to fall toward the fine and coarse ends of the most poorly sorted sediment mixture. These two sediments, along with the well sorted 1.83 mm sediment, permit a direct examination of the effect of relative grain size on the transport rates of fractions in the fine, middle, and coarse portions of a poorly sorted sediment. Because both D_i/D_m and P vary between the corresponding fine and coarse fractions, only the total relative-size effect on the fractional transport rates may be examined.

The effect of relative grain size on the fractional transport rates has been examined in two parts: the conditions necessary for initiation of sediment transport, and the variation of transport rates with bed shear stress once the grains are in motion.

We found that the different size fractions in our mixed-size sediments are transported at approximately the same rate for most of the flow conditions we measured. This effect is primarily a result of the strong control that relative grain size exerts on the conditions for initial motion of the individual fractions. Initial-motion conditions were approximated here by a reference value of dimensionless bed shear stress τ^*_{ri} which produces a small, constant value of the dimensionless transport rate W^*_i. Relatively small grains in the mixture have much higher reference shear stresses when present in a mixture than when present in a uni-size bed. This variation in τ^*_{ri} may be attributed to a decrease in exposure to the flow that the fine sediments experience, along with an increase in the roughness of the bed over which the grains must move. Relatively coarse grains in a sediment mixture exhibit changes in τ^*_{ri} values from the uni-size case that are essentially of the same magnitude as the corresponding changes for relatively fine grains, but opposite in direction. The decrease in τ^*_{ri} values we observe for the coarse fractions may be attributed to a relative increase in flow exposure compared to the uni-size case, and to a decrease in the roughness of the bed over which the grains move.

The relative-size effect on the reference shear stress is well described by the size ratio D_i/D_{50}. If the mean grain size of the mixture and the value of D_i/D_{50} are known, the τ^*_{ri} value of each fraction may be determined within 10%. The variation of τ^*_{ri} with D_i/D_{50} is virtually constant for all our sediments, meaning that the mixture sorting has little effect on the initial-motion conditions. This conclusion is also supported by the lack of variation in τ^*_{ri} values for corresponding fractions of the same size (and, hence, different values of P) in the mixtures with 1/2 Ø and 1 Ø sorting. We also find little variation in τ^*_{ri} — D_i/D_{50} relations for fractional-transport data from seven other sediment mixtures that cover a sorting range up to $\sigma_\phi = 2.1$. These other data provide additional support for the conclusion that the size ratio D_i/D_{50} explains virtually all of the relative-size effect on initial-motion conditions. In addition to a broad range of mixture sorting, these other data represent different grain-size distribution shapes, mean grain sizes, flow depths, and water temperatures. The consistency of the initial-motion relations we find with all these data, as well as our own, suggest that initial-motion conditions for many natural sediments may be relatively simple and described by functions of only the mean grain size of the sediment and the D_i/D_{50} value for each fraction.

The log slopes of τ^*_{ri} — D_i/D_{50} relations for all the sediments fall close to the special value of -1.0, which means that all fractions in the size mixture begin moving (or, more precisely, achieve the same low value of W^*_i) at close to the same bed shear stress. The implication that may be drawn from this result is that the effects of relative exposure and relative bed roughness are sufficiently strong to nearly balance an inherent increase in critical shear stress with increasing grain size and hence grain mass.

Although the τ^*_{ri} — D_i/D_{50} relations for different sediment mixtures are very similar in slope, they are separated from each other as a nearly linear function of the median size of the different sediments. This effect may be explained largely by an equivalent variation in the corresponding values of critical shear stress commonly accepted for uni-size sediment. With the

exception of one of the 11 mixtures examined here, all values of reference shear stress for the median grain size, τ^*_{r50}, fall within a factor of 1.3 of a slightly reduced (88%) position of the Shields curve for uni-size incipient motion. This level of scatter is within the range of scatter commonly associated with measurements of incipient motion.

Once the reference shear stress for each fraction is known, the relative-size dependence of the form of the relations between transport rate and shear stress may be examined in terms of the excess bed shear stress τ^*_i/τ^*_r. Most of our measured fractional transport rates (94%) fall reasonably close (within half an order of magnitude) to a common relationship that is reasonably well described by Parker's (1979) power approximation of the low-transport part of the Einstein (1950) transport function. The only significant relative-size effect on the form of the fractional transport functions occurs as a result of an underrepresentation in the transport load of the finest and coarsest fractions at intermediate transport rates. The apparent cause of this underrepresentation is the development of a coarse layer at the bed surface. Conditions for the existence, structure, and development of the coarse surface layer are poorly understood and represent a major obstacle to the developement of a general mixed-size sediment transport model. These will be discussed further in the following section.

Although the reference shear stresses for individual fractions in a mixture may be well described by only D_{50} and D_i/D_{50}, and our fractional-transport rates fall close to a common transport function, prediction of fractional transport rates from simple approximations of these empirical observations does not produce acceptable results. Because sediment transport is such a steep function of excess bed shear stress, the reference shear stress must be determined to a very accurately for an adequate prediction of the fractional transport rates. If the reference shear stress (and, hence, the excess shear stress) can be determined within a few percent, the fractional transport rates may be predicted within one order of magnitude. If the reference shear stress is known only within an accuracy of 10% or worse, the error in predicting

the transport rates increases to two or more orders of magnitude. Unfortunately, the degree to which the reference shear stress can be modeled for the best available fractional-transport data is on the order of 10% or more for many fractions. These are surprisingly accurate and consistent results for a broad range of sediment mixtures. They are not, however, sufficient to do an adequate job of predicting fractional transport rates.

THE EFFECT ON FRACTIONAL TRANSPORT RATES OF BED FORMS AND A COARSE BED-SURFACE LAYER

Sediment beds containing a mixture of sizes naturally become vertically sorted during steady-state transport when most or all of the grain sizes are in motion. The stop-and-start motion characteristic of bed-load transport, combined with the fact that the grains remain in contact with the bed during most if not all of each of their excursions, assures that finer grains will work their way beneath coarser grains. This vertical sorting process leads to a layering of the bed by grain size. A bed-surface layer that is about one (coarse) grain diameter thick and distinctly coarser than the bulk of the sediment mixture develops above a sublayer of perhaps the same thickness that is finer than the bed mixture as a whole.

We have demonstrated that this coarse surface layer can lead to underrepresentation in the transport grain-size distribution of both the finer and coarser grains in the sediment mixture. The coarse grains are underrepresented in the transport load, even though their concentration at the bed surface increases their availability for transport. The overrepresentation of the coarse grains on the bed surface is apparently more than compensated by a decrease in transportablity resulting from the decreased flow exposure and increased relative roughness experienced by the coarse surface grains. The development of the coarse surface layer eliminates the relative-size 'advantage' coarse grains experience when in well mixed portions of the bed, and makes the transportability of the coarse grains closer to that of a uni-size bed. The uni-size transport measurements we made with a sediment the same size

as the coarse grains in the 1Ø size mixture demonstrated that the reference shear stress for these coarse grains increases threefold when in a uni-size bed, and their transport rates decrease by orders of magnitude. The effect of the coarse surface layer on the proportion of the finer fractions in transport is more straightforward. By trapping disproportionate amounts of fine sediment, and hence removing them from the actively transported sediment, the coarse surface layer directly contributes to the underrepresentation of the fine fractions in the transport load. In this case, vertical sorting augments the relative-size effects of decreased exposure and increased bed roughness in producing a lower transport rate for the finer fractions in the mixture.

During bed-load motion, grains transported over bed forms come to rest on the bed-form slip face and become buried within the bed form. As the bed form moves downstream, the grains become reexposed and are transported again over the bed form to become redeposited on the slip face. If no grains are allowed to move from one bed form to another, this recycling effect prevents any size sorting on a scale larger than a single bed form. This homogenizing effect would be perfect for ideal, two-dimensional bed forms, if no grains are exchanged from one bed form to another; it should be present to some extent with any bed forms that have a depositional slip face.

Prior to this work, it was not known whether bed forms and a coarse surface layer were mutually exclusive bed states. Would the homogenizing effect of bed forms, and their tendency to scour the bed in their troughs, prevent a coarse surface layer from developing? We found that the two can, in fact, coexist, although the stability and degree of development of the coarse surface layer is to some extent dependent on the presence and shape of bed forms. With two-dimensional bed forms of fairly regular size, a well developed coarse surface layer may be present and exert a substantial influence on the transport rates of the fine and coarse fractions in the bed mixture. At higher flow strengths, the bed forms become more three-dimensional and variable in size. The variable depth to which these bed-form troughs scour and the more intense bed shear stress near reattachment apparently prevent the development

of a distinct coarse surface layer. In these cases, the transport grain-size distribution is much closer to that in the bed.

The fate of the coarse surface layer is not, of course, entirely dependent on the bed configuration — the two are interdependent. A coarse surface layer can influence the type of bed forms that may develop, particularly during moderate flow conditions, when a coarse surface layer can resist scouring in the bed-form trough and thereby contribute to the development of bed forms of a very regular size. This is a more complicated version of the classic sediment-transport problem: the transport rate is only one of several dependent variables, all of which are interrelated. Even in the simplified case of equilibrium transport of uni-size sediment, the characteristics of the sediment bed at both a large scale (bed slope, channel pattern, etc.) and a small scale (bed forms) are both determined by, and have a strong influence on, the sediment transport rate. In the case of mixed-size sediment, both the large-scale and small-scale parameters may take on different values as a function of size-mixture properties, and a second small-scale dependent variable is added to the problem: the grain-size distribution of the bed surface and subsurface. An additional interdependence is also set up: the nature of the bed forms both influences and is influenced by the development of the coarse surface.

To a first approximation, the effect of the coarse surface layer in our data may be ignored because it is present in less than 10% of our measured fractional transport rates. The effect is not trivial, however: an order-of-magnitude difference in transport rate is evident for some fractions when a well developed coarse surface layer is present. For transporting systems that operate in this range, the effect of the coarse surface layer on the fractional transport rates would be of first-order importance. Ignoring the coarse surface layer in our data also involves an implicit inclusion of the effect of bed forms on the coarse surface layer, because the transport grain-size distribution of our high-transport runs was determined in part by the presence of bed forms that were able to prevent a coarse surface layer from developing. In other sediments, such as the Oak Creek sediment (whose mean size is ten times

greater than that of our sediment), bed forms do not develop and a coarse surface layer may be present to much higher values of bed shear stress. This is suggested by the underrepresentation of both fine and coarse fractions in the highest transport rates sampled for that stream.

Because of the interdependence of fractional transport rates, bed forms, and bed-surface texture, a complete model for fractional transport rates must include the effect of the dominant mixture parameters on all three dependent variables. Our understanding of the interrelation between these three variables is not sufficient at present to do so. Further research could be profitably directed towards the following questions: How does the grain-size distribution of the coarse surface layer change with increasing flow stength? Is the composition of the coarse surface layer predictable from the bed size distribution (and particularly its standard deviation) and the flow properties? Can a threshold shear stress be determined above which the coarse surface layer begins to weaken, or above which the bed forms are able to destroy it?

HOW DO NATURAL SEDIMENTS BECOME SORTED BY GRAIN SIZE?

One of the central results of our experiments is that for flow conditions involving substantial sediment transport, the grain-size distribution of the transported sediment is nearly the same as that of the bed. We also find this result in our analysis of the fractional-transport data of others, which show the fractional reference shear stress to be nearly independent of grain size. This apparent lack of size-dependent fractional transport leaves open the question of how differential transport of individual size fractions occurs in natural settings. How are fine sediments winnowed from a poorly sorted sediment bed to leave a coarse lag deposit? How are sediment mixtures progressively sorted by size along a river or across the shelf? The particular system boundary conditions, such as sediment input and flow variability, are different between these cases, but it seems clear that size-dependent equilibrium bed-load transport rates may not be used as the driving mechanism.

A variety of other factors — none of which is well understood — may be called into play.

The overall range of fractional grain sizes considered here is limited. The largest range of fraction sizes for our mixtures is approximately 11.3 (D_{95}/D_5). The largest range for all the sediments we have considered is that for Oak Creek, for which $D_{95}/D_5 \approx 80$. Greater ranges in grain size exist in natural sediments. It is reasonable to suppose that natural limits exist for the range of grain sizes for which equal-mobility conditions hold. Grains finer than about 0.1 mm are entrained directly into suspension in uni-size beds; grains of this size (and somewhat coarser) in size mixtures may also travel in suspension most, if not all, of the time. If so, their transport functions may look substantially different from the fractions moving only as bed load. It is also likely that the size independence of the reference shear stress does not extend indefinitely to fractions much larger than the mean, if only because it is difficult to imagine boulders moving at the same transport rate as fine sand when both are in the same mixture. Although these presumed grain-size limits provide some constraint on the range over which equal-mobility conditions operate, they do not provide an explanation of how progressive sorting (in time or space) can proceed within these limits.

A second alternative is that most sorting occurs during nonequilibrium transport conditions. This is certainly the case when no sediment supply is available and the bed eventually degrades to a stable armor that can no longer be eroded by the prevailing flows. A coarse surface layer for which all grains are occasionally mobile may appear during the initial development of an immobile armor. Eventually, however, the bed would inevitably degrade to the point that only grains that are immobile for the existing range of flows would remain at the bed surface.

Nonequilibrium size-dependent transport may also prevail most of the time in transporting systems, such as alluvial rivers, that are essentially in equilibrium over periods of tens to hundreds of years. Most of the sediment transport in many rivers occurs during relatively short periods of high

discharge. Andrews (1983) has noted that during low-transport periods in some western U.S. rivers, the coarse (gravel) fractions are virtually immobile, while finer (sand) fractions move as large bed forms over a coarse-grained armor. During these periods a substantial degree of progressive sorting may be able to develop even though the transport rates are relatively low, because these periods are of much greater duration than the high-transport periods, and because the transport size distribution is entirely fine-grained. The relatively independent behavior of the sand throughput led Andrews to draw an analogy with wash load: sediment that is transported through a reach but is almost absent in the bed material. If this analogy is correct, the controls on transport rates of the throughput sand are related more to the availability of that sediment in the river system than to the nature of the sediment bed and the immediate hydraulic conditions. Other locally dependent and complex controls may act to keep the coarse grains immobile under conditions sufficient to move the finer grains. Factors controlling the stability of the bed fabric (its degree of imbrication and grain interlocking) include the shape of the coarse grains, the recent history of flow and transport variation, and the duration of low-transport periods when the bed may become stabilized by biological or cryological processes.

Time- and site-dependent nonequilibrium controls on differential fractional transport may be the dominant parameters producing progressive grain-size sorting in natural settings. If this is the case, the task of developing a general fractional-transport model that can predict this sorting will be exceedingly difficult, because an enormous number of variables will have to be included.

An additional mechanism for progressive size sorting that is appealing because it may provide a general mechanism for size-dependent fractional transport is the size-dependent entrainment of grains into suspension. Even though relative-size effects apparently make entrainment into bed-load motion nearly independent of grain size, the entrainment of grains into suspension requires the grains to be lifted into the flow and should thus show a stronger

dependence on the size and hence the weight of individual grains. Size-dependent suspension entrainment, coupled with the far greater velocities of grains in suspension transport, would produce higher transport rates of finer fractions, and this could produce progressive sorting during the major transport events that account for most of the total transport in many natural systems.

REFERENCES

Ackers, P., and W.R. White, Sediment transport: new approach and analysis, *J. Hydraul. Div., Amer. Soc. Civil Eng.*, 99(HY11), 2041-2060, 1973.

Andrews, E.D., Entrainment of gravel from naturally sorted riverbed material, *Geol. Soc. Amer. Bull.*, 94, 1225-1231, 1983.

Andrews, E.D., and D.C. Erdman, Persistence in the size distribution of surficial bed material during an extreme snowmelt flood, *Water Resour. Res.*, 22, 191-197, 1986.

Andrews, E.D., and G. Parker, The coarse surface layer as a response to gravel mobility, *Proceedings, Workshop on gravel-bed rivers*, Pingree Park, Colo., 1985.

Arya, S. P. S., A drag partition theory for determining the large-scale roughness parameter and wind stress on Arctic pack ice, *J. Geophys. Res.*, 80: 3447-3454, 1975.

Ashida, K., and M. Michiue, Study on hydraulic resistance and bedload transport rate in alluvial streams, *Trans. Jpn. Soc. Civ. Eng.*, 206, 59-69, 1972.

Borah, D.K., C.V. Alonso, and S.N. Prasad, Routing graded sediments in streams: formulations, *J. Hydraul. Div., Amer. Soc. of Civil Eng.*, 108(HY12), 1486-1503, 1982.

Carling, P.A., Threshold of coarse sediment transport in broad and narrow natural streams, *Earth Surface Processes and Landforms*, 8, 1-18, 1983.

Chepil, W.S., Dynamics of wind erosion, I, The nature of movement of soil by wind: *Soil Sci.*, 60, 305-320, 1945.

Colebrook, C. F., Turbulent flow in pipes, with particular reference to the transition between the smooth and rough pipe laws, *J. Inst. Civ. Eng. Lond.*, 99:133-156, 1938.

Day, T.J., A study of the transport of graded sediments, *Report No. IT 190*, Hydraulics Research Station, Wallingford, England, 1980a.

Day, T.J., A study of initial motion characteristics of particles in graded bed material, Geol. Survey of Canada, *Current Research, Part A*, Paper 80-1A, 281-286, 1980b.

Dhamotharan, S., A. Wood, G. Parker, and H. Stefan, Bedload transport in a model gravel stream, *Proj. Report No. 190*, St. Anthony Falls Hydr. Lab., Univ. Minnesota, 1980.

Diplas, P., Bedload transport in gravel-bed streams, *J. Hydraul. Eng.*, 113, 277-292, 1987.

Diplas, P., and G. Parker, Pollution of gravel spawning grounds due to fine sediment, *Proj. Report No. 240*, St. Anthony Falls Hydr. Lab., Univ. Minnesota, 1985.

Drake, T. G., and R. L. Shreve, High-speed motion pictures of bed-load transport in a gravel-bed stream (abstract), *EOS Trans. AGU*, 66(46), 910, 1985.

Egiazaroff, I.V., Calculation of nonuniform sediment concentrations, *J. Hydraul. Div. Am. Soc. Civ. Eng.*, 91(HY4), 225-247, 1965.

Einstein, H.A., Formulas for the transportation of bed load, *Transactions, Am. Soc. Civil Eng.*, 107, Paper No. 2140, 561-573, 1942.

Einstein, H.A., The bedload function for sediment transport in open channel flows, *Tech. Bull. 1026*, U.S. Dep. of Agric., Soil Conserv. Serv., Washington, D.C., Sept. 1950.

Einstein, H.A., and N. Chien, Transport of sediment mixtures with large range of grain size, *MRD Sediment Series No. 2*, United States Army Engineer Division, Missouri River, Corps of Engineers, Omaha, Neb, 1953.

Engelund, F., Hydraulic resistance of alluvial streams, *J. Hydraul. Div., Am. Soc. Civil Eng.*, 92(HY2), 315-327, 1966.

Engelund, F., Closure to Hydraulic resistance of alluvial streams, *J. Hydraul. Div., Am. Soc. Civil Eng.*, 93(HY4), 287-296, 1967.

Engelund, F., and J. Fredsøe, A sediment transport model for straight alluvial channels, *Nordic Hydrology*, 7:293-306, 1976.

Engelund, F., and E. Hansen, *A Monograph on Sediment Transport in Alluvial Streams*, Teknisk Vorlag, Copenhagen, 1972.

Fernandez Luque, R., and R. Van Beek, Erosion and transport of bedload sediment, *J. Hydraul. Res.*, 14(2), 127-144, 1976.

Folk, R. L., *Petrology of Sedimentary Rocks*, Hemphill, Austin, Texas, 182 p., 1980.

Guy, H.P., D.B. Simons, and E.V. Richardson, Summary of alluvial channel data from flume experiments, 1956-61, *U.S. Geol. Survey Prof. Paper 462-I*, 1966.

Hammond, F.D.C., A.D. Heathershaw, and D.N. Langhorne, A comparison between Shields' threshold criterion annd the movement of loosely packed gravel in a tidal channel, *Sedimentology*, 31, 51-62, 1984.

Harms, J. C., J. B. Southard, and R. G. Walker, *Structures and sequences in clastic rocks*, Short Course 9, Soc. Econ. Paleo. Min., 1982.

Johnson, J.W., The importance of considering side-wall friction in bed-load investigations, *Civil Engineering*, Am. Soc. Civil Eng., 12(6), 329-331, 1942.

Komar, P.D., Selective grain entrainment by a current from a bed of mixed sizes: a reanalysis, *J. Sediment. Petrol.*, 57(2), 203-211, 1987.

Li, R-M, and W. T. Fullerton, Investigation of sediment routing by size fractions in a gravel- and cobble-bed river, *Proceedings, Workshop on gravel-bed rivers*, Pingree Park, Colo., 1985.

Li, Z., and P.D. Komar, Laboratory measurements of pivoting angles for applications to selective entrainment of gravel in a current, *Sedimentology*, 33, 413-423, 1986.

McLean, S.R. and J.D. Smith, A model for flow over two-dimensional bed forms, *J. Hydraul. Eng.*, 112(4), 300-317, 1986.

Meland, N. and J.O. Norrman, Transport velocities of individual size fractions in heterogeneous bed load, *Geografiska Annaler*, 51, Ser. A, 127-144, 1969.

Meyer-Peter, E., and R. Müller, Formulation for bed load transport, *Proc. 2nd Congress*, Int. Assoc. Hydr. Res., Stockholm, Sweden, pp. 39-64, 1948.

Milhous, R.T., Sediment transport in a gravel-bottomed stream, Ph.D. thesis, Oregon State Univ., Corvallis, 1973.

Miller, M.C., I.N. McCave, and P.D. Komar, Threshold of sediment motion under unidirectional currents, *Sedimentology*, 24, 507-527, 1977.

Miller, R.L. and R.J. Byrne, The angle of repose for a single grain on a fixed rough bed, *Sedimentology*, 6, 303-314, 1966.

Misri, R. L., R. J. Garde, and K. G. Ranga Raju, Bed load transport of coarse nonuniform sediment, *J. Hydr. Eng., Am Soc. Civil Eng.*, 110(3):312-328, 1984.

Neill, C.R., A re-examination of the beginning of movement for coarse granular bed materials, Hydraul. Res. Station *Rep. No. Int 68*, 37 pp., 1968.

Neill, C.R., and M.S. Yalin, Quantitative definition of beginning of bed movement, *J. Hydraul. Div. Am. Soc. Civ. Engrs.*, 95(HYI), 585-587, 1969.

Owen, P.R., Saltation of uniform grains in air, *J. Fluid Mech.*, 20, 225-242, 1964.

Paola, C., Flow and skin friction over natural rough beds, Sc. D. Thesis, MIT/Woods Hole Ocean. Inst. WHOI-83-18, 1983.

Parker, G., Hydraulic geometry of active gravel rivers, *J. Hydraul. Div. Am. Soc. Civ. Eng.*, 105(HY9), 1185-1201, 1979.

Parker, G., and P.C. Klingeman, On why gravel bed streams are paved, *Water Resources Res.*, 18, 1409-1423, 1982.

Parker, G., P.C. Klingeman, and D.L. McLean, Bedload and size distribution in paved gravel-bed streams, *J. Hydraul. Div. Am. Soc. Civ. Eng.*, 108(HY4), 544-571, 1982.

Shields, A., Application of similarity principles and turbulence research to bedload movement, Translated from "Anwendung der Ähnlichkeitsmechanik und der Turbulenzforschung auf die Geschiebebewegung", in *Mitteilungen der Preuss. Versuchanst. für Wasserbau und Schiffbau*, Berlin, vol. 26, by W.P. Ott and J.C. von Uchelen, Calif. Inst. Technol. Hydrodyn. Lab No. 167, 1936.

Smith, J.D., Modeling of sediment transport on continental shelves, in *The Sea*, vol. 6, E.D. Goldberg, ed., Wiley-Interscience, New York, 539-577, 1977.

Smith, J. D. and S.R. McLean, Spatially averaged flow over a wavy surface, *J. Geophys. Res.*, 82(12), 1735-1746, 1977.

U.S.W.E.S., Studies of river bed materials and their movement with special reference to the lower Mississippi River, *Paper No. 17*, United States Waterways Experimental Station, Vicksburg, Miss., 1935.

Vanoni, V.A., and N.H. Brooks, Laboratory studies of the roughness and suspended load of alluvial streams, *Sedimentation Laboratory Report No. E68*, Calif. Inst. Technol., Pasadena, Calif., 1957.

White, C.M., The equilibrium of grains on the bed of a stream, *Proc. R. Soc. A*, 174, 323-338, 1940.

White, W. R., and T. J. Day, Transport of graded gravel bed material, in *Gravel-bed rivers*, edited by R. D. Hey, J. C. Bathurst, and C. R. Thorne, pp. 181-213, John Wiley, London, 1982.

Wiberg, P. L., and J. D. Smith, Calculations of the critical shear stress for motion of uniform and heterogeneous sediments, *Water Resour. Res.*, in press, 1987.

Wiberg, P.L. and J.D. Smith, A theoretical model for saltating grains in water, *J. Geophys. Res.*, 90(C4), 7341-7354, 1985.

Wilcock, P. R., and J. B. Southard, Natural variability of transport rates in beds with heterogeneous sediment sizes (abstract), *EOS Trans. AGU*, 66(46), 910, 1985.

Willams, G. P., Flume width and water depth effects in sediment transport experiments, *U.S.G.S. Prof. Paper 562-H*, 1970.

Yalin, M.S., *Mechanics of Sediment Transport*, Pergamon, New York, 1977.

APPENDIX A GRAIN-SIZE DISTRIBUTIONS OF THE TRANSPORTED SEDIMENT

TABLE A.1 1/2Ø MIXTURE GRAIN-SIZE DISTRIBUTIONS

— GRAIN SIZE GIVEN AS PERCENT RETAINED ON SIEVE —

SIEVE SIZE (mm)	BED	RUN B1	RUN B2	RUN B3	RUN B4	RUN B5	RUN B6	RUN B7
5.66	0.00	0.00	0.00	0.00	0.00	0.12	0.00	0.00
4.76	0.30	0.00	0.04	0.11	0.00	0.24	0.00	0.00
4.00	0.62	0.77	0.51	0.47	0.51	1.00	0.76	1.35
3.36	2.44	2.98	1.87	2.04	1.90	1.40	1.71	2.47
2.83	5.89	5.81	5.33	6.18	3.98	4.83	6.50	6.18
2.38	12.95	16.17	13.64	13.59	12.47	9.66	13.08	11.78
2.00	17.94	20.88	19.95	19.18	19.49	15.78	20.26	16.63
1.68	19.06	21.63	20.34	21.32	20.64	20.52	23.06	19.63
1.41	17.23	15.71	17.38	18.16	17.28	21.37	19.80	19.01
1.19	11.92	10.45	11.18	13.76	13.59	12.75	9.28	11.86
1.00	7.34	4.51	7.03	4.59	7.31	9.23	4.52	7.96
0.841	2.72	1.02	2.44	0.56	2.65	2.63	0.76	2.32
0.707	0.61	0.06	0.20	0.02	0.17	0.41	0.11	0.42
0.500	0.67	0.02	0.04	0.01	0.01	0.07	0.13	0.35
0.354	0.30	0.00	0.05	0.00	0.00	0.00	0.03	0.04

TABLE A.2 1Ø MIXTURE GRAIN-SIZE DISTRIBUTIONS

— GRAIN SIZE GIVEN AS PERCENT RETAINED ON SIEVE —

SIEVE SIZE (mm)	BED	RUN C1	RUN C2	RUN C3	RUN C4	RUN C5	RUN C6
8.00	1.67	0.00	0.00	0.00	0.00	0.15	0.52
6.73	1.93	0.00	0.00	0.00	0.02	0.26	0.85
5.66	2.66	0.00	0.45	0.25	0.16	1.75	1.87
4.76	3.29	0.55	0.50	0.41	0.75	2.77	2.34
4.00	4.47	1.12	2.34	1.26	2.23	3.88	4.82
3.36	5.38	2.83	4.80	3.59	3.90	5.90	5.48
2.83	7.47	6.30	7.17	8.45	8.07	7.67	6.55
2.38	8.07	8.02	10.07	9.52	11.00	8.13	8.05
2.00	9.93	13.34	14.32	13.98	13.95	9.43	9.00
1.68	10.23	13.77	17.14	15.93	16.55	9.54	9.58
1.41	9.73	17.88	17.53	16.30	16.18	10.02	10.17
1.19	8.52	16.19	12.91	14.22	13.11	8.91	8.70
1.00	7.62	12.05	6.96	11.21	9.75	8.56	8.16
0.84	6.20	6.12	2.96	4.23	3.71	8.26	7.60
0.71	4.60	1.24	1.68	0.54	0.48	7.10	6.65
0.50	5.43	0.56	1.08	0.07	0.11	7.37	8.59
0.35	2.81	0.03	0.08	0.03	0.02	0.29	1.10

TABLE A.3 CUNI GRAIN-SIZE DISTRIBUTIONS

— GRAIN SIZE GIVEN AS PERCENT RETAINED ON SIEVE —

SIEVE SIZE (mm)	BED	RUN D2	RUN D3	RUN D4
6.73	0.30	0.28	0.33	0.00
5.66	30.55	32.31	36.48	35.13
4.76	52.32	55.21	52.44	54.36
4.00	15.69	11.67	10.40	9.72
3.36	1.14	0.53	0.35	0.79

TABLE A.4 FUNI GRAIN-SIZE DISTRIBUTIONS

— GRAIN SIZE GIVEN AS PERCENT RETAINED ON SIEVE —

SIEVE SIZE (mm)	BED	RUN E1	RUN E2	RUN E3	RUN E4	RUN E5	RUN E6
1.000	0.71	0.55	0.38	0.71	0.36	0.50	0.32
0.841	5.69	6.36	7.82	7.69	3.99	3.68	3.55
0.707	33.58	49.07	54.67	48.66	33.61	32.18	30.89
0.595	27.89	26.57	25.97	24.20	27.91	26.78	27.91
0.500	29.15	15.73	10.63	17.43	31.17	33.32	34.05
0.420	2.63	1.29	0.46	1.13	2.76	3.27	3.06
0.354	0.35	0.42	0.08	0.20	0.21	0.28	0.22

APPENDIX B

SYMBOLS

A	Bed area	$[L^2]$
b	flume width	$[L]$
b_i	proportion of fraction *i* on the bed surface	
C_D	drag coefficient	
d	flow depth	$[L]$
d^*	d/D_i	
D	grain size	$[L]$
D_m	mean grain size of mixture	$[L]$
D_n	size with *n* percent of the mixture finer than	$[L]$
f_{ai}	area proportion of fraction *i* on bed surface	
f_i, f_{mi}	mass proportion of fraction *i* in sediment mixture	
F_D	drag force on bed forms	$[M/LT^2]$
H	bed-form height	$[L]$
l	mean excursion length of a grain in bed-load motion	$[L]$
n	number of grains moving per unit bed area and unit time	$[1/L^2T]$
p	proportion of grains on the bed surface in motion	
p_i	mass proportion of fraction *i* in the transported sediment	
P	percentile position (percent finer than) within a mixture	
q_b	unit bed-load transport rate	$[M/LT]$
q_{bi}	$(p_i)(q_b)$	$[M/LT]$
R	hydraulic radius	$[L]$
s	ρ_s/ρ	
S	water-surface slope	
S^*	$\dfrac{D_i^{3/2}\sqrt{(s-1)g}}{\nu}$	
U, V	mean flow velocity	$[L/T]$
u_*, u_{*o}	total bed shear velocity	$[L/T]$
$\forall_g$	grain volume	$[L^3]$
W^*	$\dfrac{(s-1)gq_b}{\rho_s u_*^3}$	
W^*_i	$\dfrac{(s-1)gq_{bi}}{f_i\rho_s u_*^3}$	
X	largest size in a mixture that does not experience shielding from the flow	$[L]$
z_o	bed roughness length in turbulent velocity profile	$[L]$
z_*	matching height of inner and outer velocity profiles	$[L]$
$(z_o)_o$	bed roughness length with no transport	$[L]$
$(z_o)_{st}$	bed roughness length with transport	$[L]$
δ_B	mean hop height of grains in bed-load motion	$[L]$
κ	von Karman constant (taken equal to 0.4)	

λ	bed-form spacing	[L]
μ	dynamic viscosity	[M/LT]
ν	kinematic viscosity	[L^2/T]
ξ	hiding function	
ρ	fluid density	[M/L^3]
ρ_s	sediment density	[M/L^3]
σ	mixture standard deviation	
σ_ϕ	mixture standard deviation when grain size is expressed in Ø units	
τ	shear stress	[M/LT^2]
τ_o	boundary shear stress	[M/LT^2]
τ^*	$\frac{\tau_o}{(s-1)\rho g D}$	
τ^*_i	$\frac{\tau_o}{(s-1)\rho g D_i}$	
Ø	$-\log_2(D)$ when D is expressed in millimeters	

SUBSCRIPTS

b	of the channel bed (distinct from the wall)
c	of or at critical conditions for initial grain motion
i	of an individual fraction in the mixture
lg	of or by the largest-grain initial-motion method
m	of the mean grain size in a mixture
r	of or by the reference-transport initial-motion method
w	of the channel walls (distinct from the bed)

SUPERSCRIPTS

'	of the skin friction
"	of the form drag

BIOGRAPHICAL SKETCH

I was born in 1953, the third of five children of Richard and Josephine. After a pleasant childhood in east-central Illinois, I thumbed my way about the continent and beyond for four years (including my last year of High School), working the occasional odd job to add a middle-class flavor to the tail-end of the hippie era. Thanks to the breadth and flexibility of our higher educational system, I was able to back into college at the University of Illinois in 1974. Toward the end of my undergraduate career, I discovered that science provided an outlet for the latent compulsiveness I had previously covered over with mellowness. After collecting all the honors I could and graduating in 1978, I moved on to McGill University to learn the science of geomorphology from Mike Carson. This was the formative stage of my career. I learned that the processes acting on the earth's surface were not only interesting to study, but that their study could be of some direct, immediate usefulness. After receiving my M.Sc. from McGill in 1981, affairs of the heart brought me to Boston, where I was pleasantly surprised to learn that the local technical university provided a golden opportunity for me to study the central process of geomorphology, sediment transport.